UNIVERSITY OF BELGRADE

FACULTY OF CHEMISTRY

Filip Ž. Vlahović

Density functional theory for studying electronic states of aqua- and oxo- first row transition metal complexes

Doctoral Dissertation

Belgrade, 2020.

УНИВЕРЗИТЕТ У БЕОГРАДУ

ХЕМИЈСКИ ФАКУЛТЕТ

Филип Ж. Влаховић

Теорија Функционала Густине у проучавању електронских стања аква- и оксо- комплекса прве серије прелазних метала

Докторска Дисертација

Београд, 2020.

Supervisors:

_____

dr. **Maja Gruden-Pavlović**, Full professor
University of Belgrade-Faculty of Chemistry

_____

dr. **Marcel Swart**, ICREA Research professor
Institut de Química Computacional i Catàlisi (IQCC)
University of Girona, Spain

Committee members:

_____

dr. **Matija Zlatar**, Associate research professor
University of Belgrade- Center for Chemistry,
Institute of Chemistry, Technology and Metallurgy

_____

dr. **Miloš Milčić**, Associate professor
University of Belgrade-Faculty of Chemistry

_____

dr. **Edwin Otten**, Associate professor
Faculty of Science and Engineering
University of Groningen, Netherlands

Date _____.

Acknowledgments

Before we even start with the actual science, I would like to thank my supervisor and mentor, Dr. Maja Gruden-Pavlović for the patience, support, and guidance she has provided. I need to thank her for all the help I received, not only on the professional level but also on personal. I was more than lucky to have such a devoted person for a mentor.

The present thesis wouldn't have this form without the help of Professor Dr. Marsel Swart. I am profoundly grateful for all ideas, advice, and those suggestions which were enough to move me in the moments I thought I had reached a dead-end.

I would like to express my gratitude to Dr. Matija Zlatar for the valuable experience and scientific perception he has shared with me during my research. His pragmatic way of thinking emerged as the solution to many serious chemical problems.

My sincere thanks go to Dr. Miloš Milčić, for going through the entire dissertation and for giving me many valuable comments and suggestions.

I would also like to give a lot of thanks to Dr. Edwin Otten, for being a part of the comity, as well as for numerous fruitful talks we have had during the past few years.

Although Dr. Stepan Stepanović is not a part of the comity, he deserves my special gratitude, since he has unselfishly shared all his remarkable knowledge and ideas with me, and helped me countless times in various ways. After all, he is not only a great scientist, hi is a great friend in the first place!

I would like to extend my sincere thanks to Dr. Aleksandar Nikolić, since without him my chemical sight, as well as many other skills, would be considerably reduced.

My gratitude also goes to all members of laboratory 544, without whom I wouldn't have that much fun doing science.

I would also like to thank my colleagues (and friends) from the faculty, Dalibor, Vesna, Slađana, Nataša, Konstantin, Jovana, Mima, Ivana, Mladen, and Stefan. It is a great pleasure spending time in the presence of such great scientists.

Special thanks go to my dear friends Jovica, Marija, Slobodan, Marko, Nemanja, Bojan, Luka, Aleksandar, Ivan, and Momčilo. I am really sorry for all those times I skipped gatherings and parties, but this humble peace of science required all of me- in order to see the light of the day.

I would also like to express my gratitude and respect to Dr. Miodrag Pavlović and Dr. Mihailo Marjanović.

In the end, I would like to express my deepest gratitude to my parents, Željko and Snežana, for endless love and support they are shoving in every moment of every day. Without their commitment and hard work, my high education would not be possible in the first place.

Last, but not the least, I would like to thank my sister, Žaklina, for being the most astonishing person in my life, and for teaching me how to be a good man.

Filip Ž. Vlahović

Захвалница

Пре него што почнемо са науком, желео бих да се захвалим свом супервизору и ментору Др Маји Груден-Павловић на стрпљењу, подршци и смерницама које ми је пружила. Желим се захвалити за сву помоћ коју сам добио, не само на професионалном, већ и на личном нивоу. Имао сам много среће што сам изабрао тако посвећену особу за ментора.

Ова докторска дисертација не би имала овакав облик без помоћи професора Др Марсела Сварта. Дубоко сам захвалан за све идеје, савете, и све сугестије које су биле довољне да ме покрену у тренуцима када сам сматрао да сам дошао до слепе улице.

Желео бих да се захвалим Др Матији Златару за драгоцено искуство и научну перцепцију, коју је делио са мном током свих истраживања. Његов прагматични начин размишљања био је решење за многе озбиљне хемијске проблеме.

Искрену захвалност дугујем и Др Милошу Милчићу, за детаљно прегледање дисертације и све вредне коментаре и предлоге које ми је дао.

Такође бих желео да захвалим Др Едвину Оттену што је пристао да буде део комисије, као и за бројне плодоносне разговоре које смо водили током последњих неколико година.

Иако Др Степан Степановић није део комисије, заслужује моју посебну захвалност, јер је несебично делио са мном своја изванредна знања и идеје и небројено пута ми помогао на разне начине. Уосталом, он није само сјајан научник, он је један сјајан пријатељ пре свега!

Искрено бих се захвалио Др Александру Николићу, јер би без њега мој хемијски вид, као и многе друге вештине, био знатно сужен.

Своју захвалност упућујем и свим члановима лабораторије 544, без којих ми не би било оволико забавно да се бавим науком.

Такође бих се захвалио колегама (али и пријатељима) са факултета, Далибору, Весни, Слађани, Наташи, Константину, Јовани, Мими, Ивани, Младену и Стефану. Време проведено у присуству тако великих научника представља и велико задовољство.

Посебну захвалност дугујем својим драгим пријатељима Јовици, Марији, Слободану, Марку, Немањи, Бојану, Луки, Александру, Ивану и Момчилу. Заиста ми је жао због свих ситуација када сам пропустио окупљања и славља, али овај скромни комад науке захтевао ме је целог- како би угледао светлост дана.

Такође бих хтео да укажемм на дубоку захвалност и поштовање Др Миодрагу Павловићу и Др Михаилу Марјановићу.

На крају, желим изразити своју најдубљу захвалност родитељима, Жељку и Снежани, на бескрајној љубави и подршци коју пружају у сваком тренутку свакога дана. Без њихове посвећености и напорног рада, моје високо образовање не би ни било могуће.

На крају, али не и најмање битно, хтео бих да захвалим својој сестри Жаклини јер је најневероватнија особа у мом животу и јер ме свакодневно учи како да будем добар човек.

Филип Ж. Влаховић

Мојој мајци, која ме је вештом руком усмерила на праве путеве.

Мом оцу, који је омогућио да сваки мој корак буде сигуран.

Мојој сестри, која ме је на путу у свакој одлуци безусловно подржала.

Application of methods based on Density Functional Theory, for studying electronic states of aqua- and oxo- first row transition metal complexes

SUMMARY

In the scope of present doctoral thesis, the complicated electronic structure of aqua- and oxo-complexes of the first row transition metals is studied. Energies of the ground and excited electronic states of transition metal complexes are calculated using DFT-based theoretical methods. The performance of different DFAs was investigated in order to find an unambiguous way to determine the ground spin state of oxo- and hydroxo-iron complexes, which is one of the most demanding tasks, both from theoretical and experimental point of view. The results direct us to use S12g for optimization as well as for the determination of the ground spin state.For calculation of excited states, two different methods (TD-DFT and LF-DFT) are utilized, whereas the results are rationalized and compared with those obtained experimentally. The results indicate a significantly better performance of LF-DFT method for calculation of excited states and reproduction of experimental spectra. In addition, EDA study of a series of oxo- and hydroxo- iron model complexes was performed. The binding energy is decomposed into chemically meaningful contributions. Obtained results show that the most important factor, responsible for the energy differentiation, is the destabilizing preparation energy based on excitation energy requirements and oxidation state of the metal. And the other is the stabilizing orbital interaction energy established when chemical bonds are created.

The primary challenge was to establish an appropriate level of theory able to explain the relationships between structural features and electronic structure, and in turn rationalize the experimentally obtained results. The scientific content of this dissertation proposes computational steps which make DFT reliable for explaining, interpreting and predicting the characteristics and properties of first row transition metal complexes. By rationally applying the proposed methodologies, we have an exclusive opportunity to clarify the experimental blindspots and apply the basic principles in order to understand the chemical complexities.

Keywords: Density Functional Theory, Electronic Structure, Excited States, Electronic Spectroscopy, UV/Vis Spectra, First-row Transition Metals, Oxo-iron Complexes, Hexaaqua Complexes, Energy Decomposition Analysis, Ligand-field theory

Area of science: Chemistry

Sub-area of science: Inorganic chemistry

UDC number:

Примена метода заснованих на Теорији Функционала Густине, за проучавање електронских стања аква- и оксо- комплекса прве серије прелазних метала

РЕЗИМЕ

У оквиру ове докторске тезе проучавана је компликована електронска структура аква- и оксо- комплекса прве серије прелазних метала. Теоријским методама, заснованим на *DFT*, израчунате су енергије основних и побуђених електронских стања комплекса прелазних метала. Испитано је понашање различитих *DFA* у циљу проналажења недвосмисленог начина за одређивање основног спинског стања оксо- и хидроксо- комплекса гвожђа, што је захтеван задатак, и са теоријског и са експерименталног становишта. Резултати нас усмеравају на коришћење *S12g* за оптимизацију, као и за одређивање основног спинског стања. За рачунање побуђених стања употребљене су две различите методе (*TD-DFT* и *LF-DFT*) а резултати рационализовани и упоређени са експериментално добијеним. Резултати указују на знатно боље понашање *LF-DFT* методе за рачунање побуђених стања и репродукцију експерименталних спектара. У склопу ове дисертације изведено је и *EDA* изучавање серије оксо- и хидроксо- модел комплекса гвожђа. Енергија везивања разложена је на хемијски смислене доприносе. Резултати показују да је најбитнији фактор, одговоран за енергетску диференцијацију енергија побуђивања, неопходна да се метални јон из изолованог електронског стања доведе у електронско стање које поседује у комплексном једињењу. Следећи допринос по важности је орбитална стабилизација услед успостављања метал-лиганд хемијске везе.

Примарни изазов је представљало успостављање одговарајућег нивоа теорије, објашњење међусобних односа између структурних особина и металног окружења са електронском структуром, као и рационализација добијених резултата и експерименталних података. Научни садржај ове дисертације предлаже рачунарске кораке којима чине *DFT* поузданом у објашњавању, тумачењу и предвђању карактеристика и својства комплекса прве серије прелазних метала. Рационалном применом предложених методологија, имамо прилику да разјаснимо експерименталне недоумице и искористимо основна начела како бисмо разумели хемијске сложености.

Кључне речи: Теорија функционала густине, електронска структура, побуђена стања, електронска спектроскопија, УВ/ВИС спектроскопија, први ред прелазних метала, оксо-гвожђе комплекси, хексааква комплекси, Анализа енергетске декомпозиције, теорија лигандног поља

Научна област: Хемија

Ужа научна област: Неорганска хемија

УДК број:

Useful notations

ADF: Amsterdam Density Functional

AO: Atomic Orbital

AOC: Average Of Configuration

CC: Coupled Cluster

CFT: Crystal Field Theory

CI: Configuration Interaction

CT: Charge Transfer

COSMO: Conductor Like Screening Model

DF: Density Functional

DFA: Density Functional ApproximationDFT: Density Functional Theory

EDA: Energy Decomposition Analysis

GGA: Generalized Gradient Approximation

HF: Hartree-Fock

HOMO: Highest Occupied Molecular Orbital

JT: Jahn-Teller

KS: Kohn-Sham

LDA: Local Density Approximation

LF: Ligand Field

LF-DFT: Ligand Field–Density Functional Theory

LFSE: Ligand Field Stabilization Energy

LFT: Ligand Field Theory

MAE: Mean Absolute Error

MO: Molecular Orbital

PES: Potential Energy Surface

PSE: Periodic System of Elements

SCF: Self Consistent Field

SD: Slater Determinant

SE: Schrödinger Equation

SOMO: Single Occupied Molecular Orbital

STO: Slater-Type Orbitals

TD-DFT: Time Dependent–Density Functional Theory

TM: Transition Metal

VSEPR: Valence-Shell Electron-Pair Repulsion

XC: Exchange-Correlation

ZORA: Zero-Order Regular Approximation

1. Introduction

Transition metal (TM) containing molecules are for many years earning the brightest spotlight on the chemistry stage, and stay in the main focus of the scientific audience. These diverse chemical species are always ready to perform another unexpected, and until that moment, unseen act and draw our attention again and again. Many riddles surrounding TM molecules have been solved, and many of their characteristics described, while on the other hand, many questions remain floating in the air and wait for a better time to be answered. Intriguing TM history is filled with rises and falls, Eureka's and dead ends, but one thing lingers from the very beginning and represents one of the main TM characteristics. This characteristic brings color to the story of TMs, and is in fact- their own color. The beauty of TM chemistry reflects in the color spectrum which these molecules provide, and colors are in fact one of the first things I can remember when thinking about my early introduction to TM molecules. At first, this characteristic was impressive and surprising to me, but not long after that, curiosity gave birth to the first question. Where does it come from? This question was easily resolved by my mentor many years ago and marked with a smile. Most importantly, and in this case personally, the answer to that question opened a door to a brand new horizon of more complex questions, and here we are, holding in hands my thesis while starting from the very beginning.

The world of chemistry is built on simple laws and rules, yet works in mysterious ways, which can be explained with logic formalisms. Basically, valence electrons of isolated atoms combine in order to create electron pairs which chemists like to call chemical bonds. This concept can be applied to main group element compounds while keeping in mind that the number of created chemical bonds must obey the octet rule. Chemical bonding in TM compounds is one of many features that differ from the main group elements. Unlike main group element compounds, where the covalent bond between two interacting species is formed by a combination of valence electrons of both species (in which electron pair is formed), a coordinate covalent bond is formed by means of interaction in which both electrons originate from a donor (Lewis base) and are introduced to an acceptor (Lewis acid). Using this unusual fashion for the creation of chemical bonds, coordination compounds are formed and, if they contain a TM atom/ion, are called TM complexes. TM atom or ion plays the role of Lewis acid in the creation of a chemical bond, whereas the electrophilicity originates from partially filled *d*-orbitals. On the other hand, Lewis base can be a wide variety of chemical species (ions or molecules), and the only requirement is the presence of one or more electron pairs that can be contributed to the creation of a chemical bond. These nucleophilic chemical species are called ligands. Depending on the number of available electron pairs capable of bonding, as well as on molecular size and configurational flexibility, ligands can be monodentate (capable to create only one coordination bond) and polydentate (capable to create two or more coordination bonds). The number and arrangement of specific ligands in the space around central metal atom/ion, called the first coordination sphere, are the first aspect of the complexity of resulting coordination compounds and the origin of their name. The second aspect is the central metal atom, which can exist in many different ionic states. The general picture becomes even more complicated since the central metal atom/ion, in most cases, contain partially filled *d*-orbitals, thus having a broad pallet of possible spin states. Energy requirement for the excitation of one or more electrons from the ground spin state (the most stable spin state) to some of the close-lying excited states is rather small and corresponds to the wavelength of the visible light. In this regard, complex molecules are able to absorb (and at the same time emit) a portion of energy from the visible light, which our eye can detect as color. Depending on the excitation energy requirement and the discrete portion of spectra that has been absorbed- complex molecules exist in various colors. While keeping in mind that the color originates from electronic structure, microscopic changes in the structure will lead to a change of color and many other general features of a specific complex molecule.

Ground spin state, close-lying excited states, and energy requirements needed for the excitations to take place are the main focus of the present thesis. All of the mentioned characteristics are of utmost importance for the understanding of fundamentals as well as the nature and behavior of coordination complexes. Although experimental chemistry has reached the level of maturity in which it can "catch" and examine delicate properties of molecular systems, it is in many cases not capable of unambiguous determination of the ground spin state. Besides this fundamental problem, the description and investigation of excited states are even more difficult, due to the lack of stability or the lifetime of these chemical species. Powerful tools to enforce the experiment, explain obtained results or predict missing parts of the experimental puzzle are without doubt theoretical methods. Even though many different theoretical methods exist and exhibit various advantages and limitations, our research is based on Density Functional Theory (DFT)[1] and aims to examine, elucidate and shed new light on a series of first row TM complexes.

In the present thesis, we are proposing theoretical steps that should be followed in order to get the best of DFT method. Although exact in principle, many approximations must be introduced to DFT, in order for it to work properly. In this regard, various DFT flavors are investigated in order to find the best choice for accurate geometrical optimizations, since this basic molecular characteristic will greatly influence all future calculations and final results. The most popular DFT-based method for examination of excited states, time-dependent DFT (TD-DFT), is used for the simulation of electronic spectra of a series of first row TM hexaaqua complexes. Obtained results are analyzed, correlated with the experiment, and compared with the results obtained by Ligand Field DFT (LF-DFT), which is specially designed for the determination of *d-d* excitations. DFT is further utilized for the determination of the ground spin state, and close-lying excited states of a series of iron (hydr)oxo complexes. Precise determination of the ground spin state represents a challenging task for all theoretical methods, and besides all practical difficulties, in most cases has a high computational price. Since spin states were not included in the development of most Density Functional Approximations (DFAs), we are searching for the best performing DFA in a group of some "old" and well known, as well as some new DFAs, which are specially designed for this kind of problem. The main goal of our validation study is to find the best theoretical approach, within the framework of DFT, for unambiguous determination and description of the ground spin state as well as possible close-lying excited spin states. Finally, Energy Decomposition Analysis (EDA) is used to decompose the energy of various iron-oxo and iron-hydroxo systems into chemically meaningful components, in order to gain insight into the origins of chemical bonding. EDA contributions are rationalized and correlated with the spin state energetics of investigated complexes.

With all the results in hand, obtained within the framework of the present thesis, we can go further beyond classical experiment and open a door for a new point of view on general chemistry and fundamentals that lead to the complexity of coordination compounds.

2. The general part

Forthcoming chapters contain the main concepts and chemical fundamentals essential for understanding and rationalization of the work done in this thesis.

2.1 Looking at the world through the quantum mechanical prism

The laws, on which the physical world is based, have occupied the human mind since the beginning of the time. Although we are able to see, feel, and gather various information about the surrounding environment, our sensors and detection capabilities are still very limited. Besides the fact that our senses are imperfect, many factors concerning the way in which "things work" remain a mystery due to the type of strings and patterns used to create this vivid and extremely complex picture- we call the "physical world". Namely, every piece of matter- water, wood, stone, wax, gold- has its own clearly defined characteristics and properties. The human eye is unable to describe or address these diverse features by only looking. A piece of mater can be considered as small, yet it is built from much smaller building blocks of the size, which goes way beyond our sight. Even though these delicate particles are enormously small, they are by nature complex and diverse, and for this reason, represent the origin of complexity and diversity of all the matter surrounding us. Modern quantum mechanical (QM) modeling has the power to lift the barrier, which prevents us from seeing microscopic particles and gives us insight into the laws responsible for the flawless functionality of the physical world. By having QM in hand, we are able to correlate electronic structure with macroscopic properties of molecules, and in this way understand and address chemical behavior as well as many other physico-chemical characteristics.

The central dogma of QM is the wave function ψ, which is the mathematical description of a quantum state of an isolated system, and holds all accessible information about all micro(quantum)-objects. The wave function itself is a complex construction and cannot be observed, although we can attribute a physical meaning to the square of the wave function. The mathematical form $\psi^*\psi = \psi^2$ represents the probability of finding a particle (electron) within a different predefined volume element. The measure of the probability of finding an electron in a specific region is the *electron density*, ρ. From previous statements, it can be concluded that the wave function determines the electron density, thus in turn electron density defines the wave function. Although we cannot define a wave function of a certain system, we can measure the electron density by utilizing experimental techniques such as X-ray crystallography[2] and scanning tunneling microscopy[3]. On the other hand, wave functions are the solutions of the famous *Schrödinger equation* (SE), which can describe the complete dynamics of microparticles, at least in theory. The main importance of this theoretical concept lies within the fact that it can be applicable to any system in hand, such as atoms, molecules, and materials. The non-relativistic time-independent SE takes the form

$$\hat{H}\psi = E\psi$$

Equation 2.1

where $\hat{H}$ represents the *Hamiltonian*. Hamiltonian is the *operator* of the energy and contains mathematical forms and rules that should be "performed" on the wave function in order to get the

energy of the system. Since the classic physics declares the total energy of a certain system as the sum of potential and kinetic energy, a Hamiltonian must incorporate both of these components, thus it can be written in extended form as $\hat{H} = \hat{T} + \hat{V}$. E is the energy of the system, and within the time-independent framework of SE, it is represented as an eigenvalue of the Hamiltonian, with the wave function being the corresponding eigenfunction (eigenvector).[4, 5] Although the Hamiltonian can be constructed for any system at hand, SE cannot be exactly solved except for very few simple cases.[4] Due to its nature, SE does not have a single solution, and there will be a different solution for every distribution of microparticles, which will result with different values for the energy. The energy of every possible SE solution will be quantized by discrete values. The solution with the lowest energy is known as the ground state wave function, or the *ground state*, whereas all other solutions are called the *excited states*.

2.1.1 In search for the best possible "solution"

Within the time-independent framework of SE, the energy of the system is represented as an eigenvalue of the Hamiltonian, with the wave function being the corresponding eigenfunction (eigenvector).[4, 5] Although the Hamiltonian can be constructed for any system at hand, SE cannot be exactly solved except for very few simple cases.[4] The most famous analytically solvable system is the hydrogen atom (^{1}H), containing only one proton and one electron, whereas the solutions of the SE and obtained wave functions represent the atomic orbitals (AOs)[6]. When we try to make a first step forward in the direction of more complicated cases, we will immediately hit a wall by reaching the atom of helium (^{2}He), containing two protons and two electrons. The initial difficulty, when trying to solve SE for a particular system with more than one electron, arises from well known "three-body problem".[7] Namely, the motion of three particles (three-point masses) under the influence of an interaction potential has no analytical solutions even in the classical mechanics. Luckily for us, we can simplify this problematic case by breaking this multi-electron problem into two one-electron problems, which we can solve. In other words, the Hamiltonian will represent the sum of two *hydrogen-like Hamiltonians* $\hat{H}_0 = \hat{h}_1 + \hat{h}_2$. The total two-electron wave function will be described as the product of two electrons in two orbitals (ψ_1 and ψ_2), thus the energy of such a system will be a sum of two one-electron energies. Although it can seem that we found an elegant way to avoid all complications, in this process we have neglect one important component of our multi-electron Hamiltonian. By breaking the initial Hamiltonian into two hidrohen-like Hamiltonians, we did not take into account the electron-electron interaction whereby the more accurate form will have the form $\hat{H} = \hat{H}_0 + \hat{H}_{ee}$. The electronic repulsion, as well as some other important effects, need to be taken into account in order to describe the system as realistic as possible, and this topic will be discussed in forthcoming chapters. Another factor which was putt aside by transforming our initial Hamiltonian into a so-called electronic Hamiltonian is the presence of the nucleus. The effect of this problem (as well as some other) is diminished by the introduction of various approximations to the theoretical concept. The *Born-Oppenheimer approximation* is one of the most important and most famous ones and represents a good example of how a complex problem can be significantly simplified using only scientific intuition and experience[8]. This approximation takes advantage of the significant differences between the masses of nuclei and electrons. Since even the lightest of all nuclei, the hydrogen atom, weights roughly 1800 times more than an electron, we can say that the nuclei move much slower than the electrons.[1, 8] The practical benefit of this, at first sight, simple approximation, is that we can consider the electrons as moving in the field of fixed (extremely slow) nuclei. Since there are many more approximations that need to be taken into account and introduced to the initial equation, we can conclude that the ultimate goal of almost all quantum chemical approaches is to provide the most accurate possible (approximate) solution to the time-independent, non-relativistic SE.

2.1.2 Building the core of everything (structure of the periodic system of elements)

The present form of the periodic system of elements (PSE) (*Figure 2.1.*) is based on the atomic number of each element, which further defines the electronic structure and the corresponding number of electrons. As the atomic number of an element increase, the number of electrons around the nuclei increases likewise. Electrons are organized and around the nucleus in *energy levels* called *shells*. Shells are defined by quantum[6, 9] number *n*, and contain a specific number of *subshells*, which are defined by quantum numbers *n* and *l*. These subshells are constructed of AOs, and since a maximum number of electrons populating an AO is two, a defined number of electrons can be placed in one shell. In order to understand the structure of an atomic shell, we need to start from the simplest conceptual element, and although it was already mentioned before, we need to describe an AO in more detail. An AO is a one-electron coordinate function. Since electrons move extremely fast, the precise location of an electron at a specific moment cannot be determined, yet we can use this function (solve the SE) to calculate the probability of finding any electron at a particular point. Obtained movement pattern, which resembles the most probable region for finding the specific electron, is called an AO. The function itself consists of the so-called radial part, which is a function of electron distance from the nucleus (*r*), and the second component, known as the angular part, which is a function of the angles θ and ϕ, and introduces the directional properties (and shape) of the orbital. Atomic shells are consecutively filled with electrons by the increase of quantum number *n*. While the subshells and shells are being gradually filled with electrons, at every point it is possible to distinguish between two different regions. The first region is constructed of completely filled shells and contains paired electrons which are strongly attracted to the nucleus. These electrons, called the *core electrons*, create a shield of electron density around the nucleus. The second region is the one containing partially filled shells, and electrons populating this region are named the *valence electrons*. Due to the greater distance from the nucleus, as well as due to the shielding effect of core electrons, valence electrons can be easily influenced by the surroundings. The number and arrangement of valence electrons, together with their properties, are the foundation of richness and diversity that chemistry has to offer.

According to the population scheme, valence electrons can predominantly occupy the same type of AOs, and in this regard, defined blocks within the PSE can be observed. The left side of PSE contains metals that belong to the *s*-block, and on the right side, non-metals and metalloids are present, belonging to the *p*-block. Members of different blocks strongly differ in physico-chemical properties and general behavior. In the middle of PSE, acting as a bridge between the first two blocks, there is a well-defined *d*-block. Elements located in this block are called transition elements, and their main characteristic is the presence of partially filled *d*-orbitals. TM elements show many unusual properties (if compared to the main-group elements), which can be addressed to valence *d*-orbitals. Another important consequence of having partially filled *d*-orbitals is that TMs exhibit a much broader pallet of stable ions. In this regard, a much greater variety of chemical compounds can be formed in the case of TMs than the main-group elements. The most well-known transition element is for sure iron (Fe), and we can, without a doubt, say that up to now, we live in the "Iron Age", due to versatile application of this metal in every aspect of our lives.

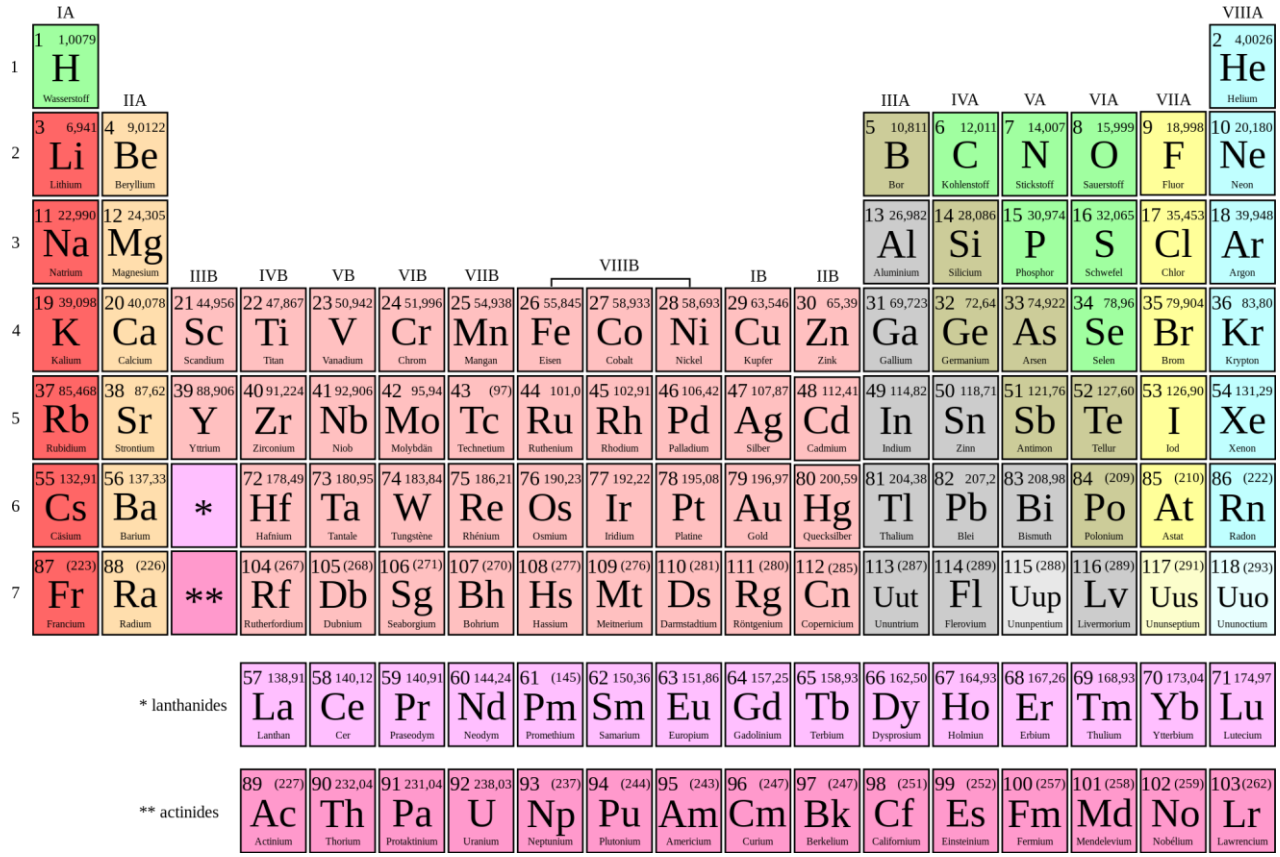

Figure 2.1. The present form of the periodic system of elements

(File URL: https://upload.wikimedia.org/wikipedia/commons/7/7a/Periodensystem_Z_A_Name_Deutsch.svg)

2.2 Electronic structure (states and configurations)

Since we scratched the surface of population patterns, before we continue we need to familiarize ourselves with few important concepts related to this phenomenon. The concept of electronic configuration holds information about the distribution of electrons in atomic orbitals. Construction of electronic configurations has its foundations in *Aufbau principle*[6, 10], whereby the orbitals are ordered by the increase in energy and populated with electrons in a "one by one" fashion, while respecting the *Pauli exclusion principle*[11]. While obeying the Pauli exclusion principle, the total wave function must be antisymmetric with respect to the interchange of any pair of electrons. In this regard, a pair of electrons can populate the same orbital using the *orbital approximation*, by which a many-electron system is described as a product of many one-electron functions, only if they are paired in opposite spin. In order to clarify this statement, let us go back to our well-known examples, hydrogen and helium. Hydrogen is described as $1s^1$ and helium as $1s^2$ ground state configuration. In both cases, the situation is clear, whereby we have one electron populating the 1*s* orbital of hydrogen, and two electrons populating the same 1*s* orbital of helium. In the case of helium, both electrons are described by the same 1*s* function, thus we can consider the orbital part of the total function as symmetric. In order for the total function to be antisymmetric, the spin part of the function must be antisymmetric. This requirement can be established only if two electrons of helium populate the same orbital with *antiparallel spin*, whereas the first is considered as α ($+\frac{1}{2}$), and the other as β ($-\frac{1}{2}$). Electron density of these antiparallel electrons can be referred to as the *spin orbitals*, whereas two electrons with the same spin orbital would correspond to a wave function that is zero everywhere. If we assign our two

electrons with, let's say, 1 and 2, we can write down an expression which will satisfie the antisymmetrization requirements and have the form:

$$\frac{1}{\sqrt{2}} = \begin{vmatrix} 1s(1)\alpha(1) & 1s(2)\alpha(2) \\ 1s(1)\beta(1) & 1s(2)\beta(2) \end{vmatrix} = \frac{1}{\sqrt{2}}\left(1s(1)\alpha(1)1s(2)\beta(2) - 1s(2)\alpha(2)1s(2)\beta(2)\right)$$
$$= 1s(1)1s(2)$$

Equation 2.2

Such an expression, able to describe a multi-electronic wave function, while obeying the Pauli exclusion principle is called a *Slater Determinant* (SD). Although for a closed-shell configuration, the total wave function can be defined with a single SD, for open-shell systems this is commonly not the case. Namely, when we go further from the nucleus, subshells will contain more than one orbital. Unoccupied orbitals within a subshell in the absence of an external perturbation will be equal in energy. This phenomenon is called *degeneracy*, and these orbitals degenerate orbitals. Due to the degeneracy, present within the subshells, there will be cases in which more than one orbital is available for occupation. Due to the *Hund's rule*[6] of maximum multiplicity, electrons will intend to be separated, which means that a specific electron will prefer to occupy a separate orbital before entering an already occupied one. In cases like this one, electronic configuration is not able to give information about precise electron arrangement, and all possible occupations within a subshell (*microstates*) are expressed as SDs. In the case of two electrons occupying three *p* orbitals, there are 15 possible arrangements, thus an *electronic state*, from which the lowest in energy represents the *ground electronic state*, is defined (approximated) by the electron configuration of the system. In order to exemplify this situation, we will consider two electrons that can be placed in two degenerate orbitals. As can be seen from *Figure 2.2.*, there are 6 possible ways to organize these two electrons, thus 6 possible SDs which satisfy the antisymmetrization principle.

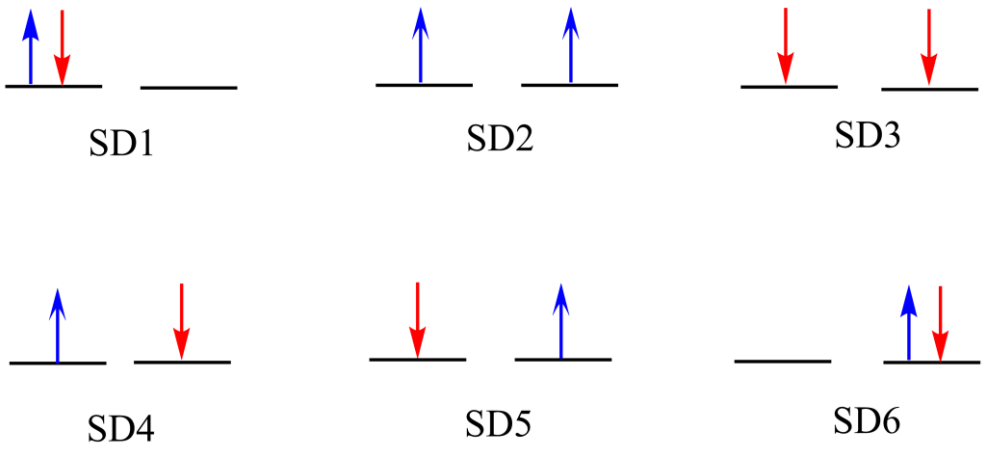

Figure 2.2. Six possible arrangements (SDs) of two electrons in two orbitals

According to the orbital approximation, in the absence of electron-electron repulsion, SD1 and SD6 would be degenerate in energy, as well as SD2, SD3, SD4, and SD5. Electron repulsion, which will differentiate our microstates in energy, will depend on two contributions *J* and *K*. The first contribution represents the *Coulombic repulsion* and thus will be positive. This contribution will contain the repulsive effect $J_{\uparrow\downarrow}$, $J_{\uparrow\uparrow}$ and $J_{\downarrow\downarrow}$, corresponding to each pair of electrons, and will increase

the energy of every single SD depending on the sum of one-electron energies. The second contribution represents the exchange factor containing $K_{\uparrow\uparrow}$ and $K_{\downarrow\downarrow}$, which occurs between two electrons of the same spin. Like the previous contribution, the effect will be positive but will favourize microstates with parallel spin (electrons in different orbitals).[9, 12-14]

2.2.1 Atomic terms (a practical main/ transition group example)

Although quantum numbers *n*, *l*, *ml*, and *ms* were enough to provide the numerical foundation for the solution of SE for one-electron hydrogen atom, this is not the case in many-electron atoms. As we have seen from the previous chapter, for a specific electronic configuration, there are various possible electronic states. All of these states can be sorted together by means of energy equivalency, whereby the formed groups are called the *atomic terms*. In many-electron atoms, the energy of an orbital, and thus of the whole system, will depend on *total spin angular momentum* and *total orbital angular momentum*, which can be determined as a (vectorial) sum of orbital and spin momenta of individual electrons ($L = \sum_i l_i$ and $S = \sum_i s_i$ respectively). These two quantities are essential for the assignation of atomic terms to electronic states. Analogously to *L* and *S*, M_L and M_S numbers can be obtained, and with the aim to exemplify, we will take into consideration the first excited state of He, heaving the electronic configuration $1s^1 2s^1$. Since *s*-orbitals have no angular momentum, in this case, we have the L = 0, and the only factor left to be considered is the spin. All possibilities (SDs) to accommodate two single electrons in two different *s*-orbitals, and resulting M_S values are shown in *Scheme 2.1*.

$$\uparrow \text{ and } \uparrow \quad M_S = \sum_i m_{s,i} = +\frac{1}{2} + \frac{1}{2} = 1$$

$$\uparrow \text{ and } \downarrow \quad M_S = \sum_i m_{s,i} = +\frac{1}{2} - \frac{1}{2} = 0$$

$$\downarrow \text{ and } \uparrow \quad M_S = \sum_i m_{s,i} = -\frac{1}{2} + \frac{1}{2} = 0$$

$$\downarrow \text{ and } \downarrow \quad M_S = \sum_i m_{s,i} = -\frac{1}{2} - \frac{1}{2} = -1$$

Scheme 2.1. Four possibilities (SDs) to accommodate two single electrons in two different s-orbitals

For the value of *S=1*, there are three microstates corresponding to the three values of M_S (1, 0, -1). After the first group of three microstates is defined and can be called a *triplet*, there is an additional state with M_S = 0 that can be attributed only to the *S* = 0 value. Since it contains only one microstate, this group can be called a *singlet*. In this regard, an atomic term can be defined as a group of microstates with same *L* and *S* values, but different M_L and M_S. The spin multiplicity is defined as 2*S*+1. Finally, atomic terms are labeled as $^{2S+1}$L. *Table 2.1.* contains the list of atomic term symbols associated with the value of *L*.

Table 2.1. Labeling of atomic terms according to the value of *L*

Value of *L*	Letter (symbol)
0	S
1	P
2	D
3	F
4	G
5	H
6	I

A list of atomic terms for s^n, p^n, and d^n electronic configurations can be found in the *Table 2.2.*, whereas the ground term represents the one with the highest multiplicity, due to the Hund's rule. One important concept that can be observed from the *Table 2.2.* is that the configurations with *N* electrons correspond to the configurations with N "holes" (empty positions within a subshell) and is known as the *hole formalism*. According to this concept, configurations p^1 and p^5, d^1 and d^9, d^2 and d^8, and so on, will be characterized with the same electronic terms.

Table 2.2. Atomic terms for s^n, p^n, and d^n electronic configurations

Electronic configuration	Number of microstates	Electronic terms
s^1	2	^{2}S
$s^2(p^6,d^{10})$	1	^{1}S
$p^1(p^5)$	6	^{2}P
$p^2(p^4)$	15	^{3}P, ^{1}D, ^{1}S
p^3	20	^{4}S, ^{2}D, ^{2}P
$d^1(d^9)$	10	^{2}D
$d^2(d^8)$	45	^{3}F, ^{3}P, ^{1}G, ^{1}D, ^{1}S
$d^3(d^7)$	120	^{4}F, ^{4}P, ^{2}H, ^{2}G, ^{2}F, ^{2}D, ^{2}D, ^{2}P
$d^4(d^6)$	210	^{5}D, ^{3}H, ^{3}G, ^{3}F, ^{3}F, ^{3}D, ^{3}P, ^{3}P, ^{1}I, ^{1}G, ^{1}G, ^{1}F, ^{1}D, ^{1}D, ^{1}S, ^{1}S
d^5	252	^{6}S, ^{4}G, ^{4}F, ^{4}D, ^{4}P, ^{2}I, ^{2}H, ^{2}G, ^{2}G, ^{2}F, ^{2}F, ^{2}D, ^{2}D, ^{2}D, ^{2}P, ^{2}S,

In order to understand the importance of atomic terms, we will discuss a practical example of two different atoms, from which the first is a main-group and second a TM element. Experimentally obtained data[15] for the ground and corresponding low-lying energy levels of carbon (C) and titanium (Ti) atom are presented in *Figure 2.3.* Besides the energy separation, every excited state is assigned with corresponding term symbol.

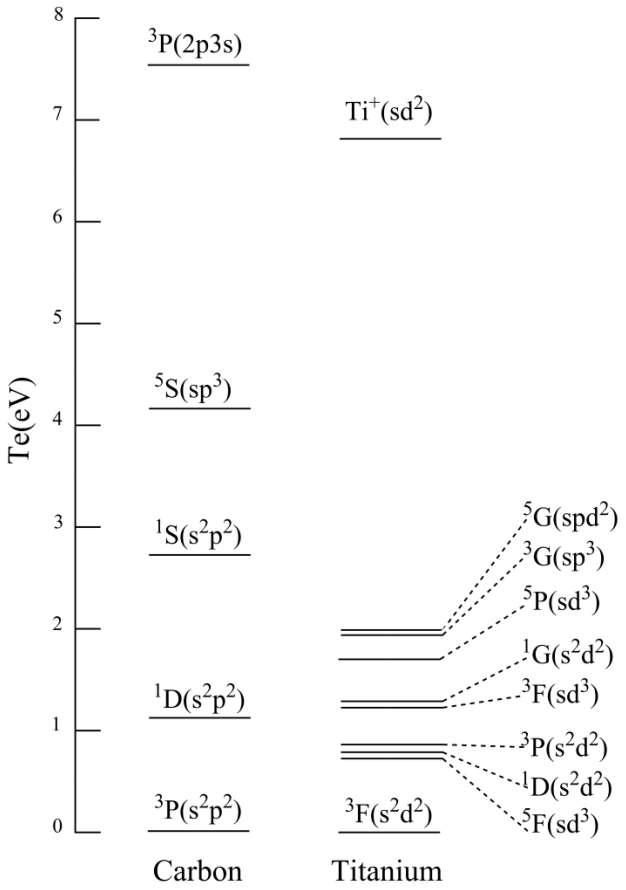

Figure 2.3. Energy separation of close-lying states, relative to the ground state, for carbon as main-group and titanium as TM group representant

The first two states of a main-group element, in our example carbon, originate from the same $1s^2 2s^2 2p^2$ configuration and show an energy separation of 1.26 and 2.69 eV, respectively, relative to the ground state. The next energy level, which is located at 4.18 eV above the ground state, corresponds to the $2s^1 2p^3$ configuration. Energetically lowest excitation state, in which an electron is excited to an unoccupied ground state orbital, is the state with configuration $2p^1 3s^1$ located at 7.5 eV. The general picture changes drastically in the case of titanium since the first excited state originates from the configuration $3d^3 4s^1$, which is different from the ground state $3d^2 4s^2$ configuration. Furthermore, the third excited state is only 1.96 eV above the ground state, whereas this energy difference for carbon atom counts 4.18 eV. The most important conclusion that can be drawn from this example is that unlike carbon, which has only four excited states within ionization energy of 7.5 eV, titanium shows a large number of close-lying excited states within the range of 6.83 eV. In this regard, we also need to remember that if we move forward from titanium deeper in the TM row the number of valence electron increases as well as the number of close-lying excited states. Our whole discussion can be summarized into one conclusion, based on which, we can expect that the absorption spectra (resulting from electron excitations) will be sufficiently different for main-group and TM

group elements. Such a broad number of TM close-lying excited states located within a limited energy domain can yield a complex spectrum that will require theoretical assistance in analysis, interpretation, and finally prediction.

Experimentally observed transitions occur between atomic terms, thus their main importance lies in such a close relation with experimentally obtained absorption spectra. As it was already described in previous chapters, the energy of a specific state is described as the sum of total orbital energy and interelectronic repulsion energy. Since orbital energy is uniform for all states originating from the same configuration, we can attribute the energy differences to the Coulumb and exchange contributions *J* and *K*. Calculation of these contributions is possible but represents a complicated and difficult task, and for this reason states energy levels are extracted from atomic spectra and further described and quantified by means of *Racah's* parameters *B* and *C*.[16] Possibility of describing all states with only two parameters lies upon the fact that atoms (and ions) exist in the highest, spherical symmetry, and although *B* and *C* posses no physical meaning, they are mathematically[16] correlated with *J* and *K*.

2.3 First-row transition metals

Since the majority of scientific results, which are going to be presented in this thesis, are devoted to chemical species which contain atoms/ions from the first-row of TM series, we should first bring to the forefront some basic information about these specific metals. First-row transition atoms and their chemical compounds are essential components of various biological and industrial processes. They are extensively employed in engineering[17] of nano-materials[18, 19], as well as remarkably potent catalyst[20-22]. Due to their great importance in various areas of life and research, they have become the main topic of the present thesis, and information about their various applications can be found elsewhere.[23-26]

As it was already stated, elements located in the first transition row are the ones with a partially filled *d*-valence subshell. The number of valence electrons varies from one to nine, depending on the metal, and is gradually increasing, starting from scandium (Sc) and going to copper (Cu). Although copper d-subshell is considered as completely filed, this metal is included in the group of TMs with partially filled *d*-subshell, due to its specific ionic form. Namely, from initial atomic configuration [Ar]3d^{10}4s^1 arises configuration in which copper is commonly found, in ionic state +2, which is [Ar]3$d^9$4s^0. Zinc is generally not considered as a TM since in both states, atomic and ionic, d-subshell stays intact and completely filled with ten electrons. Consequentially, this metal doesn't have any color, when found in chemical compounds, nor does it show paramagnetism, which is characteristic for all other elements of this row, for at least one ionic form. Another unusual example, although considered as a first row TM element, is scandium (Sc). According to experimental techniques, we know for sure that under "standard" conditions, this metal exists only in its +3 oxidation state, thus it is colorless and diamagnetic. Surpassingly, chemical behavior of Sc can be rather attributed to chemistry of aluminum (Al), than to the elements of the first transition row. The electronic configuration of all metals, located in the first transition row, can be observed from *Table 2.3.*

Table 2.3. Electronic configuration of first-row transition elements

Element	Configuration
Sc	[Ar]3$d^1$4s^2
Ti	[Ar]3$d^2$4s^2
V	[Ar]3$d^3$4s^2
Cr	[Ar]3$d^5$4s^1
Mn	[Ar]3$d^5$4s^2
Fe	[Ar]3$d^6$4s^2
Co	[Ar]3$d^7$4s^2
Ni	[Ar]3$d^8$4s^2
Cu	[Ar]3d^{10}4s^1

As it can be seen from the table, 4*s* are outlined as the frontier orbitals, even though these orbitals should be populated first, according to the Aufbau principle[6, 10], and thus be placed before 3*d* orbitals. Namely, 4*s* and 3*d* orbitals are considered as energetically similar, and as such, there can emerge many difficulties when trying to specify their exact ordering. Experimental observations have proved that TM lose electrons from 4*s* orbitals first, during an ionization process. This unusual behavior has rather complex origins, and some resources address it to the formation of the cation, whereas the 3*d* orbitals "feel" the effective potential of the nucleus stronger than the 4*s*. Other attribute this phenomenon to the stronger "diffuse character" of electrons located in 3*d* orbitals, as well as to the symmetry, whereas unlike spherically symmetric 4*s* orbital, 3*d* orbitals can cope better with the changes in the surroundings (presence of the ligands). This complicated topic exceeds the framework of the present thesis, and further information can be found elsewhere.[13, 27, 28] Nevertheless, the most important information for the understanding of TM complexes, as well as the results presented in this thesis, it that valence electrons in TM ions populate d shells, and are responsible for the chemical behavior of these molecular species.

2.4 Chemical bonding in chemistry

In the very beginning, chemists empirically determined that the chemical elements combine in a defined way and fixed ratio, in order to give chemical compounds. The force, holding these fragments together, was named the chemical bond. One of the most important conclusions at that time, originating from previous observations, was the fact that atoms of a specific element can form a defined number of chemical bonds. The maximum number of bonds formed by an element was later called the valence of that element. The first model, developed with the intention to describe chemical bonding, was the shell model. In this model, electrons are placed in spherical layers (shells) organized around the nucleus. Since at that time no noble gas compounds were known, noble gases were taken as the "stable reference". Any element could be characterized as a noble gas (with the lower atomic number) plus specific number of additional electrons in the outer shell. This outer shell was then

called the valence shell since the electrons populating this layer were responsible for the valence of a specific element, and most importantly, involved in the bond formation. Shell model was soon supported by experimental determination of free atoms ionization energies and opened a door for two different models for the description of chemical bonding.

The first one was the *ionic bond model*.[29, 30] Facts that salts, such as sodium chloride, act as insulators in solid-state, yet behave as conductors if dissolved in water, led scientists to conclude that solvated atoms exist in an ionic form. Later on, sodium has been identified as a cation and chlride on the other hand as an anion. The ionic bond model proposed an attractive interaction between oppositely charged spheres, whereby ions in solid-state organize in an arrangement which tends to minimize this charge. This phenomenon was explained by the fact that both chemical species in the ionic form have the same stable electron arrangement as a corresponding noble gas.

The ionic bond model was unable to explain the formation of a chemical bond between homonuclear molecules such as chlorine molecule. Lewis proposed a theory which could be the key to understanding such examples. Namely, Lewis noticed that most chemical compounds possess an even number of electrons, and thus assumed that the electrons could be organized in pairs. According to this model, two atoms of chlorine are held together by an electron pair. Both atoms contribute one electron in order to form an electron pair, and in this way, each atom achieves the noble gas configuration. The proposed model was named the *covalent bond model*[30, 31], whereby electron pair-like organization found its application in organic chemistry, and diagrams constructed in this way were named Lewis diagrams/structures[30].

Even though interatomic interactions and resulting chemical bonding represent the essence of chemistry in general, understanding of the nature and origin of the chemical bonds, as well as scientific novelties and general progress in this field, are in past few decades putt aside. On the other hand, fast expansion and formulation of new, advanced experimental techniques, designed to synthesize, detect, analyze and explore new chemical compounds are more than impressive. The reason for this lies in the early days of science development when classical physics was unable to describe and explain surprisingly strong covalent interaction between neutral atoms. Later, chemists invented simple models able to present this fundamental phenomenon in a graphical way, which was easy enough to be understood by people working in any scientific field. Chemical industry, as a powerful source of wealth and knowledge, has shaped the way chemistry is taught and understood in education centers and faculties while enforcing experimental techniques in order to further strengthen itself, while keeping prime fundamentals on the side.

Quantum chemical methods[32] have earned significant attention in the past few decades, but the reason for this change is still based on the simplicity of application, rather than on theoretical proof. Back in 1931 Hückel[33] already showed that theoretical methods were able to describe stability and chemical properties of aromatic compounds, but his work was neglected[34] due to the complicated mathematical formulas that were applied in order to give an explanation. The use of simple graphical models and empirically designed rules were a preferable approach used by chemists of that time. This barrier and general skepticism have been overcome during the last decade due to remarkable performance and results obtained by sophisticated methods, such as DFT.

2.4.1 Chemical bonding in transition metal compounds (metal-ligand rendezvous)

If we want to talk further about bonding models, we will immediately run into significant differences in the description of chemical bonds established between main-group elements and those

of TMs containing systems[35]. As was mentioned before, both binding partners of main-group elements will contribute one electron, in order to create an electron pair, and the resulting chemical bond can be further characterized as covalent or ionic (although the pair, in this case, is mainly located on more electronegative atom, whereby the ions are formed). In the case of TM containing systems, the chemical bond is described as coordinate covalent bond (since this bond also shows ionic characteristics), and arises from the interaction of empty *d*-orbitals of TM and doubly occupied frontier orbitals of the ligand (*Figure 2.4.).*

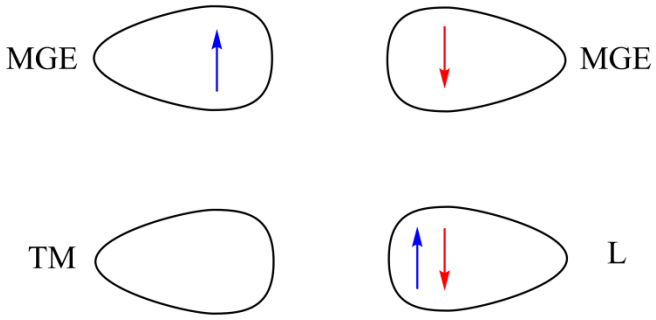

Figure 2.4. Schematic representation of bonding partners and their contribution to the formation of a covalent chemical bond (between two main-group elements (MGE) (top) and between TM and a ligand (L) (bottom))

2.4.2 Theories explaining the bonding

The first proposed bonding theory, with the intention to describe and explain the bonding properties of TM coordination compounds, was the crystal field theory (CFT)[36]. This simple theory, originally proposed by Bethe[36] and Van Vleck[37], treats coordination compounds as "ionic" (this definition must be taken with caution) molecules. Namely, central metal atom/ion is exposed to an electric field formed by the presence of surrounding ligands. Created steady "crystalline field" can be considered as analogous to what would happen if the central metal atom/ion was placed into a cavity (of the same size) inside a crystalline lattice. Although the role played by the type of ligands in this theory is rather limited, since they should provide a constant electrostatic potential, their presence have a considerable consequences on the central metal atom/ion. The symmetry and strength of a crystalline field affect the electronic levels of the gaseous metal ions, and thus the spherical symmetry is lost. The electrons belonging to the ligands are not allowed to mix with the electrons belonging to the central metal atom/ion, although they might be polarized by the presence of positively charged center. In other words, CFT considers isolated and "pure *d*-orbitals" in a field of negative point charges.

The most widely accepted model nowadays, used to describe TM compound bonding properties, is the ligand field theory (LFT)[38, 39]. Although considered as extremely simple among scientists, it represents a powerful tool for description and explanation of various physical properties of TM complexes, such as bonding energies, geometries, magnetic properties and excitation energies.[6, 40, 41] LFT represents an elegant combination of the pure CFT with the molecular-orbital theory, proposed by Mulliken[42]. In this way, the best features of both theories are merged together in order to create a superior approach for the examination of TM complexes. The main reason why LFT significantly improve CFT is because it contributes an important factor that is the chemical bond established

between the central metal atom/ion and surrounding ligands. In this way, "pure *d*-orbitals" are still taken into consideration, while placed in a field created by the ligands, but the system is additionally tuned by the existence of covalency. More practical details about the way in which LFT resolves problems arising from CFT can be found in the *Chapter 2.5.*

.

Even by having these useful models in hands, the description of TM-main group elements chemical bond is far from trivial. Many unclarified phenomena are still being hidden somewhere in the space around the metal, and well protected by the surrounding ligands. A deeper understanding of fundamentals, as well as the nature of bonding, is of utmost importance for most scientific fields, such as organometallic chemistry[43-47] or catalysis[48-50], and for this reason, different theoretical methods have been developed.

2.4.3 Formation of complex molecules (the coordination number)

So far we have discussed how the chemical bond between TM and a ligand is formed, and now we should consider how many ligands should be involved, and how should they be arranged around the TM, in order to create a coordination compound. In the very first days of coordination chemistry, it was spotted that a specific amount of TM salt requires a fixed amount of some other chemical species (later called the ligand), in order to create a complex chemical product. This was a clear indication that a certain TM requires a defined number of ligand molecules, which should be arranged in a preferred shape, thus, a defined number of coordination bonds can be established. From this observation and following experimental proofs, which were made later on, we have today the concept of coordination number.[51, 52] Coordination number defines the number of chemical (coordination) bonds that can be established between central metal atom/ion and ligating atoms/ions. The number of coordinate bonds formed in the first coordination sphere can be a good starting point for predicting the geometry of a specific complex.

Namely, ligating atoms/ions will arrange around the TM in a way in which steric and electrostatic effects (repulsion) will be the weakest. In other words, while establishing coordinate bond with the TM ligands will intend to be as far apart from each other as possible. In this regard, knowing the coordination number of a certain complex molecule will give us an opportunity to imagine and in most cases accurately predict the geometry of the first coordination sphere. Although many different geometrical entities exist, *Figure 2.5.* contains the most common molecular geometries occurring in coordination chemistry of complex compounds with different coordination number.

The basic requirement for an ion/molecule to act as a ligand is the presence of at least one lone electron pair available for donation. Although an atomic ion can establish only one coordinate bond with one metal center, a molecule on the other hand can possess more than one ligating atoms. In this regard, ligands which can offer only one electron pair for donation, and occupy only one coordination site, are called *monodentate* ligands, whereas ligands which can establish more than one coordinate bond (contain more than one ligating atom) are named *polydentate*. Nowadays, the precise determination of coordination number, as well as other structural and geometrical parameters of complex molecules, has become much easier through the use of experimental techniques, such as X-ray crystallography[2].

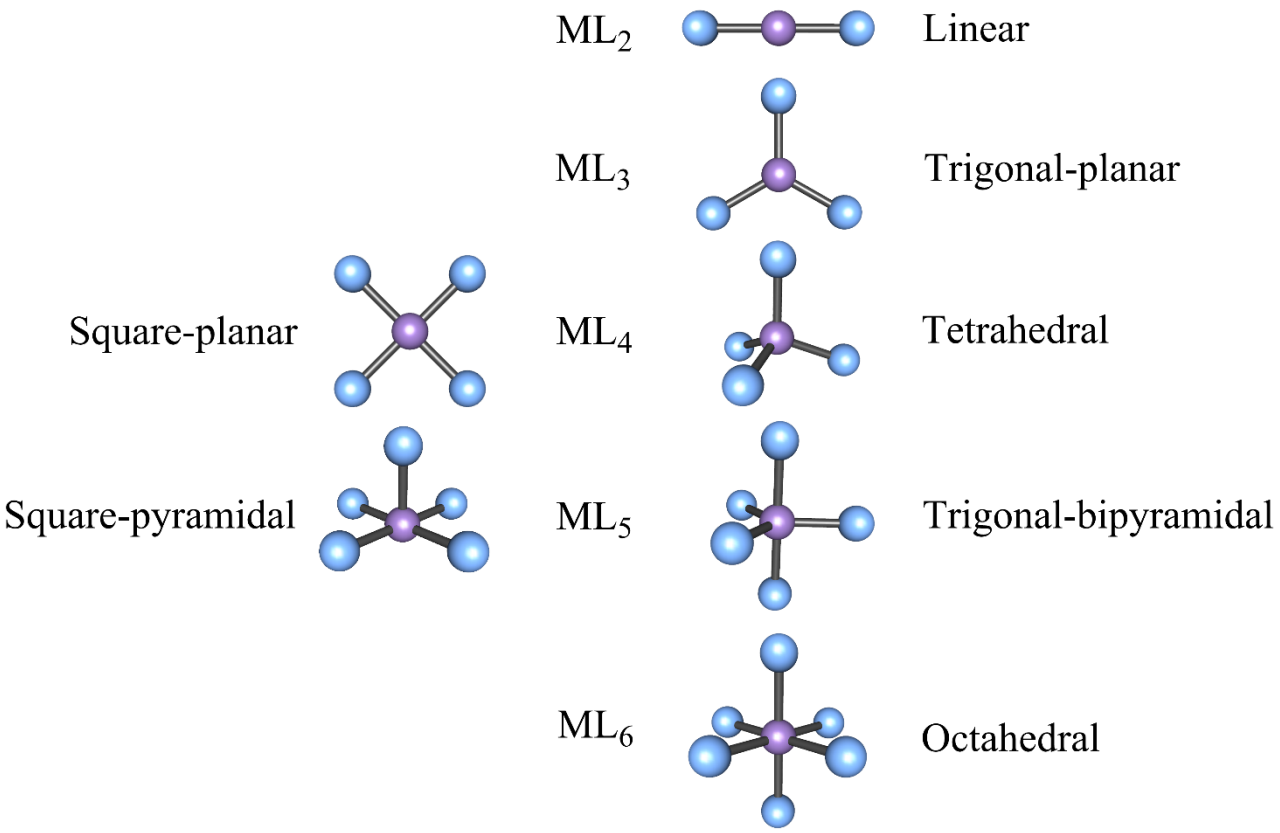

Figure 2.5. The most common geometrical entities obtained as a result of different coordination numbers

2.4.3.1 Hexaaqua TM complexes

A great number of TMs, and an even higher number of corresponding TM ions together with various molecules that can act as ligands have created a plethora of different complex molecules. This enormous amount of TM coordination compounds is being enriched every day since novel experimental techniques and tuning of experimental conditions provide a possibility to combine these small fragments in different, and until that moment unknown way. Newly synthesized complex molecules may look-alike, yet have considerably different characteristics and properties.[53-56] The first class of molecules that will be in the focus of present research is made from first-row TM hexaaqua complexes. These molecules hold great historical importance since water represents the most abundant and most affordable "universal solvent", and consequently most of the fundamental experiments have been performed in an aqueous medium. For this reason, hexaaqua coordination compounds, of general formula $[M(H_2O)_6]^{n+}$ (*Figure 2.6.*), will be in the focus of the present thesis. In our research, we will consider only six water ligands surrounding the TMs, since the first coordination sphere have the strongest impact on the electronic structure of the metal ions. Aqueous medium, in which these kinds of complexes are formed, will also create the second hydration sphere, coordinated to the first through hydrogen bonds. This phenomena has been explored both experimentally and theoretically in the past, and has no significant influence on the electronic structure of hexaaqua coordination compounds.[57-59]

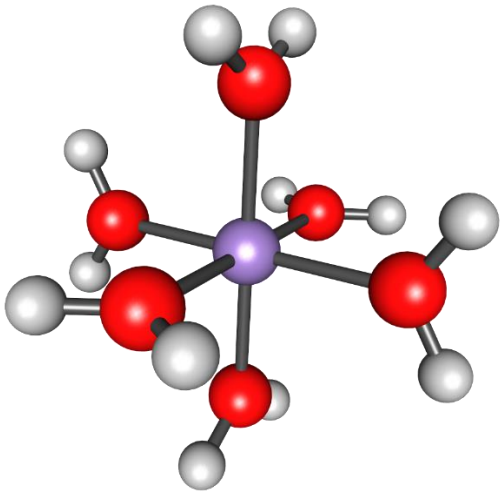

Figure 2.6. Structure of a TM hexaaqua complex of general formula $[M(H_2O)_6]^{n+}$

Another highly important aspect of complex formation in an aqueous medium is the fact that most of the reactions start with the formation of proper $[M(H_2O)_m]^{n+}$ ions[60-63], which are later transformed (due to the ligand exchange processes) into more complex ones. TM aqua complexes are useful models for investigation and elucidation of the electronic structure of metal oxide species present in photocatalytic water splitting process[64, 65] and *Fenton*[66] reactions. For all these reasons, characterization and in-depth investigation of TM hexaaqua complexes are of utmost importance for any coordination chemist. These complexes have been the subject of many scientific types of research, and much has been done in both experimental and theoretical fields. Much more should be done since nowadays we have more advanced experimental techniques able to resolve old uncertainties. On the other hand, theoretical tools, such as DFT, are powerful enough to provide us the insight into the electronic structure of these molecules and based on collected data, ensure our understanding of even more complex species.[58, 67-69]

2.4.3.2 Iron (the irreplaceable pillar)

As it was already stated, until now, we live in the "Iron Age", and Fe can be considered as one of the most important metals, for many reasons. First of all, iron, in the form of chemical compounds, is among the most abundant elements in the Earth's crust.[70] For this reason, Fe found its application in various aspects of human's daily life.[71-74] The most interesting characteristic of this metal is its behavior in the presence of an external magnetic field. Although a macroscopic piece of iron exhibits a nearly-zero overall magnetic field, the external field will magnetize the metal surface, and unpaired electrons (located in the valence shell of iron) will be utilized for reinforcement of external field.[6, 75] This phenomenon found an important application for manufacturing electric devices that are supposed to channel or transform magnetic fields.[74] This unusual effect can be "captured" with appropriate modifications of the metal, thus iron can be turned into a permanent magnet. Nanomaterial science sees iron as one of the most important metals for medical and technological applications since by rational design characteristics of this metal can be even more enriched and enhanced.[76] Second, and more sophisticated application of iron, has been established by "mother

nature" herself. An ion of this TM is located in the center of proteins, which are essential for vertebrate breathing processes and metabolism. Iron is giving these proteins the ability to transport oxygen through the bloodstream and store it in the muscles.[77, 78] Since iron can be considered as a source of life and one of the main pillars on which modern technology and industry are standing, we will pay special attention to this metal and its coordination compounds.

2.4.3.3 Iron oxo/hydroxo complexes

Iron-oxo, as well as iron-hydroxo molecular species (*Figure 2.7.*) are well known due to their great biological importance and the fact that they act as the active sites of various heme and non-heme iron enzymes, thus govern and influence reaction mechanisms.[79, 80] For this reason, they remain under constant scrutiny and consequentially various oxo and hydroxo-iron complexes were reported and well-examined.[81-98] In chemical compounds, Fe can be found in various oxidation states (from -2 to +6)[99], yet the most common ones are +2 and +3. Unlike metal salts and regular TM complexes, metal centers in hydroxo complexes are in most cases characterized by a high oxidation state[100] (such as +4), and even higher (almost exotic) oxidation states in the case of oxo complexes[98, 101, 102] (such as +5 and +6). Iron-oxo and corresponding hydroxo analogous complexes serve as extremely potent bio-organic catalysts, able to promote chemical reactions that are practically impossible to happen without their presence. Such "activation" potential can be attributed to the various possible ionic states of the central metal ion and chemical interplay between different spin states.[100, 101, 103] Since electronic structure represents the central dogma of mechanistic and energetic pathways, accurate description of this delicate property should provide us a fresh perspective, and understanding of these reactions, as well as many important processes in which they are included (for example, breathing).[104]

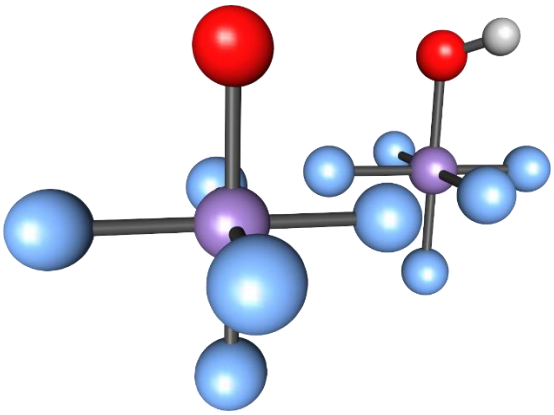

Figure 2.7. Structures of an iron-oxo and an iron-hydroxo model complex of general formula $[MO(L)_5]^{n+}$ and $[MOH(L)_5]^{n+}$

2.4.4 The concept of molecular symmetry

As it can be concluded from the *Chapter 2.4.3.*, TM complexes exist in defined geometrical shapes (with possible imperfections) depending on the coordination number and the type of the ligands. Description of geometrical aspects of complex molecules, as well as their various properties, such as spectroscopic data and magnetism, is closely related to the concept of *symmetry*[105-107]. Mathematical rationalization and systematical description of symmetry are named the *group theory*[108]. Such a complex scientific area is out of the scope of the present thesis, thus the main foundations necessary for the understanding of presented work will be covered in this chapter.

Molecular shapes and geometrical characteristics can be described in terms of the *symmetry operations* they possess. Symmetry operation (such as rotation, inversion or reflection) resembles an action performed on an object (in our case, a molecule) which permutes the object into a state which cannot be distinguished from the initial one. In other words, after the action has been carried out, the object will look the same. Molecules can be described and classified into *symmetry point groups*, which represent a combination of *symmetry elements* based on available symmetry operations. Assignation of the symmetry point group of a molecule, which requires the determination of all possible symmetry elements present in that molecule, is based on the symmetry around a point in the molecule that corresponds to the central atom or the geometric center of the molecule. In the case of TM complexes, the central metal ion is at the same time the geometric center of the molecule. Another essential information that should be kept in mind is that the examined molecule should be placed in *xyz* coordinate system in such a way that *z* axis can be considered as principal axis, and as such it should pass through the molecular center of symmetry and contain the symmetry operation of the highest order.

In order to get a clear picture, it is convenient to exemplify the concept with a practical case, thus in *Figure 2.8.* a model complex of general formula ML_5 in trigonal-bypiramidal geometry (in D_{3h} symmetry point group) is examined. The principal axis, passing through the central metal ion and two axial ligands, is characterized as C_3 axis, since the rotation by 120° will result in an indistinguishable structural arrangement. An identical structure would be obtained if a rotation by 180° is performed about any of three M-L bonds in *xy* plane, thus these three axes are characterized as C_2 axes (three C_2 elements). Combination of these specific operations declares this molecule as a member of *D* point group. Moreover, besides mentioned elements, present model system contains also three vertical planes of symmetry (each passing through one equatorial M-L bond and the principal axis), yet due to the simplicity, only one is shown in the figure (dotted square). Another plane of symmetry, containing all M-L equatorial bonds, is located in horizontal compartment passing through *x* and *y* axes (dotted triangle). When all present symmetry elements are considered together, this specific model system can be assigned as belonging to D_{3h} symmetry point group. *Table 2.4.* contains the list of point groups with corresponding symmetry elements.

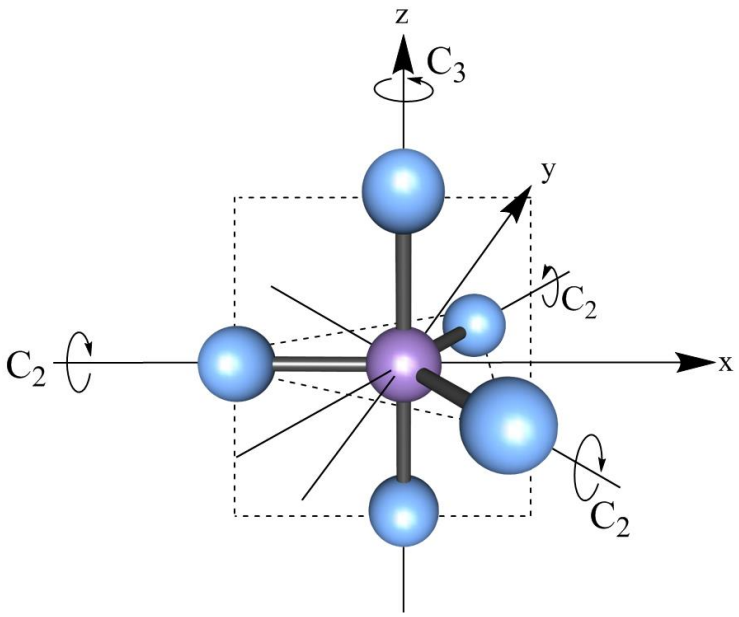

Figure 2.8. Symmetry operations for trigonal-bipyramidal model complex of general formula ML_5, in D_{3h} symmetry point group

Table 2.4. Symmetry point groups

Point group	Symmetry elements present in examined molecule
C_s	One plane of symmetry
C_i	A center of symmetry
C_n	One *n*-fold rotation axis
D_n	One *n*-fold rotation axis (about the principal axis) and *n* horizontal twofold axes
C_{nv}	One *n*-fold rotation axis (about the principal axis) and *n* vertical planes
C_{nh}	One *n*-fold rotation axis (about the principal axis) and one horizontal plane
D_{nh}	One *n*-fold rotation axis (about the principal axis, as for D_n), one horizontal plane, and n vertical planes containing the horizontal axes
D_{nd}	One n-fold rotation axis (about the principal axis, as for D_n), and vertical planes bisecting angles between the horizontal axes
S_n	Systems with alternating axes (n = 4, 6, 8)
$C_{\infty v}$, $D_{\infty h}$	Linear systems with an infinite rotation axis
T_d, O_h, O, I_h, I	Special groups: tetrahedral, octahedral, cubic and icosahedra

Energy of the molecule must be independent of the symmetry operations, thus the Hamiltonian must stay preserved in any point group. In this regard, similar to how we treat the molecules, every orbital is characterized and governed by certain point group symmetry operations. As such, orbitals form a basis for matrix representations called the irreducible representations (*irreps*). Representations are subsets of the complete point group, and they indicate the effect of the symmetry operations on different kinds of mathematical functions, such as orbitals. In other words, irreps will give us an insight how an orbital will behave if a molecule is exposed to a symmetry operation. The irreps of a point group are labeled as follows:

Table 2.5. Irreducible representations labels and corresponding characteristics

Symmetry label	Characteristics
A	Symmetric with regard to rotation about the principal axis
B	Anti-symmetric with regard to rotation about the principal axis
E	Representation is double degenerate, thus both functions must be treated as a pair and cannot be considered individually
T	Representation is triple degenerate, thus all three functions must be treated as a threesome and cannot be considered individually
g	Symmetric with respect to the inversion center
u	Anti-symmetric with respect to the inversion center

Table 2.5 contains all most important labels and their characteristics, yet for more information about irreps, as well as complete *character tables*[109] for chemically important point groups can be found elsewhere.[110]

2.4.5 Orbital Splitting (discrete layers in a nutshell)

Despite the simplicity of CFT and its successor LFT, these two models provide an extremely useful description of events that "occur" inside a TM ion surrounded by specific ligands. One important aspect, which should be highlighted here, is the fact that these methods take into account spatial and electronic symmetries that TM containing complex molecules possess. In chemical microcosms, as well as in any other layer of the world around us, symmetry will ensure stability and will be essential for many dynamical and nondynamical processes. CFT and LFT utilize symmetry properties of both metal orbitals, and ligands introduced to the metal environment. In particular, the concept of LFT describes the breaking of the degeneracy[6, 35] of metal subshell when the atom or ion is placed in any chemical environment different from the spherical.

Namely, bare TM ion in the gas phase (absence of any external field) possesses a spherical symmetry, which means that the *d*-subshell contains five *d*-orbitals of equal energy (five degenerate orbitals). However, when point charges (in our case ligands) are introduced to the system, the energy of these orbitals is lifted, and a separation in energy takes place. The way ligands are approaching the central metal ion can be defined in terms of *x*,*y* and *z* axes, thus depending on the coordination number, number of the ligands and their orientation, the symmetry of metal's environment can be determined. Since *d*-orbitals project well out to the periphery of the central metal ion, they are strongly influenced by the surrounding, and the energy of every orbital will, in turn, depend on the amount of interaction with the ligands. In other words, metal orbitals will adopt the symmetry characteristics of the environment. It is now important to realize that any possible symmetry TM complex can adopt will be lower than spherical, and in this way, the degeneracy of five *d* orbitals is shattered. Consequentially, five *d*-orbitals will no longer have the same energy and their precise occupancies (valence electron arrangement) have to be redefined. This multi-component phenomenon can be described in a step-by-step fashion, whereby on one side we have spherical symmetry of the central metal atom/ion, and on the other ligands which are approaching the metal in most symmetric way possible. The pattern of orbital differentiation and resulting orbital energies depends on the symmetry of ligand arrangement. A representative example of highly symmetric octahedral TM complex formation can be seen in *Figure 2.9.*

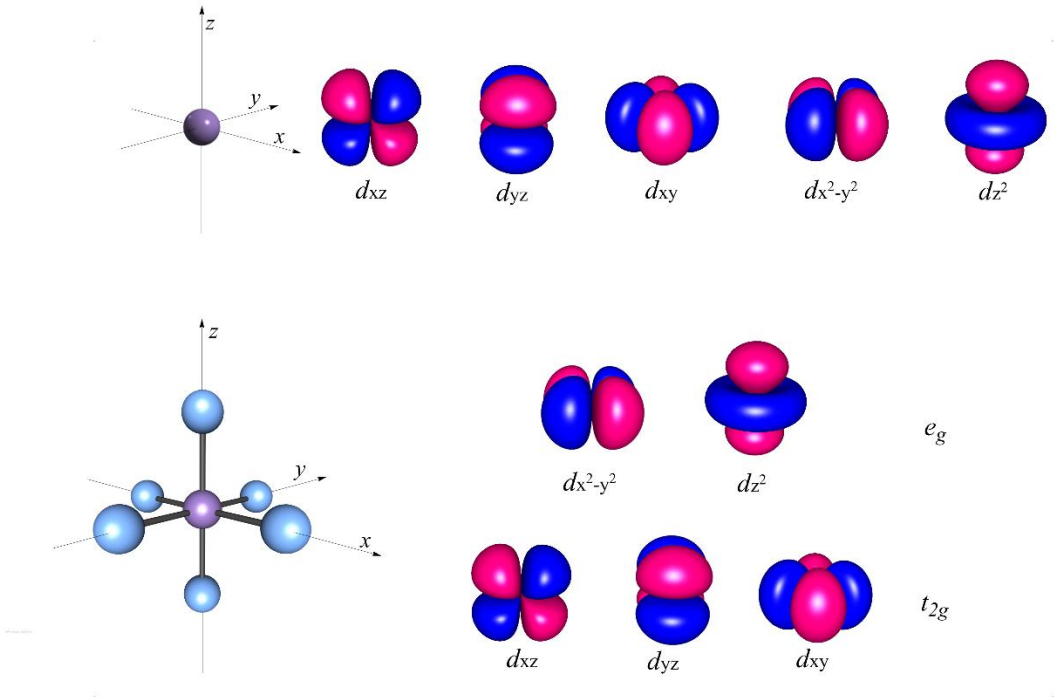

Figure 2.9. Formation of highly symmetric octahedral complex and resulting symmetry guided differentiation of *d*-orbitals

As it is shown in *Figure 2.9.*, in the first step, five d-orbitals are degenerate and energetically equivalent. In the second step, ligands have formed six coordination bonds and constructed the coordination sphere, while establishing the highest possible symmetry. As the labeling suggests, orbitals d_{xz}, d_{yz} and d_{xy} orbitals are placed between coordination axes, which make these orbitals energetically equivalent, since the amount of ligand interaction is equal for all of them. On the other hand, orbitals d_z^2 and $d_{x^2-y^2}$ pass through the coordination axes, directly towards the negatively charged ligands, which defines these two orbitals as the second set of equivalent orbitals. These two orbitals will be higher in energy, than the previous three, due to the more intense interaction with the ligands. In this way, approaching ligands are differentiating five initially degenerated *d*-orbitals into one set of triply degenerate and one set of doubly degenerate orbitals. As it can be clearly seen, the symmetry of the created coordination sphere is governing the pattern of the energetical separation (split). Triply degenerate orbitals with the symmetry label t_{2g} are lower in energy than the set of doubly degenerate orbitals with the label e_g, and the energy difference between these two sets is known as the orbital splitting Δ. This simple graphical model holds an important concept, suggesting that if the splitting is large enough available electrons will populate lower set (t_{2g}) of degenerate orbitals, but on the other hand, if the splitting is small, some of the available electrons will be able to accommodate energetically higher e_g double degenerate level (*Figure 2.10.*).

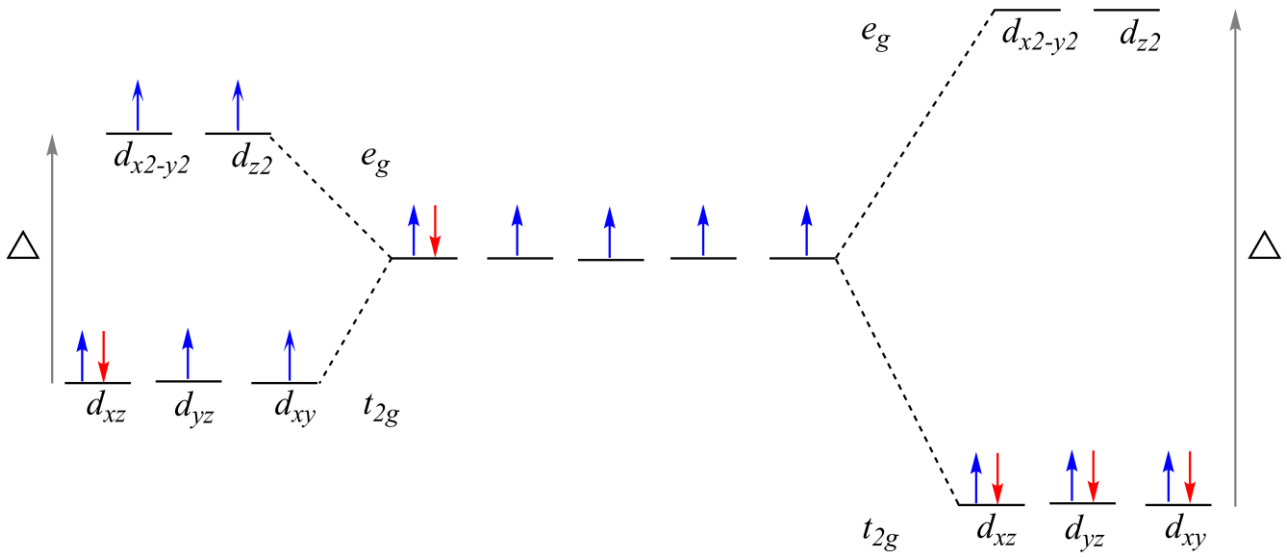

Figure 2.10. Population of *d*-orbitals in an octahedral d^6 TM complex, depending on orbital splitting Δ

The best way to obtain a precise pattern of orbital splitting, caused by the symmetry lowering, is to consult the character tables of symmetry point groups. Although different coordination geometries are attributed to different symmetry point groups, perfect geometry doesn't really exist in the world of molecules. When we describe a TM complex as octahedral, it means that the TM ion is surrounded by six ligands in the "octahedral" arrangement, thus obtained orbital sets are never completely degenerate. Nevertheless, character tables can be successfully utilized in order to sort and classify (approximate) orbitals similar in energy into defined sets like t_{2g} and e_g. According to the tables, when going from a spherical symmetric TM ion to a complex in Oh point group, *d*-orbitals are split into T_{2g} and E_g irreps. Using the tables, we are able to follow the change of specific irreps during descent in symmetry. In *Table 2.6.* the change of irreps can be observed while going from the spherical to idealized octahedral (*O*), to square-planar (D_4) and trigonal (D_3) ligand fields. As an example, we can use an octahedral complex with general formula ML_6 and assume that one ligand has dissociated, whereas five remaining ligands will rearrange and form a trigonal-bipyramidal geometry. Newly established geometry will belong to D_{3h} point group, and in turn, the splitting pattern will change. Orbitals $d_{x^2-y^2}$ and d_{xy}, as well as d_{xz} and d_{yz} will belong to two sets of degenerate *E* irreps, whereas d_{z^2} will belong assigned as A_1 irrep.

Table 2.6. Correlation table for descent in symmetry

R3	*O*	D_4	D_3
S	A_1	A_1	A_1
P	T_1	$A_2 + E$	$A_2 + E$
D	$E + T_2$	$A_1 + B_1 + B_2 + E$	$A_1 + 2E$
F	$A_2 + T_1 + T_2$	$A_2 + B_1 + B_2 + 2E$	$A_1 + 2A_2 + 2E$
G	$A_1 + E + T_1 + T_2$	$2A_1 + A_2 + B_1 + B_2 + 2E$	$2A_1 + A_2 + 3E$
H	$E + 2T_1 + T_2$	$A_1 + 2A_2 + B_1 + B_2 + 3E$	$A_1 + 2A_2 + 4E$

The convention is to label orbitals with lowercase letters and irreps, as well as states, with the uppercase symbols. The same philosophy holds for splitting of the terms upon descent in symmetry. All correlation tables can be found elsewhere.[109, 111]

2.4.5.1 Orbital splitting of Ti^{3+} octahedral aqua complex

In order to gain a feeling about the order of magnitude of orbital splitting, it is convenient to start with a practical example, and for this purpose, a hexaaqua Ti^{3+} complex will be used. This TM ion is a good example not only due to its affinity to form octahedral complexes but rather due to the simplicity of its electronic structure. Since this ion has only one electron outside the argon shell, it is the simplest example we can consider with ^2D ground term. As it was previously shown, the initial fivefold degeneracy of *d* subshell of Ti^{3+} is split by an octahedral field into two sets from which the lower is triple degenerate (T_g) and higher double degenerate (E_g). Since only one electron is present and available for an excitation, we can expect to observe only one d-d transition experimentally. Our d^1 octahedral complex experimentally indeed shows only one relatively week absorption band (*Figure 2.11.*) corresponding to $^2T_g \rightarrow {}^2E_g$ electron transition. The energy separation between two degenerate sets of orbitals for hexaaqua Ti^{3+} complex is 20,300 cm^{-1}, and although very simple, this absorption spectra holds great historical importance.[112]

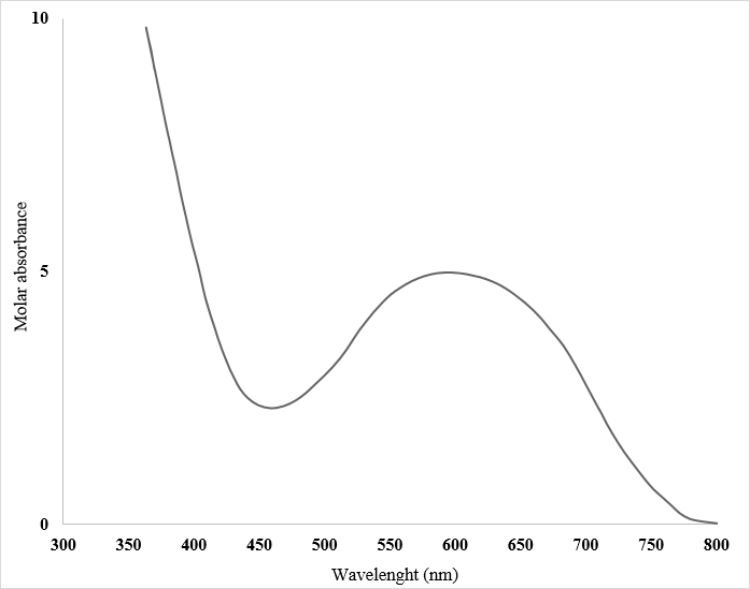

Figure 2.11. Experimentally determined electronic spectrum of $[Ti(H_2O)_6]^{3+}$ in water (spectre adopted form[113])

If it would be possible to replace all water molecules in the coordination sphere with some other ligand, the octahedral environment would be retained, and a slight change in the energy separation would be expected. By studying all known ligands in the presence of the same central metal ion we know for sure that this is not the case, thus we can expect a significant difference depending on the introduced ligand. In this regard, observations based n absorption spectra of TM complexes led to formation of a so-called *spectrochemical series*[114, 115], which sorts ligands by means of increasing ligand field strength: $I^- < Br^- < Cl^- < OH^- < F^- < H_2O <$ oxalate < pyridine < NH_3 <en $< NO_2^- < CN^-$.

Although Ti^{3+} ion has only one electron in *d*-shell, while going deeper in the TM group generated ions will have a larger number of valent electrons. Depending on the number of valence electrons and pattern of the orbital splitting, as well as on the energy separation of resulting sets of orbitals, electrons will be unpaired and distributed trough all *d*-orbitals, or paired and located in the lower-lying orbital sets.

2.5 Spin states in transition metal chemistry (the origin of versatility)

Every, but the simples one-electron system, can exist in different spin multiplicity (different spin states). The simplest example (*Figure 2.12.*) is the one in which two electrons can be pired together with opposite spin and create a singlet state, or unpaired and arranged separately with the same spin and create a triplet state. Increasing the number of electrons is expending arrangement possibilities, thus the number of spin states. Even though a certain electron system can possess numerous spin states, the general trend is to label the arrangement with a maximal number of unpaired electrons as the high spin (HS) state, and the arrangements with a maximal number of paired electrons a low spin (LS) state. Every other electron arrangement between HS and LS state is called the intermediate spin (IS) state. At this point, we have covered all basic concepts concerning the events occurring within a TM ion placed in a ligand field, and thus we can discuss how LFT is resolving the main problems arising from CFT. The answer is simple since LFT is introducing the concept of electron-electron repulsion, defined as the *pairing energy* (Π). Pairing energy is changing, starting from d^4 and going to d^7 electronic configuration in octahedral environment. In simple words, Π can be defined as the energy difference between the LS state and HS state, for a given number of *d*-electrons, divided by the number of electron pairs destroyed by the transition between these two states. Pairing energy for electronic configurations that can have close-lying spin states, can be expressed using Racah parameters *B* and *C* (defined in the *Chapter 2.2.1*) and are presented in *Scheme 2.2*.[116]

$$\Pi(d^4) = 6B + 5C$$
$$\Pi(d^5) = 7.5B + 5C$$
$$\Pi(d^6) = 2.5B + 4C$$
$$\Pi(d^7) = 4B + 4C$$

Scheme 2.2 Expression of Π for various d^n configurations, in terms of Racah's parameters *B* and *C*

Since *B* is similar for different d^n configurations, and $C \approx 4B$, any configuration at hand can be easily compared with another. It is important to keep in mind that this is just a qualitative consideration and that energy two-electron contributions for multideterminantal electronic states have to be obtained by calculating the expectation value of the two-electron operator. In this regard, LFT is combining the Π and Δ in order to determine the ground spin state.[117] Depending on the order of magnitude of these two factors, certain TM complex will be in its LS ($\Pi < \Delta$) or HS ($\Pi > \Delta$) ground state.[16]

Chemical species in different ground spin state will show considerable differences in physico-chemical properties.[118] In order to exemplify, we can take two TM complexes with the same central metal in the same ionic form, $[Fe(CN)_6]^{4-}$ and $[Fe(H_2O)_6]^{2+}$, from which the first one is yellow and diamagnetic, whereas the second one is pale-blue and paramagnetic. Although both ions have the same d^6 configuration, and the orbitals are split in the same way due to the octahedral ligand environment, the nature of surrounding ligands has a drastic impact on the final electron arrangement.

In the case of $[Fe(CN)_6]^{4-}$, strong ligand field has created a larger orbital split and resulted with pairing of all available *d*-electrons in the lower set of degenerate orbitals, thus forming a LS state. Unlike in the first case, *d*-electrons in $[Fe(H_2O)_6]^{2+}$ are distributed in all five *d* orbitals, due to the smaller energy separation between two degenerate sets, and thus result with a HS state. Besides the color of the complex, which can be easily detected by the bare eye, the ground spin state will strongly influence important characteristics such as reactivity, and for this reason, this area of research has provided a great number of experimental and theoretical investigations.[118]

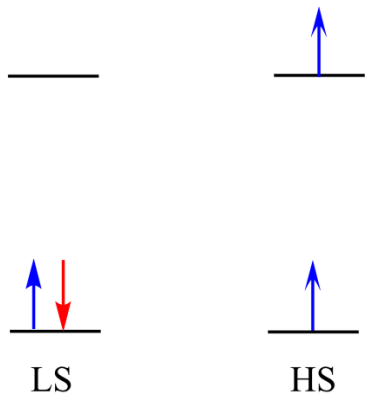

Figure 2.12. Two possible arrangements of two electrons in two orbitals, whereas LS state represents the arrangement with a maximal number of paired electrons and HS state the arrangement with a maximal number of unpaired electrons

Catalytic behavior of TMs[119-121] and their complexes[122, 123] basically originates from the fact that these elements can exist in various stable ionic forms, thus can act as mediators in redox reactions. Another important aspect is the ease with which they can reach different close-lying excited electronic states.[124-126] The possibility of reaching various energetically accessible spin states is explaining the diverse chemical behavior of TM complexes. Besides influencing the speed and reaction rate, the spin state of a reacting TM complex will, in most cases, define the reaction mechanism.[124, 127, 128] Unlike the main-group compounds, TM containing moieties are mostly found in the HS ground state, having two or more unpaired electrons located in *d*-subshell. In this regard, it is natural to presume that all chemical reactions (even the thermal ones) involving TM complexes in its HS and main-group moieties in LS should be "spin-forbidden" and most likely impossible to happen. Practically, there are numerous studies showing that these "spin-forbidden" transformations usually occur without any particular difficulties in various chemical reactions.[129, 130]

2.5.1 Electron transposition (birth of excited states)

Although we have already scratched the surface of this topic, in the scope of this chapter, we will make a short sightseeing in the world of electronic structure and its possible reshaping. For this purpose, we will utilize previously mentioned $[Fe(CN)_6]^{4-}$ complex. The ground state of the free Fe^{II} ion will be HS, since in the absence of the orbital splitting, all *d*-orbitals will stay degenerate (*Figure 2.13.*- left). After the coordination, the ion will change into LS ground state, due to the dominant effect of Δ over Π (*Figure 2.13.*- middle). Now let us introduce a perturbation (in the form of visible light, for example) to our system, and promote one electron to the higher set of degenerated *d*-orbitals

(*Figure 2.13.*- right). At this moment, we have taken the turn in the direction of excited states, and are heading to electronic arrangements of higher energy.

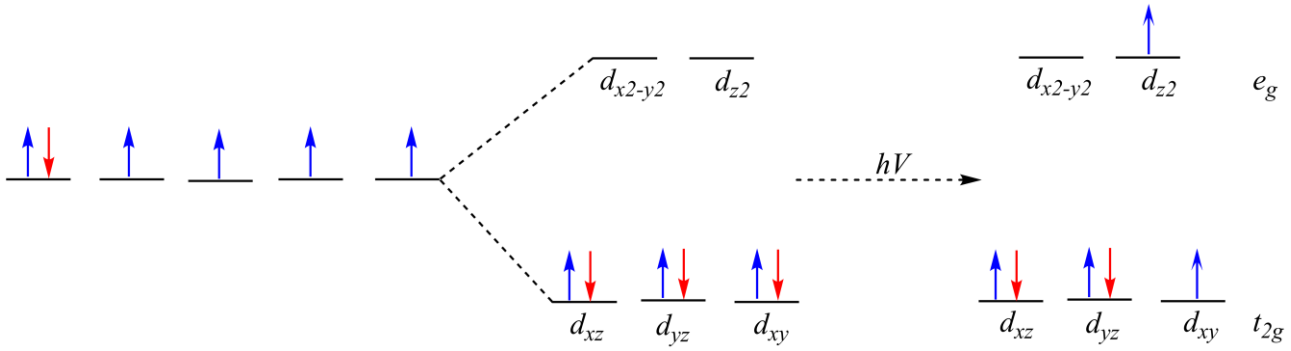

Figure 2.13. HS ground state of a free d^6 Fe^{II} ion (*left*), LS ground state of $[Fe(CN)_6]^{4-}$ (*middle*), and the first excited state of $[Fe(CN)_6]^{4-}$ coordination compound (*right*)

After this one-electron promotion is finished, we have generated a so-called excited state, and on our new path, we will have an opportunity to see many of these states (since there is a great number of possible electron arrangements) with higher energy than the ground state. Although the change we made in the electronic structure can look as delicate and negligible, in order for it to take place the molecule accumulated a portion of energy, and in this regard is completely different from the initial ground state. The excited molecule will have different electronic and vibrational spectra, thus a different reactivity and chemical behavior. The change in chemical behavior is referred to as photochemistry[131-133] because an external light source triggered it. The lifetime of an excited state is short and goes from a picosecond to a microsecond. Such a short lifetime originates from the tendency of the molecule to release an excess of energy and return to its initial stable ground spin state (keep in mind that the ground spin state for some other complexes can be HS). Nevertheless, there are many methods able to "catch" and analyze these short-living chemical species, as well as discrete partitions of energy they are realizing.

Although our tour went smoothly, it is important to point out that this path of excited states is a bumpy one. Depending on the number of *d*-electrons and the ground spin state of a complex molecule, light absorption in most cases will not initiate only one-electron excitations, nor will in result with a single excitation. Some systems will have a possibility to reach various excited states, which differ in energy, thus will be characterized by a complex photochemical response. The excited molecule relaxes and loses the excess of energy in various ways, such as radiationless relaxation (transfer of the energy to the surroundings, in the form of heat), photochemical reaction, or by back-radiation in the form of luminescence.[134] Observing these photochemical responses is the best possible way to learn about the electronic structure of molecules, as well as how a subtle change and encapsulation of a discrete portion of energy can affect and modify the chemistry of a certain chemical species.

2.5.2 d-d transitions (excitations in a nutshell)

Generally speaking, spectroscopic bands that emerge from transitions occurring in the *d*-subshell are significantly lower in intensity than, for example, those originating from charge-transfer (CT) excitations. *Selection rules*[6, 40] are defining the probability of a certain transition, and according to them, any transition between the states with the same parity (when the molecule possess the inversion center) is forbidden, which means that no *d-d* (as well as *s-s*, *p-p*, *s-d*..) transitions should be observed in the spectra of TM containing molecules. In this regard, *d-d* transitions in a highly symmetric octahedral TM complex with the same type of ligand should be forbidden, yet can be experimentally observed[135, 136]. This phenomenon can be addressed to the fact that all molecules vibrate, and these vibrations can affect and disrupt the center of symmetry which will further results with a *d-d* absorption event. In general, CT absorption bands originate from transitions allowed by the selection rules, thus are characterized by significant intensity. Another important aspect of selection rules allows only transitions between states having the same spin, and this requirement is relaxed through the introduction of the spin-orbit coupling (SOC)[137-139] mechanism.

2.5.3 Charge transfer (excitations within a region)

Another excitation class of practical interest, since they frequently occur in the experimentally measured spectrum, is the CT excitations. These excitations are defined as charge (electron) dislocation from one point in space to another and can be considered as a transfer of a discrete charge between a donor and an acceptor. The dislocation can take place between two different fragments (functional groups) within one molecule, or for example, between a metal and ligands located in the first coordination sphere. CT processes are characteristic for various kinds of chemical species and have special importance in TM chemistry since they regularly appear in the spectra of this kind of molecules.[140, 141] These excitations are characterized by broad peaks of high intensity and can in many cases mask, or cover lower intensity peaks (like, for example, *d-d* transitions), which can be of greater importance (especially in the field of TM spectroscopy). CT excitations are in most cases severely modifying the quantum mechanical state of the system, and an additional amount of energy can lead to deformations such as conformational changes of the ligands.[142] For this reason, it is important to recognize and describe the origin and location of CT phenomena, yet a model such as LFT cannot take into account CT, since it is restricted only to *d* orbitals.

2.6. Electronic spectroscopy (the insight into the electronic structure)

Spectroscopy is the technique of choice we are going to utilize in order to analyze and understand chemical systems since it is the best way to gain insight into the electronic structure. The practical importance of this experimental technique lies within the fact that electronic spectra can be measured directly in a few minutes, and the desired information can be quickly extracted from obtained data. The perturbation is initiated using ultraviolet and visible (UV/Vis) light source, which is 10 000-50 000 cm^{-1}, since most of the important excitations usually occur in this range of the spectrum. Basically, spectral properties are related to differences between the molecular ground state and the excited states, obtained by external perturbation. Due to the very complexity and varieties in the structure of different molecules, it remains very challenging to interpret the experimental spectra. Electronic spectral bands are usually very broad, thus spectroscopic data cannot be used as a molecular 'fingerprint', nor can be utilized for the determination of functional groups, as is done in

infrared spectroscopy. As we mentioned before, UV/VIS absorption spectra of TM containing systems is constructed from a broad number of close-lying excited states (metal-centered, ligand-centered, metal-to-ligand-charge-transfer and, ligand-to-ligand-charge-transfer). From such a high saturation with electronic states of different nature within a limited domain of energy, originate the differences in photophysical and photochemical properties of TM complexes- that at first glance can look quite similar. Moreover, this is the main reason for the diverse and unusual characteristics of different TM containing molecules, as well as for their versatile (sometimes even unpredictable) behavior during photochemical reactions.[84, 143-146] Interplay between various electronic states and their interaction in different points of potential energy surface (PES)[147, 148] can result in critical but well-defined changes in the overall structure. Sometimes, these changes lead to the formation of structures which can be significantly more reactive than the initial one. In this regard, the effect which we can observe during an experiment as a response of the system to external light is completely governed and defined by many concurrent sequential processes.

Hence, in order to provide a good understanding and interpretation of practical UV/VIS spectra, the assistance of theoretical methods is more than mandatory. In the beginning, a theoretical approach to excited state characteristics was mainly qualitative. Ground state electronic structure of the investigated molecular system was resolved and clarified using the molecular orbital analysis. After a successful theoretical description of ground electronic structure, the next logical step was the determination of close-lying excited states and their energy separation from the ground state. Energy differences are observed as transitions and assigned to experimentally observed bands. In time, theory has evolved and gave birth to successful electronic correlation methods. With these powerful theoretical tools, we are able to deal with multidimensional potential energy surfaces and describe the nature and reactivity of electronic excited states. Nowadays, cooperation between powerful modern computers, with impressive speed and storage capacity, and more efficient mathematical algorithms have made these extremely challenging calculations possible. However, the time required for a theoretical simulation to be finished will still depend on many factors like the chosen level of theory, size of the molecular system, density of possible excited states, number and organization of electrons populating the *d*-subshell and many others.

Depending on the level of accuracy and time required for a computation to be performed, there are various methods, based on different mathematical formalisms, suitable for the description of electronic structure and corresponding electronic spectroscopy of TM containing systems. For a long time now, DFT is considered as the best compromise between computational time and accuracy, thus forthcoming chapters will discuss DFT-based, as well as some other theoretical methods, designed for the simulation of optical spectra.

3. Theoretical and Methodological Background (the conceptual idea of physical reality)

Previous chapters introduced to us the great complexity of the chemical world and physical reality, which has its roots in the motion of microparticles. With Modern QM we can model and hopefully get close enough to the real behavior of these objects, and in turn, understand the global properties of much larger (molecular) objects. Besides the clarification and explanation of experimental results, QM insight into the electronic structure is giving us an opportunity to conduct a fine-tuning of molecular structure. In this way, scientists can rationally modify chemical and physical characteristics of interest.

The quantum mechanical methods that do not utilize any system-dependent empirical parameters are referred to as *ab initio* methods. These methods are categorized into two main divisions:[1]

1) the ones that are wrapped around the wave function as a central quantity, and
2) the ones that utilize the electron density, as a much simpler and intuitively closer starting point

In theory, both approaches should be able to calculate the same exact energy as well as to describe every observable we are interested in. Unfortunately, since the fundamental equations of quantum mechanics are not exactly solvable, except for a few simple model systems, both methodologies are practically aiming to find the best approximate approach for QM description of real-world problems and observations. Wave function-based methods are considered highly accurate and very reliable since they are in principle systematically improvable. The cost of this high accuracy is being paid through computational time requirements, which depends on the size of the system under examination. DFT methods are much faster and easier to handle, and at the same time can compete in accuracy with previously mentioned techniques. The central paradigm around which this method has successfully built itself is the idea that the energy and every experimental observable can be extracted from the electron density. This simple concept first saw the light of the day in the late 1920s, and has reached the level of maturity required to be considered as trustworthy.[1, 12, 149-151] The next chapter will cover the theoretical basis of molecular quantum mechanics. The main concepts will be discussed in the briefest way possible since there are many sources in the form of textbooks, which provide an excellent in-depth discussion of this topic.[152-157] The interested reader is encouraged to consult the literature in order to gain a more comprehensive overview of the history and the current state of the art of this vibrant and diverse field of research.

3.1. Schrödinger equation and Hartree-Fock approximation

Any problem concerning the electronic structure of matter, including time, is covered and unraveled by the SE. This famous equation, able to describe the complete dynamics of microparticles, represents the basic principle of QM. The most general form of the SE is the time-dependent non-relativistic SE:[4]

$$i\hbar\frac{\partial\psi}{\partial t}=\hat{H}\psi$$

Equation 3.1

All components of the equation are described in the first section, where we presented the reduced form of the same equation (*Equation 2.1*). The reduced form (non-relativistic time-independent SE) is commonly used one since we are practically facing problems concerning atoms

and molecules without time-dependent interaction. As it was already stated before, the "three-body" problem stands as a solid barrier between us and the real energy of a system at hand (except for a few trivial cases), since finding the solution for SE within all possible N-electron wave functions is impossible. In order to overcome this barrier, we need to simplify the initial system and transform it into a problem that can be practically solved, but more importantly, it should be a physically meaningful approximation to the exact many-electron wave function. There were many attempts to develop a suitable approximation and provide an accurate approximate solution to SE, and the most prominent one is without a doubt the Hartree-Fock (HF) approximation. Within the framework of HF the simplest, yet physically reasonable approximation to the complicated wave function is utilized. Besides being the central pillar of almost all wave function based quantum chemical methods, HF holds great conceptual importance, and most important schematic aspects will be discussed in this chapter. For a detailed outline and theoretical background of HF, as well as some other more sophisticated methods, one can consult the book written by Szabo and Ostlund.[152]

In the HF method, the complicated many-electron problem is simplified by converting it to a one-electron problem, placed in a shell created of all remaining electrons. In other words, one electron of choice is being encapsulated in the effective "field" of all other electrons (and all the nuclei), thus the electron-electron interaction is treated in an average way. The whole idea is based on a simple equation:

$$F_i\phi_i = \varepsilon_i\phi_i$$

Equation 3.2

where F_i is the so-called Fock operator, and holds information about the average potential experienced by the *i*-th electron (due to the presence of all other electrons). ϕ_i is the one-electron wave function (spin-orbital) and the ε_i is the corresponding orbital energy. The operator for the electron in orbital *i* is expressed in a form:

$$F_i = \sum_{i=1} h_i + \sum_{i=1}\sum_{j=1}\left(J_{ij} - K_{ij}\right)$$

Equation 3.3

where h_i stands for the one-electron term (holding kinetic energy and electron-nuclear attraction potential contributions) and symbols J_{ij} and K_{ij} represent the Coulumb and the Exchange matrix elements (whereas J_i and K_i represent the corresponding operators).

$$J_{ij} = \int \phi_j^*\left(r_1\right) J_i\left(r_1\right)\phi_i\left(r_1\right) d^3r_2 = \int\int \phi_j^*\left(r_1\right)\phi_i^*\left(r_2\right)\frac{1}{r_{12}}\phi_i\left(r_2\right)\phi_j\left(r_1\right) d^3r_1 d^3r_2$$

Equation 3.4

$$K_{ij} = \int \phi_j^*\left(r_1\right) K_i\left(r_1\right)\phi_j\left(r_1\right) d^3r_2 = \int\int \phi_j^*(r_1)\phi_i^*\left(r_2\right)\frac{1}{r_{12}}\phi_i\left(r_1\right)\phi_j\left(r_2\right) d^3r_1 d^3r_2$$

Equation 3.5

The first matrix element describes the classical Coulomb electron-electron repulsion, whereas the second term takes care of the fact that two electrons of the same spin cannot occupy the same region of space (*Exchange hole).*

The way to express many-electron wave function, in terms of one-electron wave functions, that satisfies the anti-symmetrization requirement is called a Slater determinant (SD). HF equations contain unknown spin orbitals, both as a solution and as an integral part of Fock operator, thus they need to be solved iteratively,and this is achived by self consisted filed (SCF) procedure , which relies on a simple mathematical idea. Namely, one can make an initial guess of spin-orbitals, and calculate the interaction of each electron with a smeared cloud of electron density originating from all other electrons. After obtaining the result for the first guess, one should solve *Equation 3.2* for a new set of spin-orbitals. Each time the chosen set is changed, a new potential field is obtained, and this process is repeated until self-consistency is reached. After wave functions, energies, and other chosen criteria differ less than a chosen threshold, the SCF procedure is finished successfully. Finished SCF procedure and the solution of HF eigenvalue problem results with a set of HF spin-orbitals. Orbitals with the lowest energy represent occupied orbitals. The SD constructed from these orbitals is the HF ground state wave function. Since there is theoretically an infinite number of HF solutions, the "real" approximate solution is achieved by introducing a set of spatial basis functions and SCF variational minimization will construct the best possible orbitals from the given basis. It is important to mention here that the application of *K* spatial functions will yield a set of 2K spin orbitals (since the general occupancy scheme, one electron per spin-orbital, combined with fermionic nature of electrons require a *K* set with α spin and a *K* set β with spin electrons). An increase in basis set functions will result in the lowering of the HF energy since there will be more flexibility in the expansion for the spin-orbitals, and this will continue till the point where the energy is not changing anymore. This point is known as the HF limit, and a further increase of basis set functions will not influence the result.

Considering the conceptual simplicity and efficiency of HF methodology, it is not unusual why it became the historical milestone of quantum chemistry. The main disadvantage, which we can consider as a serious pitfall, arises naturally at the moment when it has to describe and accurately approximate the exact particle-particle interaction. Namely, as mentioned before, our individual electrons are being surrounded with a smeared cloud of electron density originating from all other electrons, thus there is a probability for two electrons to be located within a small spatial volume (practically next to each other), and at very distant points.[152] This probability originating from the basics of HF is essentially incorrect since every electron correlates its motion relative to the motion of all other electrons in order to maximally reduce the electron-electron repulsion (*Coulomb hole*).[137] Due to the anti-symmetrization of starting wave function, required by the fermionic character of electrons, the method is prepared in advance to catch and take into account the exchange hole. On the other hand, with the lack of variational flexibility, the method is unable to "see", nor describe the Coulomb hole, leading to final energy, which is always higher than the "real" one. The absence of any correlation between the electrons of the opposite spin, as opposed to some degree of correlation for the same spin electrons, leads to the artificial stabilization of the configurations with more unpaired electrons at HF level of theory.[158]

3.1.1. Post-Hartree–Fock methods

The energy calculated by the HF method will always be higher than the "exact" one, and this well-known error, called the *correlation energy*[1], represents the main problem rooted in many-body theory. As it was discussed in the previous chapter, this technical failure originates from the incapability of the method to describe and define the correct amount of electron-electron interaction. Much progress has been made during continuous attempts to correct the error, and during this process, many sophisticated methods have been developed. These so-called post HF methods intend to take into account the electron correlation missing from the HF.[15,33,34] Electron correlation is further split into two different contributions: static correlation (originating from an inadequate single determinant

description of the ground state) and dynamical correlation (originating from the fact that electrons need to correlate their motion in order to minimize the electron-electron repulsion).[14, 137] The "exact" wave function of a many-electron system cannot be defined as a single determinant, nor a simple combination of few determinants, thus one of the most important methods, able to overcome this problem, are CI approaches, as well as Møller–Plesset perturbation theory (MP), coupled-cluster (CC) methodology, *vide infra*. CI methodologies represent a wave function as a linear combination of several SDs (electronic configurations), with variationally obtained coefficients (each SD contribution). If we would take into account all possible SDs, the method would be called a full-CI, which represents the exact solution of non-relativistic SE, within a given basis set. Unfortunately, because of the high computational cost, this calculation would require, this method is not available for most of the real-life applications. In practice, we usually have to focus our attention to some, chemically important, set of occupied and virtual orbitals and in turn create SDs within this limited "active space". Generally, this approach is able to capture most of the static correlation, but on the other hand, we need a large active space to accurately capture a significant dynamical correlation present in TM complexes. We can add a perturbational correction to the energy, and fix this problem to some extent, but the success of the correction strongly depends on the quality of the initial wave function. The perturbation approach can be utilized directly on the HF wave function (MP^n methods), but, since the initial wave function has even lower quality, and the method does not capture static correlation, it is not very useful in the case of open-shell TM systems. Finally, CC methods are the most accurate of all the abovementioned approaches but are singledeterminantal in their basic formulation (although there is multideterminantal extension of CC methodology). Besides the lack of static correlation, high computational cost is considered an additional problem, thus in order to be applicable to regular TM systems, additional approximations are required.

3.2. Density Functional Theory (a brief overview)

At this point, an introduction to DFT properties supported with a dash of raw theory will be provided, with the aim to familiarize a newcomer with the power of computational chemistry and its irreplaceable application in the field of TM coordination chemistry. I will not go into every detail hidden from the other side of the curtain, since there are many great books[1, 159-162] dealing with the theoretical background, but rather define main properties of the method responsible for its great performance on the scientific stage. A brief overview will introduce the reader to various advantages and possibilities of this methodology, as well as some well-known practical issues we are facing while working in our theoretical DFT laboratories.

The whole story started[150, 163] long ago, with two men, Llewellyn Thomas and Enrico Fermi, shortly after the introduction of the famous SE[164]. The real foundation for DFT as a (mathematically) exact theory was established by Pierre Hohenberg and Walter Kohn, who proposed a reformulation of the famous SE[165, 166].The rapid development of quantum chemistry brought scientists to realize that the wave function, which was considered as irreplaceable for a proper description of microparticle dynamics, contains much more information than they actually need. The intention was to recreate the initial equation, based on the N-electron wave function of 3N variables and reduces its complexity by developing a new equation based on electron density with only three variables.[165] Electron density is not only much simpler than the wave function but also can be determined and described experimentally. The proposed modification would give us an opportunity to step back from the search for the actual wave function of the system, and use the ground state electron density $\rho_0(\mathbf{r})$ in order to obtain the energy E_0 and all other ground state molecular properties. Suddenly this promising path which should take us to the resolution of any problem at hand, led us to a dead-end since the Hohenberg-Kohn theorem does not tell us how to extract the E_0, nor how to define and describe $\rho_0(\mathbf{r})$ without first finding the wave function. Not long after the initial idea of reformulation, an important

breakthrough was made by Kohn and Sham, who created new, simplified equations. These new equations, based on the Hohenberg-Kohn theorem, named the Kohn-Sham (KS) equations[166], have brought DFT one step further to the application to real systems and real chemical problems. Schrödinger-type description of electronic structure, in which electrons move within an external potential (produced by charges or fields external to the system of electrons- in our case by the nuclei) while interacting with each other, is being simplified by KS equation

$$\left[-\frac{\nabla^2}{2}+\upsilon_{KS}\left[\rho\right]\left(\mathbf{r}\right)\right]\varphi_i\left(\mathbf{r}\right)=\varepsilon_i\varphi_i\left(\mathbf{r}\right)$$

Equation 3.6

which is placing the electrons in defined effective potential, and describes their movement as independent and noninteracting (fictitious non-interacting system with the same density as the real one). The notation $\upsilon_{KS}[\rho]$ present in this equation is suggesting to us that the Kohn-Sham potential (υ_{KS}) has a functional dependence on electron density ($\rho(\mathbf{r})$), which is expressed as

$$\rho(\mathbf{r})=\sum_{i}^{occ}\left|\phi_i\left(\mathbf{r}\right)\right|^2$$

Equation 3.7

General potential, which can be written in a mathematical form as

$$\upsilon_{KS}\left[\rho\right]\left(\mathbf{r}\right)=\upsilon_{\text{Hartree}}\left[\rho\right]\left(\mathbf{r}\right)+\upsilon_{EXT}\left(\mathbf{r}\right)+\upsilon_{XC}\left[\rho\right]\left(\mathbf{r}\right)$$

Equation 3.8

is composed of the Hartree (Couloumb) term, the external potential generated by the nuclei, and the exchange and correlation (xc) potential. The first component $\upsilon_{\text{Hartree}}[\rho](\mathbf{r})$ is introducing to the calculation the electrostatic potential originating from the electron charge density and can be given by

$$\upsilon_{\text{Hartree}}\left(\mathbf{r}\right)=\int\frac{\rho(\mathbf{r}')}{\left[\mathbf{r}-\mathbf{r}'\right]}d^3r'$$

Equation 3.9

The external potential υ_{EXT} is constructed of bulk individual nuclear potentials located at the centers on each atom present in a specific system,

$$\upsilon_{EXT}(\mathbf{r}) = \sum_{\alpha} \upsilon_{\alpha} \frac{1}{(\mathbf{r} - \mathbf{R}_{\alpha})}$$

Equation 3.10

where υ_{α} represents the attracting force established between the fixed nucleus and surrounding electrons. Finally, the last component $\upsilon_{XC}[\rho](\mathbf{r})$ is the exchange (xc) potential, and represents the functional derivative of the exchange-correlation energy (E_{XC})

$$\upsilon_{\mathrm{XC}}(\mathbf{r}) = \frac{\delta E_{\mathrm{XC}}}{\delta \rho(\mathbf{r})}$$

Equation 3.11

In order to accurately describe and calculate the ground state energy, we need to define the electron kinetic energy, corresponding interelectronic repulsion, the electron-nuclei interaction, and correct all the terms so they could describe the real system instead of fictitious one (with noninteracting electrons). In this regard, the total energy of a certain system is described within Kohn-Sham theory as

$$E_{\mathrm{DFT}} = -\sum_{i}^{\mathrm{occ}} \int d^3\mathbf{r} \phi_i^*(\mathbf{r}) \frac{\nabla^2}{2} \phi_i(\mathbf{r}) d^3\mathbf{r} + \int d^3\mathbf{r} \upsilon_{EXT}[\rho](\mathbf{r}) d^3\mathbf{r} + \frac{1}{2} \int d^3\mathbf{r} \int d^3\mathbf{r}' \frac{\rho(\mathbf{r})\rho(\mathbf{r}')}{[\mathbf{r} - \mathbf{r}']} d^3\mathbf{r} d^3\mathbf{r}' + E_{XC}$$

Equation 3.12

The equation is composed of four terms, which are the non-interacting (Kohn–Sham) kinetic energy, the external potential, the Hartree and the E_{xc} energies, respectively. Although specific information can be found in the literature, in order to understand the advantages and limitations of this definition, we will describe all the mentioned terms in some more detail.[158, 167] First term, representing the kinetic energy of electrons cannot be accurately calculated from the density, and for this reason, we introduce KS orbitals to the calculation (their second derivative is related to the kinetic energy of the fictitious non-interacting system). The variational algorithm is being used to recombine and reorder initial KS orbitals, and these variationally generated solutions are determining the electron density ρ. This approach strongly resembles the one incorporated in HF theory, and at this point, we are backstepping from the initial attempt to describe and calculate the energy using only the electron density. Obtained kinetic energy cannot be considered as an exact and needs additional corrections since it originates from fictional KS orbitals and noninteracting electron particles. The second term can be considered as exact since it provides us information about the interaction of previously defined electron density distribution with the external potential created by the static nuclei centers. The third term, which is identical to the Coulombic interaction term in HF theory, represents a model in which electrons are placed separately in a continuous electron density distribution developed by the presence of all surrounding electrons. The final term, or exchange-correlation functional, should, in principle, contain the correction to all the previous contributions. After introducing the KS equation to the initial equation, we end up with an expression which represents the root of almost all DFT codes, and is written as:

$$E_{\mathrm{DFT}} = \sum_{i}^{\mathrm{OCC}} \varepsilon_i - \int d^3r \left[\frac{1}{2} \upsilon_{\mathrm{Hartree}}(\mathbf{r}) + \upsilon_{EXT}(\mathbf{r}) \right] \rho(\mathbf{r}) d^3r + E_{XC}$$

Equation 3.13

The previously mentioned equation is the reason why DFT was transformed into a "semi-empirical" method during its development. Since the exact form of XC term is unknown, in forthcoming chapters, we will name the various model Hamiltonians the exchange-correlation (XC) approximations. In this way, we will address the concept of exchange-correlation functional to the unknown, exact, formulation of this expression. By analogy, various approximations to the Hamiltonian in DFT will be called density functional approximations (DFAs). Approximations that we can introduce to the calculation, by means of different DFAs, will strongly influence the description of a chemical problem and will have a considerable effect on the obtained result. A vast number of DFAs have been reported during the last few decades. Many of these functionals have been specially developed for the description of specific chemical characteristics, and many more had to be designed and tuned for the treatment of new chemical problems. In order to choose a convenient DFA for a problem at hand, one must be experienced and well informed about the chemical system under investigation. Although DFT possesses a whole specter of different functionals, in the next section, we will mention and shortly describe only the ones with historical importance since they have basically given birth to all new DFAs.

At this moment, I have introduced to you the main engine parts, and hopefully clarified the basic concepts responsible for the functionality of DFT machinery. Now we can proceed further and get familiar with possibilities and capabilities, as well as with the richness of results our DFT laboratory can provide.

3.3. Why DFT and not "the others"

The main goal of computational chemistry is to provide an accurate description of electronic structure, as well as resulting physico-chemical properties, and to attribute chemical sense to these observables. Another important factor is to create a computational model that does not take a lifetime to generate the required results. Two main factors contribute to making accurate computational prediction challenging: i.) Size limitations. In many cases, a molecular system of interest is a large molecule constructed of various atoms. Many TM complexes, besides the central metal ion, which has its own complex electronic structure, contain various ligands with conformational freedom. Hence, in order to limit the length of calculations, suitable simplifications and approximations are included through the choice of DFAs. ii.) Methodological limitations. As mentioned earlier, in order to achieve higher accuracy, more computational time is required, hence some calculations can last for days or weeks, even for medium size systems. While showing a reasonable compromise between accuracy, system size and computational time requirements, DFT became the most popular method for studying and investigating small to medium size molecules, as well as troublesome TM complexes. Primary depending on the functional of choice, calculations can be further improved by including solvation effect, tuning the basis set and numerical grid, or applying an additional correction for zero-point energy, *etc*. Even though DFT has become a necessary tool for completing and further explaining the experiment, it has some well-known shortcomings[167, 168], such as self-interaction errors[169], medium- to long-range correlation errors[170] and tendency to neglect dispersion effects[171]. All these insufficiencies are being compromised because of the impressive efficiency and accuracy of this powerful theoretical engine.

3.4. DFT flavors

DFT method is, in principle exact, yet the exact form of exchange functional is unknown, meaning that the calculated energy can be more or less close to the exact one. Universal DF is still unknown, and there is no perfect algorithm that can provide the "true energy", or describe all required properties of a system under investigation. All existing DFAs have well-known advantages and drawbacks, and even though DFT has reached a level of maturity where it is considered as a trustworthy method, it still suffers from some childhood illnesses. Further development of DFT is focused on the investigation of existing functionals performances and aims to improve the exchange-correlation part within the framework of the Kohn-Sham method. All existing DFAs can be classified into six primary groups: local density approximation (LDA), generalized gradient approximation (GGA), meta-GGA, hybrid DFAs, double-hybrid DFAs, and range-separated DFAs.

3.4.1. Local Spin Density Approximation (LDA)

LDA[172] exhibits a dependence only on the electron density distribution in every point of space. The energy of a system is obtained through a simple integration of electron density point values. In other words, one specific electron at a time located at a specific point in the space is used for determining this point's contribution to the total E_{xc} of the system. Within the framework of this approximation, local exchange $\varepsilon_x\left[\rho(r)\right]$ and correlation term $\varepsilon_c\left[\rho(r)\right]$ are being treated separately as individual contributions, and mathematical form can be written as:

$$E_{xc}^{\mathrm{LDA}}\left[\rho(\mathbf{r})\right]=\int\left(\varepsilon_x\left(\rho(\mathbf{r})\right)+\varepsilon_c\left(\rho(\mathbf{r})\right)\right)\rho(\mathbf{r})d^3\mathbf{r}$$

Equation 3.14

This relatively simple description emerged from the fact that LDA uses the exchange-correlation energy of the homogeneous electron gas, evaluated from the charge density at the point r under consideration. Effectively at a specific point in the space r, $\rho = \rho(\mathrm{r})$ and E_{xc} is equal to the exchange-correlation energy for the electron-gas system, which has a homogeneous charge density ρ. This statement can be considered as correct as long as inhomogeneity $\rho(\mathrm{r})$ is negligible. Since the electronic density distribution in a molecule is certainly not homogeneous, this rudimentary LDA approximation becomes the main pitfall of this method.

Form of LDA, capable of placing electrons with an opposite spin in different spatial orbital, and in this way treating them separately, is known as Local Spin Density Approximation (LSDA). This generalization of LDA can be considered as more advanced and performs much better than the initial DFA for open-shell systems, as well as for near dissociation and weak bonds geometries (the same conclusion applies for HF and other DFAs). Considering the general simplicity of LDAs framework, this DFA can be considered as extremely efficient and applicable for the description of various physico-chemical properties.[1, 167] LDA has a well-known tendency to underestimate and shorten bond lengths during geometry optimization. This phenomenon arises from the fact that LDA works with homogeneous electron gas, and although this can be considered as an error, geometrical parameters obtained with LDA are in most cases in good agreement with the data extracted from crystal structures[173], even for the cases in which TM are involved. Good agreement can be addressed to the shortening of the bond lengths in crystal structure caused by compact crystal packing. Nevertheless, LDA showed much better performance for geometry optimization than some advanced and more sophisticated DFAs. LDA works surprisingly well for calculation of vibrational frequencies and dipole moments, as well as some molecular characteristics which depend on geometrical properties,

like, for example, the *Jahn Teller* (JT) effect[174, 175]. However, this DFA fails to accurately calculate the atomization energies, as well as molecular properties of systems with complex electronic structure (like TM systems, having a lot of close-lying electronic states with various multiplicities).[176]

In order to better understand and describe electron density, since it is not a local property of molecular systems, and provide more accurate results, various DFAs that go way beyond LDA have been developed. These advanced DFAs, which show much better performance, if compared to LDA, differ among each other by the additional functions they introduce to a particular simulation. Better performance can be established if functions of the gradient ($\nabla\rho$) are introduced, and these functionals are known as Generalized Gradient Approximation (GGA) DFAs, as well as Laplacian ($\nabla^2\rho$) of the density, which we call metaGGA DFAs. With these new functions introduced, an improvement of the results can be expected, since within the framework of these DFAs the regions where density varies rapidly with position (regions close to nuclei) are being treated differently than the regions where density varies slowly (regions far away from the nuclei).

3.4.2. Generalized Gradient Approximation (GGA)

Although LDA can be considered as highly accurate, if we take into account its conceptual simplicity, the performance of this DFA showed to be insufficient for most applications in modern chemistry. In the beginning, the moderate accuracy of this DFA was more than enough since it was mainly employed for investigations in the field of solid-state physics. Attempts to determine the reasons why a simple approximation such as LDA works so well led to the development of an enhanced approximate functional. This superior DFA was born from the idea of using not only the information about the density at a particular point, but to enrich the initial principals with valuable information about the gradient of the charge density, and in this way step much closer to the interpretation of the "real" density.

In principle, generalized gradient approximation (GGA) DFA can be considered as a function of the spin densities plus their gradient, as shown in equation:

$$E_{x,\mathrm{GGA}} = \int \varepsilon_x F(s)\, d^3r$$

Equation 3.15

As it can be seen, GGA exchange can be expressed by means of Slater's LDA exchange contribution, and supplemented with $F(s)$ factor, which is a function of reduced density gradient (s), and can be written as:

$$s = \frac{|\nabla\rho|}{2\rho^{\frac{4}{3}}\left(3\pi^2\right)^{\frac{1}{3}}}$$

Equation 3.16

The reduced density gradient (s) can be understood as a local inhomogeneity parameter.[1] Up till now, several options were proposed for the description of the explicit dependence of F on the densities and their gradients, including semiempirical functionals. It is important to mention that mathematical and systematical construction of an advanced DFA is, in most cases, dictated by the accuracy of obtained results, not the physics or chemically meaningful concepts.

3.4.3. Meta GGA Approximations

Standing as an enhancement of GGA functional, meta-GGA (MGGA) enriches the initial approximation with the Laplacian of the density ($\nabla^2\rho$) and/or the kinetic-energy density τ. The typical expression for the MGGA exchange can be written as

$$E_{XC}^{MGGA}[\rho] = \int f\left(\rho, \nabla\rho, \nabla^2\rho, \tau\right) d^3r$$

Equation 3.17

Although this DFA has extended and more complex conceptual basics, since it uses the second derivative of the electron density and/or non-interacting kinetic energy density as a part of the input information, in practice it does not ensure any significant improvement if compared with its parent GGA.[176]

3.4.4. Hybrid Approximations

As was mentioned before, LDA and GGA functionals tend to shorten the bond lengths, thus generate an overbinding effect. On the other hand, the HF method performs differently, and calculated bond lengths are somewhat weaker and longer than experimentally observed. Admix a portion of HF into the pure DFAs, will result in an increase in accuracy. Since it was many times practically confirmed that the exchange contributions are significantly larger in absolute values than the corresponding correlation effects, rational tuning of these contributions further improves the results. Thus, in order to obtain an accurate result, and create a trustworthy method, a precise expression for the exchange contribution is mandatory. Since the exchange energy of a specific SD can be calculated exactly, the most promising way to reach the "exact" exchange-correlation energy seems to be to utilize the exact exchange energy and rely on approximate functionals for providing the missing electron correlation contribution.

These classes of functionals, which supply the calculation with a certain amount of exact exchange, are known as hybrid DFAs, since they are merging information about the exact exchange from HF methodology and data obtained from pure density functionals for correlation part. Although this fusion process may sound complicated, it is done by a simple linear combination of the exact exchange interaction calculated from the HF theory and E_x and E_c from standard DFAs. The typical form of this HF exchange is expressed in the following equation:

$$E_x^{\mathrm{HF}} = -K_{ij} = -\sum_{i,j}\int \phi_j^*(r_1) K_i(r_1)\phi_j(r_1) d^3r_2 = -\sum_{i,j}\int\int \phi_j^*(r_1)\phi_i^*(r_2)\frac{1}{r_{12}}\phi_i(r_1)\phi_j(r_2) d^3r_1 d^3r_2$$

Equation 3.18

Although computational requirements are much higher for the hybrid DFAs, than for LDA or GGA, these functionals are being extensively employed and widely used as a "good standard" for obtaining accurate results, especially in the field of organic chemistry. One of the most appreciated flavors among experimentalists is, without a doubt, famous B3LYP[177]. It should be mentioned that B3LYP is not a good choice for systems that contain transition metals, and in most cases fails to describe the complicated electronic structure of the central metal atom/ion.[178]

3.5. DFT laboratory (capabilities and possibilities)

There is an impressive amount of scientific works done within the framework of DFT, and the majority of these papers focus on structural, energetic, and kinetic quantities. Generally speaking, we can say that this remarkable amount of scientific data is dedicated to the validation of DFT's capabilities and performances.[179-192] Besides proving remarkable achievements of this method, the importance of such a great number of theoretical investigations lies within the richness of available DFAs. Another important aspect is the diversity of chemical systems for which the performance of DFAs was tested during these validations. Furthermore, since the computation of different molecular properties holds different demands on the method chosen, the accuracy which a certain DFA shows is a probe for its versatility. Since DFT is still evolving, trough the persistent search for a universal DFA, a considerable number of new scientific research are published every year. The role of these papers is to track the development of DFT, and the benchmark data is collected from various sources. Although starting with experimentally obtained data is a general trend in computational chemistry, benchmark data can be taken from the high-level wave function theory (WFT) as well. While our work is predominantly TM oriented, now is the right time to warn the reader to be cautious while handling WFT results, even the high-level ones, because of the very pronounced both static and dynamical correlation within the *d*-elements. In this regard, the data obtained using the WFT based methods, in the case of TM containing systems may not be reliable[178].

DFT is a powerful tool able to use basic information about a system constructed from electrons and nuclei, in order to provide results about equilibrium geometries, corresponding bond lengths and bond angles, quantities such as bonding energies, total ground state energies, electronic density distributions, lattice constants, forces and elastic constants, dipole moments and static polarizabilities, magnetic properties and molecular characteristics such as lipophilicity.[193] Such a great amount of various results that can be generated using this theoretical engine exceeds the framework of a Ph.D. thesis, thus, in the next section, I will direct the reader's attention to the most important DFT capabilities and emphasize the ones essential for my scientific work.

3.5.1. Geometry optimizations

Almost every DFT project starts with the optimization of the structures under investigation. This kind of simulations is established through relaxation of structural parameters, in order to find stationary points on the potential energy surface. It is important to highlight that these generally simple calculations will determine the faith of all future calculations, and strongly influence the accuracy of the final results since all delicate physico-chemical properties are associated with geometrical parameters of the investigated system. Optimizing the ground state geometry of a certain molecular structure can be done easily, since there are well developed and carefully tuned algorithms for finding the minima (characterized with the absence of imaginary frequencies), while search for the transition states (this should be confirmed by a single imaginary frequency) requires more experience and information about the system at hand.[194] DFT optimized geometries are in most cases in excellent agreement with experimental data[181], although the accuracy of the result depends on the starting geometry. In cases where there is a possibility to start the optimization from crystallographic data, one can be sure that the optimization yielded a very accurate geometry.

It is convenient to stop for a moment and give some practical suggestions required for conducting an optimization of a real molecular system, which is- in our case a TM complex. There is a known fact that all-electron nonrelativistic DFT optimizations tend to overestimate weak metal-ligand bonds. In this regard, for optimization of TM complexes, a suitable basis set choice should be some polarized triple-ζ basis set, such as TZP. The relativistic effects, which is more than important for heavy atoms such as a TM, can be taken into account trough Zero Order Regular Approximation (ZORA)[195], which will tend to shrink the *s* orbitals and to lesser extent *p* orbitals. Further improvement can be established by introducing the solvation model (*e.g.*, Conductor Like Screening Model- COSMO)[196] effect (especially when we are talking about charged species in solution), and in this way compensate the net charges of an optimized moiety (TM complexes are in many cases in ionic form). Both models can be easily applied to any regular geometry optimization, at an extra cost of computational time, which is more than affordable. Another additional factor that can greatly influence the accuracy of obtained results, and should be emphasized here, is the dispersion correction[170, 171, 197, 198], *e.g.* provided by Grimme.

Since all DFAs give overall good results for the geometries, it is a general trend to use some simple and fast DFA for the optimization (like GGAs), and to utilize the time saved in this process for the calculations of some other important properties, for which computationally expensive DFAs (like hybrid ones) have a clear advantage. A good example of the previous statement is GGA functional named BP86[199-201], which is one of the favorites among computational chemists because it performs impressively well not only for the optimizations but for the calculation of the vibrational frequencies as well. Thus, BP86 represents an excellent way to finish two different jobs in a fast and accurate way.

3.5.2. Relative Energies and thermochemistry (encapsulated forces)

Extracting information about the energetic properties of a molecular system is one of the main goals of all electronic structure-based methods. DFT has reached the level where it is able to simulate and predict some of the fundamental energetic properties like ionization energies (IE) and electron affinities (EA). A precise definition of energy requirement for removal/addition of one (or more) electron from/to a certain molecular system is the basis for investigation and explanation of photoelectron spectroscopy experiments. Knowledge about these fundamental characteristics also provides us an insight of the utmost importance for understanding thermo-chemical reactions. As can

be expected, DFT results showed to be a significant improvement over the HF ones, since during the successive ionization process the number of electrons is decreasing, and lack of correlation effect within the framework of HF fails to describe this change correctly.

3.5.3. Ionization energies and electron affinities (electron interplay)

One of the most important characteristics of all atomic and molecular species, since the discovery of photoelectron spectroscopy, is their IE. The energy required for the removal of one electron from a certain compact system to an infinite distance, if measured precisely, can serve as a chemical fingerprint. Namely, every orbital (energy level) has defined energy, and the value of IE will correspond to the energy of a specific orbital, from which an electron is going to be removed (a strong radiation beam). In this regard, IE can provide us valuable information about the electronic structure of the system under investigation. DFT found some of the first applications within this field of experimental research and brought light to many dark spots by assigning complicated photoelectron spectra.

The reversal process complementary to the IE is the EA. This characteristic is described as the energy released at the moment in which an additional electron is introduced to a certain compact system. During this process, an anion is formed and a defined portion of the energy is released to the environment, nevertheless, this doesn't mean that the resulting form is stable, since in many cases generated charged species is less stable than the starting one. Even though the newly introduced electron is weakly bound, much stronger correlation effect in the ion, than in the starting form, has made the description of electronic structure a difficult task. DFT found an irreplaceable application for treating this kind of problem since it is able to apply diffuse functions and realistically distinguish this disperse spin density, scattered within an ion. Working functional should be chosen wisely since LDA, for example, is not capable of accurately describing the presence of additional electron since it is, by definition, a local DFA.

3.5.4. Atomization energies (from a molecule to single atoms)

Chemical reactions are based on structural changes associated with cleavage of chemical bonds, and the creation of new ones. Description of such multi-component processes, which are, in most cases, difficult to "catch" experimentally, has been the desire of all quantum chemical methods from the moment theoretical chemistry was born. Precise calculation of atomization energies (AE), even for the simplest reactions, is at the very heart prone to errors since it involves breaking of all bonds within a molecule, resulting in constituent atoms in the corresponding ground state. Since the HF method is missing the electron correlation effect, it is suffering from many weaknesses when it comes to the description of chemical bonding. On the other hand, post-HF methods are improving the description of the electronic structure while reaching the required level of accuracy. Even these DFT based methods show certain kinds of systematical errors associated with the correlation energy since correlation effects are greater in molecules than in corresponding subunit atoms. Even though differed DFAs vary in accuracy[202, 203], if handled properly, DFT can be used for reliable prediction of AE.

3.5.5. Bond strength (from single atoms back to a molecule)

Information about the strength of a chemical bond is a characteristic essential not only for the understanding of chemical reactions but for an understanding of fragments (atomic or molecular) between which the bond is created. This chemical property is defining how favorable is the formation of a chemical bond between two moieties, thus, how much energy is going to be released during the formation, and on the other hand how much energy is required in order to break it- after it has been successfully formed. Experimental determination of thermochemical properties holds significant importance since the precise thermochemical information can give us an opportunity to predict the chemical behavior of a certain chemical species in a specific chemical reaction. Practically, the accurate determination of thermochemical aspects is possible only for small molecules in the gas phase. The experiment is almost useless in case of complicated molecules and situations which require the presence of solvents. DFT became a favorite tool for providing deeper insight into thermochemical parameters. Even more important role it has to play for the determination of metal-ligand bond strengths within TM complexes, due to the variability of M-L bond character. Depending on the amount of ionic character within a covalent bond, the thermochemical response will change drastically. Since DFT gives us an opportunity to track and predict these changes, we are able to rationally design TM complexes with specific features and characteristics. It is important to emphasize that a certain method with the intention to predict an unknown observable, such as M-L bond strength, should firs prove itself on a set of known benchmarks typical for the molecule (and the property) under investigation. In this regard, many extensive studies dealing with this problem have been published.[204-207]

3.5.6. Population analysis

Regardless of the overall molecular charge (neutral or ionic), insight in the exact pattern by which electrons are getting together and creating the final composition has always been at the top of the quantum chemistry wish-list. Although the charge of a certain molecule can be experimentally detected, it is a property that should not be addressed to a specific atom, however, this concept showed to be more than useful in the field of organic chemistry. Association of atomic charge with a single molecular center does not make much sense, since it does not hold a clear physical meaning, nor can it be assigned using experimental techniques. Nevertheless, many various methods with the intention to describe the population pattern from which the final density (which is a physical observable) originates have been developed. Although this population-forming concept can provide valuable information about the system under investigation, this method will always stay an obscure field of research, due to the lack of physical foundation. DFT has provided many scientific works[208-210], by means of population analysis, that strongly influences the understanding of molecular properties, and one of the most important facts a newcomer should keep in mind is how to deal with the results. Besides the chosen DFA, the pattern DFT simulation is going to choose for the convergence highly depends on the size and flexibility of the basis functions, as well as the grid used. Thus, one must be cautious when comparing population analysis results, and ensure technical consistency, in order to maintain accuracy.

3.5.7. Vibrational frequencies and IR spectra

Vibrational spectroscopy has an essential role to play in almost every area of chemistry. Even though vibrational spectra are irreplaceable fingerprints useful for eliminating molecular structure or tracking chemical reactions, they can be quite complicated and difficult to resolve. Thus, theoretical methods are of great importance when it comes to an understanding and interpretation of experimentally obtained spectra, although this kind of simulations can be a demanding task. Algorithms for calculation and evaluation of vibrational frequencies have been successfully implemented, and able to generate trustworthy results in a reasonable time scale. Nowadays, frequency calculations are not considered as a luxury anymore, thanks to the development of efficient algorithms coupled with the speed of modern super-computers (especially when running in parallel), although they can remain quite challenging and/or long-lasting.

As it was mentioned in the previous sections, GGA functionals, such as BP86 and PBE, perform surprisingly well (errors usually below 10%) while maintaining the speed originating from their conceptual simplicity. Since these DFAs have been frequently employed and examined, it was concluded that such a good performance can be addressed to the error cancelation. Namely, these functionals exhibit two different systematical errors, the underestimation of harmonic frequencies and the neglect of anharmonicity, and fortunately for us, they seem to cancel each other. Source and intensities of the peaks occurring in Infra-Red (IR) spectra are in most cases accurately characterized and evaluated using DFT as an examination tool.[211-213] Validation of various DFAs for calculation of vibrational spectra, as well as a compilation of benchmark results for TM complexes, can be found elsewhere.[1]

3.6. Electronic excitations and UV/Vis spectra

In order to conduct a spectroscopic measurement, the system of interest should first be exposed to an external perturbation. The perturbation, which can be delivered from various sources (such as a beam of particles, electronic/magnetic field, laser pulse, or continual light irradiation), will initiate some delicate changes in the electronic structure, yielding to the excited states. The unstable excited state will intend to return to the initial ground state, thereby releasing the portion of energy that has been absorbed during the excitation. There are many spectroscopic methods, but the principle is the same: make a change in the probe structure, and then detect the response of the probe using an appropriate detector. While analyzing the detected spectral data, we are able to access various molecular properties and characteristics embedded within the electronic structure.

Although most of the methods, capable of excited state calculation and reproduction of optical spectra, have been mentioned in previous chapters, at this point, they will be summarized and briefly discussed. The first option is the so-called delta-self-consistent field (ΔSCF)[214-218], in which we explicitly calculate the energy of both the ground and the excited state and allow the full SCF relaxation in both cases. As a practical example, we can use a simple excitation, occurring in an octahedral ligand-field, such as the one presented in *Figure 2.13.* In this specific case, excitation energy would be obtained as the energy difference between the ground LS state (t_{2g}^6) and corresponding excited state (t_{2g}^5 e_g^1), thus calculated as ΔE = E (t_{2g}^5 e_g^1) - E (t_{2g}^6). This technique is relatively simple for application when we have a symmetric environment and, consequently, orbitals can be labeled with different irreps from the corresponding point group, enabling the straightforward construction of some excited states and their SCF procedure. Nevertheless, SCF calculation of excited states is much more complicated (from a practical and theoretical point of view) than for the ground state, thus symmetry labels of MO serve as the mathematical shortcut to the convergence. In this

regard, ΔSCF is not easily applicable to nonsymmetrical TM complexes. The problems concerning this method, can arise if a certain state is multideterminant, or on the other hand from poor excited state SCF convergence. Another more advanced method and an improvement over ΔSCF is time-dependent DFT (TD-DFT)[219-223]. This popular and computationally cheap method has shown to perform well for medium to large-size molecular systems, and although mainly applied to organic compounds, it can provide reasonable results for TM complexes.[224-226] Even though results obtained with ΔSCF can, in some cases, be comparable to TD-DFT results, this method is theoretically less founded and for this reason, is not considered accurate enough.[224] On the other hand, results generated using TD-DFT are in most cases similar to those obtained by computationally expensive highly correlated *ab initio* methods.[224, 227, 228] Another possibility within the domain of DFT is Ligand Field DFT (LF-DFT)[229, 230], which is known for its efficiency and simplicity. These two sophisticated DFT techniques (TD-DFT and LF-DFT), designed for simulation and prediction of spectroscopic characteristics, will be the topics of great importance for the present thesis, and thus will be individually described and discussed in forthcoming chapters.

Optical spectra can also be examined and interpreted by means post-Hartree-Fock (HF) methods like CI. Such an approach extends a single determinant HF wave function into a function constructed of a linear combination of many determinants with variationally optimized coefficients. This multi-determinantal technique is dealing with configuration mixing, yet the initial set of orbitals is not being reoptimized for different electronic states. It is important to highlight that the correlation effect has a strong influence on electron density, and this effect is even stronger in the case of TM containing systems. Hence, the optimization of initial molecular orbitals is of utmost importance, since only in this way we can be sure that delicate energy contributions like static correlation, will be included in the calculation. This fundamental problem can be taken into consideration by means of the multi-configuration SCF (MC-SCF)[231, 232] and extended variations of this method, called RASSCF[233] (restricted active space SCF) and CASSCF[234] (complete active space SCF). These methods have an important role to play during a theoretical observation of excited states since significant changes in the electron density triggered by electron excitations are followed by the mixing of different electronic states. Another method capable of providing very accurate transition energies by combining the multiconfigurational variation with second-order perturbation treatment of dynamic electron correlation is the so-called CASPT2[235, 236]. Cluster methods (*i.e.* Equation-of-motion coupled-cluster methods) are well known due to impressive accuracy, which is, on the other hand in most cases computationally expensive and can include single and double CCSD[237], as well as triple perturbational CCSD(T)[238]. To summarize briefly, for the sake of clarity – the main difference between the mentioned CAS and CC methods on the one side and DFT based methods on the other, is in the fact that the firs ones are based on HF and use a wavefunction as a central quantity, distinct from DFT and ρ. Also, in the wave function based methodologies, it is straightforward to increase accuracy (by a simple increase of active space/number of excitations/basis set…), but in turn, they are more computationally expensive. Details, results and accuracy validations of these various methods, designed for investigation of excited states, can be found elsewhere.[239-243]

3.6.1. DFT in a shell of time (basic concepts of Time-Dependent DFT)

The reality we live in is in the process of constant change and motion. We associate the concept of time-flow to the events occurring or changing the form during our everyday lives- breathing, changing of the moon phases, rotation of the planets… Observance of this constant time follow is limited within our natural senses and goes from a human lifetime to a segment of a second. All fields of science are occupied with the idea of dynamics of time-dependent events, but in most cases, mainly on a philosophical level. Namely, tracking and observing changes within cosmological events would require more time than anyone of us have to offer, as well as the level of detection, which goes way

beyond our sensor limitations. Thus, in order to understand such long-lasting phenomena, one has to collect and rely on some other indirect indicators of what has happened. Other similarly incomprehensible cases are the ones occurring within short time-scales, hidden in the world of microscopic events. Luckily, besides novel, highly sensible experimental techniques, able to provide an impressive time resolution, we have an opportunity to theoretically simulate these processes, undetectable for our eye. The present thesis has a particular interest in electron excitations, triggered with some external perturbation force, that takes place in a time scale of attoseconds. Walking down the path of excitation processes, we are entering an even more complex region since we are heading away from the ground state properties.

In order to familiarize a newcomer with DFT encapsulated in a shell made of time, we need first to take a look back at the time-dependent SE (*Equation 3.1*). Let us imagine a system of N interacting electrons changing their positions within an explicitly time-dependent external potential $\upsilon(\mathbf{r}, t)$, which will represent a "real" function of space and time. The Hamiltonian operator of such a system will take the form:

$$\hat{H}(t) = T + V(t) + W$$

Equation 3.19

The kinetic energy operator will retain the same form as in static case:

$$T = \sum_{j=1}^{N} -\frac{\nabla_j^2}{2}$$

Equation 3.20

The potential operator will, on the other hand, adopt the time-dependent form and will be expressed as:

$$V(t) = \sum_{j=1}^{N} \upsilon\left(\mathbf{r}_j, t\right)$$

Equation 3.21

And the Coulombic particle interaction component will be given as:

$$W = \sum_{j=1}^{N} w(\mathbf{r}_j, \mathbf{r}_j')$$

Equation 3.22

And to finalize, the time evolution of the system is determined and dictated by the time-dependent many-body Schrödinger equation:

$$i\hbar \frac{\partial \psi}{\partial t}(x_1, ..., x_N, t) = \hat{H}(t)\psi(x_1, ..., x_N, t)$$

Equation 3.23

The solution of time-dependent many-body SE is written in terms of a time evaluation operator:

$$\psi(t) = U(t, t_0)\psi_0$$

Equation 3.24

The role of time evolution operator U(t, t_0) is to derive state ψ(t) by means of initial ψ_0 state over a time interval, starting with the time t_0 and ending at some time $t \geq t_0$. The great importance of time evolution operator arises from the fact that it serves as a convenient starting point to derive numerical methods for solving time-dependent single-particle SE. Technically speaking, time-dependent SE designs a pattern by which each the external potential υ(**r**, t) produces a time-dependent wave function ψ(t), for a given conserved state ψ_0. In a physical sense, this means that the dynamical characteristics of the resulting state are determined by the time-dependent potential, generated via time-dependent SE.

$$\upsilon(\mathbf{r},t) \xrightarrow{i\partial\psi/\partial t = H(t)\psi} \psi(t) \xrightarrow{\langle\psi(t)|n|\psi(t)\rangle} n(\mathbf{r},t)$$

Scheme 3.1 Formation of a time-dependent wave function ψ(t), for a certain state ψ_0, through a specific external potential υ(**r**, t)

In order to develop a trustworthy time-dependent theory, one must look at the *Scheme 3.1* backward, and find a valid proof that time-dependent density ρ (**r**, t) can be used as variable able to fully describe the dynamics of a certain system. In this regard, it is of utmost importance to show that there is a unique one-to-one correlation between time-dependent densities and potentials. Such correlation, which is the root of TD-DFT, was recognized for the first time by Runge and Gross back in 1984.[220] Another important theoretical ingredient essential for TD-DFT is the work done by van Leeuwen, which describes the behavior of two many-body systems with different particle-particle interactions.[244] As for the first theorem, the detailed discussion, and theoretical information can be found in the original work. These two theorems stand as the basics of TD-DFT, and provide time evolution to a ground state system described and evaluated by regular static DFT. Practically speaking, this is done by starting from a system in its ground state, located at the initial time t_0. Although, one of the main characteristics of the system is the time t_0, at some point the system starts to propagate- initiated and then further lead by the effect of a defined time-dependent external potential. In this way, the effective potential is transformed into a parameter depending only on the density, which brings a great simplification to the initial theoretical scheme. Time-dependent density can be expressed in a mathematical form as:

$$\rho(\mathbf{r},t) = \sum_{j=1}^{N} \left|\varphi_j(\mathbf{r},t)\right|^2$$

Equation 3.25

While keeping in mind these two theorems, as well as the previous statement, we are able to express the time-dependent Kohn-Sham (TDKS) equation, as well as the corresponding single-particle orbitals $\left|\varphi_j\left(\mathbf{r},t\right)\right|$:

$$\left[-\frac{\nabla^2}{2}+\upsilon\left[\rho\right]\left(\mathbf{r},t\right)\right]\varphi_j\left(\mathbf{r},t\right)=i\frac{\partial}{\partial t}\varphi_j\left(\mathbf{r},t\right)$$

Equation 3.26

One important thing to mention is the selection of orbitals TD-DFT is going to take into account. Since TD-DFT is going to take the ground state density as the starting point, the orbitals that are going to be subjected to the time-evolution are the ones that were initially occupied, and the evolution is going to occur in a period between the initial time t_0 and some defined final time t_1. TD-DFT propagation is not going to take place within initially unoccupied orbitals, hence $\varphi_j\left(\mathbf{r},t_0\right)=\varphi_j^0\left(\mathbf{r}\right)$. Once the time-dependent density $\rho(\mathbf{r},t)$ is successfully generated, we can start to extract data associated with physical observables, and hopefully get the solutions for the problem in hand. As well as in the case of regular DFT calculations, TD-DFT results are in principle exact but suffer from approximate error, and in this case, exchange-correlation functional has a more demanding task, since it needs to describe the evolution of electron density in the past.[245] In this regard, most of the TD-DFT simulations utilize an important conceptual idea, called the adiabatic approximation.[221, 223] Namely, if the change occurring within the time-dependent potential is slow and smooth, without drastically fluctuations, one can approximate and use time-independent ground state exchange-correlation functional in every point of the change, instead of time-dependent one.

Although previous concepts proposed a "real-time" TD-DFT approach, there is another possibility to define and consider the excited state problem. In order to understand the approach proposed by Casida[173, 245, 246], we must first consider the equation of motion (*Equation 3.27*) and the operators $|I><0|$ which transform the ground state ($|0>|$) into *I*th excited state ($|I>|$) and stand as solutions of the equation.

$$[\hat{H},\ O^{\dagger}] = \omega O^{\dagger}$$

Equation 3.27

The excitation energy in the case of $|I><0|$ is expressed as $\omega=E_I-E_0$ (has a positive value) and give rise to the de-excitation energy $\omega=E_O-E_I$ with the same value of the opposite sign. While searching for the solution for the equation of motion, which now takes the form:

$$O^{\dagger}=\sum_{i,a}a^{\dagger}iX_{ia}+\sum_{i,a}i^{\dagger}aY_{ia}$$

Equation 3.28

we are expending the $O^{\dagger}$ (symbol † represents the Hermitian adjoint) into a basis set of so-called one-particle/one-hole excitation end de-excitation operators, which further give us an opportunity to form a matrix from the initial equation of motion (*Equation 3.29*).

$$\begin{bmatrix} \mathbf{A} & \mathbf{B} \\ \mathbf{B}^* & \mathbf{A}^* \end{bmatrix} \begin{pmatrix} \vec{X} \\ \vec{Y} \end{pmatrix} = \omega_I \begin{bmatrix} 1 & 0 \\ 0 & -1 \end{bmatrix} \begin{pmatrix} \vec{X} \\ \vec{Y} \end{pmatrix}$$

Equation 3.29

Symbols $\overrightarrow{X}$ and $\overrightarrow{Y}$ in the equation represent the column vectors, whereas the matrices **A** and **B** are defined as $A_{ij,kl} = \delta_{ik}\delta_{jl}(\varepsilon_i - \varepsilon_k) + \mathcal{K}_{ij,kl}$ and $B_{ij,kl} = \mathcal{K}_{ij,kl}$, thus the excitations can be obtained with a correction $\mathcal{K}_{ij,kl}$ to the KS transition energies $\omega_{ij} = \varepsilon_j - \varepsilon_i$. Excitations are being separated from de-excitations by the introduction of the Tamm-Dancoff approximation[247], which is neglecting the **B** matrix element. In this way, we are left to solve only the *Equation 3.29* and obtaining a clear wave function $\psi_I = \sum_{i,a} \Phi_i^a X_{ia}^I$, where Φ_i^a is the ground state determinant with an electron promoted from ψ_i to orbital ψ_a.

$$\boldsymbol{A}\overrightarrow{X_I} = \omega_I X_I$$

Equation 3.30

The excitation from a specific MO_i to a target MO_a is performed in such a way that any orbital relaxation is restricted, and depending on is it a spin-preserving or a spin-flip excitation, yields a singlet or a triplet state (*Figure 3.1.*). By solving what is in most cases referred to as "Casida's equations" vertical excitations between populated and targeted empty orbitals are obtained. One of the most important advantages of this method is the symmetry preservation of the excited state within the *Equation 3.29*, thus calculated excitations can be easily assigned and labeled. Although real-time TD-DFT can provide valuable information about excitations in large molecular systems, such as proteins, Casida's approach as more convenient and specific when it comes to small- to medium molecular structures. For this reason, this is the main TD-DFT approach implemented in most of the codes[248-250] and will be used for the calculations carried out in the present thesis.

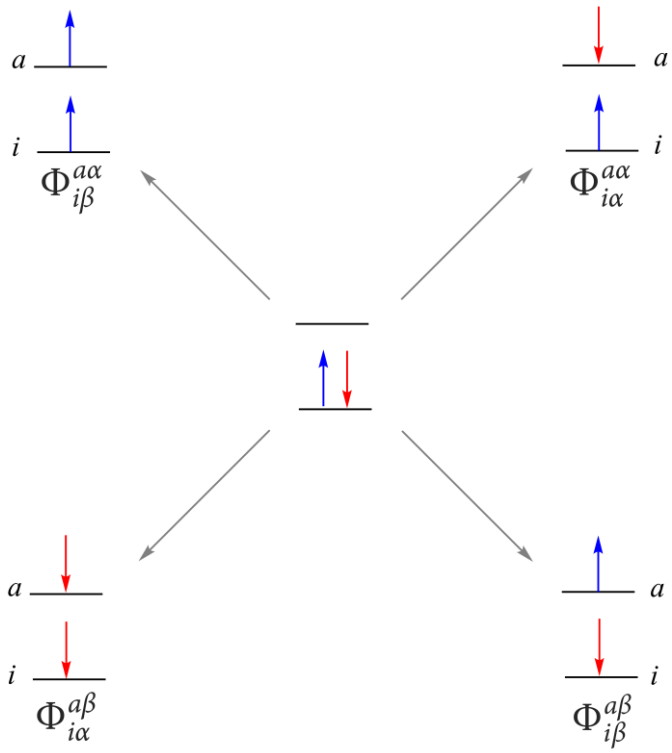

Figure 3.1. Schematic representation of one electron excitation from HOMO (*i*) to LUMO (*a*), showing both spin-flip excitations (*left*) and spin-preserving excitations (*right*)

3.6.1.1 Troublesome excitation events

As we already mentioned before, excitation energies of a certain many-body system are defined as energy differences between the ground state E_0 and some other state with higher energy E_n. In the simplest example possible, we can "dislocate" one electron from an occupied orbital in the ground state and populate an orbital which was initially unoccupied (like the example shown in *Figure 2.13.*). In this way, we would generate a new state with defined (higher) energy. Since, at the first glance, the excitation energy can be considered as the difference between these two states, one can naively think that we do not need to bother with more complications or additional equations required by TD-DFT. In the "real" particle world, the picture of this "simple" process is much different. A more realistic picture would be to consider this phenomenon as a process of rearrangement of the probability of electron density, which is a strictly defined dynamical process. The problem of defining an excitation becomes even more complex when it comes to the charge-transfer excitations. Namely, unlike linear excitations that occur between two energetically similar orbitals which are close by in space (let's say *d*-orbitals, located at the metal center), electron-transfer is taking place between two points in space which are far away from each other (let's say metal and ligand). The main difficulty in correctly describing this kind of excitation arises from the mechanistic scheme- how it happens. First of all, a discrete charge (electron) needs to "leave" a specific point in space (atom), which will be considered as a donor, and this process is defined as the ionization energy of that certain point. A portion of that energy is counteracted by the electron affinity of the second point in space, which will be the destination point, and considered as an acceptor. Although DFT is doing remarkably well in describing electronic excitations involving little or no change in the overall density, this advantage becomes a weakness when trying to describe excitations involving a transfer of charge from one point to another. Standard approximations implemented within the framework of TD-DFT fail to correctly locate and describe this class of perturbations.[251-253] Luckily for us, hybrid DFAs, especially the range-separated ones, have shown great performance for treating this kind of perturbations in a whole set of various molecular systems.[254-257] Due to the adiabatic approximation, excitations with dominant double excitation character are not properly captured.[258, 259]

3.6.2. DFT in a shell of ligands (basic concepts of Ligand Field DFT)

LF-DFT's importance is manifested through the successful consolidation of empirical (LF) and theoretical (DFT) approach, thus results obtained within the framework of this method can be directly compared with the experiment.[117, 229] This solid bridge, built between two approaches, is giving us an opportunity to extract the (implicitly incorporated) dynamical correlation from DFT, and later use it in a configuration interaction (CI) fashion to add static correlation and determine corresponding excited state properties through the LF theory. This is achieved by a so-called *multi-determinantal* DFT *calculation*, which means that we must determine all SDs for a d^n configuration, and utilize obtained energies to parameterize the LF matrix and the Racah's parameters. Since this procedure, which shows impressive performance for prediction of excitation spectra and many other properties of TM complexes[260-265], requires more than one step- a more detailed explanation will be given in the following text.

If we start from the non-relativistic SE, we can see that (within the Born-Oppenheim approximation) contributions to the total energy can be categorized as ones that depend of the coordinates of two electrons (electron-electron interaction), the ones that depend on the coordinates of only one electron (kinetic energy and electron-nuclear interaction) and the one that does not depend on the position of the electrons, and is constant shift for every specific nuclear configuration (nuclear-nuclear interaction). Since that constant shift is the same for different electronic states (in the fixed

nuclear configuration) and disappears when we calculate, for example, their relative energy with respect to the ground state (which represents the vertical excitations from which UV-vis spectra might be obtained), we will no longer be interested in it. With this in mind, we arrive at the well-known conclusion that the energy of different electronic states depends only on one-electron and two-electron contributions. Since we are interested in TM complexes, we can also rephrase this conclusion using the simple and straightforward arguments from the LFT, and state that the energy of any specific electronic configuration (which can be expressed as an SD) involving MOs with the dominant contribution of *d*-atomic orbitals, depend only on the orbitals splitting within the ligand environment (one-electron term) and the electron-electron interaction. [203,266]

$$E\left(SD_{\mu}^{d}\right) = E\left(\det\left|d_{\mu,1}\,\sigma_{\mu,1}\,d_{\mu,2}\,\sigma_{\mu,2}\ldots d_{\mu,n}\,\sigma_{\mu,n}\right|\right) = \sum_{i=1}^{n}\langle d_i|h_{LF}|d_i\rangle + \frac{1}{2}\sum_{i=1}^{n}\sum_{j=1}^{n}\left(J_{ij} - K_{ij}\delta_{\sigma_i\sigma_j}\right)$$

Equation 3.31

Specific single determinants in *Equation 3.31* for example in O_h symmetry are labeled with the subscript $\mu = 1, \ldots, \binom{10}{n}$, because there is $\binom{10}{n}$ SDs for any d^n electronic configuration, while specific electrons are labeled with *i* and *j*. Symbols *J* and *K* represent the Coulumb and the Exchange matrix elements, while h_{LF} represents, one electron, elective ligand field Hamiltonian. In order to clarify the previous statement, it is convenient to present a practical example, and for this purpose, we should take a simple d^3 electronic configuration of an octahedral complex. Four SDs (out of 120 possible), arising from the d^3 electronic configuration, are shown in *Figure 3.2.* As it can be observed from the figure, SD1, SD2 and SD4 originate from the same t_{2g}^3, and only differ in the two-electron contribution.

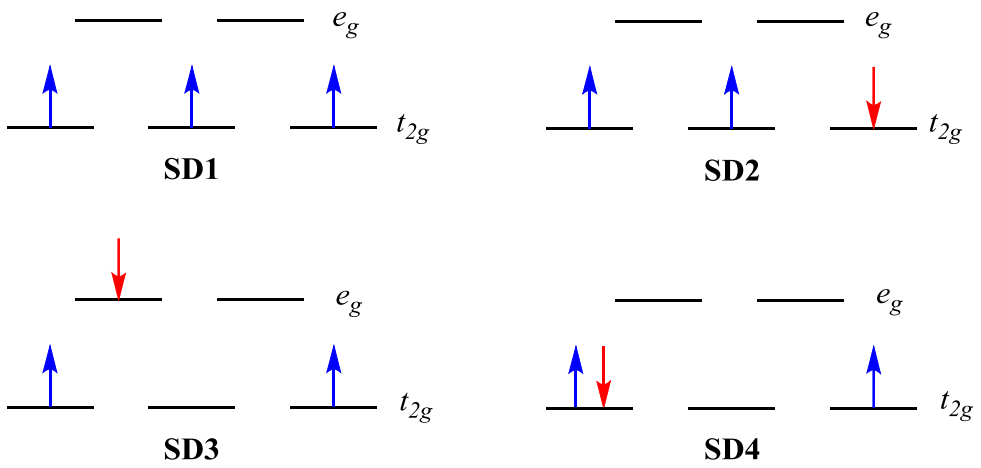

Figure 3.2. Four random electronic arrangements (SDs), arising from d^3 configuration in an octahedral complex

The two-electron matrix elements can, by the Wigner-Eckart theorem[267], be expressed as the product of two factors, from which the first depends only on the angular momentum quantum numbers involved in the specific matrix element (the Clebsch-Gordan coefficient[268]) and second, which is completely free of angular dependence (so-called reduced matrix element). In spherical symmetry (which is inherent to LF theory), all the reduced matrix elements form all 5^4 possible orbital

combinations can be expressed using only three independent parameters, so-called Radial or Slater integrals, (F_0, F_2, and F_4), which can then be recombined into Racah[40] parameters A, B, and C. This implies that by the suitable utilization of (well known) Clebsch-Gordan coefficients, we can express energy of every SD in O_h symmetry as:

$$E\left(SD_{\mu}^{d}\right) = \sum_{i=1}^{n}\langle d_i|h_{LF}|d_i\rangle + \frac{1}{2}\sum_{i=1}^{n}\sum_{j=1}^{n}\left(J_{ij} - K_{ij}\delta_{\sigma_i\sigma_j}\right) = E_{gauge} + LFSE + \beta_{\mu}B + \gamma_{\mu}C$$

Equation 3.32

where $\beta_{\mu}\ and\ \gamma_{\mu}$ are coefficients that are related to Clebsch-Gordan coefficients, B and C are obtained from F_0, F_2 and F_4, and E_{gauge} incorporates A, and represents the gauge origin within the LF and DFT methodologies. One electron matrix element $\langle d_i|h_{LF}|d_i\rangle$, present in *Equation 3.31*, are the energies of *d*-orbitals, in which each of n-electrons (from d^n configuration) are placed. Since we have obtained energies of all SDs (between 45 and 252), which represent left-hand side of the *Equation 3.32*, and, since there are only a few parameters on the right-hand side, we have the overestimated system of equations, which is then solved by making the linear square fit.

Since we established a clear relationship between one-electron terms and energies of MOs with dominant *d*-character, two-electron contribution can now be expressed using Racah parameters. Now that the working tools are provided, we should find a way to extract these necessary ingredients from the DFT calculations. In order to separate one-electron and two-electron contributions, DFT calculations (within the framework of LF-DFT) must be performed in two separate phases.

The first phase is called the *Average of Configuration* (AOC) calculation, which represents a restricted single point calculation in which available *d*-shell electrons are equally distributed over five MOs originating from *d*-orbitals in a $\frac{n}{5}$ fashion (*e.g.* 3 *d* electrons equally populating five MOs of interest result in 0.6 electrons per every orbital). The purpose of equal occupation of all five MOs is to incorporate the spherical symmetry, necessary for any LF approach, and provide the best starting point density (Janak's theorem[269]) toward the manifold of all possible d^n occupations, that will be generated in the next step. From the AOC calculation, we will extract the eigenvectors of five MOs of interest while taking only the contribution of five atomic *d*-orbitals in the form of, so-called, *U* matrix (*Scheme 3.2.*):

$$\mathrm{U} = \begin{array}{c} \\ MO_1 \\ MO_2 \\ MO_3 \\ MO_4 \\ MO_5 \end{array} \begin{array}{c} \begin{array}{ccccc} d_{xy} & d_{yz} & d_{z^2} & d_{xz} & d_{x^2-y^2} \end{array} \\ \begin{bmatrix} 0.984 & 0.005 & 0 & 0.008 & 0 \\ -0.008 & 0.005 & 0 & 0.984 & 0 \\ -0.005 & 0.984 & 0 & -0.005 & 0 \\ 0 & 0 & -0.585 & 0 & -0.791 \\ 0 & 0 & 0.791 & 0 & 0.585 \end{bmatrix} \end{array}$$

Scheme 3.2. The U matrix, for the $[Mn(H_2O)_6]^{2+}$, with labeled columns and rows
(The AOC calculation is done in *no symmetry* fashion, and in turn some off-diagonal elements are present in the *U* matrix)

The previous formulation has been generalized for any or no-symmetry systems. The symmetry of the ligand environment affects the extent of coupling between different *d*-orbitals, $\langle d_i | d_j \rangle$. For example, in a point group[40] where all *d*-orbitals belong to different irreducible representations, all $\langle d_i | d_j \rangle = 0$. Another important property of *U* matrix is that it possesses the information about the covalency of metal ligand interaction (squares of coefficients in each row do not have to produce 1, *i.e.* there is some extent of ligand orbitals present in these MOs). It is important to mention that due to the considerable contribution of ligand orbitals to the MOs, the *U* matrix is not orthogonal. This can be simply mediated by Lowdin's[270] symmetric orthogonalization ($\widetilde{U} = (U \cdot U^T)^{-\frac{1}{2}U} \cdot$). In this way we can combine the information about the symmetry of the ligand environment ($\widetilde{U}$ matrix) and extent of metal ligand interaction (energies of MOs originating from *d*-orbitals), in order to obtain the LF matrix which carries all the information regarding the metal-ligand interaction ($LF = \widetilde{U}^T \cdot E_{MO} \cdot \widetilde{U}$). Obtained LF matrix can be represented in the following form:

$$LF = \begin{bmatrix} \langle d_{xy}|h_{LF}|d_{xy}\rangle & \langle d_{yz}|h_{LF}|d_{xy}\rangle & \langle d_{z^2}|h_{LF}|d_{xy}\rangle & \langle d_{xz}|h_{LF}|d_{xy}\rangle & \langle d_{x^2-y^2}|h_{LF}|d_{xy}\rangle \\ \langle d_{xy}|h_{LF}|d_{yz}\rangle & \langle d_{yz}|h_{LF}|d_{yz}\rangle & \langle d_{z^2}|h_{LF}|d_{yz}\rangle & \langle d_{xz}|h_{LF}|d_{yz}\rangle & \langle d_{x^2-y^2}|h_{LF}|d_{yz}\rangle \\ \langle d_{xy}|h_{LF}|d_{z^2}\rangle & \langle d_{yz}|h_{LF}|d_{z^2}\rangle & \langle d_{z^2}|h_{LF}|d_{z^2}\rangle & \langle d_{xz}|h_{LF}|d_{z^2}\rangle & \langle d_{x^2-y^2}|h_{LF}|d_{z^2}\rangle \\ \langle d_{xy}|h_{LF}|d_{xz}\rangle & \langle d_{yz}|h_{LF}|d_{xz}\rangle & \langle d_{z^2}|h_{LF}|d_{xz}\rangle & \langle d_{xz}|h_{LF}|d_{xz}\rangle & \langle d_{x^2-y^2}|h_{LF}|d_{xz}\rangle \\ \langle d_{xy}|h_{LF}|d_{x^2-y^2}\rangle & \langle d_{yz}|h_{LF}|d_{x^2-y^2}\rangle & \langle d_{z^2}|h_{LF}|d_{x^2-y^2}\rangle & \langle d_{xz}|h_{LF}|d_{x^2-y^2}\rangle & \langle d_{x^2-y^2}|h_{LF}|d_{x^2-y^2}\rangle \end{bmatrix}$$

Scheme 3.3 The general form of LF matrix.

In the first phase, we have extracted the information about the symmetry of the ligand arrangement, covalency and extent of metal-ligand interaction, but we have also prepared the spherically symmetric restricted electron density, with the equally occupied MOs of interest, which is the best starting point for the second and final phase of the calculations. The final step of the calculation involves the determination of all possible SD, originating from specific d^n configuration. At this point, energy differences between obtained SDs can be considered as a consequence of electron-electron interaction. In addition, careful incorporation of spherical symmetry enables us to describe the interaction using only two Racah parameters, B and C, since A becomes a constant shift equal for all SDs.

Now it is obvious that LFSE can be obtained both from AOC and from the fitting procedure. The instructive thing to do would be to compare both results, but a general expectation is that the values should be fairly similar. More importantly, after we have used DFT obtained SDs and to fit B and C, it is interesting to compare the difference between these energies calculated by DFT and the ones obtained using the LF model with fitted B and C and one-electron parameters. The difference in the DFT calculated SD energies and SD energies from the LF model (with parameters obtained from the fit) is graphically represented in *Figure 3.3.*, for *on* $[Cr(H_2O)_6]^{3+}$. Mean Square Deviation (MSD) in this case is 77 cm^{-1}, which is a very good agreement. In general, the best fitting results are characterized by MSD bellow 50cm^{-1}, the ones in between 50-100cm^{-1} are still an indication of good agreement, and the ones in 100-200cm^{-1} are borderline acceptable. The fit >200cm^{-1} would indicate some serious failure of LF-DFT model, most probably due to strong covalency.

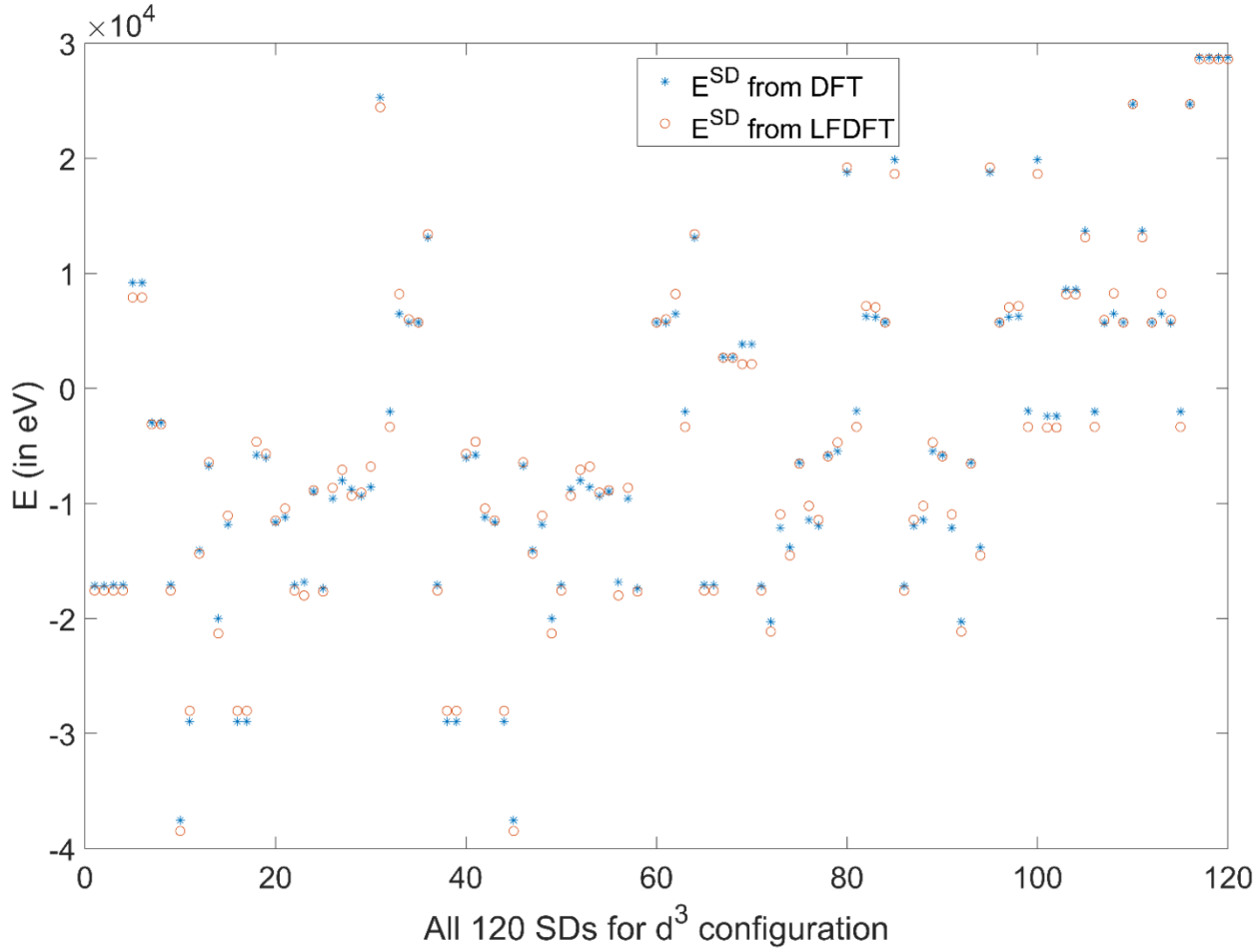

Figure 3.3. Comparison between SD energies (in eV) obtained from DFT (*) and from LF-model calculations (o). The x-axis refers to SDs and the y-axis corresponds to the energy in eV.

Since we can now easily calculate the energies of all SDs, using the obtained parameters, we can utilize any LF program to obtain the multiples. The methodology also allows simple incorporation of relativistic effects using the spin-orbit coupling constant. Since LF-DFT, beside the simple LF parameters, also possesses the wave-functions (MOs in term of *d*-orbitals, multiplets in terms of simple SDs, relativistic states as a combination of non-relativistic ones…), it is a perfect starting point for many further effective Hamiltonian applications that can be used in order to obtain electronic spin resonance (ESR), D and E magnetic anisotropy[271] parameters and many other[260-263, 265]. As well as TD-DFT, LF-DFT has been utilized with impresive success for the description of the ground and excited electronic states originating from d^n TM ions in their complexes.[67] Besides this highly important application, LF-DFT has shown great performance for simulations and predictions of optical spectra[272], calculation of the *Jahn-Teller* (JT) coupling[174], and hyperfine-coupling parameters[262], NMR shielding[263], electronic structure and transitions in *f*-elements[273], zero-field splitting[274], spin-orbit coupling[275], magnetic exchange coupling[264], as well as the covalency effects[276].

Although LF-DFT can (in mostly ionic TM complexes, with clearly separated *d*-manifold) provide very accurate results, comparable or better than CASSCF, CAS-PT2, and NEV-PT2 methodologies[67], it is not without its own limits. First of all, LF-DFT does not yet belong to procedures which can be applied routinely, and although it is a lot easier to use than the abovementioned *ab-initio* active space alternatives, it is still not recommended for utilization without, at least limited, expertise and understanding of the basic code. Additionally, since the entire LF (and thus, LF-DFT) approach is based on the clearly separated *d*-orbitals manifold, the described methodology is likely to fail in strongly covalent (organo-metallic) systems and in cases when ligand

orbitals end up in between MOs with the dominant *d* character (non-innocent, redox-active ligands and metals in very positive ionic state).

3.7. Energy Decomposition Analysis (EDA- a more realistic picture)

Many available theoretical analysis procedures, such as MO or population analysis, have been kept and applied only at a qualitative level, and all introduced changes or perturbations are taken into account as an external influence on a sum of orbital energies (election density). Since DFT has evolved in both theory and application, we are now able to use it in order to create a more realistic picture of intermolecular events, such as chemical bond formation. In this regard, the same approach of two interacting particles A and B, will be exploited, but in such a way that we can understand the complete physicochemical character of the process.[277] Interaction of two independent systems is one of the first concepts recognized by chemists, and theoretical approaches grant us unrestricted freedom to choose interacting particles. In the simplest example possible, these fragments (how we will call interacting species from now on) will be two atoms which are getting together in order to establish a chemical bond, but since we are interested in TM complexes, we will focus our attention on the interaction between the metal and corresponding ligands.[278-281] In this way, the complexity of interacting systems, bonding events, and the formation of the final product, are considerably enhanced, but on the other hand, fruitful harvest can be expected. It is important to highlight that the fragment choice can be ambiguous, and thus changing of bonding partners can yield a better insight, depending on what additional properties we are interested in.[282, 283] Fragment choice should be made by someone with experience, and strong chemical logic/intuition.

3.7.1. Splitting the bonding energy into meaningful contributions

A certain molecular species of a general formula A-B is defined by a wave function Ψ_{AB} and corresponding energy E_{AB}. EDA sees such a molecule as a final result of interaction between two fragments A_0 and B_0 in their electronic and geometric ground states Ψ_A^0 and Ψ_B^0 (corresponding energies E_A^0 and E_B^0), which they would have at an infinite separation in space. Since both electron density and geometry of the fragments must assimilate to each other and relax (a relaxed superposition of both electron densities), in order to form the final product, this process can be rationalized in few separate steps. In the first step, the fragments are distorted from their initial geometries and wave functions Ψ_A^0 and Ψ_B^0 to the geometries and wave functions Ψ_A and Ψ_B which they will have in the molecule The energy required to excite the fragments from their equilibrium geometrical and electronic ground state to state which they exhibit in the final product is termed as the preparation energy ΔE_{prep} (*Equation 3.33*).[284, 285]

$$\Delta E_{prep} = E_A - E_A^0 + E_B - E_B^0$$

Equation 3.33

This component usually has unfavorable (positive) character and will destabilize the bonding process, and since EDA represents a method designed for examination of chemical bonding, it is dominantly directed toward the analysis of interaction energy ΔE_{int}. This component represents the

energy difference between distorted (prepared) fragments and the final molecular structure (*Equation 3.34*).

$$\Delta E_{int} = E_{AB} - E_A - E_B$$

Equation 3.34

In the first step of EDA analysis, prepared fragments with retained charge densities are brought together from infinite separation to the molecular conformation. This state can be described as a product of total wave function $\Psi_A\Psi_B$ and energy E^0_{AB}. Interaction of individual charge densities within a molecular form is described as the Coulomb interaction ΔE_{elstat} (*Equation 3.35*) and, in most cases, has a stabilizing character. It is important to keep in mind that simple superposition of individual densities (ρ^A and ρ^B) considerably differs from the final equilibrium density, and the interaction of two particles with frozen charge densities (and nuclear charges Z_α and Z_β) can be formulated as:

$$\Delta E_{elstat} = \sum \frac{Z_\alpha Z_\beta}{R_{\alpha\beta}} + \int V_B(r)\,\rho^A(r)dr + \int V_A(r)\,\rho^B(r)dr + \int \frac{\rho^A(r_1)\rho^B(r_2)}{r_{12}}dr_1dr_2$$

Equation 3.36

where (and likewise for the V_B):

$$V_A(r) = -\sum \frac{Z_\alpha}{|r - R_\alpha|}$$

Equation 3.36

These two expressions hold one important chemical concept, that is, the behavior of two charged species at different positions in space. Namely, as it can be seen, two charge clouds, approaching each other, show much smaller repulsion than the one which is established between point charges at the centers of charge. In this regard, electrostatic interaction for two approaching particles becomes attractive in all cases except at very short distances, which we can consider as way too short to be of practical interest (in this hypothetical case ΔE_{elstat} becomes repulsive).

In the second step, the product of two prepared fragments is relaxed by antisymmetrization and renormalization of the summarized wave function $\Psi_A\Psi_B$. In this way, the Pauli principle requirements are satisfied and a new wave function Ψ^0 with corresponding energy E^0 is formed. The difference in energy between E^0_{AB} and E^0 is known as the exchange (Pauli) repulsion ΔE_{Pauli} (*Equation 3.37*).

$$\Delta E_{Pauli} = E^0_{AB} - E^0$$

Equation 3.37

Although theories of chemical bonding have defined various delicate attractive and repulsive contributions, the greatest interest is given to the effects responsible for the actual chemical bond formation. According to EDA, such a strong force, which acts as a "physical glue" and sticks atoms (or larger molecular species) together, is established and further enhanced in the third step of the analysis. In this step, the fragments are in final positions and are starting to relax from initial ψ^0 wave function to the final one Ψ_{AB}, with the energy E_{AB}. This attractive contribution, called the orbital interaction ΔE_{orb} (*Equation 3.38*), is practically established within the KS formalism by mixing of KS orbitals of the fragments.

$$\Delta E_{orb} = E_{AB} - E_{AB}^{0}$$

Equation 3.38

Since the stabilization originates from the orbital mixing (the wave function is optimized at this point), this term can be identified as the covalent component of a chemical bond. The type of orbital stabilization will depend on the nature of bonding fragments. Namely, if both fragments are closed-shell, the stabilization will occur due to the donor-acceptor mechanism, and the interaction of occupied orbital of one fragment, and a virtual orbital of the other. On the other hand, if unpaired electrons are included (usually located in a single occupied orbital on each fragment), orbital interaction will be based on the paring of these electrons into a bonding orbital, whereby the stabilization is established. Both cases can be observed in *Figure 3.4.* Orbital interaction component contains polarization effects, *i.e.* mixing of the filled and empty orbitals within one fragment due to the presence of the other one. It is important to highlight that ΔE_{orb} can be further decomposed into symmetry-defined components in the form of irreps, belonging to the symmetry point group of the molecule.

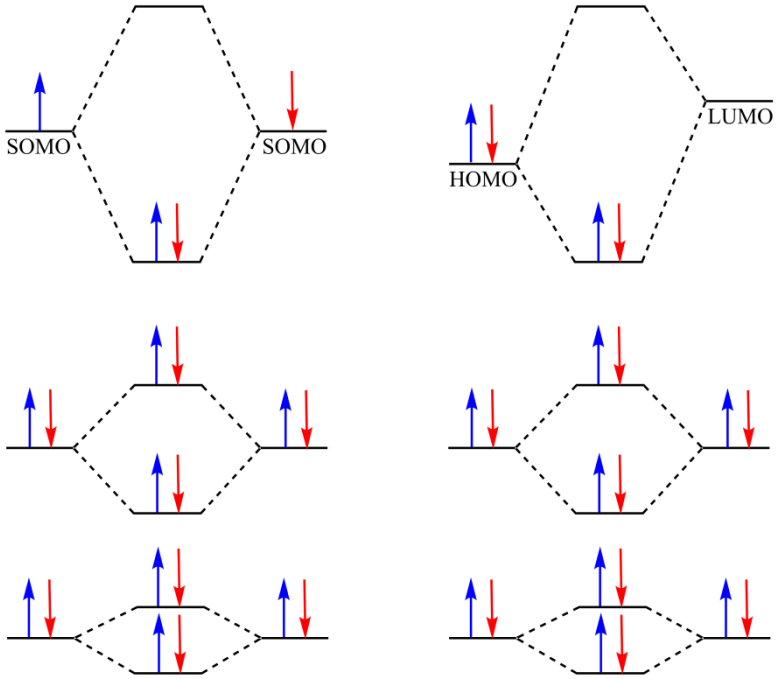

Figure 3.4. Orbital interaction diagram of two common bonding situations, wherein the case of open-shell fragments (left) a pairing mechanism occurs, and in case of closed-shell fragments (right) there is a donor-acceptor mechanism

The sum of these three contributions, ΔE_{elstat} , ΔE_{Pauli} and ΔE_{orb} , represents the total interaction energy ΔE_{int}. If the Grimme D3 dispersion correction is included in the calculation, there will be an additional ΔE_{disp} contribution to the ΔE_{int}. This insightful approach has been introduced for the first time by Ziegler and Rauk[277], and its main importance lies in the fact that the sum of ΔE_{prep} and ΔE_{int} represents the dissociation energy ΔE_{disoc} (*Equation 3.39*) for a certain molecular system, which can be determined experimentally.

$$\Delta E_{disoc} = E_{prep} + E_{int}$$

Equation 3.39

4. Our calculations and obtained results

Within this doctoral thesis, the complicated electronic structure of the aqua- and oxo- (hydroxo-) complexes of the first row TM series has been studied. The performance of various DFAs for the unambiguous determination of the ground electronic state was investigated, which is one of the most challenging tasks, from both theoretical and experimental point of view. Using the theoretical methods based on DFT, the energies of the ground and excited electronic states were calculated for the selected TM complexes. The primary challenge was to find an appropriate level of theory, able to explain the interrelationships between structural features and the electronic structure, and thus to rationalize experimentally obtained results.

The first part examines the performance of two different DFT-based methods (time-dependent density functional theory (TD-DFT) and density functional theory based on ligand field theory (LF-DFT)) for calculation of excited states and reproduction of experimentally obtained absorption spectra of a series of hexaqua complexes, where the central metal ion is $V^{2+/3+}$, $Cr^{2+/3+}$, $Mn^{2+/3+}$, $Fe^{2+/3+}$, $Co^{2+/3+,}$ and Ni^{2+}. In addition to the performance of the two methods mentioned, the influence of different DFAs is examined.[67]

The ground electronic (spin) state, as well as the close-lying excited states, are related to the geometry of the molecule. Changes in the first coordination sphere of a certain complex compound, which can look negligible, can result in significant changes in the energy and arrangement of the electronic states. For this reason, the second part of the results is devoted to the investigation of the influence of applied level of theory on the obtained geometric parameters of a series of oxo- (hydroxo-) iron complexes. For this purpose, 18 oxo- (hydroxo-) complexes, formed by the coordination of different ligands, are analyzed. Furthermore, various DFAs are tested in order to find the best choice for unambiguous determination of the ground spin state.[286]

In the third part, a detailed energy decomposition analysis (EDA) of a series of oxo- (hydroxo-) iron model complex is carried out, with the aim to collect some more insight about this kind of TM complex molecules.

Most present-day DFT calculations are performed in some of the well-developed quantum chemistry software. The most popular and the most accepted software packages are ADF[287-289] and Gaussian[290], and ORCA[291], yet there are many others like TURBOMOLE[292], Molcas[293], NWChem[294], Dalton[295], QChem[296], Quantemol[297], GAMESS[298], etc. Depending on the software chosen, one is able to work with Slater type orbitals (ADF code), Gaussian basis functions, plane waves (CPMD[299] code) or numerical basis functions (DMol[300] code), whereby all of them have certain individual advantages. For all DFT calculations that have been carried out, and presented in this thesis, we have utilized ADF program package. Specific computational details are at the end of every result subsection.

4.1. Theoretical investigation of d-d transitions of first-row TM hexaaqua complexes

From a broad palette of theoretical approaches (*Chapter 3.6*), convenient for investigation of excited states, in the present thesis we are utilizing two different methods, TD-DFT and LF-DFT, for investigation of *d-d* transitions within a series of first-row TM hexaaqua complexes. The systematic examination has been performed on six hexaaqua complexes, of general formula $[M(H_2O)_6]^{2+/3+}$ (*Figure 2.6.*), where $M^{2+/3+}$is: $V^{2+/3+}$, $Cr^{2+/3+}$, $Mn^{2+/3+}$, $Fe^{2+/3+}$, $Co^{2+/3+}$ and Ni^{2+}. Obtained results represent a good starting point for TD-DFT and LF-DFT performance validation in predicting the *d-*

d spectra of these molecular systems. Another important aspect of this study lies within the fact that different DFAs have been tested, and their influence on the final result reported. The results presented in forthcoming chapters are published, rationalized and discussed in the original paper.[67]

4.1.1. Geometry optimization of investigated first-row TM hexaaqua complexes

As a consequence of inherent water molecule symmetry, the highest possible symmetry arrangement (T_h) of six water molecules, surrounding the TM ions, has been imposed. However, ADF program package does not include T_h symmetry, thus for all geometrical optimizations, D_{2h} point group was imposed during geometry optimizations. This approach is consistent with the previous works[301-303] and is justified by the fact that spatial orientation of water ligands have no significant influence on calculated *d-d* transitions, as the orbitals are mainly localized on a metal center[304] (*Figure 4.1.*). It should be pointed out that although CT transitions can be strongly affected by the second coordination sphere[305], the *d-d* transition energies in aqua complexes are not sensitive to the inclusion of this factor.[303, 306, 307]

In T_h symmetry, five *d*-orbitals are categorized into two sets of irreps, whereas d_{x2-y2} and d_{z2} orbitals belong to the E_g, while on the other hand, the set of d_{xy}, d_{xz}, d_{yz} orbitals belong to the T_g irrep. In D_{2h} point group, d_{x2-y2} and d_{z2} orbitals belong to the same A_g irrep, while d_{xy}, d_{xz}, d_{yz} orbitals belong to the B_{1g}, B_{2g}, and B_{3g} irreducible representations. After the geometrical optimization of complexes having a non-degenerate ground spin states (d^3, d^5, and the low-spin d^6, and d^8) in D_{2h} point group orbitals belonging to B_{1g}, B_{2g}, and B_{3g} set, as well as d_{x2-y2} and d_{z2} orbitals belonging to the A_g irrep will maintain the degeneracy. For this reason, the number of transitions will be the same as in the corresponding complex in T_h symmetry. In this regard, obtained bands can be specified and assigned according to the Tanabe-Sugano[40] diagrams for octahedral coordination.

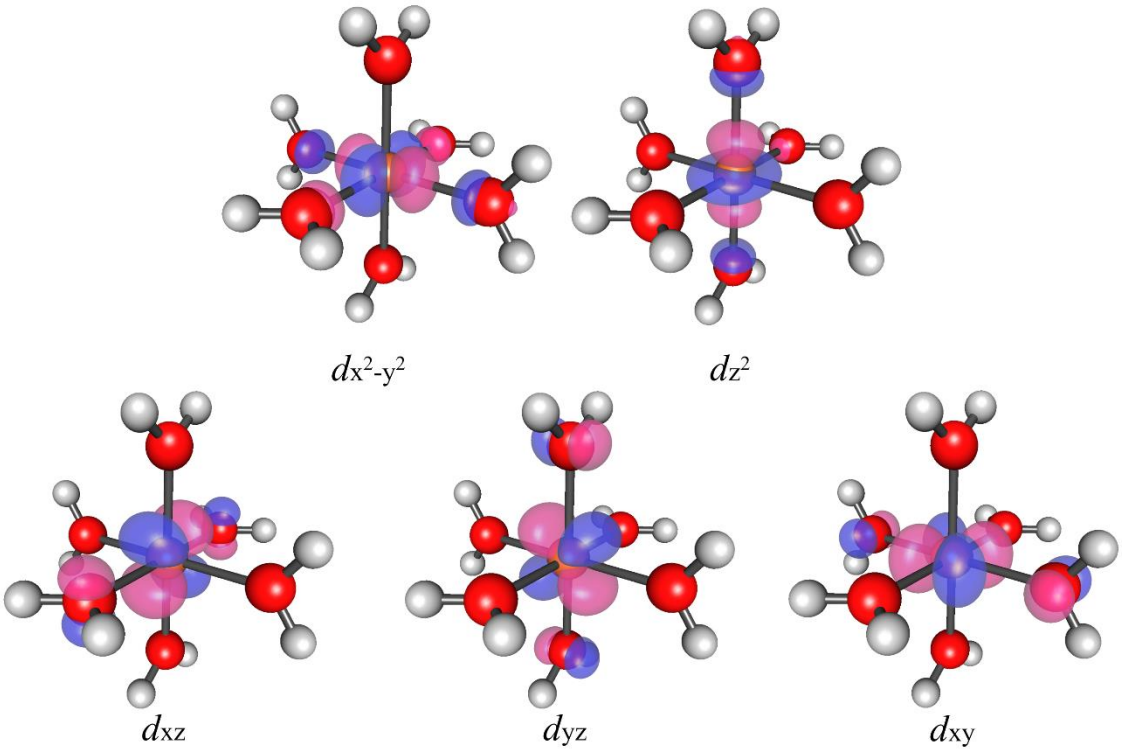

Figure 4.1. First-row TM hexaaqua complexes molecular orbitals with dominant *d*-character ($[Co(H_2O)_6]^{2+}$ complex, as an example in the figure)

Complexes $[V(H_2O)_6]^{3+}$, $[Cr(H_2O)_6]^{2+}$, $[Mn(H_2O)_6]^{3+}$, $[Fe(H_2O)_6]^{2+}$ and $[Co(H_2O)_6]^{2+}$, which are characterized with degenerate ground spin state, are considered as initialy susceptible to the JT distortion[308, 309]. Depending on the specific electronic configuration of the molecule, these complexes exhibit E_g or T_g electronic ground state, which can be observed from *Table 4.1*. This nuclear configuration is not a stationary point on the PES, thus there exists a coupling between the ground electronic state with the non-totally-symmetric vibrations, leading to the formation of distorted D_{2h} structures.[67] For this reason, orbital degeneracy present in T_h symmetry is lifted in the case of these configurations. Hence, theoretical calculations, as well as experimental observations, will report a greater number of excited states, than the one that can be expected for a complex in perfect T_h symmetry. It should be noted that, because of the single-determinant character of KS reference, for some of the investigated cases, which are slightly distorted from initial T_h symmetry, TD-DFT doesn't give a proper number of excitations.[310] All the possible splittings of the electronic states are well reproduced by means of LF-DFT, since this method respects the symmetry of the system, thus provides a complete description of the JT distortion. In order to simplify the presentation of the obtained results and create a clear conection of theoretically obtained results with experimental spectra, assignation of the electronic states for all complexes investigated in the present thesis will be given in T_h point group notation (although all complexes were optimized in D_{2h} symmetry).

The results of geometrical optimizations can be found in *Table 4.1*. Even though D_{2h} symmetry was applied during all calculations, in the case of complexes with non-degenerate ground spin state, optimized M-O bond lengths, as well as all obtained bond angles are equal. Generally speaking, theoretically obtained bond lengths, calculated on LDA level of theory are shorter than the experimentally reported ones, which can be expected for this specific functional (*Chapter 3.4.1*). Although B3LYP and OPBE functionals calculated slightly longer bond lengths, obtained values are in good agreement with experimental results. BP86 and PW91 levels of theory showed the best performance for the geometry optimization, whereby the bond lengths calculated with these two functionals are in the best agreement with experimental data. For this reason, our calculations of excited states, by utilizing TD-DFT and LF-DFT, were carried out on the structures obtained by both of these DFAs.

Table 4.1. DFT calculated M-O bond lengths [Å] of investigated complexes $[M(H_2O)_6]^{n+}$ at different levels of theory, $M^{2+/3+}$= $V^{2+/3+}$, $Cr^{2+/3+}$, $Mn^{2+/3+}$, $Fe^{2+/3+}$, $Co^{2+/3+}$, Ni^{2+}; ground state term in T_h point group, corresponding to the electronic configuration of a specific central metal ion is indicated

Complex	Electronic configuration	Ground state	LDA	BP86	PW91	OPBE	B3LYP	Exp.	Exp. Ref.
$[V(H_2O)_6]^{3+}$	d^2	^3T_g	1.915 1.987 1.989 av. 1.964	1.956 2.036 2.039 av. 2.010	1.954 2.034 2.038 av. 2.015	1.956 2.043 2.045 av. 2.015	1.965 2.033 2.039 av. 2.012	1.986 1.987 1.993 av. 1.989	311
$[V(H_2O)_6]^{2+}$	d^3	^4A_g	2.058	2.130	2.125	2.147	2.143	2.128	312
$[Cr(H_2O)_6]^{3+}$	d^3	^4A_g	1.926	1.972	1.970	1.974	1.975	1.959	313
$[Cr(H_2O)_6]^{2+}$	d^4	^5E_g	1.998 2.002 2.273 av. 2.091	2.056 2.058 2.391 av. 2.168	2.052 2.059 2.379 av. 2.163	2.061 2.069 2.553 av. 2.228	2.076 2.077 2.368 av. 2.174	2.052 2.122 2.327 av. 2.167	314
$[Mn(H_2O)_6]^{3+}$	d^4	^5E_g	1.891 1.895 2.072 av. 1.953	1.934 1.937 2.133 av. 2.001	1.932 1.936 2.130 av. 1.999	1.932 1.939 2.167 av. 2.013	1.936 1.938 2.128 av. 2.001	1.924 1.929 2.129 av. 1.994	315
$[Mn(H_2O)_6]^{2+}$	d^5	^6A_g	2.106	2.176	2.174	2.213	2.182	2.192	312
$[Fe(H_2O)_6]^{3+}$	d^5	^6A_g	2.969	2.018	2.016	2.027	2.011	1.995	313
$[Fe(H_2O)_6]^{2+}$	d^6	^5T_g	2.023 2.030 2.112 av. 2.055	2.095 2.100 2.187 av. 2.127	2.086 2.093 2.191 av. 2.123	2.121 2.122 2.244 av. 2.162	2.092 2.112 2.192 av. 2.132	2.098 2.128 2.137 av. 2.121	316
$[Co(H_2O)_6]^{3+}$	d^6	^1A_g	1.837	1.885	1.950	1.881	1.885	1.873	312
$[Co(H_2O)_6]^{2+}$	d^7	^4T_g	1.952 2.044 2.046 av. 2.014	2.016 2.113 2.125 av. 2.085	2.016 2.106 2.120 av. 2.081	2.037 2.153 2.160 av. 2.117	2.035 2.108 2.131 av. 2.091	2.044 2.084 2.094 av. 2.074	317
$[Ni(H_2O)_6]^{2+}$	d^8	^3A_g	1.979	2.049	2.047	2.074	2.057	2.061	312

4.1.2. d^2 Electronic spectrum of V(III) complex

"Electronic configuration of $[V(H_2O)_6]^{3+}$ complex cation in T_h symmetry is t_g^2, yielding a ^3T_g ground state. According to the Tanabe-Sugano diagram for d^2 configuration, the lowest excitations belong to the three spin-forbidden triplet to singlet transitions, *i.e.*, $^3T_g \rightarrow {}^1A_g$, $^3T_g \rightarrow {}^1T_g$, and $^3T_g \rightarrow {}^1E_g$, originating from the same t^2 configuration. The promotion of one electron from the t_g to e_g orbitals ($t_g^2 \rightarrow t_g^1 e_g^1$), results in two ^3T_g states ($^3T_{1g}$ and $^3T_{2g}$ in O_h point group), and two ^1T_g excited states ($^1T_{1g}$ and $^1T_{2g}$ in O_h symmetry). Experimentally obtained spectrum of $[V(H_2O)_6]^{3+}$ contains two main asymmetric absorption bands, assigned to two spin-allowed ^3T_g transitions, the first at 17100 cm^{-1} and second at 25200 cm^{-1}[1318]."[67]

"TD-DFT and LF-DFT results are listed in *Table 4.2.* and *Table 4.3.*, respectively. Splitting of the orbitally triple degenerate ground state in T_h point group, due to the JT effect, experimentally observed by the electronic Raman spectra[319], is reproduced well with both methods Generally, both TD-DFT and LF-DFT reproduced the experimental spectrum with good accuracy, for the two main transitions, as well as, for the other bands obtained by the Gaussian analysis of the spectrum. Regardless of the chosen geometry, TD-DFT on M06L and SAOP level of theory gave very poor results."[67]

"By comparing TD-DFT and LF-DFT results, one can notice far better performance of LF-DFT method. Generally, both TD-DFT and LF-DFT results are in good agreement with high-quality CASSCF/SORCI calculations by Neese *et al*[320]. Recently, Shatz at al calculated first ^3T_g state with large deviation (CASSCF ΔE=5800cm^{-1}, CASPT2 ΔE=4700 cm^{-1} MRCI ΔE=5700 cm^{-1}) from experimental value[302]. Furthermore, CASSCF/CASPT2 calculations by Laundry-Hum gave much lower values for the first ^3T_g transition.[321] Recent CASPT2/NEVPT2 calculations by Radon reproduced the first transition accurately, yet strongly overestimated the second transition[305]."[67]

Table 4.2. TD-DFT vertical excitation energies [cm^{-1}] calculated for $[V(H_2O)_6]^{3+}$ complex at different levels of theory; mean absolute error (MAE) is given in cm^{-1}; assignment (electronic state and its configuration) in formally T_h point group is indicated

BP86 geometry

Assign. (T_h)	BP86	PW91	OPBE	SSBD	B3LYP	CAMB3LYP	PBE0	OPBE0	M06L	SAOP	Exp[318]
^3Tg ($t_{2g}^2e_g^0$)	0	0	0	0	0	0	0	0	0	0	0
	2931	2859	2397	3463	2676	2492	2194	1990	6297	12287	1940[319]
^1Tg ($t_{2g}^2e_g^0$)	7127	6859	9609	9294	6630	6502	6900	8954	13612	26625	9860
	12687	12346	15409	14908	11304	11445	12602	14881	18721	25629	12200
^3Tg ($t_{2g}^1e_g^1$)	19266	19097	18046	18824	18135	18032	17586	16823	24019	12287	17200
	23069	22756	24161	24370	22323	22381	22342	23645	30390	40142	19600
^3Tg ($t_{2g}^1e_g^1$)	24853	24679	22921	24212	25658	25779	25234	24121	29630	28497	25200
	26218	26576	28351	28364	27234	27450	27092	28437	35057	44841	27900
MAE ($^3T_g \rightarrow {}^3\Gamma$)	1711	1563	1719	1874	1103	1039	845	1217	6711	11208	
MAE ($^3T_g \rightarrow {}^1\Gamma$)	1610	1570	1730	1637	2063	2056	1681	1793	5136	15097	
MAE	1682	1566	1722	1806	1377	1329	1084	1382	6261	12319	

PW91 geometry

Assign. (T_h)	BP86	PW91	OPBE	SSBD	B3LYP	CAMB3LYP	PBE0	OPBE0	M06L	SAOP	Exp[318]
^3Tg ($t_{2g}^2e_g^0$)	0	0	0	0	0	0	0	0	0	0	0
	2958	2885	2422	3491	2700	2515	2218	2012	6330	12314	1940[319]
^1Tg ($t_{2g}^2e_g^0$)	7222	6956	9740	9320	6626	6480	6915	8992	13613	26557	9860
	12683	12341	15399	14901	11299	11440	12597	14874	18716	25587	12200
^3Tg ($t_{2g}^1e_g^1$)	18228	18228	18228	18228	18228	18228	18228	18228	18228	18228	17200
	23170	22859	24580	24470	22418	22475	22435	23736	30493	40201	19600
^3Tg ($t_{2g}^1e_g^1$)	24937	24762	23009	24296	25737	25858	25317	24206	29721	28623	25200
	26354	26646	28417	28429	27305	27522	27169	28511	35123	44865	27900
MAE ($^3T_g \rightarrow {}^3\Gamma$)	1485	1385	1839	1776	1147	1103	998	1368	5611	10478	
MAE ($^3T_g \rightarrow {}^1\Gamma$)	1560	1522	1659	1620	2067	2070	1671	1771	5134	15042	
MAE	1506	1424	1788	1732	1410	1379	1190	1483	5474	11782	

Table 4.3. LF-DFT vertical excitation energies [cm^{-1}] calculated for $[V(H_2O)_6]^{3+}$ complex at different levels of theory; mean absolute error (MAE) is given in cm^{-1}; assignment (electronic state and its configuration) in formally T_h point group is indicated

BP86 geometry

Assign. (T_h)	BP86	PW91	OPBE	SSBD	B3LYP	CAMB3LYP	PBE0	OPBE0	Exp[318]
	0	0	0	0	0	0	0	0	0
^3Tg ($t_{2g}^2e_g^0$)	909	899	841	900	855	844	837	798	1940[319]
	1092	1086	1074	1056	961	930	955	941	
	9654	9557	10520	10407	9506	9494	10006	10713	9860
^1Tg ($t_{2g}^2e_g^0$)	10611	10508	11479	11320	10319	10300	10811	11512	12200
	11032	10925	11857	11763	10772	10731	11254	11931	
	15255	15212	14814	14408	14995	15229	15146	14848	17200
^3Tg ($t_{2g}^1e_g^1$)	16235	16186	15776	15351	15829	16025	15974	15663	19600
	17590	17547	17221	16697	17374	17687	17578	17309	
	23862	23796	22909	22882	24047	24134	23755	23193	25200
^3Tg ($t_{2g}^1e_g^1$)	25884	25811	24900	24917	26285	26493	26016	25429	27900
	27159	27079	26150	26159	27442	27621	27162	26556	
MAE ($^3T_g \rightarrow {}^3\Gamma$)	1424	1472	1986	2173	1447	1290	1492	1844	
MAE ($^3T_g \rightarrow {}^1\Gamma$)	792	893	596	602	1004	1025	656	665	
MAE	1243	1306	1589	1724	1320	1214	1253	1507	

PW91 geometry

Assign. (T_h)	BP86	PW91	OPBE	SSBD	B3LYP	CAMB3LYP	PBE0	OPBE0	Exp[318]
	0	0	0	0	0	0	0	0	0
^3Tg ($t_{2g}^2e_g^0$)	917	907	848	908	863	852	845	805	1940[319]
	1113	1107	1094	1077	981	949	975	960	
	9648	9550	10512	10401	9499	9487	10000	10705	9860
^1Tg ($t_{2g}^2e_g^0$)	10630	10526	11496	11339	10324	10304	10828	11527	12200
	11046	10938	11870	11777	10784	10742	11266	11942	
	15343	15299	14902	14494	15081	15317	15234	14936	17200
^3Tg ($t_{2g}^1e_g^1$)	16321	16272	15863	15434	15912	16109	16058	15748	19600
	17715	17672	17348	16819	17499	17815	17704	17435	
	23940	23873	22989	22957	24120	24207	23830	23269	25200
^3Tg ($t_{2g}^1e_g^1$)	25971	25897	24989	25002	26371	26582	26105	25518	27900

	27291	27210	26283	26289	27573	27755	27295	26689
MAE ($^3T_g \rightarrow {}^3\Gamma$)	1341	1390	1902	2092	1366	1207	1410	1762
MAE ($^3T_g \rightarrow {}^1\Gamma$)	787	889	584	591	1003	1025	646	655
MAE	1183	1246	1526	1663	1262	1155	1191	1445

4.1.3. d^3 Electronic spectra of V(II) and Cr(III) hexaaqua complexes

"Ground electronic configuration of $[V(H_2O)_6]^{2+}$ and $[Cr(H_2O)_6]^{3+}$ complexes in T_h symmetry is t_g^3. The ground electronic state in both investigated structures is ^4A_g. According to the lowest three excitations belong to the spin-flip forbidden transitions within the ground t_g^3 electronic configuration, *i.e.* ^2E_g, ^2T_g and ^2T_g states. The first two spin-allowed transitions are from the ground ^4A_g state to the two ^4T_g states, one corresponding to $^4T_{1g}$ and other to the $^4T_{2g}$ in O_h symmetry. These transitions represent the promotion of the one-electron from the t_g orbitals to the eg orbitals, and transition to the $^4T_{2g}$ state corresponds to the LF splitting Δ. The doublets originating from the same excited electronic configuration are the two ^2A_g, two ^2E_g, and four ^2T_g. The promotion of two electrons from t_g orbitals into e_g orbitals, without changing the spin yields ^4T_g as a high lying excited state ($^4T_{1g}$ in O_h symmetry). The same excitation $t_g^3 \rightarrow t_g^1 e_g^2$, accompanied by the spin-flip, gives four ^2T_g states. Simultaneous excitation of all three electrons from t_g orbitals to e_g orbitals, *i.e.* $t_g^3 \rightarrow t_g^0 e_g^3$ ($^4A_g \rightarrow {}^2E_g$), is also spin forbidden. Despite all these excitation possibilities, only three transitions are observed in the case of $[V(H_2O)_6]^{2+}$, and four transitions in the case of $[Cr(H_2O)_6]^{3+}$ complex cation[322]."[67]

"TD-DFT failed to reproduce experimental data for both $[V(H_2O)_6]^{2+}$ and $[Cr(H_2O)_6]^{3+}$, *Table 4.4.* and *Tables 4.6.*, in particular, the relative position of the first two bands. Furthermore, adiabatic TD-DFT was not able to calculate the experimentally observed double excitation ($t^3 \rightarrow t^1e^2$), although this transition was clearly seen experimentally[323]. However, the spin-forbidden transition, $^4A_g \rightarrow {}^2E_g$, of $[Cr(H_2O)_6]^{3+}$ is calculated with very good accuracy with B3LYP, BP86, PW91, and CAM-B3LYP."[67]

Table 4.4. TD-DFT vertical excitation energies [cm^{-1}] calculated for $[V(H_2O)_6]^{2+}$ complex at different levels of theory; mean absolute error (MAE) is given in cm^{-1}; assignment (electronic state and its configuration) in formally T_h point group is indicated

BP86 geometries

Assign. (T_h)	BP86	PW91	OPBE	SSBD	B3LYP	CAMB3LYP	PBE0	OPBE0	M06L	SAOP	Exp[322]
^4A_g ($t_{2g}^3e_g^0$)	0	0	0	0	0	0	0	0	0	0	0
^4T_g ($t_{2g}^2e_g^1$)	17435	17201	15827	16813	16466	16335	15702	14630	23298	24474	12350
^4T_g ($t_{2g}^2e_g^1$)	20010	18483	18496	19460	20753	20781	20407	19421	26026	27121	18500
^4T_g ($t_{2g}^1e_g^2$)	-	-	-	-	-	-	-	-	-	-	27900
MAE	3297	2434	1715	2686	3159	3108	2604	1575	9212	10347	

PW91 geometries

Assign. (T_h)	BP86	PW91	OPBE	SSBD	B3LYP	CAMB3LYP	PBE0	OPBE0	M06L	SAOP	Exp[322]
^4A_g ($t_{2g}^3e_g^0$)	0	0	0	0	0	0	0	0	0	0	0
^4T_g ($t_{2g}^2e_g^1$)	17560	17279	15938	16892	16604	16476	15836	14754	23427	24586	12350
^4T_g ($t_{2g}^2e_g^1$)	20124	18297	18599	19522	20880	20917	20534	19537	26146	27222	18500
^4T_g ($t_{2g}^1e_g^2$)	-	-	-	-	-	-	-	-	-	-	27900
MAE	3392	2541	1818	2757	3292	3246	2735	1695	9336	10454	

"In contrast, LF-DFT shows remarkably well performance for both $[V(H_2O)_6]^{2+}$ and $[Cr(H_2O)_6]^{3+,}$ *Table 4.5.* and *Tables 4.7.*, and the only discrepancy is observed at CAM-B3LYP level of theory for $[V(H_2O)_6]^{2+}$, because of the overestimation of the ligand-field splitting. LF-DFT results are also in good agreement with previous INDO/S[324], SORCI[320], and MRCI[302] calculations. In addition, in the case of $[Cr(H_2O)_6]^{3+}$, the third spin-allowed transition, arising from the double excitation, is calculated with even higher precision with LF-DFT than with *ab initio* methods. Transition to ^4T_g state is calculated with even higher precision using LF-DFT method. LF-DFT proved to be more accurate in comparison to recent CASSCF/CASPT2[302] calculations. The transition to the first ^4T_g state, experimentally found at ~17400 cm^{-1}, was calculated with the deviation of 3800 cm^{-1} (CASSCF) and 3100 cm^{-1} (CASPT2)[302]. Furthermore, the transition experimentally found at ~ 37800 was calculated with the error of 3300 cm^{-1} using CASPT2[302]and the error of 1900 cm^{-1} (2300 cm^{-1}) with CASPT2/NEVPT2[305]."[67]

Table 4.5. LF-DFT vertical excitation energies [cm^{-1}] calculated for $[V(H_2O)_6]^{2+}$ complex at different levels of theory; mean absolute error (MAE) is given in cm^{-1}; assignment (electronic state and its configuration) in formally T_h point group is indicated

BP86 geometries									
Assign. (T_h)	BP86	PW91	OPBE	SSBD	B3LYP	CAMB3LYP	PBE0	OPBE0	Exp[322]
^4A_g ($t_{2g}^3e_g^0$)	0	0	0	0	0	0	0	0	0
^4T_g ($t_{2g}^2e_g^1$)	12311	12343	11605	11563	12899	15251	13048	12432	12350
^4T_g ($t_{2g}^2e_g^1$)	18189	18107	17119	17206	18864	21228	19006	18217	18500
^4T_g ($t_{2g}^1e_g^2$)	28266	28148	26605	26743	29332	33431	29566	28322	27900
MAE	239	216	1140	1079	782	3720	957	262	
PW91 geometries									
Assign. (T_h)	BP86	PW91	OPBE	SSBD	B3LYP	CAMB3LYP	PBE0	OPBE0	Exp[322]
^4A_g ($t_{2g}^3e_g^0$)	0	0	0	0	0	0	0	0	0
^4T_g ($t_{2g}^2e_g^1$)	12460	12530	11761	11706	13086	15732	13224	12621	12350
^4T_g ($t_{2g}^2e_g^1$)	18354	18226	17298	17352	19093	21716	19180	18428	18500
^4T_g ($t_{2g}^1e_g^2$)	28525	28358	26886	26967	29696	34316	29855	28659	27900
MAE	244	254	985	958	992	4288	1120	317	

Table 4.6. TD-DFT vertical excitation energies [cm^{-1}] calculated for $[Cr(H_2O)_6]^{3+}$ complex at different levels of theory; mean absolute error (MAE) is given in cm^{-1}; assignment (electronic state and its configuration) in formally T_h point group is indicated

BP86 geometry

Assign. (T_h)	BP86	PW91	OPBE	SSBD	B3LYP	CAMB3LYP	PBE0	OPBE0	M06L	SAOP	Exp[322]
^4A_g ($t_{2g}^3e_g^0$)	0	0	0	0	0	0	0	0	0	0	0
^2E_g ($t_{2g}^3e_g^0$)	16295	15969	19876	19414	15890	16183	17614	20680	24392	32569	15000
^4T_g ($t_{2g}^2e_g^1$)	21410	21308	19388	20748	21158	21246	20451	19266	26403	25872	17400
^4T_g ($t_{2g}^2e_g^1$)	23512	23422	21390	22792	25305	25642	25057	19254	28451	27617	24600
^4T_g ($t_{2g}^1e_g^2$)	-	-	-	-	-	-	-	-	-	-	37800
MAE ($^4T_g \rightarrow {}^4\Gamma$)	2549	2543	2599	2578	2231	2444	1754	3606	6427	5744	
MAE ($^4T_g \rightarrow {}^2\Gamma$)	1295	969	4876	44414	890	1183	2614	5680	9329	17569	
MAE	2131	2018	3358	3190	1784	2023	2041	4297	7415	9686	

PW91 geometry

Assign. (T_h)	BP86	PW91	OPBE	SSBD	B3LYP	CAMB3LYP	PBE0	OPBE0	M06L	SAOP	Exp[322]
^4A_g ($t_{2g}^3e_g^0$)	0	0	0	0	0	0	0	0	0	0	0
^2E_g ($t_{2g}^3e_g^0$)	16291	15966	19866	19407	15885	16177	17607	20667	24392	32538	15000
^4T_g ($t_{2g}^2e_g^1$)	21492	21391	19472	20833	21233	21321	25971	19342	26483	20527	17400
^4T_g ($t_{2g}^2e_g^1$)	23594	23504	21474	22883	25379	25712	25133	23915	28537	27719	24600
^4T_g ($t_{2g}^1e_g^2$)	-	-	-	-	-	-	-	-	-	-	37800
MAE ($^4T_g \rightarrow {}^4\Gamma$)	2599	2593	2649	2625	2256	2466	4502	1365	6460	3073	
MAE ($^4T_g \rightarrow {}^2\Gamma$)	1291	966	4866	4407	885	1177	2607	5667	9392	17538	
MAE	2163	2051	3388	3219	1799	2037	3870	2798	7437	7895	

Table 4.7. LF-DFT vertical excitation energies [cm^{-1}] calculated for $[Cr(H_2O)_6]^{3+}$ complex at different levels of theory; mean absolute error (MAE) is given in cm^{-1}; assignment (electronic state and its configuration) in formally T_h point group is indicated

BP86 geometry

Assign.(T_h)	BP86	PW91	OPBE	SSBD	B3LYP	CAMB3LYP	PBE0	OPBE0	Exp[322]
^4A_g ($t_{2g}^3e_g^0$)	0	0	0	0	0	0	0	0	0
^2E_g ($t_{2g}^3e_g^0$)	12886	12769	14325	14120	12674	12758	13630	14736	15000
^4T_g ($t_{2g}^2e_g^1$)	17078	17043	16665	16167	16730	16861	16812	16559	17400
^4T_g ($t_{2g}^2e_g^1$)	24052	24004	23182	22950	24102	24245	23998	23497	24600
^4T_g ($t_{2g}^1e_g^2$)	37718	37642	36518	35900	37562	37801	37482	36760	37800
MAE ($^4T_g \rightarrow {}^4\Gamma$)	317	370	1145	1594	469	298	503	995	
MAE ($^4T_g \rightarrow {}^2\Gamma$)	2114	2231	675	880	2326	2242	1370	264	
MAE	766	835	1027	1416	933	784	719	812	

PW91 geometry

Assign. (T_h)	BP86	PW91	OPBE	SSBD	B3LYP	CAMB3LYP	PBE0	OPBE0	Exp[322]
^4A_g ($t_{2g}^3e_g^0$)	0	0	0	0	0	0	0	0	0
^2E_g ($t_{2g}^3e_g^0$)	12905	12786	14336	14140	12682	12756	13640	14745	15000
^4T_g ($t_{2g}^2e_g^1$)	17154	17119	16743	16240	16806	16938	16888	16636	17400
^4T_g ($t_{2g}^2e_g^1$)	24140	24095	23266	23036	24197	24332	24096	23594	24600
^4T_g ($t_{2g}^1e_g^2$)	37866	37793	36664	36043	37716	37945	37639	36918	37800
MAE ($^4T_g \rightarrow {}^4\Gamma$)	291	298	1075	1527	394	325	425	917	
MAE ($^4T_g \rightarrow {}^2\Gamma$)	2095	2214	664	860	2318	2244	1360	255	
MAE	546	578	513	1360	612	805	659	407	

"High overestimation of the first transition to the ^4T_g excited state by TD-DFT is obviously due to the lack of orbital relaxation. Lack of orbital relaxation in TD-DFT, has been recently analyzed by Ziegler *et al*.[325] In TM complexes, this is a particularly important issue for the excitations that depend only on the ligand field splitting Δ, like in these two cases ($^4A_{2g}$ to $^4T_{2g}$). On the other hand, orbitals used in LF-DFT are prepared utilizing the variational DFT-AOC-SCF procedure, circumventing problems related to the orbital relaxation. Another important issue in d^3 systems is CI mixing between $^4T_{1g}(F)$ and $^4T_{1g}(P)$ states. Since later one nominally corresponds to double excitation, this mixing is missing in adiabatic TD-DFT methodology. If we consider LF parameters for $[V(H_2O)_6]^{2+}$ and $[Cr(H_2O)_6]^{3+}$, the double excitation character of, lower, $^4T_{1g}(F)$ state is 16.5% and 9.5%, respectively. This leads to the stabilization of this state due to its double excitation character for around 1,600 and 1,300 cm^{-1}, respectively, which is however in the range of precision of these calculations. LF-DFT, as a non-empirical approach to the LFT, is performing very well for such situations."[67]

4.1.4. d^4 Electronic spectra of Cr(II) and Mn(III) hexaaqua complexes

"Electronic configuration of both, $[Cr(H_2O)_6]^{2+}$ and $[Mn(H_2O)_6]^{3+}$ complexes, in T_h symmetry is $t_g^3e_g^1$. The ground electronic state is ^5E_g. The only spin-allowed excitation belongs to the transition of one electron from t_g orbitals to e_g orbitals ($t_g^3e_g^1 \rightarrow t_g^2e_g^2$), resulting with ^5T_g excited state ($^5T_{2g}$ in O_h symmetry). The unequal population of the anti-bonding e_g orbitals in the ground state leads to the strong JT distortion that can be clearly reflected in the absorption spectra of these two complexes.[68, 326] Instead of a single $^5E_g \rightarrow {}^5T_g$ band, two major bands are observed. The first one, lower in energy, originates from the JT splitting of the ground state, and the second, broad asymmetric band, from the splitting of the excited ^5T_g state. The spectrum of $[Cr(H_2O)_6]^{2+}$ consists of two major bands centered at 8000 cm^{-1} and 14550 cm^{-1}, with a shoulder at 18050 cm^{-1} (*Tables 14.* and *15.*). On the other hand, in the spectrum of $[Mn(H_2O)_6]^{3+}$, the bands occur at 9800 cm^{-1} and 20000 - 21000 cm^{-1} (*Tables 16.* and *17.*)."[67]

Table 4.8. TD-DFT vertical excitation energies [cm^{-1}] calculated for $[Cr(H_2O)_6]^{2+}$ complex at different levels of theory; mean absolute error (MAE) is given in cm^{-1}; assignment (electronic state and its configuration) in formally T_h point group is indicated

BP86 geometries

Assign. (T_h)	BP86	PW91	OPBE	SSBD	B3LYP	CAMB3LYP	PBE0	OPBE0	M06L	SAOP	Exp[68]
$^5E_g\,(t_{2g}^3e_g^1)$	0 8070	0 7800	0 7313	0 8443	0 7973	0 7864	0 7709	0 7246	0 12385	0 14066	0 8000
$^5T_g\,(t_{2g}^2e_g^2)$	15277 17424 18006	15219 15219 17946	14156 16128 16329	15102 17196 17574	14697 16431 17063	14576 16233 16948	14288 16023 16089	13583 14831 15306	20988 23121 23375	20536 22464 22506	14550 18050
MAE	377	426	967	553	492	540	849	1567	5340	5495	

PW91 geometries

Assign. (T_h)	BP86	PW91	OPBE	SSBD	B3LYP	CAMB3LYP	PBE0	OPBE0	M06L	SAOP	Exp[68]
$^5E_g\,(t_{2g}^3e_g^1)$	0 7905	0 7968	0 7147	0 8291	0 7823	0 7717	0 7559	0 7095	0 12230	0 13921	0 8000
$^5T_g\,(t_{2g}^2e_g^2)$	15345 17465 18061	15154 17285 17892	14227 16185 16369	15172 17245 17637	14751 16471 17114	14629 16274 16999	14347 16064 16142	13646 14884 15347	21044 23169 23433	20600 22499 22561	14550 18050
MAE	654	620	1063	787	724	745	1001	1297	5723	5810	

Table 4.9. LF-DFT vertical excitation energies [cm^{-1}] calculated for $[Cr(H_2O)_6]^{2+}$ complex at different levels of theory; mean absolute error (MAE) is given in cm^{-1}; assignment (electronic state and its configuration) in formally T_h point group is indicated

BP86 geometries

Assign. (T_h)	BP86	PW91	OPBE	SSBD	B3LYP	CAMB3LYP	PBE0	OPBE0	Exp[68]
$^5E_g\,(t_{2g}^3e_g^1)$	0 7308	0 7229	0 6820	0 7019	0 7362	0 7461	0 7304	0 7028	0 8000
$^5T_g\,(t_{2g}^2e_g^2)$	13069 13075 15139	12988 12995 15037	12376 12501 14325	12278 12407 14382	12824 13090 14817	13034 13339 14984	12839 13070 14750	12428 12577 14178	14550 18050
MAE	1694	1780	2338	2285	1821	1656	1863	2297	

PW91 geometries

Assign. (T_h)	BP86	PW91	OPBE	SSBD	B3LYP	CAMB3LYP	PBE0	OPBE0	Exp[68]
$^5E_g\,(t_{2g}^3e_g^1)$	0 7170	0 7092	0 6697	0 6886	0 7231	0 7332	0 7177	0 6910	0 8000
$^5T_g\,(t_{2g}^2e_g^2)$	13130 13163 15185	13056 13075 15083	12463 12562 14373	12337 12489 14423	12890 13171 14864	13105 13422 15037	12906 13153 14801	12495 12659 14229	14550 18050
MAE	1699	1786	2339	2293	1824	1656	1864	2295	

"TD-DFT reproduced the experimental transitions of $[Cr(H_2O)_6]^{2+}$ with high accuracy (*Table 4.8.)*, with a mean absolute error (MAE) less than 1000 cm^{-1}. SAOP and M06-L gave transitions intensely shifted toward higher wave-numbers. TD-DFT results for this complex ion are somewhat better than those obtained with LF-DFT. Although LF-DFT reproduced the first band with high accuracy, regardless of the level of theory (*Table 4.9.*), the second transition is underestimated, and shoulder at 18,050 cm^{-1} is not observed. Schatz *et al.*[302] highly underestimated the first transition with the error of ~4400 cm^{-1}, 3800 cm^{-1}, and 4700 cm^{-1} by using CASSCF, CASPT2 and MRCI, respectively. Recent calculations[305] using CASPT2/NEVPT2 bigger basis sets/active space overestimated this transition with the error of ~1200 cm^{-1}. The second transition was calculated with a deviation of ~3300 cm^{-1} (CASSCF) and ~3100 cm^{-1} (MRCI). Neese *et al.*[327], using CASSCF and SORCI, also reported values for the splitting of the ^5E_g term that are underestimated by ~3500 - 4000 cm^{-1}, if compared with experimental observation. The authors suggested that strain influences the splitting of the ^5E_g state, shifting the first experimental transition to the higher energy for approximately 1500 cm^{-1}."[67]

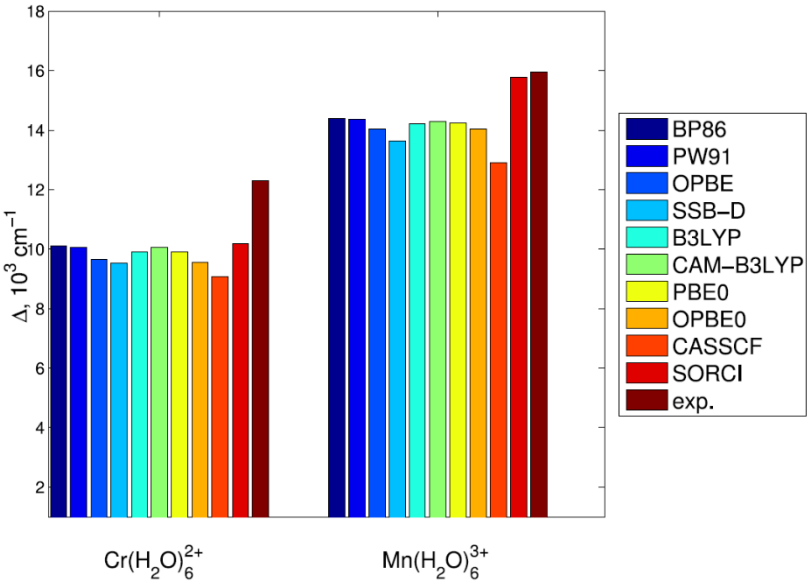

Figure 4.2. Ligand field strength of $[Cr(H_2O)_6]^{2+}$ and $[Mn(H_2O)_6]^{3+}$ obtained from LF-DFT calculations with different XC functionals, and compared with CASSCF and SORCI results and experiment

"In the case of $[Mn(H_2O)_6]^{3+}$, TD-DFT calculations on B3LYP, M06-L, CAM-B3LYP, and PBE0 level of theory show good agreement with the experimental data. Again, TD-DFT showed better performance than LF-DFT. Both TD-DFT and LF-DFT match better the experimental spectrum, than CASSCF/MRCI study done by Schatz *et al.* [302], who obtained the deviation of calculated value for the first transition of ∼3400 cm−1 (CASSCF) and ∼3100 cm−1 (MRCI). Good agreement with the experimental values was obtained using CASPT2/NEVPT2[305], yet the comparison was carried out on the spectra obtained from a solution."[67]

"LF-DFT calculated ligand-field strength, Δ, (*Appendix section*), for both $[Cr(H_2O)_6]^{2+}$ and $[Mn(H_2O)_6]^{3+}$ in perfect octahedral coordination environment, is in a good agreement with the high-level *ab initio* calculations by Neese *et al*[320]."[67]

Table 4.10. TD-DFT vertical excitation energies [cm^{-1}] calculated for $[Mn(H_2O)_6]^{3+}$ complex at different levels of theory; mean absolute error (MAE) is given in cm^{-1}; assignment (electronic state and its configuration) in formally T_h point group is indicated

BP86 geometries

Assign. (T_h)	BP86	PW91	OPBE	SSBD	B3LYP	CAMB3LYP	PBE0	OPBE	M06L	SAOP	Exp[326]
$^5E_g\,(t_{2g}^3e_g^1)$	0 6554	0 6489	0 5782	0 6827	0 7216	0 7371	0 7104	0 5782	0 9577	0 10048	0 9800
$^5T_g\,(t_{2g}^2e_g^2)$	15347 16517 18494	15356 16484 18474	11636 14313 15701	11695 14555 16026	18001 19743 20004	18550 20651 20876	17950 19565 20019	11636 14313 15701	15858 18641 20037	12646 16401 17436	20000 21100
MAE	3307	3339	5481	2911	1602	1017	1673	5481	1345	3129	

PW91 geometries

Assign. (T_h)	BP86	PW91	OPBE	SSBD	B3LYP	CAMB3LYP	PBE0	OPBE	M06L	SAOP	Exp[326]
$^5E_g\,(t_{2g}^3e_g^1)$	0 6568	0 6501	0 5796	0 6839	0 7227	0 7380	0 7113	0 5796	0 9595	0 10085	0 9800
$^5T_g\,(t_{2g}^2e_g^2)$	15539 16639 18629	15547 16604 18608	11853 14451 15855	11911 14690 16183	18110 19882 20109	18653 20746 20992	18061 19667 20150	11853 14451 15855	16090 18782 20212	12887 16563 17632	20000 21100
MAE	3204	3238	5365	3446	1522	942	1591	5365	1219	3009	

Table 4.11. LF-DFT vertical excitation energies [cm^{-1}] calculated for $[Mn(H_2O)_6]^{3+}$ complex at different levels of theory; mean absolute error (MAE) is given in cm^{-1}; assignment (electronic state and its configuration) in formally T_h point group is indicated

BP86 geometries									
Assign. (T_h)	BP86	PW91	OPBE	SSBD	B3LYP	CAMB3LYP	PBE0	OPBE0	Exp[326]
$^5E_g\,(t_{2g}^3e_g^1)$	0 6437	0 6420	0 6286	0 6272	0 6474	0 6531	0 6475	0 6387	0 9800
$^5T_g\,(t_{2g}^2e_g^2)$	16826 16984 18985	16800 16961 18950	16403 16642 18498	16041 16131 18103	16747 16809 18742	16862 16958 18839	16814 16861 18754	16619 16623 18472	20000 21100
MAE	2858	2883	3198	3479	2969	2873	2944	3140	
PW91 geometries									
Assign. (T_h)	BP86	PW91	OPBE	SSBD	B3LYP	CAMB3LYP	PBE0	OPBE0	Exp[326]
$^5E_g\,(t_{2g}^3e_g^1)$	0 6449	0 6433	0 6300	0 6285	0 6486	0 6543	0 6488	0 6400	0 9800
$^5T_g\,(t_{2g}^2e_g^2)$	16935 17075 19092	16908 17051 19056	16513 16734 18607	16147 16219 18206	16833 16913 18841	16949 17061 18937	16902 16965 18853	16711 16723 18573	20000 21100
MAE	2784	2810	3123	3408	2900	2805	2875	3070	

4.1.5. d^5 Electronic spectra of Mn(II) and Fe(III) hexaaqua complexes

"Electronic configuration of both $[Mn(H_2O)_6]^{2+}$ and $[Fe(H_2O)_6]^{3+}$ complex in T_h symmetry is $t_g^3e_g^2$. The ground electronic state is ^6A_g. There are no spin-allowed *d-d* transitions in d^5 high spin configuration. The lowest excitations (two ^4A_g, two ^4E_g, two ^4T_g, three ^2A_g, three ^2E_g, four ^1T_g and four ^1T_g) belong to the same electronic configuration. The transition of one electron from t_g orbitals to e_g orbitals gives two ^4T_g, two ^2A_g, two ^2E_g and four ^2T_g states. Promotion of two electrons from t_g orbitals to e_g orbitals, as a result, gives two spin-forbidden ^2T_g states. Experimentally, quartet states are seen in the spectrum, as low-intensity bands. More precisely, there are five[328] bands in the case of $[Mn(H_2O)_6]^{2+}$, and three[329] in the case of $[Fe(H_2O)_6]^{3+}$."[67]

"In the case of $[Mn(H_2O)_6]^{2+}$ complex, five experimentally observed absorption bands (*Tables 18.* and *19.*) are attributed to the transitions from the ground ^6A_g state to two ^4T_g ($^4T_{1g}$ and $^4T_{2g}$ in O_h symmetry), ^4E_g + $^4A_{1g}$, ^4T_g and ^4E_g states, respectively. [328]TD-DFT obtained results are in poor agreement with the experiment (*Table 4.12.*) The absorption spectrum was reproduced with excellent accuracy using LF-DFT approach at SSBD, PBE0, OPBE0 and OPBE levels of theory (*Table 4.13.*). Furthermore, LF-DFT calculations are also in good agreement with calculations using INDO/s model[324], and with CASSCF/CASPT2/MRCI[302] and NEVPT2[305] obtained results."[67]

Table 4.12. TD-DFT vertical excitation energies [cm^{-1}] calculated for $[Mn(H_2O)_6]^{3+}$ complex at different levels of theory; mean absolute error (MAE) is given in cm^{-1}; assignment (electronic state and its configuration) in formally T_h point group is indicated

BP86 geometries

Assign. (T_h)	BP86	PW91	OPBE	SSBD	B3LYP	CAMB3LYP	PBE0	OPBE0	M06L	SAOP	Exp[328]
$^4A_g\,(t_{2g}^3e_g^2)$	0	0	0	0	0	0	0	0	0	0	0
$^4T_g\,(t_{2g}^4e_g^1)$	20134	19785	26952	27811	18964	18978	21679	27137	32131	42723	18870
$^4T_g\,(t_{2g}^4e_g^1)$	20257	19908	27063	27918	19955	20038	22932	28374	32253	42832	23120
$^4A_g+^4E_g\,(t_{2g}^3e_g^2)$	24720	24397	30816	36308	23840	24040	26400	31391	36308	45574	24960
	25238	24890	31529	32496	23885	24066	26504	31471	37053	46565	25270
$^4T_g\,(t_{2g}^3e_g^2)$	25832	25445	32470	32742	24382	24458	27376	32747	38007	47943	27980
$^4E_g\,(t_{2g}^3e_g^2)$	25841	25457	32496	32771	23886	25358	28011	33158	38022	46902	29750
MAE	1742	1983	5229	6682	2537	2204	1335	5721	10637	20431	

PW91 geometries

Assign. (T_h)	BP86	PW91	OPBE	SSBD	B3LYP	CAMB3LYP	PBE0	OPBE0	M06L	SAOP	Exp[328]
$^4A_g\,(t_{2g}^3e_g^2)$	0	0	0	0	0	0	0	0	0	0	0
$^4T_g\,(t_{2g}^4e_g^1)$	20059	19710	26875	27744	18897	18910	21610	27067	32050	42584	18870
$^4T_g\,(t_{2g}^4e_g^1)$	20183	19833	26985	27851	19892	19973	22869	28309	32171	42694	23120
$^4A_g+^4E_g\,(t_{2g}^3e_g^2)$	24705	24376	30799	36404	23832	24032	26388	31379	36291	24425	24960
	25226	24874	31516	32326	23878	24032	26493	31459	37037	24432	25270
$^4T_g\,(t_{2g}^3e_g^2)$	25825	25438	32463	32701	24373	24449	27366	32735	37996	47869	27980
$^4E_g\,(t_{2g}^3e_g^2)$	25833	25448	32491	32798	23878	25351	28001	33147	38015	46909	29750
MAE	1749	1991	5196	6645	2542	2213	1334	5691	10601	13618	

Table 4.13. LF-DFT vertical excitation energies [cm^{-1}] calculated for $[Mn(H_2O)_6]^{3+}$ complex at different levels of theory; mean absolute error (MAE) is given in cm^{-1}; assignment (electronic state and its configuration) in formally T_h point group is indicated

BP86 geometries

Assign.(T_h)	BP86	PW91	OPBE	SSBD	B3LYP	CAMB3LYP	PBE0	OPBE0	Exp[328]
$^4A_g\,(t_{2g}^3e_g^2)$	0	0	0	0	0	0	0	0	0
$^4T_g\,(t_{2g}^4e_g^1)$	16118	15912	20105	19218	15527	15606	17814	20739	18870
$^4T_g\,(t_{2g}^4e_g^1)$	20237	20038	23614	22931	19695	19734	21656	24146	23120
$^4A_g+{}^4E_g$ $(t_{2g}^3e_g^2)$	22754	22547	25750	25015	21834	21853	23679	25922	24960 25270
$^4T_g\,(t_{2g}^3e_g^2)$	26344	26137	29264	28770	25768	25768	27546	29782	27980
$^4E_g\,(t_{2g}^3e_g^2)$	28397	28188	31080	30639	27760	27744	29432	31498	29750
MAE	2197	2403	996	463	2850	2826	942	1450	

PW91 geometries

Assign.(T_h)	BP86	PW91	OPBE	SSBD	B3LYP	CAMB3LYP	PBE0	OPBE0	Exp[328]
$^4A_g\,(t_{2g}^3e_g^2)$	0	0	0	0	0	0	0	0	0
$^4T_g\,(t_{2g}^4e_g^1)$	16044	15838	20031	19151	15458	15536	17744	20668	18870
$^4T_g\,(t_{2g}^4e_g^1)$	20186	19988	23564	22889	19650	19688	21611	24102	23120
$^4A_g+{}^4E_g$ $(t_{2g}^3e_g^2)$	22749	22542	25742	25012	21829	21847	23672	25913	24960 25270
$^4T_g\,(t_{2g}^3e_g^2)$	26323	26116	29239	28750	25745	25744	27522	29754	27980
$^4E_g\,(t_{2g}^3e_g^2)$	28390	28181	31070	30635	27753	27736	29423	31486	29750
MAE	2784	2810	3123	3408	2900	2805	2875	3123	

"The experimental spectrum of $[Fe(H_2O)_6]^{3+}$ is characterized by three absorption bands at 12600, 18500 and 24300 cm^{-1}.[329] These bands are assigned as transitions from the ground ^6A_g state to two ^4T_g ($^4T_{1g}$ and $^4T_{2g}$ in O_h symmetry) and ^4E_g + $^4A_{1g}$ states, respectively. TD-DFT calculations failed to reproduce experimentally obtained transitions (*Table 4.14.*)."[67]

"LF-DFT theoretical transitions agree rather well with the experimental values (*Table 4.15.*). The best agreement was achieved with OPBE0, SSBD and OPBE XC functionals, for both, BP86 and PW91 optimized structures. However, slightly better results were obtained on PW91 optimized geometry (*Table 4.15.*). LF-DFT vertical excitation energies were also in good agreement with INDO/S calculations[324]. Furthermore, LF-DFT proved to be significantly better than high-level wave function based methods[302, 305, 320], that showed a strong dependence on the chosen basis set, the active space and correlation of the outer-core orbitals. In general, wave-function based, post-HF methods, tend to highly overestimate transitions within d^5 TM ion systems. This phenomenon reflects the importance of the dynamic correlation in the sextet-quartet splitting. Electron correlation between the electrons of opposite spins is completely missing in the HF, and in the post-HF methods, very extensive correlation treatments, with very large basis sets, are needed to achieve more precise results. As already mentioned, these correlation effects are included in LF-DFT through the XC functional. This proves that the LF-DFT calculations with either one of chosen DFAs can be the method of choice for studying vertical excitation energies. and corresponding UV/Vis spectra."[67]

Table 4.14. TD-DFT vertical excitation energies [cm^{-1}] calculated for $[Fe(H_2O)_6]^{3+}$ complex at different levels of theory; mean absolute error (MAE) is given in cm^{-1}; assignment (electronic state and its configuration) in formally T_h point group is indicated

BP86 geometries

Assign. (T_h)	BP86	PW91	OPBE	SSBD	B3LYP	CAMB3LYP	PBE0	OPBE0	M06L	SAOP	Exp[329]
$^4A_g\,(t_{2g}^3e_g^2)$	0	0	0	0	0	0	0	0	0	0	0
$^4T_g\,(t_{2g}^4e_g^1)$	11757	11515	16368	18197	13200	13770	15350	19476	22314	24024	12600
$^4T_g\,(t_{2g}^4e_g^1)$	11893	11650	16512	18311	14437	15117	16916	21021	22439	24369	18500
$^4A_g+^4E_g\,(t_{2g}^3e_g^2)$	17421 19309	17239 19158	19329 20499	20171 21255	22194 26517	23676 29047	24899 29644	28015 31481	23587 24495	24491 24608	24300
MAE	4461	4678	3380	3124	1572	2204	2435	4106	4637	5847	

PW91 geometries

Assign. (T_h)	BP86	PW91	OPBE	SSBD	B3LYP	CAMB3LYP	PBE0	OPBE0	M06L	SAOP	Exp[329]
$^4A_g\,(t_{2g}^3e_g^2)$	0	0	0	0	0	0	0	0	0	0	0
$^4T_g\,(t_{2g}^4e_g^1)$	11695	11453	16310	18138	13137	13709	15289	19417	22272	24127	12600
$^4T_g\,(t_{2g}^4e_g^1)$	11830	11587	16452	18282	14401	15056	16857	20963	22396	24351	18500
$^4A_g+^4E_g\,(t_{2g}^3e_g^2)$	17470 19382	17288 19230	19399 20585	20246 21343	22223 26591	23695 29110	24927 29722	28063 31577	23678 24598	24473 24720	24300
MAE	4483	4700	3355	3087	1581	2218	2452	4121	4576	5891	

Table 4.15. LF-DFT vertical excitation energies [cm^{-1}] calculated for $[Fe(H_2O)_6]^{3+}$ complex at different levels of theory; mean absolute error (MAE) is given in cm^{-1}; assignment (electronic state and its configuration) in formally T_h point group is indicated

BP86 geometries

Assign. (T_h)	BP86	PW91	OPBE	SSBD	B3LYP	CAMB3LYP	PBE0	OPBE0	Exp[329]
^4A_g ($t_{2g}^3e_g^2$)	0	0	0	0	0	0	0	0	0
^4T_g ($t_{2g}^4e_g^1$)	11102	10946	14112	14240	10079	9990	11683	13784	12600
^4T_g ($t_{2g}^4e_g^1$)	16013	15866	18523	18809	15313	15243	16701	18481	18500
$^4A_g+^4E_g$ ($t_{2g}^3e_g^2$)	21301	21155	23463	23386	20663	20942	22019	23597	24300
MAE	2328	2477	790	954	3115	3157	1665	635	

PW91 geometries

Assign. (T_h)	BP86	PW91	OPBE	SSBD	B3LYP	CAMB3LYP	PBE0	OPBE0	Exp[329]
^4A_g ($t_{2g}^3e_g^2$)	0	0	0	0	0	0	0	0	0
^4T_g ($t_{2g}^4e_g^1$)	11040	10885	14047	14178	10001	9906	11600	13688	12600
^4T_g ($t_{2g}^4e_g^1$)	15968	15823	18475	18765	15244	15163	16623	18388	18500
$^4A_g+^4E_g$ ($t_{2g}^3e_g^2$)	21313	21169	23472	23395	20650	20672	21998	23563	24300
MAE	2359	2507	766	916	3168	3219	1726	645	

4.1.6. d^6 Electronic spectra of Co(III) and Fe(II) hexaaqua complexes

"In the case of $[Fe(H_2O)_6]^{2+}$ complex, the electronic configuration in T_h symmetry is $t_g^4e_g^2$. The ground electronic state is ^5T_g. According to the Tanabe-Sugano diagram for d^6 high-spin configuration, one spin-allowed transition to ^5E_g state is expected. This transition corresponds to the promotion of one electron from t_g orbitals to e_g orbitals ($t_g^4e_g^2 \rightarrow t_g^3e_g^3$). Experimentally, two absorption picks are observed, one at 8300 and one at 10400 cm^{-1} (*Table 4.16.*)[330], as a consequence of the JT distortion, present in the excited ^5E_g state. Splitting of the ground ^5T_g state is experimentally not observed, because of the relatively weak JT effect, associated with the unequal population of the nonbonding t_g orbitals."[67]

"DFT calculations with B3LYP, CAM-B3LYP, OPBE0, and PBE0 reproduced the first component of spin-allowed transition with reasonable accuracy (<2500 cm^{-1})on both BP86 and PW91 optimized geometries (*Table 4.16.*). The second transition is calculated on too high energy. This discrepancy can be explained in the same way as in the case of d^3 systems, due to the lack of orbital excitation in TD-DFT, since upon descent in symmetry ^5E_g state splits into two states."[67]

"LF-DFT calculations reproduced the spectrum with excellent agreement with experimental data (*Table 4.17.*). Slightly better results were obtained with PW91 optimized geometry. In general, LF-DFT calculations provided better results than TD-DFT in the particular case of $[Fe(H_2O)_6]^{2+}$. The transition energies obtained using the LF-DFT approach are in accordance with previous CASSCF/SORCI calculations by Neese *at al.*[320]. Furthermore study utilizing the CASSCF/CASPT2/MRCI done by Shatz *et al.* calculated the first transition with the error above the 3000 cm^{-1}, depending on the chosen method.[302] This fact gives an obvious advantage to the low cost of DFT-based methods."[67]

Table 4.16. TD-DFT vertical excitation energies [cm^{-1}] calculated for $[Fe(H_2O)_6]^{2+}$ complex at different levels of theory; mean absolute error (MAE) is given in cm^{-1}; assignment (electronic state and its configuration) in formally T_h point group is indicated

BP86 geometries											
Assign. (T_h)	BP86	PW91	OPBE	SSBD	B3LYP	CAMB3LYP	PBE0	OPBE0	M06L	SAOP	Exp[330]
^5T_g ($t_{2g}^4e_g^2$)	0	0	0	0	0	0	0	0	0	0	0
^5E_g ($t_{2g}^3e_g^3$)	11887	11700	11699	12499	10429	10324	10741	10828	16938	22954	8300
	16846	16581	15743	17298	14267	14075	14266	13774	24047	24970	10400
MAE	5016	4790	4371	5548	2998	2849	3153	2951	11142	14612	
PW91 geometries											
Assign. (T_h)	BP86	PW91	OPBE	SSBD	B3LYP	CAMB3LYP	PBE0	OPBE0	M06L	SAOP	Exp[330]
^5T_g ($t_{2g}^4e_g^2$)	0	0	0	0	0	0	0	0	0	0	0
^5E_g ($t_{2g}^3e_g^3$)	12104	11916	11878	12642	10628	10523	10928	10986	17165	23035	8300
	16956	16689	15847	17357	14394	14204	14394	21947	24117	25116	10400
MAE	5180	4952	4512	5649	3161	3013	3311	7116	11291	14725	

Table 4.17. LF-DFT vertical excitation energies [cm^{-1}] calculated for $[Fe(H_2O)_6]^{2+}$ complex at different levels of theory; mean absolute error (MAE) is given in cm^{-1}; assignment (electronic state and its configuration) in formally T_h point group is indicated

BP86 geometries									
Assign. (T_h)	BP86	PW91	OPBE	SSBD	B3LYP	CAMB3LYP	PBE0	OPBE0	Exp[330]
^5T_g ($t_{2g}^4e_g^2$)	0	0	0	0	0	0	0	0	0
^5E_g ($t_{2g}^3e_g^3$)	8199	8289	8008	7885	7632	7508	7476	7198	8300
	9987	10037	9638	9533	9355	9237	9171	8821	10400
MAE	257	187	527	641	856	977	1026	1340	
PW91 geometries									
Assign. (T_h)	BP86	PW91	OPBE	SSBD	B3LYP	CAMB3LYP	PBE0	OPBE0	Exp[330]
^5T_g ($t_{2g}^4e_g^2$)	0	0	0	0	0	0	0	0	0
^5E_g ($t_{2g}^3e_g^3$)	8392	8400	8050	7915	7656	7531	7501	7226	8300
	10403	10394	9939	9826	9642	9523	9455	9099	10400
MAE	47	53	355	479	701	823	872	1187	

"Complex $[Co(H_2O)_6]^{3+}$ represents the only low-spin aqua complex in the first row TM series, with a closed-shell ground state configuration in t_g^6. The ground electronic state is ^1A_g. Experimentally, four bands were observed, centered at 8000 cm^{-1}, 12500 cm^{-1}, 16600 cm^{-1}, and 24900 cm^{-1} .[331] All four transitions (*Table 4.18.*) originate due to the promotion of one electron from t_g orbitals to e_g orbitals, $t_g^6 \rightarrow t_g^5e_g^1$. First two bands at 8000 cm^{-1} and 12500 cm^{-1} are assigned to spin-forbidden one-electron transition to ^3T_g states ($^3T_{1g}$ and $^3T_{2g}$ in O_h symmetry). The bands observed at 16600 cm^{-1}, and 24900 cm^{-1} correspond to spin-allowed transition to two ^1T_g states ($^1T_{1g}$ and $^1T_{2g}$ in O_h symmetry)."[67]

"Generally speaking, TD-DFT reproduced the experimental spectrum with good accuracy only at BP86 optimized geometry using CAM-B3LYP and PBE0 functional (*Table 4.18.*). LF-DFT calculations at BP86 optimized geometry reproduced experimental spectrum with excellent accuracy with all performed XC functionals (*Table 4.19.*). LF-DFT results obtained on BP86 geometries are consistent with previous LF-DFT calculations done by Atanasov *et al.*[303], as well as with SORCI[320] and INDO/S[324] calculations. Furthermore, LF-DFT showed remarkably better performance than CASSCF[302, 320], CASPT2, NEVPT2[305] and MRCI calculations[302]. CASSCF calculations[239] calculated the first spin-allowed transition with the error of ~5400 cm^{-1} and the second ^1Tg with the error of ~4300 cm^{-1}. The same transitions were calculated with the error of ~4900 cm^{-1} and ~3500 cm^{-1} using CASPT2.[302] MRCI gave errors of ~6100 cm^{-1} for the first singlet transition and ~3900 cm−1 for the second singlet transition.[302] CASSCF calculations by Neese *et al*. also underestimated the first ^1T_g transition with the error of ~3886 cm^{-1}."[67]

"In the case of PW91 geometry, LF-DFT and TD-DFT failed to provide accurate values for both spin allowed transitions with all investigated functionals (*Tables 22.* and *24.*). This discrepancy is due to the higher deviation of Co-O bond lengths in PW91 optimized geometry (1.950 Å), with respect to BP86 optimized bond lengths (1.885 Å), which is in better agreement with crystal bond distances (1.873 Å)."[67]

Table 4.18. TD-DFT vertical excitation energies [cm^{-1}] calculated for $[Co(H_2O)_6]^{3+}$ complex at different levels of theory; mean absolute error (MAE) is given in cm^{-1}; assignment (electronic state and its configuration) in formally T_h point group is indicated

BP86 geometries

Assign. (T_h)	BP86	PW91	OPBE	SSBD	B3LYP	CAMB3LYP	PBE0	OPBE0	M06L	SAOP	Exp[331]
^1A_g ($t_{2g}^6e_g^0$)	0	0	0	0	0	0	0	0	0	0	0
^3T_g ($t_{2g}^5e_g^1$)	11936	11882	10066	11668	11610	6458	9930	8547	18329	18745	8000
^3T_g ($t_{2g}^5e_g^1$)	12175	12115	10314	11829	13367	12361	12119	10766	18597	19091	12500
^1T_g ($t_{2g}^5e_g^1$)	16608	16554	14799	16402	17491	17716	15976	14683	22783	22742	16600
^1T_g ($t_{2g}^5e_g^1$)	19463	19409	17659	19124	23818	24510	23048	21734	25267	24709	24900
MAE ($^1\Gamma \rightarrow {}^1\Gamma$)	2130	2133	2126	2169	2238	840	1155	1140	8213	8668	
MAE ($^1\Gamma \rightarrow {}^3\Gamma$)	2722	2768	4521	2987	986	753	1238	2541	3275	3166	
MAE	2426	2451	3323	2578	1612	797	1197	1841	5744	5917	

PW91 geometries

Assign. (T_h)	BP86	PW91	OPBE	SSBD	B3LYP	CAMB3LYP	PBE0	OPBE0	M06L	SAOP	Exp[331]
^1A_g ($t_{2g}^6e_g^0$)	0	0	0	0	0	0	0	0	0	0	0
^3T_g ($t_{2g}^5e_g^1$)	8826	8789	7106	8612	8915	7858	7233	5984	14940	15248	8000
^3T_g ($t_{2g}^5e_g^1$)	9059	9018	7333	8851	10610	12214	9342	8109	15241	15581	12500
^1T_g ($t_{2g}^5e_g^1$)	13055	13019	11415	12814	14486	14781	13051	11816	18850	18704	16600
^1T_g ($t_{2g}^5e_g^1$)	15384	15351	13764	14990	20239	21188	19697	18447	20723	20180	24900
MAE ($^1\Gamma \rightarrow {}^1\Gamma$)	2133	2135	3030	2130	1402	214	1962	3203	4840	5164	
MAE ($^1\Gamma \rightarrow {}^3\Gamma$)	6530	6565	8160	6848	3387	2765	4376	5618	3213	3412	
MAE	4332	4350	5595	4489	2395	1489	3169	4411	4027	4288	

Table 4.19. LF-DFT vertical excitation energies [cm^{-1}] calculated for $[Co(H_2O)_6]^{3+}$ complex at different levels of theory; mean absolute error (MAE) is given in cm^{-1}; assignment (electronic state and its configuration) in formally T_h point group is indicated

BP86 geometries

Assign. (T_h)	BP86	PW91	OPBE	SSBD	B3LYP	CAMB3LYP	PBE0	OPBE0	Exp[331]
^1A_g ($t_{2g}^6e_g^0$)	0	0	0	0	0	0	0	0	0
^3T_g ($t_{2g}^5e_g^1$)	9271	9329	7737	7403	10186	10845	10734	9539	8000
^3T_g ($t_{2g}^5e_g^1$)	13898	13958	12008	11808	15115	15917	15949	14436	12500
^1T_g ($t_{2g}^5e_g^1$)	15329	15335	14718	14310	15727	16127	15986	15600	16600
^1T_g ($t_{2g}^5e_g^1$)	24590	24598	23357	23167	25518	26181	26281	25352	24900
MAE ($^1\Gamma \rightarrow {}^1\Gamma$)	1334	1393	377	644	2400	3131	3091	1737	
MAE ($^1\Gamma \rightarrow {}^3\Gamma$)	790	783	1712	2011	745	877	997	726	
MAE	1062	1088	1045	1328	1573	2004	2044	1232	

PW91 geometries

Assign. (T_h)	BP86	PW91	OPBE	SSBD	B3LYP	CAMB3LYP	PBE0	OPBE0	Exp[331]
^1A_g ($t_{2g}^6e_g^0$)	0	0	0	0	0	0	0	0	0
^3T_g ($t_{2g}^5e_g^1$)	6253	6312	4783	4617	7706	7999	7212	6281	8000
^3T_g ($t_{2g}^5e_g^1$)	10311	10375	8532	8454	12076	12410	11488	10369	12500
^1T_g ($t_{2g}^5e_g^1$)	13109	12031	11403	11147	13109	13374	13080	12747	16600
^1T_g ($t_{2g}^5e_g^1$)	21756	20088	18918	18774	21757	22112	21589	20934	24900
MAE ($^1\Gamma \rightarrow {}^1\Gamma$)	1968	1906	3592	3714	359	45	900	1925	
MAE ($^1\Gamma \rightarrow {}^3\Gamma$)	3317	4690	5589	5789	3317	3007	3415	3909	
MAE	2643	3298	4591	4752	1838	1526	2158	2917	

4.1.7. d^7 Electronic spectrum of Co(II) hexaaqua complex

"Electronic configuration of $[Co(H_2O)_6]^{2+}$ complex in T_h symmetry is $t_g^5e_g^2$. The ground electronic state is ^4T_g. Two bands that correspond to spin-allowed transitions. Two spin-allowed transitions belong to the promotion of one electron from the ground state t_g orbitals to e_g orbitals ($t_g^5e_g^2 \rightarrow t_g^4e_g^3$), resulting in two ^4T_g states ($^4T_{1g}$ and $^4T_{2g}$ in O_h symmetry). Splitting of the second ^4T_g state because of the ground state JT effect is experimentally not observed.[323] Possible spin-forbidden transitions are two ^2A_g, two ^2E_g, and four ^2T_g. Promotion of the two electrons from t_g orbitals to e_g orbitals ($t_g^5e_g^2 \rightarrow t_g^3e_g^4$) gives one spin-allowed ^4A_g state ($^4A_{2g}$ in O_h symmetry), and spin-forbidden doublet states ^2E_g and two ^2T_g."[67]

"TD-DFT calculations (*Table 4.20.*), overestimated the first transition to the ^4T_g state, while not able to calculate the two-electron excitation to the ^4A_g state. The third transition is satisfactorily reproduced. It should be noted that M06-L and SAOP completely failed to reproduce the experimental values."[67]

"LF-DFT calculated transition energies are in excellent agreement with the experimentally obtained transitions, and the best agreement was obtained with BP86 and PW91 functionals, using either the BP86 or PW91 geometries (*Table 4.21.*).

LF-DFT underestimates the spin-forbidden transition $^4T_g \rightarrow {}^2E_g$, even though results with OPBE, OPBE0, and SSB-D are in reasonable agreement with the experiment. Our LF-DFT results are in agreement with the previously reported LF-DFT calculations with PW91 functional by Atanasov *et al.*[303] and with recent CASPT2/NEVPT2[305] calculations."[67]

Table 4.20. TF-DFT vertical excitation energies [cm^{-1}] calculated for $[Co(H_2O)_6]^{2+}$ complex at different levels of theory; mean absolute error (MAE) is given in cm^{-1}; assignment (electronic state and its configuration) in formally T_h point group is indicated

BP86 geometries

Assign. (T_h)	BP86	PW91	OPBE	SSBD	B3LYP	CAMB3LYP	PBE0	OPBE0	M06L	SAOP	Exp[323]
^4T_g ($t_{2g}^5e_g^2$)	0	0	0	0	0	0	0	0	0	0	0
^4T_g ($t_{2g}^4e_g^3$)	12676	12501	11876	14006	10102	9927	9881	9488	19406	19523	8100
	13396	13236	12624	14614	11161	11003	10983	10547	19762	20369	
^2E_g ($t_{2g}^6e_g^1$)	6791	6362	11333	12864	7168	7342	9443	12658	17435	15685	11300
	11481	11041	16077	17705	11616	11924	13295	16556	22730	20165	
^4A_g ($t_{2g}^3e_g^4$)	-	-	-	-	-	-	-	-	-	-	16000
^4T_g ($t_{2g}^4e_g^3$)	20146	19902	18669	21799	19021	18899	19240	18550	29558	25253	19400
	20748	20512	19231	22257	20104	20026	20309	19525	30040	26016	21550
MAE ($^4\Gamma \rightarrow {}^4\Gamma$)	2161	2103	2400	3105	1452	1463	1244	1597	10044	7388	
MAE ($^4\Gamma \rightarrow {}^2\Gamma$)	2164	2598	2405	3984	1908	1667	69	3307	8782	6625	
MAE	2162	2227	2401	3325	1566	1514	950	2025	9729	7197	

PW91 geometries

Assign. (T_h)	BP86	PW91	OPBE	SSBD	B3LYP	CAMB3LYP	PBE0	OPBE0	M06L	SAOP	Exp[323]
^4T_g ($t_{2g}^5e_g^2$)	0	0	0	0	0	0	0	0	0	0	0
^4T_g ($t_{2g}^4e_g^3$)	12776	12608	11966	14066	10219	10048	9997	9595	19449	19634	8100
	13473	13317	12689	14665	11231	11075	11048	10604	19811	20434	
^2E_g ($t_{2g}^6e_g^1$)	6683	6471	10404	12762	7070	7243	9349	12560	17325	15567	11300
	11337	11186	15082	17571	11482	11789	13156	16414	22588	20014	
^4A_g ($t_{2g}^3e_g^4$)	-	-	-	-	-	-	-	-	-	-	16000
^4T_g ($t_{2g}^4e_g^3$)	20255	20020	18770	21893	19144	19025	19358	18661	29610	25364	19400
	20785	20554	19260	22282	20133	20055	20336	19547	30036	26067	21550
MAE ($^4\Gamma \rightarrow {}^4\Gamma$)	2215	2159	2382	3163	1433	1444	1226	1580	10075	7471	
MAE ($^4\Gamma \rightarrow {}^2\Gamma$)	2290	2471	1443	3866	2024	1784	47	3187	8656	6490	
MAE	2234	2237	2148	3339	1580	1529	931	1982	9721	7226	

Table 4.21. TF-DFT vertical excitation energies [cm^{-1}] calculated for $[Co(H_2O)_6]^{2+}$ complex at different levels of theory; mean absolute error (MAE) is given in cm^{-1}; assignment (electronic state and its configuration) in formally T_h point group is indicated

BP86 geometries

Assign. (T_h)	BP86	PW91	OPBE	SSBD	B3LYP	CAMB3LYP	PBE0	OPBE0	Exp[323]
^4T_g ($t_{2g}^5e_g^2$)	0	0	0	0	0	0	0	0	0
^4T_g ($t_{2g}^4e_g^3$)	7684	7670	7363	7191	7029	6890	6862	6649	8100
	8196	8185	7853	7678	7300	7100	7074	6832	
	9368	9353	9039	8813	8535	8377	8342	8116	
^2E_g ($t_{2g}^6e_g^1$)	5446	5336	7728	7753	5580	5738	6937	8546	11300
	7540	7426	9770	9785	7595	7749	8904	10468	
^4A_g ($t_{2g}^3e_g^4$)	17642	17616	16947	16566	16121	15806	15742	15274	16000
^4T_g ($t_{2g}^4e_g^3$)	19028	19018	18005	18490	18821	18618	18382	17743	19400
	20482	20468	19480	19991	20299	20110	19857	19225	21550
	21453	21434	20406	20892	21043	20798	20534	19860	
MAE ($^4\Gamma \rightarrow {}^4\Gamma$)	602	594	691	397	317	406	557	1058	
MAE ($^4\Gamma \rightarrow {}^2\Gamma$)	4807	4919	2551	2531	4712	4556	3379	1793	
MAE	1443	1459	1063	824	1196	1236	1122	1205	

PW91 geometries

Assign. (T_h)	BP86	PW91	OPBE	SSBD	B3LYP	CAMB3LYP	PBE0	OPBE0	Exp[323]
^4T_g ($t_{2g}^5e_g^2$)	0	0	0	0	0	0	0	0	0
^4T_g ($t_{2g}^4e_g^3$)	7821	7807	7501	7318	7156	7017	6989	6776	8100
	8255	8245	7915	7734	7365	7169	7143	6902	
	9413	9398	9084	8855	8574	8417	8382	8155	
^2E_g ($t_{2g}^6e_g^1$)	5363	5253	7646	7678	5514	5674	6873	8483	11300
	7372	7258	9603	9628	7447	7603	8760	10326	
^4A_g ($t_{2g}^3e_g^4$)	17829	17801	17133	16740	16292	15980	15914	15445	16000
^4T_g ($t_{2g}^4e_g^3$)	19159	19147	18129	18611	16292	18739	18500	17855	19400
	20493	20478	19485	19997	18941	20119	19864	19227	21550
	21484	21464	20429	20915	20306	20837	20570	19892	
MAE ($^4\Gamma \rightarrow {}^4\Gamma$)	679	671	728	400	930	332	470	974	
MAE ($^4\Gamma \rightarrow {}^2\Gamma$)	4932	5044	2675	2647	4819	4661	3483	1895	
MAE	1530	1545	1118	850	1708	1198	1072	1158	

4.1.8. d^8 Electronic spectrum of Ni(II) hexaaqua complex

"The ground electronic state of $[Ni(H_2O)_6]^{2+}$ complex in T_h symmetry is ^3A_g, with electronic configuration $t_g^6e_g^2$. Three spin-allowed transitions to ^3T_g ($^3T_{2g}$, corresponding to Δ, and $^3T_{1g}$ (*F*) and $^3T_{1g}$ (*P*) states in O_h point group) are observed. [332] The first two transitions originate from the excitation of one electron from t_g orbital to e_g orbital ($t_g^6e_g^2 \rightarrow t_g^5e_g^3$). The third transition represents the double excitation from t_g orbitals to e_g orbitals ($t_g^6e_g^2 \rightarrow t_g^4e_g^4$). Additionally, the two spin-forbidden transitions are experimentally observed."[67]

"Our TD-DFT calculations failed to reproduce correctly experimental spectrum (*Table 4.22.*). Generally, TD-DFT was not proved to be a good choice for electronic spectrum calculations of nickel hexaaqua complex, as previously shown by Neese *at al.*[320] Reason behind the failure of TD-DFT to describe the spectrum is a consequence of two factors. The first one is a lack of orbital relaxation in TD-DFT, resulting in the overestimation of the first transition that corresponds to the ligand field splitting. The second reason is CI mixing between two $^3T_{1g}$ states. As already mentioned, the second $^3T_{1g}$ transition corresponds to a double excitation from the ground state and is ignored within the framework of adiabatic TD-DFT. LF analysis shows that this mixing is much more significant for $[Ni(H_2O)_6]^{2+}$ than for $[Cr(H_2O)_6]^{3+}$ and $[V(H_2O)_6]^{2+}$. The contribution of the double excitation to the $^3T_{1g}(F)$ is very large, 45%. Thus, this $^3T_{1g}(F)$ - $^3T_{1g}$ (*P*) mixing should lead to the stabilization of $^3T_{1g}$ (*F*) for around 4600 cm^{-1}. Neese[333] pointed out that TD-DFT predicts only one $^3T_{1g}$ transition, almost half in between experimentally observed $^3T_{1g}$ (*F*) and $^3T_{1g}$ (*P*) states."[67]

Consequently, LF-DFT calculations were almost perfectly accurate in predicting the spectrum and provided good agreement with experimental data at most of the investigated levels of theory (*Table 4.23.*). The best match was obtained with OPBE, SSBD and OPBE0 functionals. Our LF-DFT calculations are in good agreement with results obtained with INDO/S model[324], CASPT2/NEVPT2[305] and with SORCI approach[320].

Table 4.22. TF-DFT vertical excitation energies [cm^{-1}] calculated for $[Ni(H_2O)_6]^{2+}$ complex at different levels of theory; mean absolute error (MAE) is given in cm^{-1}; assignment (electronic state and its configuration) in formally T_h point group is indicated

BP86 geometries

Assign. (T_h)	BP86	PW91	OPBE	SSBD	B3LYP	CAMB3LYP	PBE0	OPBE0	M06L	SAOP	Exp[332]
^3A_g ($t_{2g}^6e_g^2$)	0	0	0	0	0	0	0	0	0	0	0
^3T_g ($t_{2g}^5e_g^3$)	16137	15984	14355	16895	14401	13926	18485	14361	12814	24973	8700
^3T_g ($t_{2g}^5e_g^3$)	19539	19388	17865	20417	20417	20480	20554	19544	28573	21367	13750
^1E_g ($t_{2g}^6e_g^2$)	14105	13839	15012	18134	14768	15226	16269	15506	24923	17344	15250
^1T_g ($t_{2g}^5e_g^3$)	20220	19988	20711	23315	20125	20244	20080	21010	31693	23540	22000
^3T_g ($t_{2g}^4e_g^4$)	-	-	-	-	-	-	-	-	-	-	25144
MAE ($^3\Gamma \rightarrow {}^3\Gamma$)	6613	6461	4885	7431	6184	5978	8294	5727	9468	11945	
MAE ($^3\Gamma \rightarrow {}^1\Gamma$)	1462	1712	763	2099	1178	890	1469	623	9683	1817	
MAE	4038	4086	2824	4765	3681	3434	4882	3175	9576	6881	

PW91 geometries

Assign. (T_h)	BP86	PW91	OPBE	SSBD	B3LYP	CAMB3LYP	PBE0	OPBE0	M06L	SAOP	Exp[332]
^3A_g ($t_{2g}^6e_g^2$)	0	0	0	0	0	0	0	0	0	0	0
^3T_g ($t_{2g}^5e_g^3$)	16211	16064	14420	16963	14463	14423	13987	12870	25038	18562	8700
^3T_g ($t_{2g}^5e_g^3$)	19625	19480	17946	20485	20481	20543	20607	19592	28656	21468	13750
^1E_g ($t_{2g}^6e_g^2$)	14105	13845	15005	18128	14766	15494	16263	17333	24920	15223	15250
^1T_g ($t_{2g}^5e_g^3$)	20301	20076	20795	23401	20186	20304	20138	23644	31783	21063	22000
^3T_g ($t_{2g}^4e_g^4$)	-	-	-	-	-	-	-	-	-	-	25144
MAE ($^3\Gamma \rightarrow {}^3\Gamma$)	6918	6772	5183	7724	6472	6483	6297	5231	15847	9015	
MAE ($^3\Gamma \rightarrow {}^1\Gamma$)	1497	1739	800	2064	1224	895	1362	1788	9651	557	
MAE	4207	4256	2991	4894	3848	3689	3830	3510	12749	4786	

Table 4.23. LF-DFT vertical excitation energies [cm^{-1}] calculated for $[Ni(H_2O)_6]^{2+}$ complex at different levels of theory; mean absolute error (MAE) is given in cm^{-1}; assignment (electronic state and its configuration) in formally T_h point group is indicated

BP86 geometries

Assign. (T_h)	BP86	PW91	OPBE	SSBD	B3LYP	CAMB3LYP	PBE0	OPBE0	Exp[332]
^3A_g ($t_{2g}^6e_g^2$)	0	0	0	0	0	0	0	0	0
^3T_g ($t_{2g}^5e_g^3$)	9529	9521	9201	8992	9316	9233	9229	9114	8700
^3T_g ($t_{2g}^5e_g^3$)	15518	15506	14919	14735	15273	15148	15110	14870	13750
^1E_g ($t_{2g}^6e_g^2$)	12478	12410	13258	13465	12232	12218	12759	13321	15250
^1T_g ($t_{2g}^5e_g^3$)	21647	21569	22129	22089	21162	21065	21614	22081	22000
^3T_g ($t_{2g}^4e_g^4$)	26040	26026	24807	25100	26059	25889	25684	25061	25144
MAE ($^3\Gamma \rightarrow {}^3\Gamma$)	1164	1153	669	440	1018	892	810	539	
MAE ($^3\Gamma \rightarrow {}^1\Gamma$)	1562	1635	1060	937	1928	1984	1438	1005	
MAE	1324	1346	825	639	1382	1329	1061	725	

PW91 geometries

Assign. (T_h)	BP86	PW91	OPBE	SSBD	B3LYP	CAMB3LYP	PBE0	OPBE0	Exp[332]
^3A_g ($t_{2g}^6e_g^2$)	0	0	0	0	0	0	0	0	0
^3T_g ($t_{2g}^5e_g^3$)	9594	9586	9268	9056	9362	9276	9272	9157	8700
^3T_g ($t_{2g}^5e_g^3$)	15610	15598	15013	14827	15340	15210	15172	14930	13750
^1E_g ($t_{2g}^6e_g^2$)	12480	12412	13262	13471	12231	12215	12758	13321	15250
^1T_g ($t_{2g}^5e_g^3$)	21715	21638	22201	22160	21209	21107	21657	22126	22000
^3T_g ($t_{2g}^4e_g^4$)	26145	26131	24915	25202	26131	25956	25752	25127	25144
MAE ($^3\Gamma \rightarrow {}^3\Gamma$)	1350	1338	889	660	1178	1047	965	753	
MAE ($^3\Gamma \rightarrow {}^1\Gamma$)	1602	1675	1169	1044	1980	2039	1492	1102	
MAE	1451	1473	1001	814	1499	1444	1176	893	

4.1.9. Conclusions

The present theoretical investigation represents a comparative study of two different DFT-based methods, TD-DFT and LF-DFT. The main goal was to investigate *d-d* transitions for a series of first row TM aqua complexes, and in this regard test performance and accuracy of proposed methods, as well as the influence of chosen functional. For this purpose, we have utilized ten different DFAs. Generally, TD-DFT shoved good performance in specific cases of d^2, d^3 and low-spin d^6 TM complexes with most of the investigated DFAs, although failed on M06L and SAOP level of theory. We addressed the failure of TD-DFT, in the case $[Ni(H_2O)_6]^{2+}$, $[V(H_2O)_6]^{2+}$ and $[Cr(H_2O)_6]^{3+}$ complex molecules to the absence of the orbital relaxation. In this regard, the overestimation of the first transition originates from the fact that this transition depends only on the ligand field splitting Δ. Another important factor is the nature of the second state in the case of these molecules. Namely, this state has a substantial contribution of the double excitation, that goes beyond the reach of regular adiabatic TD-DFT. In this regard, in cases with stronger mixing, we can expect a lower accuracy of the method.

According to our results, LF-DFT has proven to be very accurate for the determination and characterization of excited states for all complex molecules under investigation. The reason for such a good performance lies in the fact that we can observe the orbitals with dominant *d*-character in a CI-based fashion. In this way, we are able to examine an active space constructed from KS orbitals dominantly belonging to the TM. It is important to emphasize that LF-DFT proved to be accurate for the calculation of spin-allowed transitions, regardless of the chosen level of theory. On the other hand, excellent performance in the case of spin-forbidden excitations was obtained only with OPBE and SSB-D, and OPBE0, which are generally considered as convenient DFA choices for the determination of the spin state splitting. Considered together, our LF-DFT results are comparable with those obtained by high-level *ab initio* methods. Most importantly, LF-DFT performed even better than the *ab initio* methods in the case $[Mn(H_2O)_6]^{2+}$ and $[Fe(H_2O)_6]^{3+}$, for calculation of sextet-quartet transitions. This remarkable performance can be addressed to the ability of LF-DFT to treat consistently non-dynamic, as well as the dynamic correlation effect, when the level of theory is properly chosen. These two complexes emerged as challenging examples and good examples for validation of different functionals, as well as other methods designed for the examination of excited states.

Based on our results, it can be concluded that LF-DFT can be considered as a powerful tool for the examination of *d-d* transitions in hexaaqua TM complex molecules. This method showed to be a reliable choice for calculation of excited states, and a good alternative to popular TD-DFT. Most importantly, LF-DFT can provide accurate results that are comparable, or even better, than those obtained with *ab initio* methods. Based on all previous statements, this method deserves a special position in the field of excited states of inorganic compounds. LF-DFT takes advantage of both standard ligand field theory and modern DFT and sheds light on the coordination chemistry of TM ions.[67] However, since LF-DFT is rooted in the LF theory itself, it is not possible to elucidate CT transitions with this approach. In addition to metal-centered, CT transitions are obviously also important and can dominate in the absorption spectra of TM compounds.[67]

4.1.10. Computational details

The calculations using the unrestricted formalism have been performed with the Amsterdam Density Functional (ADF) [287, 334] program package, version 2013.01. All electron Triple-ζ STOs plus one polarization (TZP) function basis set has been used for all present atoms. [306] All the complexes

are treated in the HS electronic configuration, except $[Co(H_2O)_6]^{3+}$, which is the only one known to have an LS ground state.[335] Symmetry constrained geometry optimizations in D_{2h} point group were performed with the LDA[172], BP86[199-201], PW91[336], OPBE[337], and B3LYP[177] XC functionals. TD-DFT calculations, as implemented in ADF program package[338], were performed with the BP86, PW91, OPBE, SSB-D[339], B3LYP, CAM-B3LYP[340], PBE0[341, 342], OPBE0[337], M06-L[186, 343], and SAOP[344] XC functionals, on the BP86 and PW91 optimized geometries. Spin-forbidden transitions were calculated with the spin-flip formalism[345, 346] and Tamm-Dancoff approximation[247]. All *d-d* transitions were identified by examination of the corresponding orbitals involved in the excitations. LF-DFT calculations were carried out on the BP86 and PW91 optimized geometries, using BP86, PW91, OPBE, SSBD, B3LYP, CAM-B3LYP, PBE0, and OPBE0 XC functionals. LF-DFT is based on a multi-determinant description of the multiplet structures [277, 347] originating from the d^n configuration of the TM ions surrounded by coordinating ligands, by combining the CI and the KS-DFT approaches. In all the calculations, the solvent effects of water have been implicitly modeled, according to the conductor-like screening model (COSMO)[196, 348], as implemented in ADF.

4.2. *Theoretical determination of ground spin state and corresponding spin state splitting for a series of iron-oxo and iron-hydroxo complexes with different oxidation state of central metal ion*

"One of the major research areas that stay in the focus of the scientific eye are those where different oxidation and spin states of first-row TM ions are involved. This can be confirmed by a great number of valuable experimental and theoretical studies. As it was already discussed, changes in the orbital occupation patterns (and hence spin states) have a great effect on catalysis[349-353] but also can lead to changes in the reaction paths that are being followed.[354] Unfortunately, the resulting intermediates and transition states are in most cases too short-lived for experimental characterization, leading to discussions about their existence and character. For this reason, DFT emerged as an irreplaceable tool for investigation and explanation of chemical events in this field of research."[286]

"Among many systems containing first row TM ions, high-valent iron-oxo molecules hold a special value due to the fact that they play an essential role in the mechanism of heme and non-heme iron enzymes, and are widely used in various fields, such as industrial catalysis, biology, and medicine.[80, 355] Various iron-oxo complexes have been experimentally and theoretically examined, however many questions still remain. Answers about their structure, oxidation state, ground spin state, and the effect these characteristics have on their properties and reactivity are still required.[98, 356] Many of these uncertainties have been illuminated and clarified in the past with the help of theoretical methods.[357-363] Such an example is without a doubt the intriguing Sc^{3+}-capped iron-oxo complex $[(TMC)(Fe^{III/IV}\text{-}O\text{-}Sc^{III})(OTf)_4(OH_x)]$ (TMC = 1,4,8,11-tetramethyl-1,4,8,11-tetraazacyclotetradecane), synthesized by Fukuzumi, Nam and co-workers and later characterized by X-ray crystallography.[364] Initial experimental investigations created additional uncertainties about the assignment of the oxidation state of central metal ion, and thus this interesting complex remained under scientific scrutiny.[98, 356] Later on, DFT was successfully utilized to illuminate structural characteristics and give a proposition that the complex should be reformulated as $[(TMC)(Fe^{III}\text{-}O\text{-}Sc^{III})(OTf)_4(OH_2)]$, with an iron(III) oxidation state in the high-spin configuration.[357] With newly collected insight in hand, experimentalists soon after confirmed theoretical findings.[365] Namely, the complex was reinvestigated by X-ray crystallography, Mössbauer and EPR spectroscopy, whereas the high-spin iron(III) ground state was unambiguously confirmed. Most importantly, this example resembles the true power of DFT, proving its remarkable accuracy and affirming this method as trustworthy, even in cases when correct experimental data is unavailable."[286]

Thought by the mentioned example, we decided to provide a detailed study with the aim to test various DFAs for reproduction and confirmation of experimental data. For this purpose, 18 iron complexes (12 oxo and 6 hydroxo), with a broad pallet of ligands, are selected. Although it was already shown[357] in 2013, that accurate structural parameters could be obtained for a set of iron(III/IV) complexes, in present research we expand this set with recently characterized complexes to perform a thorough study of the influence of starting geometry and choice of DFA on obtained results. The examined set of iron molecules includes Fe^{II}-hydroxo, Fe^{III}-oxo, Fe^{III}-hydroxo complexes, as well as Fe^{IV}-oxo complexes, together with the challenging Sc^{3+}-capped complexes (*vide supra*). All investigated molecules are presented in *Figure 4.3.* Our study represents a search for the best DFA choice for accurate geometry optimization and unambiguous determination of the ground spin state for the chosen series of TM complexes. Furthermore, we have studied the thermodynamic aspects of the formation process for scandium triflate adduct with the Fe^{IV}-oxo complex,[356, 364] which gives detailed insight into the complex formation and confirms the oxidation state of iron in this Sc^{3+}-capped complex. All results that are going to be presented in forthcoming chapters are already publisched and discussed in the original paper.[286]

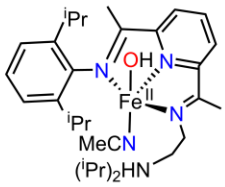

1. $[Fe^{II}(OH)(Hdidpa)CH_3CN]^{2+}$

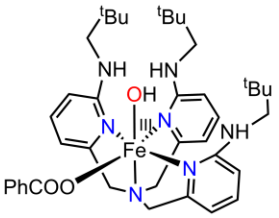

7. $[Fe^{III}(OH)(tnpa)(COOPh)]^{+}$

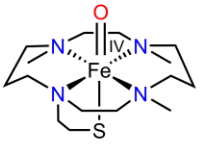

14. $[Fe^{IV}(O)(TMCS)]^{+}$

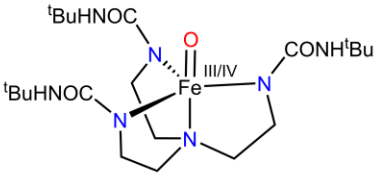

2. $[Fe^{III}(O)(H_3buea)]^{2-}$
9. $[Fe^{IV}(O)(H_3buea)]^{-}$

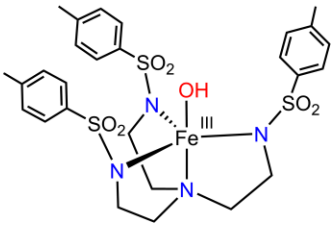

8. $[Fe^{III}(OH)(TST)]^{-}$

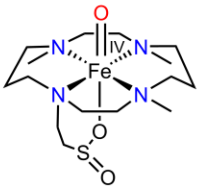

15. $[Fe^{IV}(O)(TMCSO_2)]^{+}$

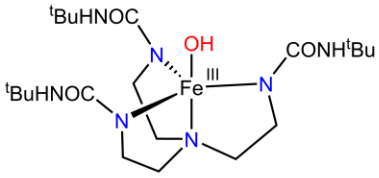

3. $[Fe^{III}(OH)(H3buea)]^{-}$

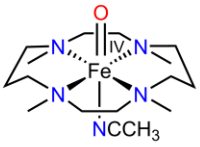

10. $[Fe^{IV}(O)(TMC)(NCCH_3)]^{2+}$

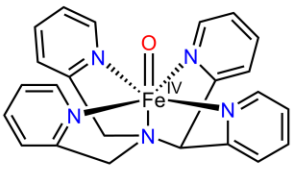

16. $[Fe^{IV}(O)(N_4Py)]^{2+}$

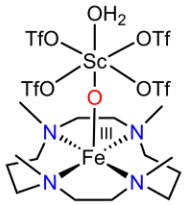

4. $[(TMC)Fe^{III}(O)(Sc^{3+}(OTf)_4OH_2)]$

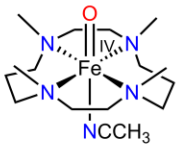

11. $[Fe^{IV}(O)(TMC^{i})(NCCH_3)]^{2+}$

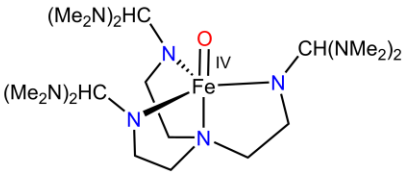

17. $[Fe^{IV}(O)(TMG_3tren)]^{2+}$

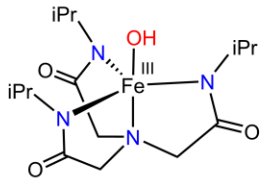

5. $[Fe^{III}(2,2',2''$-nitrilo-*k*N)tris(N-(1-methylethyl)acetamidato-kN)(OH)$]^{-}$

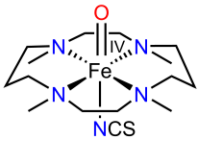

12. $[Fe^{IV}(O)(TMC)(NCS)]^{+}$

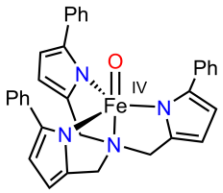

18. $[Fe^{IV}(O)(tpaPh)]^{-}$

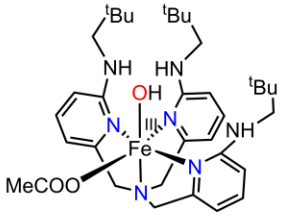

6. $[Fe^{III}(OH)(tnpa)(COOMe)]^{+}$

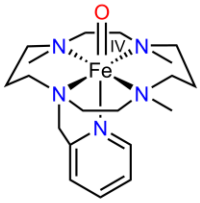

13. $[Fe^{IV}(O)(TMC\text{-}Py)]^{2+}$

Figure 4.3. Structures of 18 investigated $Fe^{II}/Fe^{III}/Fe^{IV}$-(hydr)oxo complexes

4.2.1. Geometry optimizations

In the first step of our research, we have tested various DFAs for the geometrical optimization of a broad set of complexes, containing $Fe^{II}/Fe^{III}/Fe^{IV}$ iron-oxo and iron-hydroxo chemical species coordinated with different types of ligands. Experimentally obtained data (if available), including structural and spectroscopic characteristics, is indicated in *Table 4.24*. In order to find the best functional for the optimization of investigated structures, we have used three classes of DFAs: (i) the local density approximation (LDA); (ii) three general gradient approximation (GGA) functionals, S12g, BP86-D_3, and PBE-D_2; and (iii) two hybrid functionals, B3LYP and S12h. Geometrical parameters obtained from our geometrical optimizations are in good agreement with the results from previous theoretical study[357], as well as with the experimental data. All details can be found in *Figure 4.4.* and *Tables 30-33*. "It should be noted that in ref.[357] two outliers were reported, $[Fe^{III}(OH)(H_3buea)]^-$ and $[Fe^{III}(OOH)(TMC^i)]^{2+}$ that showed apparent deviations of ca. 0.08-0.10 Å. However, upon reinvestigating the original sources[61, 86], it was found that the experimental data mentioned in ref.[357] were referring to complexes with iron in a different oxidation state; the actual experimental Fe-O distances for $[Fe^{III}(OH)(H_3buea)]^-$ (1.93 Å)[366] and $[Fe^{III}(OOH)(TMC^i)]^{2+}$ (1.85 Å)[367] are in fact in excellent agreement with the computed data of 1.932 Å and 1.842 Å, respectively. Since $[Fe^{III}(OH)(H_3buea)]^-$ is a complex of interest for the present research, here we use the corrected data (*Tables 2.24-2.26.*)."[286]

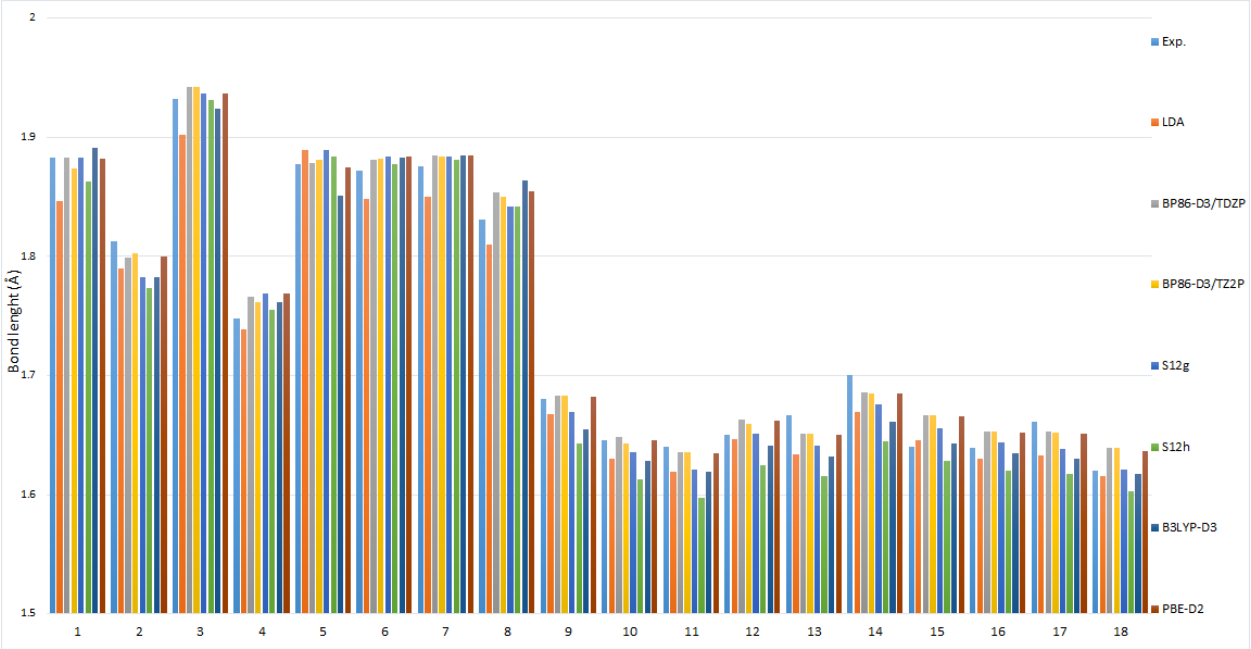

Figure 4.4. The difference between the experimentally obtained $Fe^{II/}Fe^{III}/Fe^{IV}$-oxygen bond lengths and those from different DFAs. for all 18 investigated complexes

"First of all, we focus on the optimized geometries of the experimentally observed spin ground state for each of the 18 complexes. Bond lengths of interest for our work are in all cases the axial iron-oxygen (Fe-O) distance (related to oxo, hydroxo) the axial iron-nitrogen (Fe-N_{ax}) distance and the average of the *in-plane* iron-nitrogen/oxygen (Fe-N/O_{eq}) distances. The best agreement with experimentally observed Fe-O bond lengths was obtained using the dispersion corrected BP86-D_3 PBE-D2/TZ2P and S12g/TZ2P, with a mean absolute deviation of 0.011-0.014 Å (*Table 4.24.*)."[286]

Table 4.24. $Fe^{II}/Fe^{III}/Fe^{IV}$–O ligand distances (Å) for 18 investigated complexes, calculated with different DFAs and basis sets

DFA:	Exp.	Exp.	LDA	PBE-D_2	BP86-D_3	BP86-D_3	S12g	S12h	B3LYP-D_3	*Ref.*
Basis:			TZ2P	TZ2P	TDZP	TZ2P	TZ2P	TZ2P	TZ2P	
Molecule 1.	HS	1.883	1.853	1.890	1.890	1.874	1.874	1.886	1.903	368
Molecule 2.	HS	1.813	1.790	1.793	1.799	1.803	1.783	1.773	1.783	86
Molecule 3.	HS	1.932	1.902	1.932	1.942	1.942	1.937	1.931	1.924	366
Molecule 4.	HS	1.748	1.739	1.762	1.766	1.762	1.769	1.755	1.762	369
Molecule 5.	HS	1.877	1.889	1.875	1.878	1.881	1.889	1.884	1.851	370
Molecule 6.	HS	1.872	1.848	1.884	1.881	1.882	1.884	1.877	1.883	371
Molecule 7.	HS	1.876	1.850	1.885	1.885	1.884	1.884	1.881	1.885	372
Molecule 8.	HS	1.831	1.810	1.855	1.854	1.850	1.842	1.842	1.864	373
Molecule 9.	HS	1.680	1.668	1.678	1.683	1.683	1.669	1.643	1.655	87
Molecule 10.	IS	1.646	1.630	1.645	1.648	1.643	1.636	1.613	1.628	88
Molecule 11.	IS	1.64	1.619	1.634	1.636	1.636	1.621	1.597	1.619	89
Molecule 12.	IS	1.65	1.647	1.659	1.663	1.659	1.651	1.625	1.641	93, 94
Molecule 13.	IS	1.667	1.634	1.648	1.651	1.651	1.641	1.616	1.632	90
Molecule 14.	IS	1.70	1.669	1.683	1.686	1.685	1.676	1.645	1.661	374
Molecule 15.	IS	1.64	1.646	1.662	1.667	1.667	1.656	1.628	1.643	91
Molecule 16.	IS	1.639	1.630	1.648	1.653	1.653	1.644	1.620	1.635	83, 84
Molecule 17.	HS	1.661	1.633	1.646	1.653	1.652	1.638	1.617	1.630	81, 82
Molecule 18.	HS	1.62	1.616	1.630	1.639	1.639	1.621	1.603	1.617	92
max. abs. error			0.033	0.024	0.027	0.027	0.030	0.055	0.039	
mean error			-0.017	0.002	0.006	0.004	-0.003	-0.019	-0.009	
mean abs. error			0.019	0.011	0.012	0.011	0.014	0.023	0.019	

**L=((2,2',2"-nitrilo-kN)tris(N-(1-methylethyl)acetamidato-kN))

Excellent agreement with experimental data, for the in-plane (equatorial) Fe-N_{eq}/Fe-O_{eq} bond distances, is obtained on BP86-D3 and PBE-D2 levels of theory, with a mean absolute error value of 0.060 Å for Fe-N_{eq} (*Table 4.25.*), and 0.024 and 0.027 Å for Fe-O_{eq} . (*Table 4.24.*). Larger deviations can be observed for the axial Fe-N_{ax} bond lengths (0.05-0.08 Å). Such disagreement between experimental results and DFT calculations can be attributed most likely to the influence of crystal packing, which can significantly shorten the M-L bond lengths in real systems. If considered together, obtained geometrical parameters clearly indicate the best performing functional for the optimization is BP86-D3, in particular with the TDZP basis, which is, therefore, a fast and effective route to accurate TM complexes geometry optimization.

Table 4.25. $Fe^{II}/Fe^{III}/Fe^{IV}$–N_{av}(in-plane) ligand distances (Å) for 18 investigated complexes, calculated with different DFAs and basis sets

DFA:	Exp.	Exp.	LDA	PBE-D_2	BP86-D_3	BP86-D_3	S12g	S12h	B3LYP-D_3	*Ref.*
Basis:			TZ2P	TZ2P	TDZP	TZ2P	TZ2P	TZ2P	TZ2P	
Molecule 1.	HS	2.065	2.134	2.123	2.124	2.093	2.150	2.168	2.064	[368]
Molecule 2.	HS	2.089	2.014	2.075	2.078	2.070	2.095	2.112	2.110	[86]
Molecule 3.	HS	2.016	1.973	2.021	2.014	2.012	2.022	2.037	2.034	[366]
Molecule 4.	HS	2.175	2.157	2.202	2.191	2.194	2.233	2.259	2.207	[369]
Molecule 5.	HS	2.022	1.990	2.045	2.031	2.034	2.054	2.050	2.049	[370]
Molecule 6.	HS	2.179	2.134	2.199	2.208	2.200	2.241	2.216	2.212	[371]
Molecule 7.	HS	2.198	2.128	2.193	2.197	2.195	2.241	2.210	2.209	[372]
Molecule 8.	HS	2.035	2.003	2.030	2.040	2.031	2.023	2.023	2.009	[373]
Molecule 9.	HS	2.007	1.951	1.999	1.997	1.995	2.012	2.008	2.011	[87]
Molecule 10.	IS	2.084	2.056	2.100	2.103	2.203	2.140	2.122	2.126	[88]
Molecule 11.	IS	2.08	2.045	2.097	2.089	2.089	2.138	2.126	2.113	[89]
Molecule 12.	IS	2.07	2.057	2.109	2.104	2.112	2.143	2.128	2.131	[93, 94]
Molecule 13.	IS	2.090	2.040	2.086	2.083	2.083	2.116	2.101	2.107	[90]
Molecule 14.	IS	2.09	2.051	2.103	2.098	2.098	2.137	2.123	2.127	[374]
Molecule 15.	IS	2.05	2.060	2.110	2.106	2.106	2.143	2.129	2.131	[91]
Molecule 16.	IS	1.972	1.913	1.967	1.958	1.958	1.983	1.982	1.986	[83, 84]
Molecule 17.	HS	2.032	1.947	1.998	1.990	1.989	2.024	2.018	2.012	[81, 82]
Molecule 18.	HS	1.99	1.914	1.964	1.952	1.952	1.979	1.976	1.973	[92]
max. abs. error			0.085	0.060	0.059	0.119	0.093	0.103	0.081	
mean error			-0.038	0.010	0.007	0.009	0.035	0.030	0.020	
mean abs. error			0.046	0.021	0.021	0.025	0.038	0.035	0.028	

Table 4.26. $Fe^{II}/Fe^{III}/Fe^{IV}–N_{ax}$ ligand distances (Å) for 18 investigated complexes, calculated with different DFAs and basis sets

DFA:	Exp.	Exp.	LDA	PBE-D_2	BP86-D_3	BP86-D_3	S12g	S12h	B3LYP-D_3	*Ref.*
Basis:			TZ2P	TZ2P	TDZP	TZ2P	TZ2P	TZ2P	TZ2P	
Molecule 1.	HS	2.063	1.924	2.004	2.000	1.999	2.044	2.066	1.926	[368]
Molecule 2.	HS	2.271	2.293	2.367	2.316	2.316	2.359	2.331	2.325	[86]
Molecule 3.	HS	2.171	2.287	2.338	2.346	2.327	2.272	2.320	2.313	[366]
Molecule 4.	HS	-	-	-	-	-	-	-	-	[369]
Molecule 5.	HS	2.194	2.244	2.269	2.278	2.273	2.273	2.247	2.264	[370]
Molecule 6.	HS	2.150	2.173	2.213	2.191	2.190	2.207	2.198	2.200	[371]
Molecule 7.	HS	2.158	2.172	2.216	2.191	2.193	2.207	2.198	2.200	[372]
Molecule 8.	HS	2.358	2.421	2.525	2.454	2.421	2.601	2.550	2.617	[373]
Molecule 9.	HS	2.064	2.041	2.103	2.082	2.081	2.111	2.190	2.108	[87]
Molecule 10.	IS	2.058	1.921	1.988	1.986	1.986	2.044	2.060	2.034	[88]
Molecule 11.	IS	2.10	1.961	2.071	2.058	2.061	2.298	2.341	2.134	[89]
Molecule 12.	IS	2.07	1.879	1.944	1.933	1.930	1.988	1.928	1.984	[93, 94]
Molecule 13.	IS	2.118	2.044	2.134	2.128	2.129	2.187	2.182	2.164	[90]
Molecule 14.	IS	-	-	-	-	-	-	-	-	[374]
Molecule 15.	IS	-	-	-	-	-	-	-	-	[91]
Molecule 16.	IS	2.033	2.019	2.074	2.059	2.064	2.085	2.096	2.094	[83, 84]
Molecule 17.	HS	2.112	2.055	2.137	2.105	2.109	2.139	2.153	2.134	[81, 82]
Molecule 18.	HS	1.99	1.914	1.964	1.952	1.952	1.979	1.976	1.973	[92]
max. abs. error			0.191	0.167	0.175	0.156	0.243	0.241	0.259	
mean error			-0.035	0.033	0.015	0.011	0.064	0.067	0.041	
mean abs. error			0.076	0.074	0.061	0.057	0.080	0.087	0.077	

Table 4.27. $Fe^{III}–O_{eq}$ ligand distances (Å) for 2 investigated complexes, calculated with different DFAs and basis sets

DFA:	Exp.	Exp.	LDA	PBE-D_2	BP86-D_3	BP86-D_3	S12g	S12h	B3LYP-D_3	*Ref.*
Basis:			TZ2P	TZ2P	TDZP	TZ2P	TZ2P	TZ2P	TZ2P	
Molecule 6.	HS	1.998	1.989	1.994	1.992	1.990	1.987	1.963	1.969	[371]
Molecule 7.	HS	1.988	1.993	1.996	1.992	1.988	1.987	1.970	1.975	[372]
max. abs. error			0.009	0.008	0.006	0.008	0.011	0.035	0.029	
mean error			-0.002	0.002	-0.001	-0.004	-0.006	-0.027	-0.021	
mean abs. error			0.007	0.006	0.005	0.004	0.006	0.027	0.021	

4.2.2. Spin state energetics

In the second part of the investigation, we are confronting the main goal of this research, that is, the unambiguous determination of the correct ground spin state. Since all of the complex molecules of interest for this study contain iron as the central metal ion we are dealing with partially filled *d*-orbitals. For this reason, there is more than one possible spin state, and in most cases, these spin states are close in energy. After optimizations have been done with all previously mentioned DFAs, obtained structures are further examined. Various DFAs are utilized for energy calculation of all possible spin states, with the aim to find the most convenient level of theory for unambiguous determination of the ground spin state. The calculations have been carried out in a single point fashion using one standard (BP86-D_3), two hybrid (B3LYP-D_3 and S12h), and three functionals specially designed for this particular kind of problem (OPBE, SSBD and S12g). In the present study, we also tested the performance of newly designed meta-GGA 'made very simple' functional (MGGA-MVS)[375]. While keeping in mind all previous statements about the tight relationship between geometrical parameters and spin state energetics[376], we present here the calculations carried out with all employed DFAs on BP86-D3 optimized geometries (*Table 4.28. and 4.29.*), since the geometries obtained on this level of theory are the closest to the experimentally obtained ones. Nevertheless, the complete data, obtained by energy calculation with eight different functionals, using structures from every level of theory optimization, is presented in the *Appendix section* of the resent thesis.

Table 4.28. Spin state energies (kcal·mol^{-1}) for Fe $^{II/III/IV}$-(hydr)oxo species calculated on BP86-D_3/TDZP optimized geometries, using four different density functionals (TZ2P basis)

DFA:		S12g			OPBE			BP86			SSB-D		
	Exp.	l.s.	i.s.	h.s.	l.s.	i.s.	h.s.	l.s.	i.s.	h.s.	l.s.	i.s.	h.s.
Molecule 1.	HS	3.8	0.0	0.8	4.8	0.0	4	0.0	0.3	10.8	11.6	3.7	0.0
Molecule 2.	HS	24.6	9.4	0.0	27.3	10.0	0.0	9.2	0.3	0.0	32.6	14.3	0.0
Molecule 3.	HS	13.6	5.6	0.0	13.7	5.2	0.0	1.5	0.0	3.6	21.7	10.3	13.6
Molecule 4.	HS	26.1	5.9	0.0	29.6	8.5	0.0	14.5	0.0	4.9	31.7	9.2	26.1
Molecule 5.	HS	12.4	9.6	0.0	10.8	7.6	0.0	10.7	8.7	0.0	11.3	9.3	12.4
Molecule 6.	HS	11.8	8.8	0.0	18.3	10.5	0.0	0.0	4.2	3.2	20.1	11.1	11.8
Molecule 7.	HS	7.8	12.2	0.0	12.2	21.6	0.0	0.0	12.0	9.9	12.8	13.1	0.0
Molecule 8.	HS	22.2	7.3	0.0	28.3	7.2	0.0	7.9	0.0	2.2	28.9	12.1	0.0
Molecule 9.	HS	25.9	17.5	0.0	23.0	19.6	0.0	14.5	9.6	0.0	31.3	19.8	0.0
Molecule 10.	IS	9.7	0.0	4.1	10.8	0.0	2.9	15.4	0.0	11.6	10.4	0.0	3.8
Molecule 11.	IS	9.4	0.0	5.0	10.8	0.0	5.4	7.7	0.0	13.1	9.9	0.0	4.6
Molecule 12.	IS	9.2	0.0	1.5	10.2	0.0	1.2	7.4	0.0	10.3	10.3	0.0	1.6
Molecule 13.	IS	9.6	0.0	4.3	11.1	0.0	3.8	7.8	0.0	12.8	10.7	0.0	4.6
Molecule 14.	IS	10.7	1.1	0.0	11.9	1.9	0.0	7.2	0.0	7.4	10.1	1.3	0.0
Molecule 15.	IS	10.4	0.5	0.0	12.5	1.1	0.0	8.0	0.0	7.8	11.1	1.0	0.0
Molecule 16.	IS	30.2	0.0	14.3	31.4	0.0	14.9	28.1	0.0	23.8	32.6	0.0	9.3
Molecule 17.	HS	27.1	22.3	0.0	29.6	24.1	0.0	18.1	16.6	0.0	30.6	24.9	0.0
Molecule 18.	HS	20.4	24.2	0.0	23.9	26.4	0.0	12.4	19.4	0.0	24.2	28.2	0.0

Table 4.29. Spin state energies (kcal·mol^{-1}) for Fe $^{II/III/IV}$-(hydr)oxo species calculated on BP86-D_3/TDZP optimized geometries, using three different density functionals (TZ2P basis)

DFA:		B3LYP			S12h			MVS		
	Exp.	l.s.	i.s.	h.s.	l.s.	i.s.	h.s.	l.s.	i.s.	h.s.
Molecule 1.	HS	16.8	9.7	0.0	31.8	18.4	0.0	19.4	7.9	0.0
Molecule 2.	HS	28.9	10.1	0.0	43.9	18.0	0.0	43.6	20.9	0.0
Molecule 3.	HS	0.0	12.7	4.5	0.0	29.7	13.2	0.0	33.5	16.7
Molecule 4.	HS	0.0	25.9	6.4	0.0	41.3	15.3	0.0	43.6	15.5
Molecule 5.	HS	0.0	11.8	8.9	0.0	10.7	8.1	0.0	40.5	17.9
Molecule 6.	HS	0.0	14.0	7.8	0.0	28.6	16.2	0.0	23.8	18.7
Molecule 7.	HS	9.1	12.5	0.0	23.9	19.9	0.0	24.4	21.8	0.0
Molecule 8.	HS	23.9	7.2	0.0	40.1	15.6	0.0	42.2	18.3	0.0
Molecule 9.	HS	28.3	17.8	0.0	41.1	24.8	0.0	41.7	29.1	0.0
Molecule 10.	IS	28.2	0.0	2.4	35.6	3.9	0.0	14.9	0.0	0.7
Molecule 11.	IS	28.5	0.0	3.9	35.0	2.9	0.0	20.4	5.7	0.0
Molecule 12.	IS	27.9	0.0	1.5	37.3	6.0	0.0	10.6	0.7	0.0
Molecule 13.	IS	28.4	0.0	3.8	31.7	0.0	-3.4	9.0	0.0	1.9
Molecule 14.	IS	28.9	3.0	0.0	39.8	10.0	0.0	18.9	4.6	0.0
Molecule 15.	IS	29.4	0.4	0.0	40.1	7.6	0.0	11.8	3.8	0.0
Molecule 16.	IS	29.9	0.0	10.0	33.3	0.0	1.6	38.3	0.0	7.2
Molecule 17.	HS	31.1	25.1	0.0	42.4	32.3	0.0	43.5	34.0	0.0
Molecule 18.	HS	23.8	56.9	0.0	34.3	69.3	0.0	37.6	37.4	0.0

As it is can be seen from *Chapter 3.4.1*, LDA is by design derived from a uniform electron gas and thus we can not expect from this DFA to give a proper description of different spin states and corresponding energetics. Because of that, results obtained with this DFA are not included in the examination of the spin state energetics, although they can be found in the *Appendix section*. According to the experiment, the ground spin state of all investigated Fe^{II}, Fe^{III} and Fe^{IV} species is either intermediate (IS, 10-16) or high spin (HS, 1-9, 17, 18). According to the general properties of HF, and hybrid functionals that include a certain portion of HF (*Chapter 3.1* and *3.4.4.*), it can be expected that they will favor HS over other spin states. Another phenomenon that can occur, while using these DFAs for spin state energetics, is a considerable amount of spin contamination.[377] In this regard, it is not surprising that our hybrid S12g functional (which contains 25% of HF) indeed favors the HS state for complexes 10-15, yet predicts the correct IS state for complex 16. Surprisingly, our second hybrid functional of choice (B3LYP-D3, which includes 20% HF exchange) determined the right IS ground spin for five of the investigated complexes (*e.g.* 10-13 and 16), although it predicts the wrong ground spin state in the case of complexes 14 and 15. Our research indicates inaccuracy of LDA and BP86-D3 for the determination of the ground spin state (even in the case of HS complexes), which was reported and discussed many times in the literature. According to our results, the best performance for the description of the spin states, an unambiguous determination of the ground spin state is attributed to OPBE, S12g, and SSB-D functionals. These three levels of theory are in general considered as the best choices for dealing with spin state energetics, and they showed success in many similar types of research from the past[337, 360, 378-381] Although S12g failed in prediction of IS ground state for complexes 14 and 15, this negligible energy difference of 0.5 and 1.1 kcal·mol^{-1} can be

attributed to the methodological error, but this conclusion should be taken with caution. Another aspect when it comes to energetically close lying spin states (IS and HS in this case), is that such molecules could be considered as examples of TM systems that can exhibit spin-crossover properties. Spin ground states determined with OPBE, S12g and SSB-D are in accordance with the experiment for all examined iron-oxo complexes, except for complexes $[Fe^{IV}(O)(TMCS)]^{+}$, $[Fe^{IV}(O)(TMCSO_2)]^{+}$, and complex $[Fe^{II}(OH)(Hdidpa)CH_3CN]^{2+}$. Since the first two complexes we may consider as spin-crossover examples (and will be the topic of future examinations), the only troublesome system is remaining complex 1. The wrong ground spin state is obtained as a result of keeping the attention focused on the electronic energy. However, if we extend our sight, and take int consideration the Gibbs free energy, it can be noted that the ΔG correction is 4.06 $kcal \cdot mol^{-1}$ in favor of the high-spin. Although in the case of OPBE the stabilization can be considered as almost negligible (0.1 $kcal \cdot mol^{-1}$), we have a significant stabilization in the case of S12g (3.3 $kcal \cdot mol^{-1}$). For this reason, we can say that S12g actually performs well for the complex molecule **1** and predicts the right HS state. While considering all results together, we can conclude that the best approach to obtain reliable results for the spin state energetics, and unambiguously determine the ground spin state is to employ dispersion corrected S12g. Although BP86-D3/TDZP provided better geometries, this functional fails when it comes to the description of the spin states. For this reason, it is important to emphasize that both good geometries and correct ground spin state can be obtained in one step by use of S12g, which might be sped up in some cases using the BP86-D3/TDZP geometries.

4.2.3. Thermochemical description of $[Fe^{n}(O)(Sc(OTf)_4(OH_m)]$ moiety formation

Now, when an appropriate method for investigation of spin state energetics is established, we can return and with confidence provide some additional theoretical insight for the mentioned scandium-containing iron-oxo complex. In 2013 it was already shown that Fe(III) represents the real chemical moiety present in this unusual molecule. The confirmation came from all previously mentioned experimental techniques and additionally enforced by a study using chromium as a central metal ion.[382] Although much has been done in order to investigate and characterize this complex, we still don't know anything about the character and the strength of the bond formed between the $[Sc(OTf)_4(OH_2)]^{-}$ moiety and the iron-oxo compartment. In forthcoming research, we will utilize the previously proposed approach for geometry optimization and energy calculation of involved chemical species. According to our previous results, we can be sure that geometrical parameters, as well as the obtained energies, will be precise and accurate. Therefore, we studied the $[Fe^{n}(O)(Sc(OTf)_4(OH_m)]$ molecule with S12g/TZ2P energies on BP86-D3/TDZP optimized structures (*Scheme 6.* and *Figure 4.5.*). It is important to highlight that n our research, the main focus is directed to thermochemistry, thus we do not consider the kinetics of the reaction.

	Reaction	ΔE_{elec} (kcal·mol^{-1})	ΔG (kcal·mol^{-1})
1	$[Fe^{IV}(O)(TMC)(NCCH_3)]^{2+} \rightarrow [Fe^{IV}(O)(TMC)]^{2+} + MeCN$	11.82	-0.9
2	$[Fe^{IV}(O)(TMC)]^{2+} + Fe(Cp)_2 \rightarrow [Fe^{III}(O)(TMC)]^{1+} + [Fe(Cp)_2]^{+1}$	15.20	13.02
3	$H_2O + MeCN \rightarrow OH^{-1} + MeCNH^{+1}$	62.79	58.32
4	$Sc(OTf)_3 + Sc(OTf)_3 + H_2O \rightarrow [Sc(OTf)_4(H_2O)]^{-1} + [Sc(OTf)_2]^{+1}$	-24.86	-7.29
5	$Sc(OTf)_3 + Sc(OTf)_3 + OH^{-1} \rightarrow [Sc(OTf)_4(OH)]^{-2} + [Sc(OTf)_2]^{+1}$	-55.57	-40.77
6	$[Sc(OTf)_4(OH)]^{-2} + [Fe^{IV}(O)(TMC)]^{2+} \rightarrow [Fe^{IV}(O)(Sc(OTf)_4(OH)]$	-12.66	4.83
7	$[Sc(OTf)_4(H_2O)]^{-1} + [Fe^{IV}(O)(TMC)]^{2+} + Fe(Cp)_2 \rightarrow [Fe^{III}(O)(Sc(OTf)_4(OH_2)] + [Fe(Cp)_2]^{+1\cdot}$	-50.49	-32.7
8	$[Sc(OTf)_4(H_2O)]^{-1} + [Fe^{III}(O)(TMC)]^{1+} \rightarrow [Fe^{III}(O)(Sc(OTf)_4(OH_2)]$	-65.69	-36.51

Scheme 6. Thermochemistry of sequential reactions included in the formation of the scandium-capped iron-oxygen complex $[Fe^{III}(O)Sc(OTf)_4(OH_2)]$

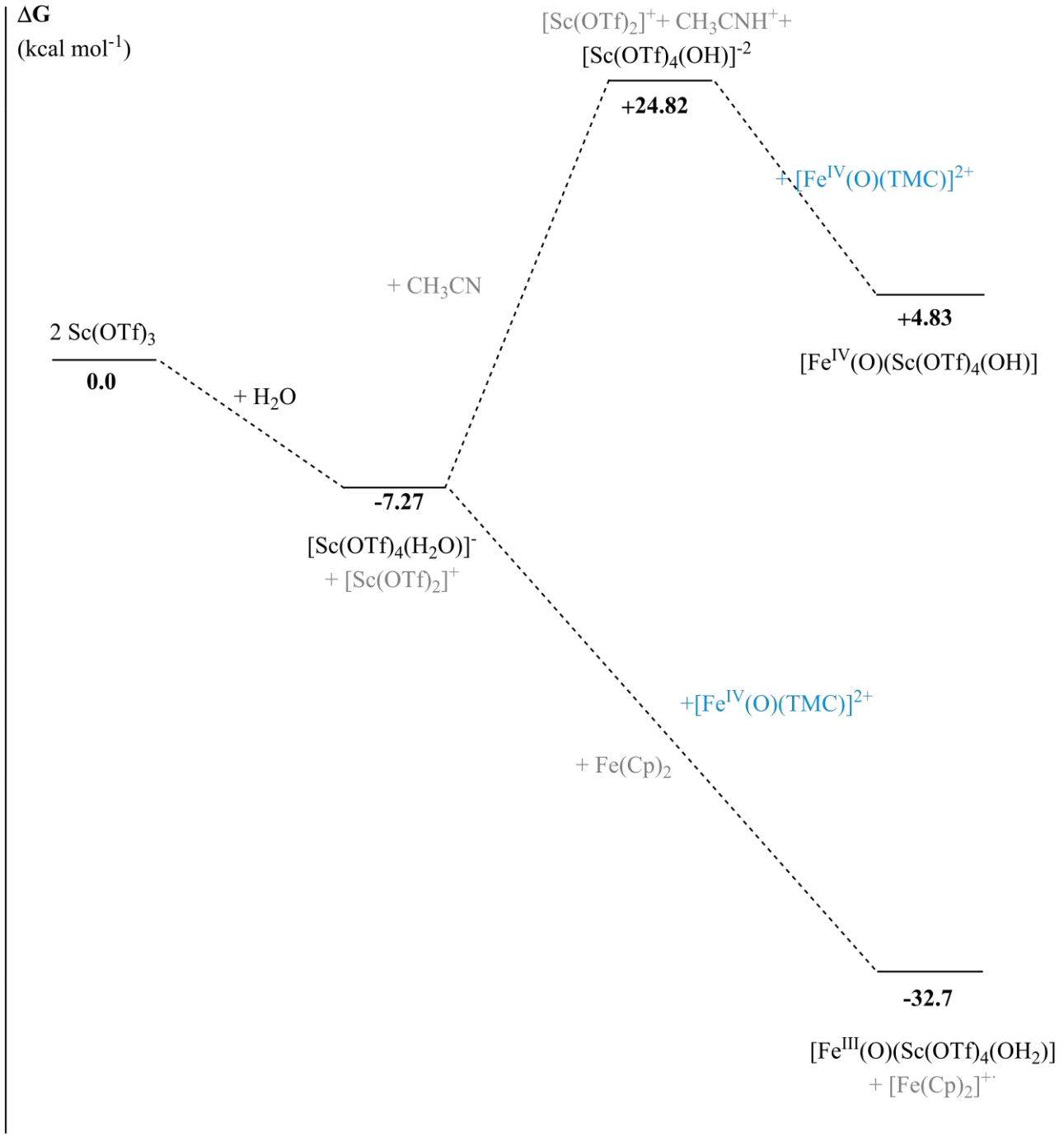

Figure 4.5. The Formation of the scandium-capped iron-oxygen complex $[Fe^{III}(O)Sc(OTf)_4(OH_2)]$

Our research indicates that the capping process of the $[Fe^{IV}(O)(TMC)]^{2+}$ which includes the scandium moiety, has an exergonic character in case of forming the Fe(III) complex. On the other hand, the same chemical process showed to be endergonic in the case of Fe(IV)-oxygen complex. These findings are fully consistent with the Fe-O and Sc-O distances found in the crystal structure[364], and the DFT study[357], and the Mössbauer studies (both the computational prediction[357] and experimental corroboration[365]).

4.2.4. Conclusions

"Within this study, the extension of the previous validation[357] of various DFAs for a correct description of spin state energetics for a series of $Fe^{II}/Fe^{III}/Fe^{IV}$ iron-oxo and iron-hydroxo complexes is presented. Bearing in mind that the change of the spin state is often associated with changes occurring in the geometry, structure relaxation of the LS, IS and HS state of 18 iron-oxo and iron-hydroxo species was allowed with six density functionals. Our theoretical findings, in accordance with experimental data, suggest that the HS or IS configuration is favored for all investigated species by the means of DFAs using OPBE, SSB-D, S12g, MVS and B3LYP-D3. However, LDA, BP86-D3 and S12h showed a tendency to predict a wrong spin ground state on the BP86-D3 optimized geometries. Overall geometries, obtained at S12g/TZ2P and BP86-D3/TDZP level of theories (including COSMO solvation and ZORA relativistic corrections) are in excellent agreement with the experimental data, for all molecules under study. It is noteworthy that BP86-D3/TDZP gave the best agreement with experimentally observed Fe-O and Fe-N_{eq} distances, while results for Fe-N_{ax} are satisfactory. When considered together, obtained data support few important conclusions: although one should be cautious while choosing the DFA for a correct prediction of the spin ground state, accurate spin state energies can be easily derived performing fast and efficient high-level theory single point calculations on correct geometry (for mononuclear metal complexes!). For all complexes under investigation, the best performance in determination of the spin ground state was obtained with OPBE, S12g, and SSB-D, which makes them an important tool for exploring and describing different spin states of various TM containing systems. With the caution that different research groups would recommend the use of different functionals, encouraged with these results we suggest S12g/TZ2P as the most reliable choice for both geometry optimization and determination of spin state and splittings in transition complexes: it provides both good geometries and accurate description of the electronic structure. This comprehensive validation study gives us the confidence to use S12g for studying and predicting properties of unknown TM compounds, which ultimately is one of the aims of theoretical (bio)inorganic chemistry."[286]

"After many discussions in the past[357, 364, 365] about oxidation and spin state of iron in scandium-capped iron-oxygen complex, here we provide additional computational support for the assignment of a Fe(III) oxidation state. The thermo-chemically most stable iron complex is unambiguously $[Fe^{III}(O)(Sc(OTf)_4(H_2O)]$, with a high-spin ground state."[286]

4.2.5. Computational details

All DFT calculations were performed with the Amsterdam Density Functional (ADF)[287, 334] and QUILD[383] programs. Molecular orbitals were expanded in an uncontracted set of STOs of triple-ζ quality with double polarization functions (TZ2P), or the TDZP basis set which consists of triple-ζ quality on the metal and double-ζ quality on all other atoms, in both cases including one polarization function. [384, 385] Core electrons were not treated explicitly during geometry optimizations (frozen core approximation). An auxiliary set of s, p, d, f, and g STOs was used to fit the molecular density and to represent the Coulomb and exchange potentials accurately for each SCF cycle.

Geometries of all possible spin states were optimized with the QUILD[383] program using adapted delocalized coordinates[379] until the maximum gradient component was less than 10^{-4} a.u. Energies and gradients were calculated using LDA, PBE-D_2[198], S12g[386], BP86-D_3, B3LYP-D_3 and S12h[386] functionals, in all cases by including solvation effects through the COSMO dielectric continuum model with appropriate parameters for each solvent used. Scalar relativistic corrections have been included self-consistently in all calculations by using the zeroth-order regular approximation (ZORA)[387, 388]. Geometry optimizations at the BP86-D_3 level of theory were performed with both TDZP and TZ2P, and optimizations with LDA (Slater exchange[389, 390] with Vosko-Wilk-Nusair[172]

correlation), PBE-D_2, S12g, B3LYP, S12h were performed with the TZ2P basis set. Subsequent single-point calculations (with the all-electron TZ2P basis set) have been performed on all optimized geometries, with S12g, BP86-D_3, OPBE, SSB-D, B3LYP-D_3, S12h, and MVS[375]. For all calculations carried out with LDA, PBE-D_2, OPBE, BP86-D_3, and B3LYP the Becke[391, 392] grid of normal quality was used; calculations performed with SSB-D, S12g and S12h were performed with a Becke grid of very good quality, and for MVS a grid of good quality with five times radial-grid boost was applied. Note that BP86-D_3, S12g, B3LYP-D_3 and S12h include Grimme's D_3, while PBE-D_2 and SSB-D functional include Grimme's D_2 dispersion energy scheme[197] with appropriate parameters; MVS was shown to already include a large part of the dispersion interactions implicitly for short- and medium-range weak interactions,[375] and hence there is less need to combine MVS with Grimme's D_3 scheme (although efforts to also describe long-range interactions correctly may be forthcoming). All DFA calculations were performed using the unrestricted Kohn-Sham scheme.

4.3. Energy decomposition analysis of iron-oxo and iron-hydroxo complexes

As it was highlighted and explained in previous sections, iron exists in various oxidation states, thus consequentially exhibits a broad pallet of spin states. Ground spin state and corresponding low lying excited states of a certain chemically active moiety are in most cases the driving force which defines and governs the chemical reaction they are included in. As we mentioned before, this is of utmost importance in the case of iron, since it plays an essential role in various biochemical reactions. In present work we will utilize DFT method supported by trustworthy S12g functional, which showed good performance for consistent description of spin state energetics (previous section), in order to investigate simple iron model-complexes of general formula $[(NH_3)_xFe^n(O)(Y)_{ax}]^{m+}$ and $[(NH_3)_xFe^n(OH)(Y)_{ax}]^{m+}$ presented in *Figure 4.6.* Similar model systems have been used before[351, 393], but the research has been mainly focused on reactivity. These simple models are in the focus of present work since their molecular properties and chemical behavior can be representative of much larger and more diverse molecular and biological systems. Our main goal is to use EDA approach in order to go beyond simple spin state energetics and illuminate the factors leading to spin state splitting.

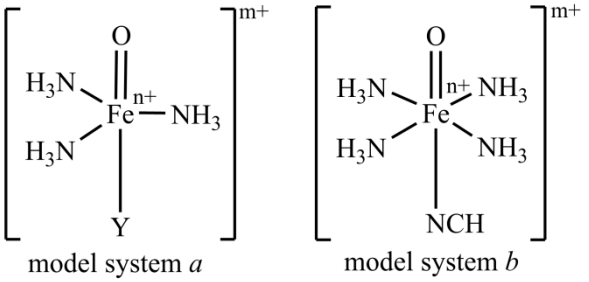

Y = NH3, NCH
n = 2, 3, 4
m = 0, 1, 2

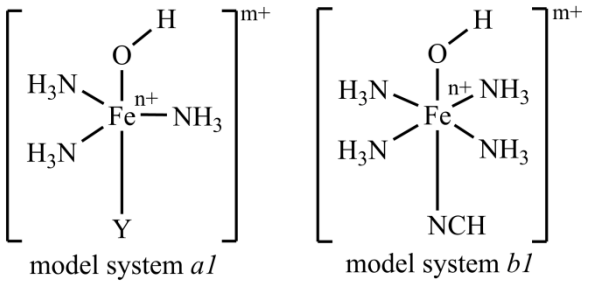

Y = NH_3, NCH
n = 3, 4
m = 2, 3

Figure 4.6. Investigated model systems with three different oxidation states of iron

4.3.1. Geometry optimizations

As well as in previous researches, the first step was the geometry optimization of all investigated complexes in three oxidation states (+2, +3 and +4) of a central metal ion. As we already discussed, the geometry of a certain complex is closely related to the ground spin state and thus, the population of close-lying excited states, as well as with spin state splitting between these states. Small changes in the coordination environment will lead to extreme changes in energy and ordering of present spin states. In order to obtain good geometries, we decided to use dispersion-corrected S12g functional with solvation effects included since it showed excellent performance for geometry optimization of iron-oxo and iron-hydroxo complexes in the previous study. According to the obtained results, we can consider this DFA as a smart and elegant one-step approach for obtaining good geometries and accurate spin state energetics. In the present research, we are investigating small and highly symmetric molecules in several spin states, corresponding to a specific oxidation state of iron. In this regard, some of these spin states are formally JT active, meaning that symmetry-lowering may result in more favorable energies. We started our geometry optimizations by applying the most symmetric ligand arrangement around central metal ion (C_{3v} and C_{4v} for *a* and *b* respectively, and C_s for both *a1* and *b1* model systems) in all three iron oxidation states. For all spin states that showed the JT activity, we allowed the distortion to take place by performing another geometry optimization and relaxing the structures to corresponding lower symmetry point group (C_s and C_{2v} respectively for *a* and *b* model systems *Figure 4.6.*). As expected, symmetry lowering for complexes in spin states prone to the JT effect resulted in geometries that are more stable than those of higher symmetry. The label of final symmetry point-group for all spin states can be found in *Tables 4.30-4.35*. Unlike in the case of

iron-oxo systems, geometry optimization of iron-hydroxo complexes was in most cases followed by the rotation of at least two axial ammonia ligands. This geometrical diversity combined with the change of oxo into hydroxo-group are taking place in the first coordination sphere, and is strongly influencing not only the atomic orbital overlap but the energy split between molecular orbitals. In this regard, a noticeable change in the overall spin state energetics picture of hydroxo complexes relative to corresponding oxo complexes can be expected. All geometrical details can be found included in the *Appendix section*.

4.3.2. Spin state splitting

Due to the simplicity, from this point forward, we will observe iron-oxo complexes separately from iron-hydroxo complexes. As it can be clearly seen from the *Figure 4.7*, in the case of iron-oxo complexes we have a consistent ground spin state for first two complexes (HS, IS and HS for +2, +3 and +4oxidation states respectively), although spin state energetics and resulting spin state splitting is rather different even for these two model systems which on the first glance we may say geometrically look alike. The third complex does not even follow the same trend for the ground spin state (LS, IS and IS for +2, +3 and +4 oxidation states respectively) and has significantly different values for the spin state splitting. These diversities originate from delicate differences in geometry and electronic structure.

In the case of iron-hydroxo complexes the same trend of ground state consistency can be observed for the first two model systems (HS and HS for +3 and +4 respectively), and a change for the third (HS and IS for III and IV respectively). Spin state splitting is even more diverse than for the previous models. One important thing to notice is that iron oxidation state +4 has the same ground spin state in all model systems (both oxo and hydroxo), whereas oxidation state +3 shows a change depending on the type of oxygen-containing group.

In order to locate, define and rationalize these differences we will apply EDA approach and generate physically meaningful contributions responsible for the stability of a certain complex.

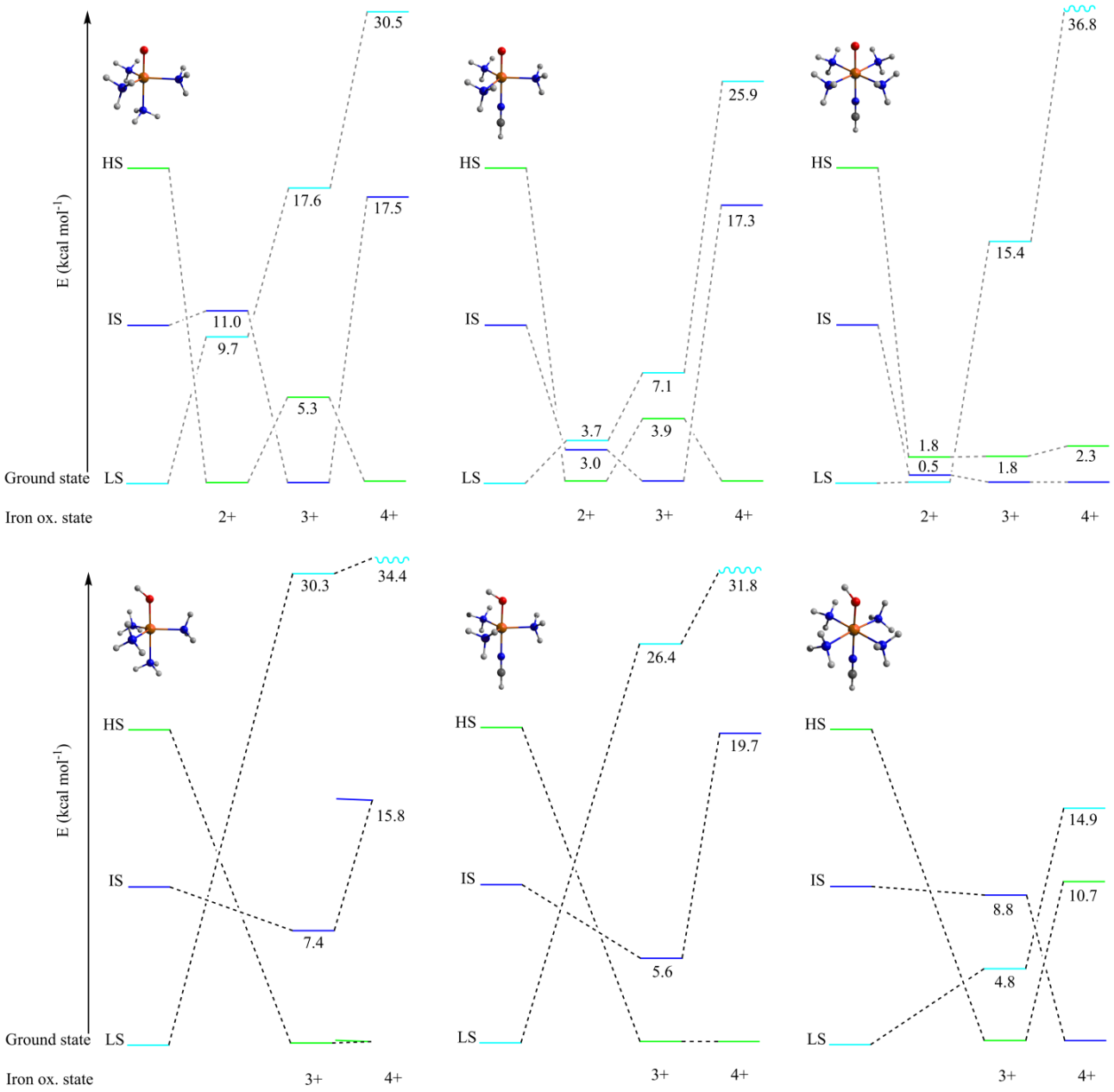

Figure 4.7. Spin state splitting for examined iron-oxo and iron-hydroxo model-complexes

4.3.3. Energy Decomposition Analysis

Details about EDA procedure, and information about corresponding contributions to the overall energy of a certain molecular system, can be found in *Chapter 3.7*. After the geometry optimization and relaxation of structures that were JT active, we decomposed all final geometries into two fragments from which one is iron in its specific oxidation state coordinated with oxygen atom or hydroxyl group (since this is the mutual unit for all complexes) and the other is constructed of all remaining ligands creating the coordination sphere (*Figure 4.8.*). In this way, we will be able to observe and investigate the form and amount of ligand interaction with iron-oxo/hydroxo compartment.[192] During the discussion, EDA contributions will be defined and rationalized relative to the ground spin state of a specific model system.

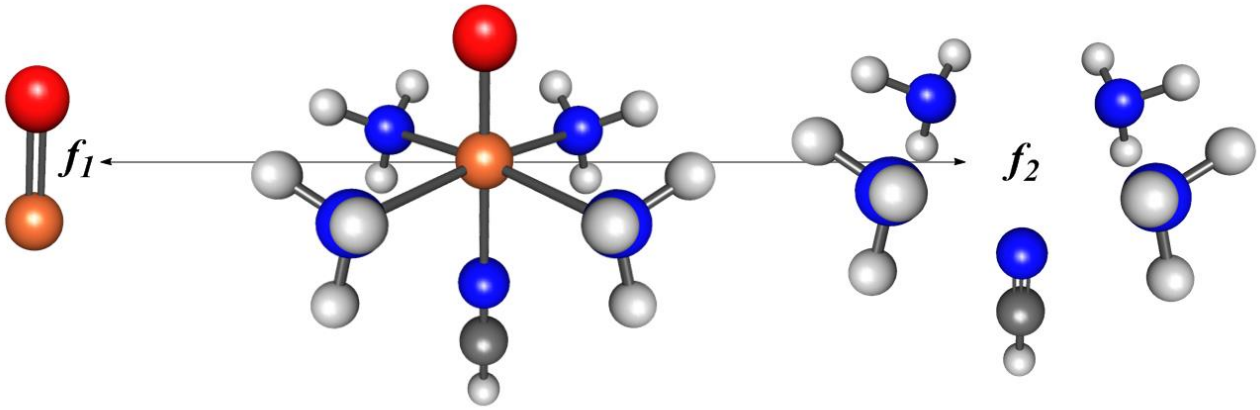

Figure 4.8. Decomposition of a molecule into fragments (iron coordinated with oxygen as *fragment 1* and all remaining ligands (four NH_3 and one NCH) as *fragment 2*)

4.3.3.1. EDA of $[(NH_3)_3Fe^n(O)(NH_3)]^{m+}$ complex

We will start the discussion with iron-oxo complexes, more precisely with the first model system containing three equatorial and one axial NH_3 ligand (*Figure 4.9.a.*). Mentioned complex in 2+ oxidation state of iron has an HS ground state. It is important to mention that iron-oxo $[Fe(O)]^{n+}$ unit on its own has an HS ground state, and the preparation energy needed to bring the $[Fe(O)]^{n+}$ from its preferred ground state to IS or LS is almost similar (~70 kcal mol^{-1} and ~64 kcal mol^{-1} respectively). This electronic effect is additionally boosted by strong Pauli repulsion (~34 kcal mol^{-1} and ~105 kcal mol^{-1} respectively, relative to the HS) lifting the IS and LS states in energy and explaining the HS character of this complex. It is important to notice that the sum of individual components for IS and LS is almost the same (although the EDA components vary), which explains small splitting between these two states. As it can be seen from the *Table 4.24.*, less energy is needed to bring HS iron-oxo component to LS, and at the same time, this excited state shows much stronger orbital interaction than the IS (~156 kcal mol^{-1} and ~126 kcal mol^{-1}, respectively), making LS the first excited state.

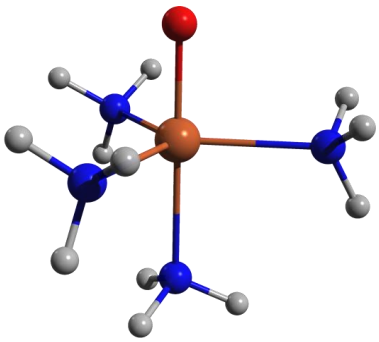

Figure 4.9.a. Geometry of $[(NH_3)_3Fe^n(O)(NH_3)]^{m+}$ complex

In the case of oxidation state 3+ the overall picture changes drastically. Preparation energy needed to excite preferred HS iron-oxo component to IS now counts only 15 kcal mol^{-1}. This energy requirement and negligibly stronger effect of Pauli repulsion in IS (~5 kcal mol^{-1}, relative to HS) can be easily counteracted by a favorable combination of Orbital interaction and Electrostatic interaction, making IS the ground state. Sum of Pauli, Orbital and Electrostatic interaction, known as the Interaction energy, has a stabilizing (~-24 kcal mol^{-1}, relative to HS) effect and is strong enough to overcome the excitation energy. Preparation energy needed for excitation of HS component to LS state is even larger than in the case of oxidation state 2+, and this unfavorable contribution is accompanied by even stronger Pauli repulsion, lifting this spin state in energy and creating much larger splitting.

Table 4.30. EDA parameters (kcal mol^{-1}) for $[(NH_3)_3Fe^n(O)(NH_3)]^{m+}$ model system calculated on ZORA/S12g/TZ2P level of theory

Ox. State		+2			+3			+4	
Spin state	LS	IS	HS	LS	IS	HS	LS	IS	HS
Symmetry	C_s	C_{3v}	C_s	C_s	C_s	C_{3v}	C_{3v}	C_s	C_{3v}
E	-2113.04	-2111.76	-2122.76	-2020.39	-2038.01	-2032.70	-1766.24	-1779.27	-1796.76
ΔEprep	102.30	100.07	28.45	125.38	42.14	23.91	68.91	44.39	25.35
ΔEdeform	0.50	0.03	0.01	0.01	0.04	0.03	0.17	0.19	0.15
ΔElig-lig	22.22	14.52	12.57	21.88	16.68	13.57	25.71	22.77	18.09
ΔEval.xc	79.58	85.52	15.92	103.49	25.42	10.31	43.03	21.43	7.11
ΔEint	-130.50	-126.03	-65.73	-259.69	-193.64	-169.93	-383.67	-372.06	-370.25
ΔEpauli	258.52	186.98	153.22	280.16	157.63	152.62	238.25	199.88	184.37
ΔEelstat	-233.02	-187.15	-135.56	-260.92	-211.55	-198.61	-302.70	-286.33	-287.25
ΔEorbint	-156.00	-125.86	-83.39	-278.93	-139.72	-123.94	-319.22	-285.61	-267.37
C_{3v} C_s									
A1 *A`*	-114.64	-38.60	-63.42	-240.22	-103.77	-53.38	-111.64	-176.93	-122.61
A2 *A``*	-41.36	-0.86	-19.97	-38.71	-35.94	-1.90	-5.68	-108.68	-5.38
E1 -	-	-86.40	-	-	-	-68.66	-201.89	-	-139.38
ΔEdisp	-5.39	-6.35	-6.04	-5.82	-6.28	-6.47	-5.72	-5.78	-6.02
ΔEtotal	-28.2	-25.96	-37.28	-134.31	-151.5	-146.02	-314.76	-327.67	-344.9

In 4+ oxidation state of iron, the ground spin state is reversed again. As it can be seen, the preparation energy for the excitation of preferred HS to IS is still small and affordable (~14 kcal mol^{-1}, relative to HS), but cannot be overcame by small stabilizing effect of Interaction energy, since there is not enough stabilization, originating from Orbital interaction and Electrostatic interaction, needed to counteract destabilizing Pauli repulsion. The interaction energy of LS is only ~13 kcal mol^{-1} higher and the driving force creating large splitting is unfavorable excitation energy needed to bring the preferred component to LS state.

4.3.3.2. EDA of $[(NH_3)_3Fe^n(O)(NCH)]^{m+}$ complex

As mentioned before, geometrical aspects are one of the main factors governing the spin state ordering. Our second model system has a similar coordination environment, containing three equatorial NH_3 and one axial NCH ligand (*Figure 4.9.b.*), and all optimized structures of this model system are similar to the previous one (*Appendix section*). As expected, the qualitative picture did not change, and spin state ordering is the same as for the previous (*Figure 4.7.*, *Table 4.31.*). Although the ground spin state is retained for all three oxidation states, spin state splitting changed, and a closer look at the geometries reveals slight but important geometrical differences that influence the general result.

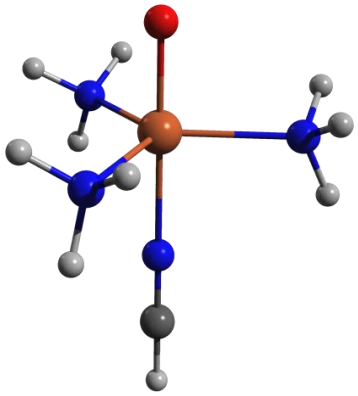

Figure 4.9.b. Geometry of $[(NH_3)_3Fe^n(O)(NCH)]^{m+}$ complex

Namely, in oxidation state 2+, the distance between the central metal ion and equatorial ammonia ligands stayed almost the same as in the first model system, yet bond length between a metal ion and axial NCH is shorter (~ 0.3Å) than in the case of axial NH_3. This bond shortening is causing destabilizing Pauli repulsion energy to increase, but at the same time it is providing stronger orbital overlap, and as a general result, we have stronger Interaction energy. Excitation energy is almost the same as for the first model system, yet we have dominantly stronger Interaction, which is lowering the energy and reducing the spin state splitting.

Spin state splitting for iron oxidation state 3+ changed drastically. In HS, shortening (~ 0.1Å) of M-$L_{(eq)}$ took place and was accompanied by an elongation (~ 1.3Å) of M-$L_{(ax)}$. This effect can be clearly noticed in Orbital interaction contribution, since stabilization decreased for orbitals of A_1 symmetry (corresponding to axial *d* orbitals), and increased for orbitals of E_1 symmetry (corresponding to equatorial *d* orbitals). Although the overall effect is weaker Orbital interaction energy, we have a decrease of destabilizing Ligand-Ligand interaction (due to the elongation of M-$L_{(ax)}$) and reduction of the orbital splitting. The ground spin state remains IS, showing a negligible shortening of all M-L bonds followed by a rotation of equatorial ligands. This geometrical change is causing a less favorable Orbital interaction, thus a slight destabilization of IS and smaller spin state splitting between the ground and remaining excited spin states. In LS state a shortening of M-$L_{(ax)}$ took place resulting in more favorable Orbital interaction and stronger Interaction energy, which further stabilizes this spin state. Synergic effect of IS destabilization and stabilization of LS state led to a sufficient decrease of splitting between these two spin states, and as a final result, we have almost the same energy requirement for the excitation of the ground spin state either to HS or LS.

Table 4.31. EDA parameters (kcal mol^{-1}) for $[(NH_3)_3Fe^n(O)(NCH)]^{m+}$ model system calculated on ZORA/S12g/TZ2P level of theory

Ox. State		+2			+3			+4	
Spin state	LS	IS	HS	LS	IS	HS	LS	IS	HS
Symmetry	C_s	C_{3v}	C_s	C_s	C_s	C_{3v}	C_{3v}	C_s	C_{3v}
E	-2142.08	-2142.79	-2145.81	-2035.01	-2042.12	-2038.26	-1775.58	-1784.21	-1801.49
ΔEprep	109.87	99.67	25.81	122.54	37.81	13.16	63.71	38.84	20.08
ΔEdeform	13.49	1.35	0.43	0.10	0.10	0.05	0.37	0.37	0.38
ΔElig-lig	19.62	13.44	11.00	19.11	12.97	4.75	18.06	17.41	13.10
ΔEval.xc	76.76	84.88	14.38	103.34	24.75	8.36	45.28	21.06	6.60
ΔEint	-162.10	-151.91	-80.99	-266.63	-188.54	-160.48	-383.12	-366.55	-364.88
ΔEpauli	374.67	258.23	222.57	320.40	162.46	163.6	230.97	201.55	184.24
ΔEelstat	-281.56	-220.66	-165.95	-269.57	-208.88	-204.04	-300.76	-282.65	-281.76
ΔEorbint	-255.21	-189.48	-137.61	-317.46	-142.12	-120.04	-313.33	-285.45	-267.36
C_{3v} C_s									
A_1 $A`$	-186.44	-50.14	-91.45	-266.90	-101.91	-40.38	-93.63	-167.96	-109.35
A_2 $A``$	-68.77	-0.95	-46.16	-50.56	-40.21	-2.42	-5.82	-117.49	-5.45
E_1 -	-	-138.39	-	-	-	-77.24	-213.87	-	-152.56
ΔEdisp	-4.56	-5.29	-5.32	-4.88	-5.32	-4.88	-4.56	-4.76	-5.01
ΔEtotal	-52.23	-52.24	-55.18	-144.09	-150.73	-147.32	-319.41	-327.71	-344.8

As it can be seen from *Figure 4.7.*, as well as from *Table 4.31.*, there are no drastic changes in the case of oxidation state 4+. This phenomenon is explained by the fact that both model systems have similar optimized geometries in all spin states.

4.3.3.3. EDA of $[(NH_3)_4Fe^n(O)(NCH)]^{m+}$ complex

Geometry of the third model system is noticeably different (*Figure 4.9.c.*), since it has an additional equatorial NH_3 ligand, and in this regard, we have sufficiently different results for EDA components (*Table 4.32.*), as well as for the resulting spin state splitting (*Figure 4.7.*).

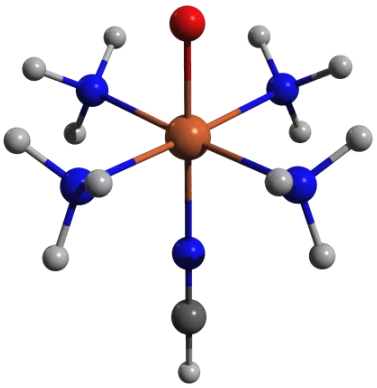

Figure 4.9.c. Geometry of $[(NH_3)_4Fe^n(O)(NCH)]^{m+}$ complex

On a first glance EDA components for complex in which iron has oxidation state 2+ look considerably different for three possible spin states. As it can be expected and noted from *Table 4.32.*, this complex shows stronger orbital interaction starting from HS and going to LS due to the shortening of M-L distances (*Appendix section*), but at the same time a stronger destabilizing effect of the Pauli repulsion and Ligand-Ligand interaction energy. After we add the unfavorable Excitation energy effect to the interplay of previously mentioned contributions we obtain almost the same amount of stabilization for all three spin states (-45.86, -41.43 and -40.78 kcal mol^{-1} for LS, IS and HS respectively). As a final result, LS stands out as a ground state with negligible spin state splitting (*Figure 4.7.*), thus we can consider this model system as a transition complex.

Complex with iron oxidation state 3+ shows much smaller energy requirement for excitation from preferred HS to IS, which is overcome by stronger stabilizing interaction effect based on more favorable Orbital interaction in IS. After the addition of the Ligand-Ligand destabilizing component, we have IS as ground state and HS negligibly higher in energy. Unlike HS, LS is considerably higher in energy. If we take into account that the sum of stabilizing Interaction contribution and destabilizing Excitation energy is almost the same for all three spin states (-180.76, -181.38, and -176.03 kcal mol^{-1} for LS, IS and HS respectively), it is obvious that the reason for this larger spin state splitting lies in strong destabilizing Ligand-Ligand effect which lifts LS in energy.

Table 4.32. EDA parameters (kcal mol^{-1}) for $[(NH_3)_4Fe^n(O)(NCH)]^{m+}$ model system calculated on ZORA/S12g/TZ2P level of theory

Ox. State	+2			+3			+4		
Spin state	LS	IS	HS	LS	IS	HS	LS	IS	HS
Symmetry	C_{4v}	C_{4v}	C_{4v}	C_{2v}	C_{4v}	C_{4v}	C_{2v}	C_{4v}	C_{4v}
E	-2587.29	-2586.77	-2585.46	-2493.43	-2508.86	-2507.09	-2248.91	-2285.66	-2283.36
ΔEprep	162.71	112.77	27.34	135.09	43.32	24.06	122.78	90.72	28.94
ΔEdeform	2.09	0.20	-0.05	0.29	0.04	0.00	0.17	0.14	0.20
ΔElig-lig	33.34	22.31	10.91	31.34	18.72	14.77	29.36	30.62	22.31
ΔEval.xc	127.28	90.26	16.48	103.48	24.56	9.30	93.25	59.96	6.43
ΔEint	-206.48	-154.00	-68.17	-284.24	-205.94	-185.33	-460.73	-466.54	-400.62
ΔEpauli	347.58	260.90	158.20	230.54	130.80	154.89	194.66	196.32	149.82
ΔEelstat	-290.98	-224.90	-137.13	-274.37	-201.79	-206.80	-312.04	-312.51	-278.68
ΔEorbint	-263.08	-190.00	-89.24	-240.41	-134.95	-133.42	-343.35	-350.35	-271.76
C_{4v} C_{2v}									
A_1 A_1	-60.52	-54.48	-37.60	-149.84	-52.84	-44.09	-225.07	-96.17	-100.74
A_2 A_2	-1.13	-0.65	-0.32	-10.57	-1.25	-1.57	-14.61	-4.41	-3.58
B_1 B_1	-9.18	-1.73	-8.05	-41.80	-4.97	-3.45	-57.90	-10.13	-7.37
B_2 B_2	-53.29	-15.85	-5.48	-38.20	-21.47	-25.25	-45.77	-133.96	-56.96
E_1	-138.97	-117.27	-37.80	-	-54.42	-59.06	-	-105.69	-103.11
ΔEdisp	-5.32	-7.22	-6.45	-5.32	-7.27	-6.84	-6.35	-5.23	-7.11
ΔEtotal	-43.77	-41.23	-40.83	-149.15	-162.62	-161.27	-337.95	-375.82	-371.68

In the case of oxidation state 4+ (relative to previous two model systems) a considerable change in spin state ordering took place (*Figure 4.7.*). IS became the ground state, and as it was stated before[192], the reason for this phenomenon arises from stronger stabilizing Interaction effect dominating over destabilizing Preparation energy. The same concept rationalizes the spin state splitting for this model system.

4.3.3.4. EDA of $[(NH_3)_3Fe^n(OH)(NH_3)]^{m+}$ complex

As well as for iron-oxo model systems, transition metal-containing unit $[Fe(OH)]^{n+}$ on its own has an HS ground state. The first hydroxo model system (*Figure 4.9..d.*), containing three equatorial and one axial NH_3 ligand, in the case of 3+ oxidation state of iron has an HS ground state.

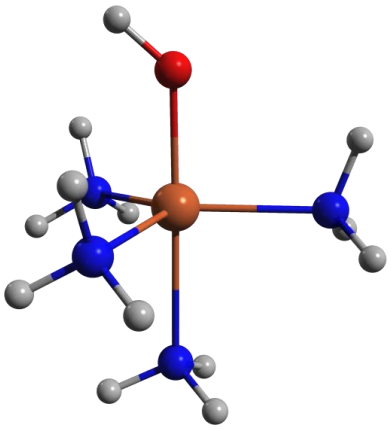

Figure 4.9.d. Geometry of $[(NH_3)_3Fe^n(OH)(NH_3)]^{m+}$ complex

This is not in accordance with the corresponding iron-oxo complex having the IS as the ground state. During the geometry optimization of all three spin states of iron-hydroxo complex, an elongation of Fe-O and shortening of Fe-L bonds took place (*Appendix section*), and in this regard, we can expect a change in overall results. As we mentioned earlier, preparation energy needed to excite preferred HS iron-oxo component to IS is rather small (~15 kcal mol^{-1}) and can easily be overcome by favorable Interaction energy. Unlike in the case of iron-oxo complex corresponding hydroxo complex shows noticeably higher preparation (*Table 4.33.*), based on energy requirement for excitation of preferred HS iron-hydroxo to first excited IS state (~38.41 kcal mol^{-1}). Since the stabilizing Interaction energy effect is not strong enough to counteract this energy requirement we have HS as the ground state and IS as the first excited state. The change of the ground spin state between iron-oxo and iron-hydroxo model systems is in this way addressed to the Preparation energy component. Since the preparation energy requirement for the excitation of iron-hydroxo HS ground state to LS is greater than in the case of iron-oxo, where ground IS must be excited to LS, we can say that the same factor is responsible for a larger spin state splitting in the case of the iron-hydroxo complex.

Table 4.33. EDA parameters (kcal mol^{-1}) for $[(NH_3)_3Fe^n(OH)(NH_3)]^{m+}$ model system calculated on ZORA/S12g/TZ2P level of theory

Ox. State		+3			+4	
Spin state	LS	IS	HS	LS	IS	HS
Symmetry	*Cs*	*Cs*	*Cs*	*Cs*	*Cs*	*Cs*
E	-1880.26	-1903.21	-1910.61	-1477.04	-1495.61	-1511.42
ΔEprep	124.82	70.27	28.24	450.36	298.32	228.95
ΔEdeform	0.08	0.05	0.05	0.44	0.44	0.42
ΔElig-lig	24.78	18.15	14.53	31.73	27.22	20.54
ΔEval.xc	99.96	52.07	13.66	418.19	270.66	207.99
ΔEint	-373.28	-341.38	-306.54	-763.74	-629.85	-576.12
ΔEpauli	229.32	186.50	161.95	227.81	230.01	204.45
ΔEelstat	-287.05	-278.55	-255.18	-340.7	-339.6	-335.01
ΔEorbint	-315.55	-249.33	-213.31	-650.85	-520.26	-445.56
Cs						
A`	-193.38	-177.04	-145.22	-429.55	-428.85	-325.03
A``	-122.17	-72.29	-68.09	-221.30	-91.41	-120.52
ΔEdisp	-5.92	-6.29	-6.43	-5.6	-5.61	-6.02
ΔEtotal	-246.48	-271.11	-278.3	-313.38	-331.53	-347.17

The overall picture of spin state ordering in the case of the iron-hydroxo complex with 4+ oxidation state of the metal is the same as for the corresponding iron-oxo complex. Geometrical parameters (*Appendix section*) of this iron-hydroxo complex, unlike in the previous example stayed almost the same with negligible changes. Although each EDA component changed drastically, in comparison with the corresponding iron-oxo complex, obtained values relative to the ground HS state are the same, resulting with almost equal spin state splitting.

4.3.3.5. EDA of $[(NH_3)_3Fe^n(OH)(NCH)]^{m+}$ complex

The geometrical parameters of the next model system, containing three equatorial NH_3 and one axial NCH ligand (*Figure 4.9.e.*), are almost the same (*Appendix section*) for both 3+ and 4+ oxidation state of central metal ion if compared with previous iron-hydroxo complex.

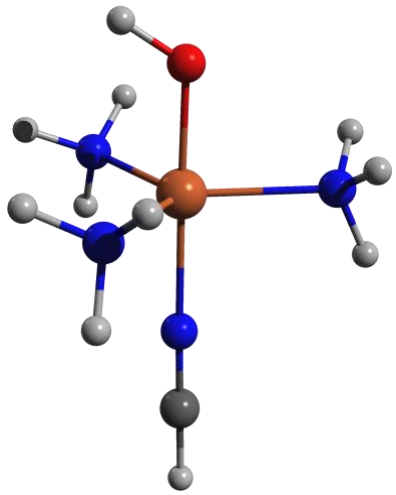

Figure 4.9.e. Geometry of $[(NH_3)_3Fe^n(OH)(NCH)]^{m+}$ complex

For this reason, EDA contributions (*Table 4.34.*), as well as resulting spin state ordering and spin state splitting are similar. In this regard, the same concept as for the previous model system can be applied. Moreover, oxidation state 3+ shows the same trend and a change of the ground spin state from IS to HS, if compared with the corresponding iron-oxo complex. This phenomenon is once more explained with Preparation contribution, based on excitation energy requirements.

Table 4.34. EDA parameters (kcal mol^{-1}) for $[(NH_3)_3Fe^n(OH)(NCH)]^{m+}$ model system calculated on ZORA/S12g/TZ2P level of theory

Ox. State		+3			+4	
Spin state	LS	IS	HS	LS	IS	HS
Symmetry	*Cs*	*Cs*	*Cs*	*Cs*	*Cs*	*Cs*
E	-1888.09	-1908.68	-1914.33	-1483.57	-1495.68	-1515.36
ΔEprep	119.79	65.78	23.34	445.15	293.11	224.87
ΔEdeform	0.22	0.20	0.14	0.90	0.90	0.75
ΔElig-lig	20.39	14.14	23.34	25.89	22.32	15.48
ΔEval.xc	99.18	51.44	12.77	418.36	269.89	208.64
ΔEint	-372.33	-338.77	-301.88	-759.78	-619.09	-570.48
ΔEpauli	245.64	194.71	165.88	241.3	230.57	209.46
ΔEelstat	-287.96	-276.11	-255.6	-345.13	-338.18	-330.79
ΔEorbint	-330.01	-257.37	-212.16	-655.95	-511.48	-449.15
Cs						
A`	-196.66	-176.15	138.38	-408.15	-283.67	-313.83
A``	-133.35	-81.23	-73.77	-247.80	-227.81	-135.32
ΔEdisp	-4.94	-5.29	-5.43	-4.59	-4.82	-5.22
ΔEtotal	-252.54	-272.99	-278.54	-314.63	-325.98	-345.61

4.3.3.6. EDA of $[(NH_3)_4Fe^n(OH)(NCH)]^{m+}$ complex

The last investigated model system, containing four equatorial NH_3 and one axial NCH ligand (*Figure 4.9.f.*), shows similar geometrical parameters to the previous model system (*Appendix section*), but more importantly, bond lengths are almost similar to corresponding iron-oxo complex with the same number of ligands around the central metal ion.

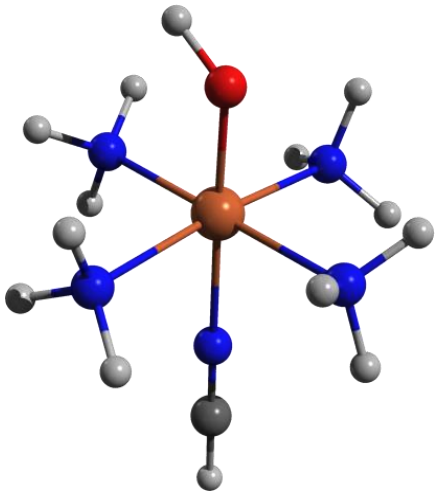

Figure 4.9.f. Geometry of $[(NH_3)_4Fe^n(OH)(NCH)]^{m+}$ complex

Besides a slight elongation of Fe-O distance, due to the change of double to a single bond, and rotation of two parallel NH_3 ligands in an equatorial sphere, optimized structures of the corresponding iron-oxo and iron-hydroxo complexes look-alike. As well as in the previous two cases, the first system, having 3+ oxidation state of iron, shows a change of ground spin state. As we mentioned before, the iron-oxo complex having 3+ oxidation state of iron has a small spin state splitting (~ 1.8 kcal mol^{-1}) between IS ground state and first excited HS state by cause of, in this case, more dominant Interaction energy that can overtake destabilizing Excitation energy requirement. Unlike iron-oxo complex, corresponding iron-hydroxo analog shows the superiority of Preparation energy (*Table 4.35.*), which cannot be counteracted and overcame by weaker Interaction energy present in LS and IS states, thus making HS the ground state. The interplay of Excitation energy and Interaction energy results with LS being the first excited state. Although LS has the strongest Preparation energy contribution, this destabilizing effect is weakened by Interaction energy based on the stronger orbital overlap. In the case of IS state, the destabilizing excitation energy is stronger than the stabilizing Interaction effect resulting in a stronger split while making IS the second excited state.

Table 4.35. EDA parameters (kcal mol^{-1}) for $[(NH_3)_4Fe^n(OH)(NCH)]^{m+}$ model system calculated on ZORA/S12g/TZ2P level of theory

Ox. State		+3			+4	
Spin state	LS	IS	HS	LS	IS	HS
Symmetry	*Cs*	*Cs*	*Cs*	*Cs*	*Cs*	*Cs*
E	-2393.15	-2389.21	-2397.98	-2010.83	-2025.74	-2015.05
ΔEprep	128.92	74.26	33.4	444.36	305.33	234.52
ΔEdeform	0.08	0.13	0.47	0.44	0.34	0.47
ΔElig-lig	31.27	21.92	21.00	34.38	33.39	24.96
ΔEval.xc	97.57	52.21	11.93	409.54	271.6	209.09
ΔEint	-433.53	-373.46	-341.22	-833.9	-709.46	-626.55
ΔEpauli	216.43	171.69	153.15	240.84	220.22	176.73
ΔEelstat	-304.68	-276.83	-261.33	-369.71	-358.79	-333.43
ΔEorbint	-345.28	-268.32	-233.04	-705.03	-570.89	-469.85
Cs						
A`	-273.73	-204.43	-169.56	-493.56	-464.05	-362.55
A``	-71.55	-63.88	-63.48	-211.47	-106.84	-107.31
ΔEdisp	-5.59	-7.23	-7.16	-5.43	-5.48	-7.17
ΔEtotal	-304.61	-299.2	-307.82	-389.54	-404.13	-392.03

In the case of the last iron-hydroxo model system, having 4+ oxidation state of iron, we have nearly identical geometrical parameters with corresponding iron-oxo complex. As well as in the previous case, a slight elongation of Fe-O distance and a rotation of two parallel NH_3 ligands took place, but this change did not affect the qualitative picture. This complex has the same spin ordering as corresponding iron-oxo analog, with a noticeable difference in energy split between ground IS and corresponding excited states. Splitting between the ground and first excited HS state is substantially smaller in the case of iron-oxo, and can be addressed to much stronger Interaction energy present in iron-hydroxo IS ground state and compensation of strong Preparation energy. In this way, a stronger differentiation between the ground and the first excited state is established. Unlike the first excited state, splitting between the ground and second LS state is much larger and originates from the combination of destabilizing Excitation energy requirement and less stabilizing Interaction energy contribution. Although the corresponding iron-hydroxo complex has a higher value for the Excitation energy, this factor is counteracted with sufficiently stronger Interaction, which is much stronger in the case of LS than IS state.

4.3.4. Conclusions

In the present work an in-depth examination of a series of iron-oxo and iron-hydroxo model systems in three different oxidation states (2+, 3+ and 4+) of a central metal ion. In this regard, our model systems can exist in many different close-lying spin- states, and in order to understand the ground spin state as well as the corresponding excited states, EDA approach has been utilized. In this way, we have successfully decomposed the interaction energy between fragments, from which one is the central metal ion bearing the oxo/hydroxo component and the other is the composition of surrounding ligands. This study shows that the utilized fragment-based approach represents an excellent method for analysis of the interaction between chemically meaningful moieties. Our main conclusion is that within the interplay of EDA contributions, central roles are played by destabilizing preparation energy based on excitation energy requirements and oxidation state of the metal, as well as stabilizing interaction energy based on orbital overlap during which chemical bonds are created. Our model systems are chosen due to the fact that similar chemical species are present as active sites in much more complex biochemical systems and are responsible for a broad pallet of different functions. We hope that in the future our present work will be used to define and explore these complex systems and resolve phenomena, such as the change of the ground spin state, ligand exchange or overall reactivity.

4.3.5. Computational details

All DFT calculations were performed with the Amsterdam Density Functional (ADF) and QUILD program. Molecular orbitals were expanded in an uncontracted set of STOs of triple-ζ quality with double polarization functions TZ2P. Core electrons were not treated explicitly during geometry optimizations (frozen core approximation). An auxiliary set of s, p, d, f, and g STOs was used to fit the molecular density and to represent the Coulomb and exchange potentials accurately for each SCF cycle.

Geometries of all possible spin states were optimized with the QUILD program using adapted delocalized coordinates until the maximum gradient component was less than 10^{-4} a.u. Energies and gradients were calculated using dispersion corrected S12g functional. Calculations related to the fragments were carried out in gas phase and restricted form, whereas all other calculations were done including the solvation effect and in unrestricted fashion (according to the general EDA procedure). The solvation effect has been included through the COSMO dielectric continuum model with appropriate parameters for acetonitrile as solvent.[394] Scalar relativistic corrections have been included self-consistently in all calculations by using ZORA. All DFA calculations were performed using the unrestricted Kohn-Sham scheme.

5. General conclusions

The versatility of results presented in this thesis demonstrates a modern theoretical approach for investigation of various aspects and characteristics of first row transition metal (TM) complexes. Considering all results together, Density Functional Theory (DFT) has once again proven to be an accurate and reliable method for extensive investigations in the field of coordination chemistry.

In the present thesis, we propose a systematization of computational steps and DFT flavors that should be used in order to get the best of this theoretical method. In this regard, we have tested, rationalized and tuned computational conditions in order to get the best performance. Performance of some old and some newly-designed density functional approximations (DFAs) have been tested firstly for the geometry optimizations of aqua- and oxo- complexes of the first row TMs.. Although accurate geometries are obtained with some other DFAs, we are putting forward the dispersion corrected S12g functional. The reason for this lies in the fact that besides remarkable efficiency for the geometrical optimization, this DFA emerged as an irreplaceable tool for an accurate description of electronic structure, which is one of the most demanding tasks in the field of TM sciences. Accurate prediction of the ground spin state in all investigated cases has been achieved. In this regard, we have utilized this specific functional for description and understanding of the connection between geometrical aspects, ground spin state and corresponding low-lying excited states. With all these results in hand, we gained an opportunity to investigate and deeper understand the excitation spectra of a series of first row TM hexaaqua complexes. Namely, the energy difference between the ground spin state and excited states can be correlated with the absorption spectra, thus we utilized DFT for the necessary calculations. For this purpose, we have applied two different approaches, TD-DFT and LF-DFT. Our results show far better performance of LF-DFT, for determination of excitation energies, and prediction of electronic spectra. Such a good performance can be addressed to the theoretical foundations of the method, whose focus is on the *d*-orbitals, where the excitations of interest will occur. TD-DFT obviously failed due to the lack of orbital relaxation and showed to be inconvenient due to its incapability to calculate the double excitations. Although this method can be a good choice for organic compounds, it showed to be an insufficient choice for simulations of excitation events located within a TM *d*-orbitals. In addition, one must be careful when choosing a DFA, since M06L and SAOP turned out to be a bad choice. For all these reasons, LF-DFT can be considered as a valuable, fast and accurate alternative not only for TD-DFT, but for computationally expensive high-level *ab initio* methods.

At the end, Energy Decomposition Analysis (EDA) has been successfully applied, and the energy of various iron-oxo and iron-hydroxo systems has been split into chemically meaningful components. These components, which contribute and define the final energy provided further insight into the origins of chemical bonding. According to our results, the bonding energy is influenced by two dominant factors. The first one is the destabilizing preparation energy, which turned to be based on excitation energy requirements and the oxidation state of the metal. The other is the stabilizing interaction energy based on orbital overlap during which chemical bonds are created. More importantly, investigated molecular systems were chosen due to the fact that their molecular properties and chemical behavior can be representative of much larger and more diverse molecular and biological systems.

Although universal DFA doesn't exist, and one should be cautious when making a choice, in the present thesis we propose theoretical steps and DFAs which should be used for unambiguous investigation of the complicated electronic structure of TM containing molecules. I hope that in the future this piece of science will be used, in the first place, to teach a newcomer the basics and capabilities of DFT. More importantly, although much has been done within the framework of this thesis, I hope that the obtained results will be utilized to further understand and illuminate molecular systems (and their characteristics) which are even more complex than the ones presented.

6. Appendix

In the forthcoming section, supplementary material for all investigations presented in the thesis can be found.

6.1. Theoretical investigation of d-d transitions of first-row TM hexaaqua complexes

6.1.1. Non-empirical parameters obtained from LF-DFT / Racah's parameters (B and C) and ligand field splitting Δ

TABLE A1. All non-empirically determined parameters (Racah's parameters B and C, and ligand field splitting **Δ**) obtained by the LF-DFT procedure (in cm^{-1}) for $[V(H_2O)_6]^{2+}$ on different levels of theory

Geometry	XC	B	C	Δ
BP86	B3LYP	839	2,437	17,119
	BP86	635	2,519	12,311
	CAMB3LYP	594	2,400	15,251
	OPBE	594	3,142	11,605
	OPBE0	616	3,040	12,432
	PBE0	629	2,590	13,048
	PW91	615	2,501	12,343
	SSB-D	617	2,904	11,563
PW91	B3LYP	635	2,258	13,086
	BP86	633	2,516	12,460
	CAMB3LYP	589	2,458	15,732
	OPBE	593	3,135	11,761
	OPBE0	615	3,035	12,621
	PBE0	624	2,600	13,224
	PW91	599	2,519	12,530
	SSB-D	613	2,905	11,706

TABLE A2. All non-empirically determined parameters (Racah's parameters B and C, and ligand field splitting **Δ**) obtained by the LF-DFT procedure (in cm^{-1}) for $[Cr(H_2O)_6]^{3+}$ on different levels of theory

Geometry	XC	B	C	Δ
BP86	B3LYP	765	2,389	16,730
	BP86	702	2,582	17,078
	CAMB3LYP	764	2,416	16,861
	OPBE	647	3,174	16,665
	OPBE0	705	3,187	16,559
	PBE0	736	2,758	16,812
	PW91	701	2,547	17,043
	SSB-D	690	3,022	16,167
PW91	B3LYP	766	2,388	16,806
	BP86	703	2,586	17,154
	CAMB3LYP	764	2,415	16,938
	OPBE	647	3,177	16,743
	OPBE0	707	3,186	16,636
	PBE0	738	2,757	16,888
	PW91	702	2,550	17,119
	SSB-D	691	3,026	16,240

TABLE A3. All non-empirically determined parameters (Racah's parameters B and C, and ligand field splitting **Δ**) obtained by the LF-DFT procedure (in cm^{-1}) for $[Mn(H_2O)_6]^{2+}$ on different levels of theory

Geometry	XC	B	C	Δ
BP86	B3LYP	847	2,674	8,066
	BP86	806	2,939	8,671
	CAMB3LYP	842	2,687	8,019
	OPBE	762	3,627	8,176
	OPBE0	797	3,591	7,618
	PBE0	822	3,092	7,958
	PW91	806	2,898	8,637
	SSB-D	804	3,396	8,135
PW91	B3LYP	846	2,673	8,134
	BP86	806	2,938	8,744
	CAMB3LYP	841	2,687	8,087
	OPBE	761	3,626	8,247
	OPBE0	796	3,590	7,685
	PBE0	821	3,092	8,026
	PW91	806	2,897	8,710
	SSB-D	803	3,396	8,204

TABLE A4. All non-empirically determined parameters (Racah's parameters B and C, and ligand field splitting **Δ**) obtained by the LF-DFT procedure (in cm^{-1}) for $[Fe(H_2O)_6]^{3+}$ on different levels of theory

Geometry	XC	B	C	Δ
BP86	B3LYP	822	2,488	12,389
	BP86	779	2,702	12,219
	CAMB3LYP	822	2,494	12,517
	OPBE	726	3,240	11,836
	OPBE0	768	3,184	12,237
	PBE0	801	2,803	12,428
	PW91	779	2,673	12,203
	SSB-D	765	3,148	11,515
PW91	B3LYP	822	2,486	12,454
	BP86	780	2,702	12,294
	CAMB3LYP	821	2,492	12,581
	OPBE	727	3,240	11,912
	OPBE0	766	3,180	12,300
	PBE0	799	2,801	12,492
	PW91	780	2,673	12,279
	SSB-D	766	3,148	11,588

TABLE A5. All non-empirically determined parameters (Racah's parameters B and C, and ligand field splitting **Δ**) obtained by the LF-DFT procedure (in cm^{-1}) for $[Co(H_2O)_6]^{3+}$ on different levels of theory

Geometry	XC	B	C	Δ
BP86	B3LYP	839	2,437	17,119
	BP86	787	2,723	16,911
	CAMB3LYP	859	2,299	17,434
	OPBE	733	3,213	16,594
	OPBE0	842	2,695	17,139
	PBE0	894	2,262	17,245
	PW91	787	2,697	16,902
	SSB-D	771	3,151	16,112
PW91	B3LYP	771	2,383	14,432
	BP86	733	2,578	13,440
	CAMB3LYP	774	2,370	14,697
	OPBE	687	3,029	13,074
	OPBE0	729	2,939	14,398
	PBE0	757	2,625	14,551
	PW91	733	2,555	13,440
	SSB-D	716	2,964	12,753

TABLE A6. All non-empirically determined parameters (Racah's parameters B and C, and ligand field splitting **Δ**) obtained by the LF-DFT procedure (in cm^{-1}) for $[Ni(H_2O)_6]^{2+}$ on different levels of theory

Geometry	XC	B	C	Δ
BP86	B3LYP	892	2,785	9,316
	BP86	865	3,001	9,529
	CAMB3LYP	889	2,791	9,233
	OPBE	808	3,596	9,201
	OPBE0	839	3,520	9,114
	PBE0	874	3,116	9,229
	PW91	865	2,967	9,521
	SSB-D	857	3,532	8,992
PW91	B3LYP	892	2,784	9,362
	BP86	865	3,000	9,594
	CAMB3LYP	889	2,789	9,276
	OPBE	808	3,596	9,268
	OPBE0	839	3,520	9,157
	PBE0	874	3,114	9,272
	PW91	865	2,966	9,586
	SSB-D	857	3,533	9,056

TABLE A7. All non-empirically determined parameters (Racah's parameters B and C, and ligand field splitting **Δ**) obtained by the LF-DFT procedure (in cm^{-1}) for $[Ni(H_2O)_6]^{2+}$ on different levels of theory

Geometry	XC	B	C	Δ
BP86	B3LYP	892	2,785	9,316
	BP86	865	3,001	9,529
	CAMB3LYP	889	2,791	9,233
	OPBE	808	3,596	9,201
	OPBE0	839	3,520	9,114
	PBE0	874	3,116	9,229
	PW91	865	2,967	9,521
	SSB-D	857	3,532	8,992
PW91	B3LYP	892	2,784	9,362
	BP86	865	3,000	9,594
	CAMB3LYP	889	2,789	9,276
	OPBE	808	3,596	9,268
	OPBE0	839	3,520	9,157
	PBE0	874	3,114	9,272
	PW91	865	2,966	9,586
	SSB-D	857	3,533	9,056

6.2. *Theoretical determination of ground spin state and corresponding spin state splitting for a series of iron-oxo and iron-hydroxo complexes with a different oxidation state of central metal ion*

TABLE A8.a. Relative spin state energies (kcal·mol^{-1}) for [Fe^{II}(OH)(Hdidpa)CH$_3$CN]$^{2+}$ **(1)** complex calculated at LDA, S12g, PBE-D2, BP86-D3, B3LYP, S12h optimized geometries, with four different DFAs

		Single point calculations on a different level of theory:											
Geometry:		LDA			S12g			OPBE			BP86-D3		
	Exp.	ls	is	hs	ls	is	hs	ls	is	hs	ls	is	hs
LDA	h.s.	-29.3	-21.8	0.0	4.0	1.9	0.0	2.3	1.4	0.0	-7.6	-6.7	0.0
S12g	h.s.	-27.4	-20.0	0.0	3.7	-1.4	0.0	0.1	-4.0	0.0	-10.7	-11.3	0.0
PBE-D2	h.s.	-29.5	-20.9	0.0	4.3	-1.4	0.0	3.6	-4.0	0.0	-8.7	-11.3	0.0
BP86-D3	h.s.	-25.6	-20.2	0.0	3.0	-0.8	0.0	0.8	-4.0	0.0	-10.8	-10.5	0.0
B3LYP	h.s.	-9.9	-3.4	0.0	-2.9	5.6	0.0	1.5	8.4	0.0	-15.2	-1.0	0.0
S12h	h.s.	-25.1	-18.9	0.0	5.5	-0.2	0.0	2.0	-2.4	0.0	-8.8	-9.6	0.0

TABLE A8.b. Relative spin state energies (kcal·mol^{-1}) for [Fe^{II}(OH)(Hdidpa)CH$_3$CN]$^{2+}$ **(1)** complex calculated at LDA, S12g, PBE-D2, BP86-D3, B3LYP, S12h optimized geometries, with four different DFAs

		Single point calculations on different level of theory:											
Geometry:		SSBD			B3LYP			S12h			MVS		
	Exp.	ls	is	hs	ls	is	hs	ls	is	hs	ls	is	hs
LDA	h.s.	0.0	10.1	3.8	0.0	20.6	13.7	0.0	33.7	20.8	0.0	17.7	9.4
S12g	h.s.	0.0	11.0	3.0	0.0	17.2	8.6	0.0	32.1	17.8	0.0	19.2	7.8
PBE-D2	h.s.	0.0	10.9	3.3	0.0	19.8	9.1	0.0	33.9	18.3	0.0	17.4	7.6
BP86-D3	h.s.	0.0	11.6	3.7	0.0	16.8	9.7	0.0	31.8	18.4	0.0	19.4	7.9
B3LYP	h.s.	0.0	8.5	10.9	0.0	1.0	11.1	0.0	19.7	20.5	0.0	16.5	8.0
S12h	h.s.	0.0	12.9	4.3	0.0	17.0	9.4	0.0	31.7	18.6	0.0	17.1	11.1

TABLE A9.a. Relative spin state energies (kcal·mol^{-1}) for [Fe^{III}(O)(H$_3$buea)]$^{2-}$ **(2)** complex calculated at LDA, S12g, PBE-D2, BP86-D3, B3LYP, S12h optimized geometries, with four different DFAs

		Single point calculations on different level of theory:											
Geometry:		LDA			S12g			OPBE			BP86-D3		
	Exp.	ls	is	hs	ls	is	hs	ls	is	hs	ls	is	hs
LDA	h.s.	0.6	-*	0.0	30.4	-	0.0	28.2	-	0.0	15.9	-	0.0
S12g	h.s.	2.9	0.6	0.0	27.1	8.8	0.0	30.6	11.0	0.0	10.5	0.4	0.0
PBE-D2	h.s.	1.2	-1.8	0.0	24.0	8.3	0.0	27.6	10.8	0.0	7.9	-1.5	0.0
BP86-D3	h.s.	2.9	-3.9	0.0	24.6	9.4	0.0	27.3	10.0	0.0	9.2	0.3	0.0
B3LYP	h.s.	-	-2.7	0.0	-	9.2	0.0	-	10.0	0.0	-	0.8	0.0
S12h	h.s.	2.9	-2.2	0.0	24.9	8.9	0.0	28.6	10.2	0.0	8.8	0.8	0.0

**not converged structure*

TABLE A9.b. Relative spin state energies (kcal·mol^{-1}) for [[Fe^{III}(O)(H$_3$buea)]$^{2-}$ **(2)** complex calculated at LDA, S12g, PBE-D2, BP86-D3, B3LYP, S12h optimized geometries, with four different DFAs

		Single point calculations on different level of theory:											
Geometry:		SSBD			B3LYP			S12h			MVS		
	Exp.	ls	is	hs	ls	is	hs	ls	is	hs	ls	is	hs
LDA	h.s.	35.0	-	0.0	32.9	-	0.0	48.0	-	0.0	47.1	-	0.0
S12g	h.s.	33.5	13.2	0.0	27.8	9.3	0.0	42.5	17.1	0.0	45.2	21.0	0.0
PBE-D2	h.s.	30.3	12.4	0.0	7.7	-10.3	0.0	41.7	15.9	0.0	44.4	21.2	0.0
BP86-D3	h.s.	32.6	14.3	0.0	28.9	10.1	0.0	43.9	18.0	0.0	43.6	20.9	0.0
B3LYP	h.s.	-	13.5	0.0	-	9.7	0.0	-	17.4	0.0	-	21.5	0.0
S12h	h.s.	31.5	13.3	0.0	25.1	9.4	0.0	39.4	16.8	0.0	43.5	21.2	0.0

TABLE A10.a. Relative spin state energies (kcal·mol^{-1}) for [Fe^{III}(OH)(H$_3$buea)]$^{-}$**(3)** complex calculated at LDA, S12g, PBE-D2, BP86-D3, B3LYP, S12h optimized geometries, with four different DFAs

		Single point calculations on different level of theory:											
Geometry:		LDA			S12g			OPBE			BP86-D3		
	Exp.	ls	is	hs	ls	is	hs	ls	is	hs	ls	is	hs
LDA	h.s.	-13.5	-9.6	0.0	15.9	7.7	0.0	15.1	4.9	0.0	0.9	-0.5	0.0
S12g	h.s.	-14.8	-10.2	0.0	11.5	4.7	0.0	14.8	4.0	0.0	-4.6	-4.0	0.0
PBE-D2	h.s.	-12.3	-8.9	0.0	13.8	5.5	0.0	14.6	5.2	0.0	-2.2	-3.6	0.0
BP86-D3	h.s.	-12.0	-9.4	0.0	13.6	5.6	0.0	13.7	5.2	0.0	-2.1	-3.6	0.0
B3LYP	h.s.	-9.9	-8.4	0.0	14.0	6.0	0.0	16.4	7.0	0.0	-2.1	-3.4	0.0
S12h	h.s.	-	-7.2	0.0	-	6.4	0.0	-	8.8	0.0	-	-2.8	0.0

TABLE A10.b. Relative spin state energies (kcal·mol^{-1}) for $[Fe^{III}(OH)(H_3buea)]^-$ **(3)** complex calculated at LDA, S12g, PBE-D2, BP86-D3, B3LYP, S12h optimized geometries, with four different DFAs

		Single point calculations on different level of theory:											
Geometry:		SSBD			B3LYP			S12h			MVS		
	Exp.	ls	is	hs	ls	is	hs	ls	is	hs	ls	is	hs
LDA	h.s.	21.5	11.0	0.0	18.3	8.5	0.0	31.7	16.0	0.0	31.8	17.2	0.0
S12g	h.s.	18.2	9.3	0.0	11.0	5.1	0.0	27.9	13.3	0.0	30.9	16.3	0.0
PBE-D2	h.s.	21.0	10.5	0.0	13.6	4.6	0.0	30.2	13.5	0.0	31.2	17.2	0.0
BP86-D3	h.s.	21.7	10.3	0.0	12.7	4.5	0.0	29.7	13.2	0.0	33.5	16.7	0.0
B3LYP	h.s.	21.0	10.5	0.0	13.1	5.6	0.0	30.3	13.7	0.0	33.5	17.9	0.0
S12h	h.s.	-	10.4	0.0	-	6.3	0.0	-	14.6	0.0	-	17.8	0.0

TABLE A11.a. Relative spin state energies (kcal·mol^{-1}) for $[(TMC)Fe^{III}(O)(Sc^{III}(OTf)_4OH_2)]^0$ **(4)** complex calculated at LDA, S12g, PBE-D2, BP86-D3, B3LYP, S12h optimized geometries, with four different DFAs

		Single point calculations on different level of theory:											
Geometry:		LDA			S12g			OPBE			BP86-D3		
	Exp.	ls	is	hs	ls	is	hs	ls	is	hs	ls	is	hs
LDA	h.s.	1.0	-9.9	0.0	30.8	9.0	0.0	32.3	10.7	0.0	15.2	-2.0	0.0
S12g	h.s.	3.9	-8.4	0.0	26.3	6.7	0.0	31.1	10.7	0.0	9.2	-3.8	0.0
PBE-D2	h.s.	1.9	-10.4	0.0	25.6	5.6	0.0	30.9	10.1	0.0	8.1	-5.5	0.0
BP86-D3	h.s.	2.5	-10.3	0.0	26.1	5.9	0.0	29.6	8.5	0.0	9.6	-4.9	0.0
B3LYP	h.s.	-	-8.9	0.0	-	6.2	0.0	-	9.0	0.0	-	-4.3	0.0
S12h	h.s.	-	-7.2	0.0	-	6.4	0.0	-	8.8	0.0	-	-2.8	0.0

TABLE A11.b. Relative spin state energies (kcal·mol^{-1}) for $[(TMC)Fe^{III}(O)(Sc^{III}(OTf)_4OH_2)]^0$ **(4)** complex calculated at LDA, S12g, PBE-D2, BP86-D3, B3LYP, S12h optimized geometries, with four different DFAs

		Single point calculations on different level of theory:											
Geometry:		SSBD			B3LYP			S12h			MVS		
	Exp.	ls	is	hs	ls	is	hs	ls	is	hs	ls	is	hs
LDA	h.s.	33.5	12.0	0.0	31.6	10.4	0.0	45.9	19.4	0.0	43.1	16.8	0.0
S12g	h.s.	32.5	10.0	0.0	29.7	9.5	0.0	41.2	15.9	0.0	44.0	15.6	0.0
PBE-D2	h.s.	31.1	8.7	0.0	24.7	6.0	0.0	40.6	14.9	0.0	42.0	13.5	0.0
BP86-D3	h.s.	31.7	9.2	0.0	25.9	6.4	0.0	41.3	15.3	0.0	43.6	15.5	0.0
B3LYP	h.s.	-	9.7	0.0	-	6.6	0.0	-	15.8	0.0	-	15.4	0.0
S12h	h.s.	-	10.4	0.0	-	6.3	0.0	-	14.6	0.0	-	2.6	0.0

TABLE A12.a. Relative spin state energies (kcal·mol^{-1}) for [Fe^{III}((2,2',2"-nitrilo-kN)tris(N-(1-methylethyl)acetamidato-kN)(OH)]$^{-}$ **(5)** complex calculated at LDA, S12g, PBE-D2, BP86-D3, B3LYP, S12h optimized geometries, with four different DFAs

		Single point calculations on different level of theory:											
Geometry:		LDA			S12g			OPBE			BP86-D3		
	Exp.	ls	is	hs	ls	is	hs	ls	is	hs	ls	is	hs
LDA	h.s.	-4.1	-7.8	0.0	23.9	9.1	0.0	25.0	12.1	0.0	9.2	1.3	0.0
S12g	h.s.	3.0	3.3	0.0	10.1	8.0	0.0	8.4	5.9	0.0	8.3	7.1	0.0
PBE-D2	h.s.	4.6	4.8	0.0	11.6	9.6	0.0	9.9	7.3	0.0	9.9	8.6	0.0
BP86-D3	h.s.	5.7	4.8	0.0	12.4	9.6	0.0	10.8	7.6	0.0	10.7	8.7	0.0
B3LYP	h.s.	3.3	4.0	0.0	9.7	8.3	0.0	8.1	6.3	0.0	8.3	7.5	0.0
S12h	h.s.	4.8	4.3	0.0	12.5	8.6	0.0	11.2	6.6	0.0	10.6	7.7	0.0

TABLE A12.b. Relative spin state energies (kcal·mol^{-1}) [Fe^{III}((2,2',2"-nitrilo-kN)tris(N-(1-methylethyl)acetamidato-kN)(OH)]$^{-}$ **(5)** complex calculated at LDA, S12g, PBE-D2, BP86-D3, B3LYP, S12h optimized geometries, with four different DFAs

		Single point calculations on different level of theory:											
Geometry:		SSBD			B3LYP			S12h			MVS		
	Exp.	ls	is	hs	ls	is	hs	ls	is	hs	ls	is	hs
LDA	h.s.	27.9	11.9	0.0	25.1	10.9	0.0	-	17.8	0.0	41.1	18.2	0.0
S12g	h.s.	8.9	7.5	0.0	9.2	7.2	0.0	8.1	6.4	0.0	40.0	17.7	0.0
PBE-D2	h.s.	10.4	9.1	0.0	11.4	9.4	0.0	10.2	8.5	0.0	40.0	17.8	0.0
BP86-D3	h.s.	11.3	9.3	0.0	11.8	8.9	0.0	10.7	8.1	0.0	40.5	17.9	0.0
B3LYP	h.s.	8.6	7.8	0.0	9.0	7.6	0.0	7.8	6.8	0.0	40.5	18.0	0.0
S12h	h.s.	10.9	8.2	0.0	11.8	7.8	0.0	10.5	7.3	0.0	40.3	18.4	0.0

TABLE A13a. Relative spin state energies (kcal·mol^{-1}) for [Fe^{III}(OH)(tnpa)(COOCH$_3$)]$^{+}$ **(6)** complex calculated at LDA, S12g, PBE-D2, BP86-D3, B3LYP, S12h optimized geometries, with four different DFAs

		Single point calculations on different level of theory:											
Geometry:		LDA			S12g			OPBE			BP86-D3		
	Exp.	ls	is	hs	ls	is	hs	ls	is	hs	ls	is	hs
LDA	h.s.	-25.6	-6.2	0.0	6.8	7.3	0.0	8.0	8.4	0.0	-12.2	-2.0	0.0
S12g	h.s.	-25.2	-5.8	0.0	8.3	7.2	0.0	11.6	8.5	0.0	-9.4	-2.1	0.0
PBE-D2	h.s.	-24.9	-6.3	0.0	8.5	9.1	0.0	11.6	11.0	0.0	-9.2	1.1	0.0
BP86-D3	h.s.	-24.1	-4.9	0.0	11.8	8.8	0.0	18.3	10.5	0.0	-3.2	1.0	0.0
B3LYP	h.s.	-23.3	-4.4	0.0	8.1	6.8	0.0	12.6	8.3	0.0	-8.8	-1.6	0.0
S12h	h.s.	-23.4	-4.4	0.0	8.0	6.8	0.0	13.4	8.8	0.0	-9.1	-1.7	0.0

TABLE A13.b. Relative spin state energies (kcal·mol^{-1}) [Fe^{III}(OH)(tnpa)(COOCH$_3$)]$^+$ **(6)** complex calculated at LDA, S12g, PBE-D2, BP86-D3, B3LYP, S12h optimized geometries, with four different DFAs

		Single point calculations on different level of theory:											
Geometry:		SSBD			B3LYP			S12h			MVS		
	Exp.	ls	is	hs	ls	is	hs	ls	is	hs	ls	is	hs
LDA	h.s.	14.0	11.5	0.0	8.8	6.4	0.0	25.1	15.1	0.0	24.1	19.3	0.0
S12g	h.s.	13.3	11.6	0.0	8.3	7.2	0.0	24.5	15.1	0.0	24.4	19.3	0.0
PBE-D2	h.s.	13.3	11.2	0.0	10.2	7.3	0.0	25.6	16.2	0.0	24.9	19.4	0.0
BP86-D3	h.s.	20.1	11.1	0.0	14.0	7.8	0.0	28.6	16.2	0.0	23.8	18.7	0.0
B3LYP	h.s.	13.2	11.6	0.0	9.5	6.2	0.0	24.2	15.1	0.0	25.4	20.4	0.0
S12h	h.s.	13.1	11.8	0.0	11.9	7.5	0.0	24.6	15.3	0.0	25.3	20.5	0.0

TABLE A14.a. Relative spin state energies (kcal·mol^{-1}) for [Fe^{III}(OH)(tnpa)(COOPh)]$^+$ **(7)** complex calculated at LDA, S12g, PBE-D2, BP86-D3, B3LYP, S12h optimized geometries, with four different DFAs

		Single point calculations on different level of theory:											
Geometry:		LDA			S12g			OPBE			BP86-D3		
	Exp.	ls	is	hs	ls	is	hs	ls	is	hs	ls	is	hs
LDA	h.s.	-25.1	-6.2	0.0	7.6	7.6	0.0	10.1	9.4	0.0	-11.4	-1.9	0.0
S12g	h.s.	-25.9	-5.9	0.0	7.9	7.0	0.0	10.9	8.3	0.0	-9.6	-1.9	0.0
PBE-D2	h.s.	-24.8	-5.8	0.0	8.7	9.6	0.0	12.1	11.5	0.0	-8.7	1.8	0.0
BP86-D3	h.s.	-25.8	-3.1	0.0	7.8	12.2	0.0	12.2	21.6	0.0	-9.9	2.1	0.0
B3LYP	h.s.	-22.1	-4.1	0.0	8.8	6.9	0.0	15.4	8.8	0.0	-8.5	-1.5	0.0
S12h	h.s.	-22.1	-3.7	0.0	8.5	7.2	0.0	11.7	8.4	0.0	-8.6	-1.3	0.0

TABLE A14.b. Relative spin state energies (kcal·mol^{-1}) [Fe^{III}(OH)(tnpa)(COOPh)]$^+$ **(7)** complex calculated at LDA, S12g, PBE-D2, BP86-D3, B3LYP, S12h optimized geometries, with four different DFAs

		Single point calculations on different level of theory:											
Geometry:		SSBD			B3LYP			S12h			MVS		
	Exp.	ls	is	hs	ls	is	hs	ls	is	hs	ls	is	hs
LDA	h.s.	14.4	11.8	0.0	9.8	6.8	0.0	25.6	15.5	0.0	24.6	19.7	0.0
S12g	h.s.	12.9	11.6	0.0	9.3	5.2	0.0	24.0	15.0	0.0	23.5	19.1	0.0
PBE-D2	h.s.	13.6	11.8	0.0	10.8	9.8	0.0	25.3	16.8	0.0	28.4	15.7	0.0
BP86-D3	h.s.	12.8	13.1	0.0	9.1	12.5	0.0	23.9	19.9	0.0	24.4	21.8	0.0
B3LYP	h.s.	14.1	11.8	0.0	10.1	6.8	0.0	24.6	15.6	0.0	24.9	21.0	0.0
S12h	h.s.	13.8	12.3	0.0	9.9	6.8	0.0	23.9	15.2	0.0	24.8	21.0	0.0

TABLE A15.a. Relative spin state energies (kcal·mol^{-1}) for [Fe^{III}(OH)(TST)]$^{-}$ **(8)** complex calculated at LDA, S12g, PBE-D2, BP86-D3, B3LYP, S12h optimized geometries, with four different DFAs

		Single point calculations on different level of theory:											
Geometry:		LDA			S12g			OPBE			BP86-D3		
	Exp.	ls	is	hs	ls	is	hs	ls	is	hs	ls	is	hs
LDA	h.s.	-3.3	-5.0	0.0	25.8	12.9	0.0	26.2	10.3	0.0	11.2	5.4	0.0
S12g	h.s.	-0.8	-5.0	0.0	24.0	9.2	0.0	27.2	11.4	0.0	6.7	-0.1	0.0
PBE-D2	h.s.	11.1	-5.7	0.0	26.0	10.2	0.0	26.1	8.3	0.0	6.8	-1.3	0.0
BP86-D3	h.s.	3.2	-7.0	0.0	22.2	7.3	0.0	28.3	7.2	0.0	5.7	-2.2	0.0
B3LYP	h.s.	2.5	-4.3	0.0	26.9	9.8	0.0	27.4	9.1	0.0	10.4	1.2	0.0
S12h	h.s.	21.0	-8.6	0.0	30.6	7.3	0.0	34.9	4.4	0.0	19.7	0.4	0.0

TABLE A15.b. Relative spin state energies (kcal·mol^{-1}) [Fe^{III}(OH)(TST)]$^{-}$ **(8)** complex calculated at LDA, S12g, PBE-D2, BP86-D3, B3LYP, S12h optimized geometries, with four different DFAs

		Single point calculations on different level of theory:											
Geometry:		SSBD			B3LYP			S12h			MVS		
	Exp.	ls	is	hs	ls	is	hs	ls	is	hs	ls	is	hs
LDA	h.s.	31.6	16.1	0.0	26.7	14.2	0.0	41.1	21.4	0.0	42.1	20.8	0.0
S12g	h.s.	30.5	13.5	0.0	22.4	9.5	0.0	38.2	17.8	0.0	41.8	20.5	0.0
PBE-D2	h.s.	31.5	14.1	0.0	20.5	9.9	0.0	41.1	19.0	0.0	43.8	20.8	0.0
BP86-D3	h.s.	28.9	12.1	0.0	23.9	7.2	0.0	40.1	15.6	0.0	42.2	18.3	0.0
B3LYP	h.s.	32.8	14.6	0.0	24.8	9.0	0.0	40.2	17.2	0.0	44.6	21.5	0.0
S12h	h.s.	37.3	11.5	0.0	34.1	6.2	0.0	49.8	14.3	0.0	-	-	-

TABLE A16.a. Relative spin state energies (kcal·mol^{-1}) for [Fe^{IV}(O)(H$_3$buea)]$^{-}$ **(9)** complex calculated at LDA, S12g, PBE-D2, BP86-D3, B3LYP, S12h optimized geometries, with four different DFAs

		Single point calculations on different level of theory:											
Geometry:		LDA			S12g			OPBE			BP86-D3		
	Exp.	ls	is	hs	ls	is	hs	ls	is	hs	ls	is	hs
LDA	h.s.	-0.7	2.3	0.0	25.8	17.9	0.0	20.8	22.2	0.0	15.3	10.7	0.0
S12g	h.s.	1.7	4.3	0.0	25.5	15.4	0.0	24.1	21.2	0.0	14.1	7.8	0.0
PBE-D2	h.s.	0.1	2.9	0.0	26.9	14.6	0.0	24.2	20.6	0.0	15.4	6.1	0.0
BP86-D3	h.s.	2.1	3.5	0.0	25.9	17.5	0.0	23.0	19.6	0.0	14.5	9.6	0.0
B3LYP	h.s.	3.7	-	0.0	25.9	-	0.0	25.0	-	0.0	14.6	-	0.0
S12h	h.s.	15.9	-2.7	0.0	27.5	10.2	0.0	35.7	18.4	0.0	17.2	1.6	0.0

TABLE A16.b. Relative spin state energies (kcal·mol^{-1}) $[Fe^{IV}(O)(H_3buea)]^-$ **(9)** complex calculated at LDA, S12g, PBE-D2, BP86-D3, B3LYP, S12h optimized geometries, with four different DFAs

		Single point calculations on different level of theory:											
Geometry:		SSBD			B3LYP			S12h			MVS		
	Exp.	ls	is	hs	ls	is	hs	ls	is	hs	ls	is	hs
LDA	h.s.	29.2	18.5	0.0	32.3	20.1	0.0	42.6	25.8	0.0	36.4	27.6	0.0
S12g	h.s.	30.8	18.1	0.0	28.0	16.2	0.0	40.1	23.1	0.0	41.1	27.2	0.0
PBE-D2	h.s.	31.4	16.7	0.0	30.5	15.1	0.0	41.9	21.6	0.0	39.4	26.4	0.0
BP86-D3	h.s.	31.3	19.8	0.0	28.3	17.8	0.0	41.1	24.8	0.0	41.7	29.1	0.0
B3LYP	h.s.	30.7	-	0.0	27.6	-	0.0	40.0	-	0.0	40.6	-	0.0
S12h	h.s.	29.9	13.1	0.0	26.6	9.8	0.0	38.3	17.0	0.0	36.4	21.6	0.0

TABLE A17.a. Relative spin state energies (kcal·mol^{-1}) for $[Fe^{IV}(O)(TMC)(NCCH_3)]^{2+}$ **(10)** complex calculated at LDA, S12g, PBE-D2, BP86-D3, B3LYP, S12h optimized geometries, with four different DFAs

		Single point calculations on different level of theory:											
Geometry:		LDA			S12g			OPBE			BP86-D3		
	Exp.	ls	is	hs	ls	is	hs	ls	is	hs	ls	is	hs
LDA	h.s.	-15.4	-23.9	0.0	3.9	-5.4	0.0	6.2	-4.1	0.0	-7.2	-14.8	0.0
S12g	h.s.	-14.3	-22.5	0.0	5.4	-4.4	0.0	7.5	-3.4	0.0	-4.1	-11.8	0.0
PBE-D2	h.s.	-14.7	-24.0	0.0	5.4	-4.4	0.0	7.5	-3.2	0.0	-4.0	-11.6	0.0
BP86-D3	h.s.	-14.8	-23.4	0.0	5.6	-4.1	0.0	7.9	-2.9	0.0	-3.8	-11.6	0.0
B3LYP	h.s.	-14.3	-22.1	0.0	5.3	-4.5	0.0	7.8	-2.6	0.0	-4.0	-11.6	0.0
S12h	h.s.	-14.4	-22.4	0.0	4.8	-4.3	0.0	6.9	-3.7	0.0	-4.5	-11.5	0.0

TABLE A17.b. Relative spin state energies (kcal·mol^{-1}) $[Fe^{IV}(O)(TMC)(NCCH_3)]^{2+}$ **(10)** complex calculated at LDA, S12g, PBE-D2, BP86-D3, B3LYP, S12h optimized geometries, with four different DFAs

		Single point calculations on different level of theory:											
Geometry:		SSBD			B3LYP			S12h			MVS		
	Exp.	ls	is	hs	ls	is	hs	ls	is	hs	ls	is	hs
LDA	h.s.	7.5	-2.9	0.0	23.5	-4.4	0.0	34.2	2.9	0.0	14.1	-0.6	0.0
S12g	h.s.	7.1	-3.9	0.0	25.6	-2.9	0.0	35.9	3.6	0.0	14.3	-0.2	0.0
PBE-D2	h.s.	6.5	-4.8	0.0	25.7	-2.9	0.0	32.2	3.3	0.0	14.1	-1.9	0.0
BP86-D3	h.s.	6.6	-3.8	0.0	25.8	-2.4	0.0	35.6	3.9	0.0	14.2	-0.7	0.0
B3LYP	h.s.	7.0	-3.9	0.0	25.7	-2.7	0.0	36.0	3.8	0.0	14.5	0.2	0.0
S12h	h.s.	6.0	-4.3	0.0	25.7	-2.5	0.0	35.8	3.9	0.0	13.9	0.0	0.0

TABLE A18.a. Relative spin state energies (kcal·mol^{-1}) for $[Fe^{IV}(O)(TMC^{i})(NCCH_3)]^{2+}$ **(11)** complex calculated at LDA, S12g, PBE-D2, BP86-D3, B3LYP, S12h optimized geometries, with four different DFAs

		Single point calculations on different level of theory:											
Geometry:		LDA			S12g			OPBE			BP86-D3		
	Exp.	ls	is	hs	ls	is	hs	ls	is	hs	ls	is	hs
LDA	h.s.	8.5	0.0	25.3	9.6	0.0	6.5	10.5	0.0	5.9	8.2	0.0	16.3
S12g	h.s.	9.2	0.0	20.0	9.7	0.0	6.9	11.2	0.0	4.1	7.9	0.0	15.2
PBE-D2	h.s.	8.6	0.0	24.6	9.8	0.0	5.4	10.5	0.0	4.4	7.7	0.0	13.2
BP86-D3	h.s.	8.5	0.0	25.4	9.4	0.0	5.0	10.8	0.0	5.4	7.7	0.0	13.1
B3LYP	h.s.	8.6	0.0	23.5	10.4	0.0	5.3	11.5	0.0	4.0	8.3	0.0	12.8
S12h	h.s.	9.5	0.0	19.0	10.8	0.0	6.8	12.2	0.0	4.4	8.7	0.0	14.7

TABLE A18.b. Relative spin state energies (kcal·mol^{-1}) $[Fe^{IV}(O)(TMC^{i})(NCCH_3)]^{2+}$ **(11)** complex calculated at LDA, S12g, PBE-D2, BP86-D3, B3LYP, S12h optimized geometries, with four different DFAs

		Single point calculations on different level of theory:											
Geometry:		SSBD			B3LYP			S12h			MVS		
	Exp.	ls	is	hs	ls	is	hs	ls	is	hs	ls	is	hs
LDA	h.s.	10.7	0.0	3.5	28.6	0.0	5.7	34.2	2.0	0.0	15.1	0.0	1.4
S12g	h.s.	10.9	0.0	3.5	28.9	0.0	6.7	34.4	1.8	0.0	17.5	2.3	0.0
PBE-D2	h.s.	10.6	0.0	4.6	28.5	0.0	4.2	32.1	2.7	0.0	14.5	0.0	1.7
BP86-D3	h.s.	9.9	0.0	4.6	28.5	0.0	3.9	35.0	2.9	0.0	20.4	5.7	0.0
B3LYP	h.s.	10.9	0.0	4.6	28.3	0.0	4.0	35.0	2.9	0.0	15.4	0.0	0.4
S12h	h.s.	11.2	0.0	3.1	28.5	0.0	6.3	34.2	2.0	0.0	18.4	3.1	0.0

TABLE A19.a. Relative spin state energies (kcal·mol^{-1}) for $[Fe^{IV}(O)(TMC)(NCS)]^{+}$ **(12)** complex calculated at LDA, S12g, PBE-D2, BP86-D3, B3LYP, S12h optimized geometries, with four different DFAs

		Single point calculations on different level of theory:											
Geometry:		LDA			S12g			OPBE			BP86-D3		
	Exp.	ls	is	hs	ls	is	hs	ls	is	hs	ls	is	hs
LDA	h.s.	8.0	0.0	21.7	9.3	0.0	2.9	10.0	0.0	1.8	7.3	0.0	12.8
S12g	h.s.	7.8	0.0	20.5	9.7	0.0	1.6	10.1	0.0	1.2	7.1	0.0	9.8
PBE-D2	h.s.	7.8	0.0	21.1	9.7	0.0	1.5	10.0	0.0	0.5	7.4	0.0	9.8
BP86-D3	h.s.	8.1	0.0	21.9	9.2	0.0	1.5	10.2	0.0	1.2	7.4	0.0	10.3
B3LYP	h.s.	7.6	0.0	20.2	9.1	0.0	1.8	10.3	0.0	0.4	7.3	0.0	9.8
S12h	h.s.	7.4	0.0	20.7	8.9	0.0	1.6	10.3	0.0	1.8	7.5	0.0	9.9

TABLE A19.b. Relative spin state energies (kcal·mol^{-1}) $[Fe^{IV}(O)(TMC)(NCS)]^{+}$ **(12)** complex calculated at LDA, S12g, PBE-D2, BP86-D3, B3LYP, S12h optimized geometries, with four different DFAs

		Single point calculations on different level of theory:											
Geometry:		SSBD			B3LYP			S12h			MVS		
	Exp.	ls	is	hs	ls	is	hs	ls	is	hs	ls	is	hs
LDA	h.s.	10.2	0.0	0.7	27.2	0.0	2.7	36.0	5.0	0.0	15.9	1.5	0.0
S12g	h.s.	10.1	0.0	1.9	27.6	0.0	1.3	37.6	5.9	0.0	15.9	2.1	0.0
PBE-D2	h.s.	10.1	0.0	1.7	27.3	0.0	0.9	37.6	6.1	0.0	15.0	1.7	0.0
BP86-D3	h.s.	10.3	0.0	1.6	27.9	0.0	1.5	37.3	6.0	0.0	10.6	0.7	0.0
B3LYP	h.s.	10.3	0.0	1.9	28.0	0.0	1.3	37.7	6.0	0.0	16.7	2.0	0.0
S12h	h.s.	10.2	0.0	2.0	28.4	0.0	1.1	38.2	6.5	0.0	16.8	1.9	0.0

TABLE A20.a. Relative spin state energies (kcal·mol^{-1}) for $[Fe^{IV}(O)(TMC\text{-}Py)]^{2+}$ **(13)** complex calculated at LDA, S12g, PBE-D2, BP86-D3, B3LYP, S12h optimized geometries, with four different DFAs

		Single point calculations on different level of theory:											
Geometry:		LDA			S12g			OPBE			BP86-D3		
	Exp.	ls	is	hs	ls	is	hs	ls	is	hs	ls	is	hs
LDA	h.s.	8.7	0.0	23.9	10.1	0.0	5.8	11.0	0.0	4.8	8.2	0.0	15.3
S12g	h.s.	8.9	0.0	22.7	9.6	0.0	4.4	10.8	0.0	4.3	8.1	0.0	12.5
PBE-D2	h.s.	8.6	0.0	23.5	9.5	0.0	6.6	11.0	0.0	5.5	8.0	0.0	16.0
BP86-D3	h.s.	8.8	0.0	24.9	9.6	0.0	4.3	11.1	0.0	3.8	7.8	0.0	12.8
B3LYP	h.s.	8.7	0.0	22.9	10.1	0.0	4.8	11.7	0.0	3.8	8.4	0.0	12.6
S12h	h.s.	8.2	0.0	23.2	10.2	0.0	4.5	11.5	0.0	4.8	7.7	0.0	12.6

TABLE A20.b. Relative spin state energies (kcal·mol^{-1}) $[Fe^{IV}(O)(TMC\text{-}Py)]^{2+}$ **(13)** complex calculated at LDA, S12g, PBE-D2, BP86-D3, B3LYP, S12h optimized geometries, with four different DFAs

		Single point calculations on different level of theory:											
Geometry:		SSBD			B3LYP			S12h			MVS		
	Exp.	ls	is	hs	ls	is	hs	ls	is	hs	ls	is	hs
LDA	h.s.	10.7	0.0	3.6	28.1	0.0	5.1	31.6	0.0	-2.5	14.7	0.0	1.3
S12g	h.s.	10.7	0.0	4.8	28.6	0.0	3.7	32.3	0.0	-3.7	14.9	0.0	0.7
PBE-D2	h.s.	10.6	0.0	4.7	28.6	0.0	6.7	30.0	0.0	-1.9	14.8	0.0	0.4
BP86-D3	h.s.	10.7	0.0	4.6	28.4	0.0	3.8	31.7	0.0	-3.4	9.0	0.0	1.9
B3LYP	h.s.	11.3	0.0	4.9	28.7	0.0	3.7	32.3	0.0	-3.5	15.2	0.0	0.6
S12h	h.s.	10.9	0.0	4.5	28.4	0.0	4.0	32.0	0.0	-3.3	15.3	0.0	0.8

TABLE A21.a. Relative spin state energies (kcal·mol^{-1}) for $[Fe^{IV}(O)(TMCS)]^{+}$ **(14)** complex calculated at LDA, S12g, PBE-D2, BP86-D3, B3LYP, S12h optimized geometries, with four different DFAs

		Single point calculations on different level of theory:											
Geometry:		LDA			S12g			OPBE			BP86-D3		
	Exp.	ls	is	hs	ls	is	hs	ls	is	hs	ls	is	hs
LDA	h.s.	8.2	0.0	19.2	9.2	0.0	0.5	10.8	0.1	0.0	7.4	0.0	10.4
S12g	h.s.	7.6	0.0	18.0	9.8	0.8	0.0	11.8	1.2	0.0	7.6	0.0	7.3
PBE-D2	h.s.	8.3	0.0	18.7	10.2	0.6	0.0	11.6	1.6	0.0	7.2	0.0	7.6
BP86-D3	h.s.	7.8	0.0	19.3	10.7	1.1	0.0	11.9	1.9	0.0	7.2	0.0	7.4
B3LYP	h.s.	7.5	0.0	17.7	9.8	0.8	0.0	12.8	2.3	0.0	7.2	0.0	7.2
S12h	h.s.	7.2	0.0	17.8	10.4	1.0	0.0	10.7	0.9	0.0	6.9	0.0	7.0

TABLE A21.b. Relative spin state energies (kcal·mol^{-1}) $[Fe^{IV}(O)(TMCS)]^{+}$ **(14)** complex calculated at LDA, S12g, PBE-D2, BP86-D3, B3LYP, S12h optimized geometries, with four different DFAs

		Single point calculations on different level of theory:											
Geometry:		SSBD			B3LYP			S12h			MVS		
	Exp.	ls	is	hs	ls	is	hs	ls	is	hs	ls	is	hs
LDA	h.s.	12.4	2.2	0.0	25.1	0.0	0.3	36.6	7.5	0.0	19.2	4.9	0.0
S12g	h.s.	11.1	1.0	0.0	28.4	2.4	0.0	39.4	9.4	0.0	20.4	5.4	0.0
PBE-D2	h.s.	11.2	1.1	0.0	28.3	2.4	0.0	39.3	9.4	0.0	19.4	5.2	0.0
BP86-D3	h.s.	10.1	1.3	0.0	28.9	3.0	0.0	39.8	10.0	0.0	18.9	4.6	0.0
B3LYP	h.s.	11.2	1.3	0.0	27.9	2.4	0.0	38.9	9.5	0.0	20.0	5.6	0.0
S12h	h.s.	11.8	1.3	0.0	27.8	2.5	0.0	38.5	9.4	0.0	20.3	5.4	0.0

TABLE A22.a. Relative spin state energies (kcal·mol^{-1}) for $[Fe^{IV}(O)(TMCSO_2)]^{+}$ **(15)** complex calculated at LDA, S12g, PBE-D2, BP86-D3, B3LYP, S12h optimized geometries, with four different DFAs

		Single point calculations on different level of theory:											
Geometry:		LDA			S12g			OPBE			BP86-D3		
	Exp.	ls	is	hs	ls	is	hs	ls	is	hs	ls	is	hs
LDA	h.s.	8.9	0.0	18.9	10.5	0.0	0.8	10.9	0.0	0.0	8.1	0.0	11.1
S12g	h.s.	9.0	0.0	17.9	11.1	0.7	0.0	12.1	1.1	0.0	8.5	0.0	7.8
PBE-D2	h.s.	9.0	0.0	18.7	11.2	0.8	0.0	12.8	1.8	0.0	8.0	0.0	7.9
BP86-D3	h.s.	9.0	0.0	18.6	10.4	0.5	0.0	12.5	1.1	0.0	8.0	0.0	7.8
B3LYP	h.s.	9.1	0.0	17.9	11.2	0.5	0.0	12.0	1.8	0.0	8.6	0.0	7.8
S12h	h.s.	8.8	0.0	18.0	11.6	0.6	0.0	12.3	0.5	0.0	8.8	0.0	7.7

TABLE A22.b. Relative spin state energies (kcal·mol^{-1}) $[Fe^{IV}(O)(TMCSO_2)]^+$ **(15)** complex calculated at LDA, S12g, PBE-D2, BP86-D3, B3LYP, S12h optimized geometries, with four different DFAs

		Single point calculations on different level of theory:											
Geometry:		SSBD			B3LYP			S12h			MVS		
	Exp.	ls	is	hs	ls	is	hs	ls	is	hs	ls	is	hs
LDA	h.s.	12.9	1.8	0.0	28.6	0.0	1.7	38.7	6.7	0.0	18.9	3.7	0.0
S12g	h.s.	12.2	1.0	0.0	29.3	0.4	0.0	40.2	7.8	0.0	20.4	4.2	0.0
PBE-D2	h.s.	12.6	1.0	0.0	29.7	0.9	0.0	40.6	8.3	0.0	19.7	4.5	0.0
BP86-D3	h.s.	11.1	1.0	0.0	29.4	0.4	0.0	40.1	7.6	0.0	11.8	3.8	0.0
B3LYP	h.s.	12.7	0.9	0.0	29.0	0.3	0.0	40.0	7.7	0.0	20.0	0.0	4.4
S12h	h.s.	12.5	0.9	0.0	29.0	0.4	0.0	39.8	7.7	0.0	20.4	4.2	0.0

TABLE A23.a. Relative spin state energies (kcal·mol^{-1}) for $[Fe^{IV}(O)(N_4Py)]^{2+}$ **(16)** complex calculated at LDA, S12g, PBE-D2, BP86-D3, B3LYP, S12h optimized geometries, with four different DFAs

		Single point calculations on different level of theory:											
Geometry:		LDA			S12g			OPBE			BP86-D3		
	Exp.	ls	is	hs	ls	is	hs	ls	is	hs	ls	is	hs
LDA	h.s.	26.8	0.0	35.1	31.8	0.0	14.6	31.5	0.0	15.0	29.9	0.0	23.9
S12g	h.s.	26.6	0.0	37.1	30.2	0.0	13.8	32.8	0.0	14.6	28.1	0.0	23.1
PBE-D2	h.s.	28.4	0.0	33.9	32.0	0.0	14.3	31.8	0.0	14.7	28.5	0.0	23.9
BP86-D3	h.s.	28.0	0.0	34.2	30.2	0.0	14.3	31.4	0.0	14.9	28.1	0.0	23.8
B3LYP	h.s.	26.8	0.0	31.9	30.3	0.0	13.6	31.4	0.0	13.4	29.5	0.0	22.7
S12h	h.s.	26.5	0.0	36.2	31.2	0.0	13.1	31.2	0.0	13.9	29.2	0.0	22.2

TABLE A23.b. Relative spin state energies (kcal·mol^{-1}) $[Fe^{IV}(O)(N_4Py)]^{2+}$ **(16)** complex calculated at LDA, S12g, PBE-D2, BP86-D3, B3LYP, S12h optimized geometries, with four different DFAs

		Single point calculations on different level of theory:											
Geometry:		SSBD			B3LYP			S12h			MVS		
	Exp.	ls	is	hs	ls	is	hs	ls	is	hs	ls	is	hs
LDA	h.s.	31.7	0.0	9.9	30.2	0.0	9.0	33.5	0.0	0.9	36.9	0.0	8.5
S12g	h.s.	31.6	0.0	10.6	29.9	0.0	9.7	33.2	0.0	2.3	36.8	0.0	10.4
PBE-D2	h.s.	32.0	0.0	9.5	30.3	0.0	10.1	33.6	0.0	1.7	36.6	0.0	7.2
BP86-D3	h.s.	32.6	0.0	9.3	29.9	0.0	10.0	33.3	0.0	1.6	38.3	0.0	7.2
B3LYP	h.s.	32.8	0.0	8.7	29.8	0.0	9.7	33.3	0.0	1.3	38.3	0.0	6.1
S12h	h.s.	32.6	0.0	9.7	29.6	0.0	9.0	33.1	0.0	1.9	38.0	0.0	9.6

TABLE A24.a. Relative spin state energies (kcal·mol^{-1}) for [Fe^{IV}(O)(TMG$_3$tren)]$^{2+}$ **(17)** complex calculated at LDA, S12g, PBE-D2, BP86-D3, B3LYP, S12h optimized geometries, with four different DFAs

		Single point calculations on different level of theory:											
Geometry:		LDA			S12g			OPBE			BP86-D3		
	Exp.	ls	is	hs	ls	is	hs	ls	is	hs	ls	is	hs
LDA	h.s.	11.3	12.5	0.0	29.2	24.2	0.0	30.5	25.0	0.0	20.9	17.9	0.0
S12g	h.s.	11.8	13.6	0.0	27.2	22.3	0.0	31.5	24.9	0.0	18.0	16.5	0.0
PBE-D2	h.s.	11.8	13.0	0.0	27.4	22.4	0.0	30.3	24.3	0.0	18.4	16.4	0.0
BP86-D3	h.s.	11.7	13.1	0.0	27.1	22.3	0.0	29.6	24.1	0.0	18.1	16.6	0.0
B3LYP	h.s.	12.7	13.6	0.0	27.4	22.7	0.0	31.2	25.0	0.0	18.5	15.5	0.0
S12h	h.s.	12.6	14.2	0.0	27.5	22.5	0.0	32.2	24.9	0.0	18.7	17.0	0.0

TABLE A24.b. Relative spin state energies (kcal·mol^{-1}) [Fe^{IV}(O)(TMG$_3$tren)]$^{2+}$ **(17)** complex calculated at LDA, S12g, PBE-D2, BP86-D3, B3LYP, S12h optimized geometries, with four different DFAs

		Single point calculations on different level of theory:											
Geometry:		SSBD			B3LYP			S12h			MVS		
	Exp.	ls	is	hs	ls	is	hs	ls	is	hs	ls	is	hs
LDA	h.s.	31.5	25.2	0.0	34.1	27.1	0.0	44.0	33.3	0.0	43.6	33.9	0.0
S12g	h.s.	30.5	24.7	0.0	31.2	25.5	0.0	42.5	32.2	0.0	44.1	31.6	0.0
PBE-D2	h.s.	30.4	24.7	0.0	31.4	25.4	0.0	42.5	32.4	0.0	44.0	34.3	0.0
BP86-D3	h.s.	30.6	24.9	0.0	31.1	25.1	0.0	42.4	32.3	0.0	43.5	34.0	0.0
B3LYP	h.s.	30.5	25.0	0.0	30.7	24.8	0.0	41.9	32.0	0.0	38.2	-6.1	0.0
S12h	h.s.	30.5	24.8	0.0	30.4	25.0	0.0	41.9	32.0	0.0	44.7	32.4	0.0

TABLE A25.a. Relative spin state energies (kcal·mol^{-1}) for [Fe^{IV}(O)(tpa^{Ph})]$^{-}$ **(18)** complex calculated at LDA, S12g, PBE-D2, BP86-D3, B3LYP, S12h optimized geometries, with four different DFAs

		Single point calculations on different level of theory:											
Geometry:		LDA			S12g			OPBE			BP86-D3		
	Exp.	ls	is	hs	ls	is	hs	ls	is	hs	ls	is	hs
LDA	h.s.	6.9	14.4	0.0	21.2	25.2	0.0	26.0	28.3	0.0	13.1	20.2	0.0
S12g	h.s.	7.5	15.4	0.0	20.9	24.8	0.0	25.6	27.9	0.0	13.1	20.6	0.0
PBE-D2	h.s.	6.7	14.5	0.0	20.5	24.7	0.0	25.2	27.6	0.0	12.4	19.9	0.0
BP86-D3	h.s.	6.6	13.9	0.0	20.4	24.2	0.0	23.9	26.4	0.0	12.4	19.4	0.0
B3LYP	h.s.	7.9	15.2	0.0	21.4	24.7	0.0	24.6	27.7	0.0	15.3	19.8	0.0
S12h	h.s.	7.6	15.9	0.0	21.2	24.6	0.0	26.3	28.6	0.0	13.1	20.1	0.0

TABLE A25.b. Relative spin state energies (kcal·mol^{-1}) [Fe^{IV}(O)(tpa^{Ph})]$^{-}$ **(18)** complex calculated at LDA, S12g, PBE-D2, BP86-D3, B3LYP, S12h optimized geometries, with four different DFAs

		Single point calculations on different level of theory:											
Geometry:		SSBD			B3LYP			S12h			MVS		
	Exp.	ls	is	hs	ls	is	hs	ls	is	hs	ls	is	hs
LDA	h.s.	24.5	28.9	0.0	24.5	58.1	0.0	34.8	71.1	0.0	38.0	38.0	0.0
S12g	h.s.	24.9	29.0	0.0	26.3	59.5	0.0	34.6	70.4	0.0	38.2	37.8	0.0
PBE-D2	h.s.	24.4	28.6	0.0	23.8	57.5	0.0	34.3	69.9	0.0	38.1	37.6	0.0
BP86-D3	h.s.	24.2	28.2	0.0	23.8	56.9	0.0	34.3	69.3	0.0	37.6	37.4	0.0
B3LYP	h.s.	24.5	28.7	0.0	25.5	57.6	0.0	34.5	70.1	0.0	38.4	38.0	0.0
S12h	h.s.	24.7	29.2	0.0	24.1	57.9	0.0	34.8	70.2	0.0	38.8	38.3	0.0

6.3. Energy decomposition analysis of iron-oxo and iron-hydroxo complexes (unpublished results)

6.3.1. Geometrical parameters of all investigated complexes

TABLE A26 Metal-Ligand distances (Å) for $[(NH_3)_3Fe^n(OH)(NH_3)]^{m+}$ model system (ZORA/S12g/TZ2P)

Iron Ox. State	+2			+3			+4		
Spin state	LS	IS	HS	LS	IS	HS	LS	IS	HS
Fe-O	1.76	1.75	1.77	1.65	1.65	1.74	1.57	1.60	1.64
Fe-N_{eq} (*average*)	2.06	2.18	2.36	2.04	2.16	2.21	1.99	2.03	2.07
Fe-N_{ax}	2.10	2.18	2.27	2.16	2.14	2.30	2.23	2.12	2.09

TABLE A27. Metal-Ligand distances (Å) for $[(NH_3)_3Fe^n(OH)(NCH)]^{m+}$ model system (ZORA/S12g/TZ2P)

Iron Ox. State	+2			+3			+4		
Spin state	LS	IS	HS	LS	IS	HS	LS	IS	HS
Fe-O	1.73	1.74	1.76	1.64	1.65	1.71	1.55	1.59	1.63
Fe-N_{eq} (*average*)	2.05	2.14	2.33	2.08	2.14	2.12	1.98	2.02	2.06
Fe-N_{ax}	1.74	1.87	1.98	1.83	2.08	3.62	2.26	2.09	2.06

TABLE A28. Metal-Ligand distances (Å) for $[(NH_3)_4Fe^n(OH)(NCH)]^{m+}$ model system (ZORA/S12g/TZ2P)

Iron Ox. State	+2			+3			+4		
Spin state	LS	IS	HS	LS	IS	HS	LS	IS	HS
Fe-O	1.85	1.81	1.78	1.74	1.64	1.73	1.62	1.63	1.62
Fe-N_{eq} (*average*)	2.05	2.25	2.33	2.05	2.25	2.21	2.03	2.03	2.17
Fe-N_{ax}	1.80	1.83	3.80	1.97	2.14	3.40	2.29	2.16	2.11

TABLE A29. Metal-Ligand distances (Å) for $[(NH_3)_3Fe^n(O)(NH_3)]^{m+}$ model system (ZORA/S12g/TZ2P)

Iron Ox. State	+2			+3		
Spin state	LS	IS	HS	LS	IS	HS
Fe-O	1.83	1.80	1.78	1.72	1.72	1.69
Fe-N_{eq} (*average*)	2.02	2.07	2.00	2.04	1.97	1.95
Fe-N_{ax}	2.14	2.04	2.09	2.01	2.00	2.08

TABLE A30. Metal-Ligand distances (Å) for $[(NH_3)_3Fe^n(O)(NCH)]^{m+}$ model system (ZORA/S12g/TZ2P)

Iron Ox. State	+2			+3		
Spin state	LS	IS	HS	LS	IS	HS
Fe-O	1.82	1.79	1.77	1.71	1.70	1.68
Fe-N_{eq} (*average*)	2.10	2.06	1.99	2.04	1.97	1.94
Fe-N_{ax}	2.33	1.96	1.96	1.93	1.97	2.02

TABLE A31. Metal-Ligand distances (Å) for $[(NH_3)_4Fe^n(O)(NCH)]^{m+}$ model system (ZORA/S12g/TZ2P)

Iron Ox. State	+2			+3		
Spin state	LS	IS	HS	LS	IS	HS
Fe-O	1.82	1.81	1.81	1.72	1.72	1.73
Fe-N_{eq} (*average*)	2.61	2.01	1.96	1.99	1.99	1.99
Fe-N_{ax}	2.17	2.17	2.03	2.14	2.01	2.00

6.3.2. Energy Decomposition Analysis component values relative to ground spin state (kcal mol^{-1}) of every specific complex

TABLE A32. EDA contributions for $[(NH_3)_3Fe^{II}(O)(NH_3)]^0$ model system (ZORA/S12g/TZ2P)

Spin state	LS	LS-HS	IS	IS-HS	HS
E	-2113.04	9.72	-2111.76	11.00	-2122.76
ΔEprep	102.30	73.85	100.07	71.62	28.45
ΔEdeform	0.50	0.49	0.03	0.02	0.01
ΔElig-lig	22.22	9.65	14.52	1.95	12.57
ΔEvalexc	79.58	63.66	85.52	69.60	15.92
ΔEint	-130.50	-64.77	-126.03	-60.30	-65.73
ΔEpauli	258.52	105.30	186.98	33.76	153.22
ΔEelstat	-233.02	-97.46	-187.15	-51.59	-135.56
ΔEorbint	-156.00	-72.61	-125.86	-42.47	-83.39
ΔEdisp	-5.39	0.65	-6.35	-0.31	-6.04
ΔEtotal	-28.20	9.08	-25.96	11.32	-37.28

TABLE A33. EDA contributions for $[(NH_3)_3Fe^{III}(O)(NH_3)]^{+1}$ model system (ZORA/S12g/TZ2P)

Spin state	LS	LS-IS	IS	HS-IS	HS
E	-2020.39	17.62	-2038.01	5.31	-2032.70
ΔEprep	125.38	83.24	42.14	-18.23	23.91
ΔEdeform	0.01	-0.03	0.04	-0.01	0.03
ΔElig-lig	21.88	5.20	16.68	-3.11	13.57
ΔEvalexc	103.49	78.07	25.42	-15.11	10.31
ΔEint	-259.69	-66.05	-193.64	23.71	-169.93
ΔEpauli	280.16	122.53	157.63	-5.01	152.62
ΔEelstat	-260.92	-49.37	-211.55	12.94	-198.61
ΔEorbint	-278.93	-139.21	-139.72	15.78	-123.94
ΔEdisp	-5.82	0.46	-6.28	-0.19	-6.47
ΔEtotal	-134.31	17.19	-151.50	5.48	-146.02

TABLE A34. EDA contributions for $[(NH_3)_3Fe^{IV}(O)(NH_3)]^{+2}$ model system (ZORA/S12g/TZ2P)

Spin state	LS	LS-HS	IS	IS-HS	HS
E	-1766.24	30.52	-1779.27	17.49	-1796.76
ΔEprep	68.91	43.56	44.39	19.04	25.35
ΔEdeform	0.17	0.02	0.19	0.04	0.15
ΔElig-lig	25.71	7.62	22.77	4.68	18.09
ΔEvalexc	43.03	35.92	21.43	14.32	7.11
ΔEint	-383.67	-13.42	-372.06	-1.81	-370.25
ΔEpauli	238.25	53.88	199.88	15.51	184.37
ΔEelstat	-302.70	-15.45	-286.33	0.92	-287.25
ΔEorbint	-319.22	-51.85	-285.61	-18.24	-267.37
ΔEdisp	-5.72	0.30	-5.78	0.24	-6.02
ΔEtotal	-314.76	30.14	-327.67	17.23	-344.90

TABLE A35. EDA contributions for $[(NH_3)_3Fe^{II}(O)(NCH)]^{0}$ model system (ZORA/S12g/TZ2P)

Spin state	LS	LS-HS	IS	IS-HS	HS
E	-2142.08	3.73	-2142.79	3.02	-2145.81
ΔEprep	109.87	84.06	99.67	73.86	25.81
ΔEdeform	13.49	13.06	1.35	0.92	0.43
ΔElig-lig	19.62	8.62	13.44	2.44	11.00
ΔEvalexc	76.76	62.38	84.88	70.50	14.38
ΔEint	-162.10	-81.11	-151.91	-70.92	-80.99
ΔEpauli	374.67	152.10	258.23	35.66	222.57
ΔEelstat	-281.56	-115.61	-220.66	-54.71	-165.95
ΔEorbint	-255.21	-117.60	-189.48	-51.87	-137.61
ΔEdisp	-4.56	0.76	-5.29	0.03	-5.32
ΔEtotal	-52.23	2.95	-52.24	2.94	-55.18

TABLE A36. EDA contributions for $[(NH_3)_3Fe^{III}(O)(NCH)]^{+1}$ model system (ZORA/S12g/TZ2P)

Spin state	LS	LS-IS	IS	HS-IS	HS
E	-2035.01	7.11	-2042.12	3.86	-2038.26
ΔEprep	122.54	84.73	37.81	-24.65	13.16
ΔEdeform	0.10	0.00	0.10	-0.05	0.05
ΔElig-lig	19.11	6.14	12.97	-8.22	4.75
ΔEvalexc	103.34	78.59	24.75	-16.39	8.36
ΔEint	-266.63	-78.09	-188.54	28.06	-160.48
ΔEpauli	320.40	157.94	162.46	1.14	163.60
ΔEelstat	-269.57	-60.69	-208.88	4.84	-204.04
ΔEorbint	-317.46	-175.34	-142.12	22.08	-120.04
ΔEdisp	-4.88	0.44	-5.32	0.44	-4.88
ΔEtotal	-144.09	6.64	-150.73	3.41	-147.32

TABLE A37. EDA contributions for $[(NH_3)_3Fe^{IV}(O)(NCH)]^{+2}$ model system (ZORA/S12g/TZ2P)

Spin state	LS	LS-HS	IS	IS-HS	HS
E	-1775.58	25.91	-1784.21	17.28	-1801.49
ΔEprep	63.71	43.63	38.84	18.76	20.08
ΔEdeform	0.37	-0.01	0.37	-0.01	0.38
ΔElig-lig	18.06	4.96	17.41	4.31	13.10
ΔEvalexc	45.28	38.68	21.06	14.46	6.60
ΔEint	-383.12	-18.24	-366.55	-1.67	-364.88
ΔEpauli	230.97	46.73	201.55	17.31	184.24
ΔEelstat	-300.76	-19.00	-282.65	-0.89	-281.76
ΔEorbint	-313.33	-45.97	-285.45	-18.09	-267.36
ΔEdisp	-4.56	0.45	-4.76	0.25	-5.01
ΔEtotal	-319.41	25.39	-327.71	17.09	-344.80

TABLE A38. EDA contributions for $[(NH_3)_4Fe^{II}(O)(NCH)]^0$ model system (ZORA/S12g/TZ2P)

Spin state	LS	IS-LS	IS	HS-LS	HS
E					
ΔEprep	-2587.29	1.83	-2586.77	1.31	-2585.46
ΔEdeform	162.71	-135.37	112.77	-85.43	27.34
ΔElig-lig	2.09	-2.14	0.20	-0.25	-0.05
ΔEvalexc	33.34	-22.43	22.31	-11.40	10.91
ΔEint	127.28	-110.80	90.26	-73.78	16.48
ΔEpauli	-206.48	138.31	-154.00	85.83	-68.17
ΔEelstat	347.58	-189.38	260.90	-102.70	158.20
ΔEorbint	-290.98	153.85	-224.90	87.77	-137.13
ΔEdisp	-5.32	-1.13	-7.22	0.77	-6.45
ΔEtotal	-43.77	2.94	-41.23	0.40	-40.83

TABLE A39. EDA contributions for $[(NH_3)_3Fe^{III}(O)(NCH)]^{+1}$ model system (ZORA/S12g/TZ2P)

Spin state	LS	LS-IS	IS	HS-IS	HS
E	-2493.43	15.43	-2508.86	1.77	-2507.09
ΔEprep	135.09	91.77	43.32	-19.26	24.06
ΔEdeform	0.29	0.25	0.04	-0.04	0.00
ΔElig-lig	31.34	12.62	18.72	-3.95	14.77
ΔEvalexc	103.48	78.92	24.56	-15.26	9.30
ΔEint	-284.24	-78.30	-205.94	20.61	-185.33
ΔEpauli	230.54	99.74	130.80	24.09	154.89
ΔEelstat	-274.37	-72.58	-201.79	-5.01	-206.80
ΔEorbint	-240.41	-105.46	-134.95	1.53	-133.42
ΔEdisp	-5.32	1.95	-7.27	0.43	-6.84
ΔEtotal	-149.15	13.47	-162.62	1.35	-161.27

TABLE A40. EDA contributions for $[(NH_3)_3Fe^{IV}(O)(NCH)]^{+2}$ model system (ZORA/S12g/TZ2P)

Spin state	LS	LS-IS	IS	HS-IS	HS
E	-2248.91	36.75	-2285.66	2.30	-2283.36
ΔEprep	122.78	32.06	90.72	-61.78	28.94
ΔEdeform	0.17	0.03	0.14	0.06	0.20
ΔElig-lig	29.36	-1.26	30.62	-8.31	22.31
ΔEvalexc	93.25	33.29	59.96	-53.53	6.43
ΔEint	-460.73	5.81	-466.54	65.92	-400.62
ΔEpauli	194.66	-1.66	196.32	-46.50	149.82
ΔEelstat	-312.04	0.47	-312.51	33.83	-278.68
ΔEorbint	-343.35	7.00	-350.35	78.59	-271.76
ΔEdisp	-6.35	-1.12	-5.23	-1.88	-7.11
ΔEtotal	-337.95	37.87	-375.82	4.14	-371.68

TABLE A41. EDA contributions for $[(NH_3)_3Fe^{III}(OH)(NH_3)]^{+2}$ model system (ZORA/S12g/TZ2P)

Spin state	LS	LS-HS	IS	IS-HS	HS
E	-1880.26	30.35	-1903.21	7.40	-1910.61
ΔEprep	124.82	96.58	70.27	42.03	28.24
ΔEdeform	0.08	0.03	0.05	0.00	0.05
ΔElig-lig	24.78	10.25	18.15	3.62	14.53
ΔEvalexc	99.96	86.30	52.07	38.41	13.66
ΔEint	-373.28	-66.74	-341.38	-34.84	-306.54
ΔEpauli	229.32	67.37	186.50	24.55	161.95
ΔEelstat	-287.05	-31.87	-278.55	-23.37	-255.18
ΔEorbint	-315.55	-102.24	-249.33	-36.02	-213.31
ΔEdisp	-5.92	0.51	-6.29	0.14	-6.43
ΔEtotal	-246.48	31.82	-271.11	7.19	-278.30

TABLE A42. EDA contributions for $[(NH_3)_3Fe^{IV}(OH)(NH_3)]^{+3}$ model system (ZORA/S12g/TZ2P)

Spin state	LS	LS-HS	IS	IS-HS	HS
E	-1477.04	34.38	-1495.61	15.81	-1511.42
ΔEprep	450.36	221.41	298.32	69.37	228.95
ΔEdeform	0.44	0.02	0.44	0.02	0.42
ΔElig-lig	31.73	11.19	27.22	6.68	20.54
ΔEvalexc	418.19	210.20	270.66	62.67	207.99
ΔEint	-763.74	-187.62	-629.85	-53.73	-576.12
ΔEpauli	227.81	23.36	230.01	25.56	204.45
ΔEelstat	-340.70	-5.69	-339.60	-4.59	-335.01
ΔEorbint	-650.85	-205.29	-520.26	-74.70	-445.56
ΔEdisp	-5.60	0.42	-5.61	0.41	-6.02
ΔEtotal	-313.38	33.79	-331.53	15.64	-347.17

TABLE A43. EDA contributions for $[(NH_3)_3Fe^{III}(OH)(NCH)]^{+2}$ model system (ZORA/S12g/TZ2P)

Spin state	LS	LS-HS	IS	IS-HS	HS
E	-1888.09	26.24	-1908.68	5.65	-1914.33
ΔEprep	119.79	96.45	65.78	42.44	23.34
ΔEdeform	0.22	0.08	0.20	0.06	0.14
ΔElig-lig	20.39	-2.95	14.14	-9.20	23.34
ΔEvalexc	99.18	86.41	51.44	38.67	12.77
ΔEint	-372.33	-70.45	-338.77	-36.89	-301.88
ΔEpauli	245.64	79.76	194.71	28.83	165.88
ΔEelstat	-287.96	-32.36	-276.11	-20.51	-255.60
ΔEorbint	-330.01	-117.85	-257.37	-45.21	-212.16
ΔEdisp	-4.94	0.49	-5.29	0.14	-5.43
ΔEtotal	-252.54	26.00	-272.99	5.55	-278.54

TABLE A44. EDA contributions for $[(NH_3)_3Fe^{IV}(OH)(NCH)]^{+3}$ model system (ZORA/S12g/TZ2P)

Spin state	LS	LS-HS	IS	IS-HS	HS
E	-1483.57	31.79	-1495.68	19.68	-1515.36
ΔEprep	445.15	220.28	293.11	68.24	224.87
ΔEdeform	0.90	0.15	0.90	0.15	0.75
ΔElig-lig	25.89	10.41	22.32	6.84	15.48
ΔEvalexc	418.36	209.72	269.89	61.25	208.64
ΔEint	-759.78	-189.30	-619.09	-48.61	-570.48
ΔEpauli	241.30	31.84	230.57	21.11	209.46
ΔEelstat	-345.13	-14.34	-338.18	-7.39	-330.79
ΔEorbint	-655.95	-206.80	-511.48	-62.33	-449.15
ΔEdisp	-4.59	0.63	-4.82	0.40	-5.22
ΔEtotal	-314.63	30.98	-325.98	19.63	-345.61

TABLE A45. EDA contributions for $[(NH_3)_3Fe^{III}(OH)(NCH)]^{+2}$ model system (ZORA/S12g/TZ2P)

Spin state	LS	LS-HS	IS	IS-HS	HS
E	-2393.15	4.83	-2389.21	8.77	-2397.98
ΔEprep	128.92	95.52	74.26	40.86	33.40
ΔEdeform	0.08	-0.39	0.13	-0.34	0.47
ΔElig-lig	31.27	10.27	21.92	0.92	21.00
ΔEvalexc	97.57	85.64	52.21	40.28	11.93
ΔEint	-433.53	-92.31	-373.46	-32.24	-341.22
ΔEpauli	216.43	63.28	171.69	18.54	153.15
ΔEelstat	-304.68	-43.35	-276.83	-15.50	-261.33
ΔEorbint	-345.28	-112.24	-268.32	-35.28	-233.04
ΔEdisp	-5.59	1.57	-7.23	-0.07	-7.16
ΔEtotal	-304.61	3.21	-299.20	8.62	-307.82

TABLE A46. EDA contributions for $[(NH_3)_3Fe^{IV}(OH)(NCH)]^{+3}$ model system (ZORA/S12g/TZ2P)

Spin state	LS	LS-IS	IS	HS-IS	HS
E	-2010.83	14.91	-2025.74	10.69	-2015.05
ΔEprep	444.36	139.03	305.33	-70.81	234.52
ΔEdeform	0.44	0.10	0.34	0.13	0.47
ΔElig-lig	34.38	0.99	33.39	-8.43	24.96
ΔEvalexc	409.54	137.94	271.60	-62.51	209.09
ΔEint	-833.90	-124.44	-709.46	82.91	-626.55
ΔEpauli	240.84	20.62	220.22	-43.49	176.73
ΔEelstat	-369.71	-10.92	-358.79	25.36	-333.43
ΔEorbint	-705.03	-134.14	-570.89	101.04	-469.85
ΔEdisp	-5.43	0.05	-5.48	-1.69	-7.17
ΔEtotal	-389.54	14.59	-404.13	12.10	-392.03

7. References

1. Koch, W.; Holthausen, M. C., *A chemist's guide to density functional theory*. Wiley-VCH: 2000.
2. Ladd, M.; Palmer, R., *Structure Determination by X-ray Crystallography: Analysis by X-rays and Neutrons*. Springer US: **2014**.
3. Warner, J. H.; Schäffel, F.; Bachmatiuk, A.; Rümmeli, M. H. Chapter 5 - Characterisation Techniques. In *Graphene*, Warner, J. H.; Schäffel, F.; Bachmatiuk, A.; Rümmeli, M. H., Eds.; Elsevier: **2013**, 229-332.
4. Zettili, N., *Quantum Mechanics: Concepts and Applications*. Wiley: **2009**.
5. Perić, M., *Struktura i spektri molekula*. Srpska Akademija Nauka i Umetnosti: **2009**.
6. Cotton, F. A.; Wilkinson, G.; Gaus, P. L., *Basic inorganic chemistry*. J. Wiley: **1995**.
7. Schmid, E. W.; Zieǵelmann, H.; Stumpf, H., *The Quantum Mechanical Three-Body Problem: Vieweg Tracts in Pure and Applied Physics*. Elsevier Science: **1974**.
8. Demtröder, W., *Atoms, Molecules and Photons: An Introduction to Atomic-, Molecular- and Quantum-physics* Springer: **2006**.
9. Griffiths, D. J., *Introduction to Quantum Mechanics*. Cambridge University Press: **2017**; 207-210.
10. Boeyens, J. C. A., *Chemistry from First Principles*. Springer Netherlands: **2008**.
11. Pauli, W., Über den Zusammenhang des Abschlusses der Elektronengruppen im Atom mit der Komplexstruktur der Spektren. *Zeitschrift für Physik* **1925**, 31, 765-783.
12. Dirac, P. A. M., Quantum Mechanics of Many-Electron Systems. *Proceedings of the Royal Society A* **1931**, 123, 714- 733.
13. Dirac, P. A. M., *The principles of quantum mechanics*. Clarendon press: **1992**.
14. Levine, I. N., *Quantum Chemistry*. Pearson Education: **2013**.
15. Moore, C. E., *Atomic energy levels as derived from the analyses of optical spectra*. U.S. National Bureau of Standards: Washington DC, **1949**; Vol. 1 and 2.
16. Bersuker, I. B., *Electronic Structure and Properties of Transition Metal Compounds: Introduction to the Theory*. Wiley: **2010**.
17. Kosinov, N.; Liu, C.; Hensen, E. J. M.; Pidko, E. A., Engineering of Transition Metal Catalysts Confined in Zeolites. *Chemistry of Materials* **2018**, 30, 3177-3198.
18. Jin, W.; Maduraiveeran, G., Recent advances of porous transition metal-based nanomaterials for electrochemical energy conversion and storage applications. *Materials Today Energy* **2019**, 13, 64-84.
19. Yang, W.; Rehman, S.; Chu, X.; Hou, Y.; Gao, S., Transition Metal (Fe, Co and Ni) Carbide and Nitride Nanomaterials: Structure, Chemical Synthesis and Applications. *ChemNanoMat* **2015**, 1, 376-398.
20. Miao, J.; Ge, H., Recent Advances in First-Row-Transition-Metal-Catalyzed Dehydrogenative Cou-pling of C(sp3)–H Bonds. *European Journal of Organic Chemistry* **2015**, 2015, 7859-7868.
21. Liu, Y.; Bandini, M., Nickel Catalyzed Functionalization of Allenes. *Chinese Journal of Chemistry* **2019**, 37, 431-441.
22. Alig, L.; Fritz, M.; Schneider, S., First-Row Transition Metal (De)Hydrogenation Catalysis Based On Functional Pincer Ligands. *Chemical Reviews* **2019**, 119, 2681-2751.
23. Abu-Dief, A. M.; Mohamed, I. M. A., A review on versatile applications of transition metal complexes incorporating Schiff bases. *Beni-Suef University Journal of Basic and Applied Sciences* **2015**, 4, 119-133.
24. Zweig, J. E.; Kim, D. E.; Newhouse, T. R., Methods Utilizing First-Row Transition Metals in Natural Product Total Synthesis. *Chemical Reviews* **2017**, 117, 11680-11752.
25. Beaumier, E. P.; Pearce, A. J.; See, X. Y.; Tonks, I. A., Modern applications of low-valent early transition metals in synthesis and catalysis. *Nature Reviews Chemistry* **2019**, 3, 15-34.
26. Deronzier, A.; Moutet, J. C. Electrochemical Reactions Catalyzed by Transition Metal Complexes. In *Comprehensive Coordination Chemistry II*, McCleverty, J. A.; Meyer, T. J., Eds.; Pergamon: Oxford, **2003**, 471-507.
27. Sakurai, J. J.; Napolitano, J., *Modern Quantum Mechanics*. Addison-Wesley: **2011**.
28. Greiner, W.; Bromley, D. A., *Relativistic Quantum Mechanics. Wave Equations*. Springer: **2000**.
29. Camargo, P. H. C., I. David Brown: The chemical bond in inorganic chemistry: the bond valence model, 2nd ed. *Journal of Materials Science* **2017**, 52, 9959-9962.

30. Gillespie, R. J.; Popelier, P. L. A.; Popelier, P. L. A., *Chemical Bonding and Molecular Geometry: From Lewis to Electron Densities*. Oxford University Press: **2001**.
31. Muller, U., *Inorganic Structural Chemistry*. Wiley: **2007**.
32. Gavroglou, K.; Simões, A.; Buchwald, J. Z., *Neither Physics Nor Chemistry: A History of Quantum Chemistry*. MIT Press: **2012**.
33. Hückel, E., Quantentheoretische Beiträge zum Benzolproblem. *Zeitschrift für Physik* **1931**, 70, 204-286.
34. Berson, J. A., Erich Hückel, Pioneer of Organic Quantum Chemistry: Reflections on Theory and Experiment. *Angewandte Chemie International Edition in English* **1996**, 35, 2750-2764.
35. Frenking, G.; Fröhlich, N., The Nature of the Bonding in Transition-Metal Compounds. *Chemical Reviews* **2000**, 100, 717-774.
36. Bethe, H., Termaufspaltung in Kristallen. *Annalen der Physik* **1929**, 395, 133-208.
37. Vleck, J. H. V., The Group Relation Between the Mulliken and Slater-Pauling Theories of Valence. *The Journal of Chemical Physics* **1935**, 3, 803-806.
38. Ballhausen, C. J., *Introduction to ligand field theory*. McGraw-Hill: **1962**.
39. König, E., C. K. Jørgensen: Modern Aspects of Ligand Field Theory. North-Holland Publishing Co. **1971**. VIII, 538 p., Preis: Hfl. 100.–. *Berichte der Bunsengesellschaft für physikalische Chemie* **1971**, 75, 1150-1150.
40. Cotton, F. A., *Advanced Inorganic Chemistry*. Wiley: **1999**.
41. Elias, H., M. Gerloch, E. C. Constable: Transition Metal Chemistry – The Valence Shell in d-Block Chemistry. VCH Weinheim, **1994**; XI, 211 Seiten, gebunden (ISBN 3-527-29218-7). Preis: DM 128,–. Paperback, ISBN 3-527-29219-5: DM 58,–. *Berichte der Bunsengesellschaft für physikalische Chemie* **1995**, 99, 901-901.
42. Mulliken, R. S., Electronic Structures of Polyatomic Molecules and Valence. *Physical Review* **1932**, 40, 55-62.
43. Veillard, A., Ab initio calculations of transition-metal organometallics: structure and molecular properties. *Chemical Reviews* **1991**, 91, 743-766.
44. Koga, N.; Morokuma, K., Ab initio molecular orbital studies of catalytic elementary reactions and catalytic cycles of transition-metal complexes. *Chemical Reviews* **1991**, 91, 823-842.
45. Lee, Y.-J.; Kim, S.-J.; Kang, C.-H.; Ko, J.; Kang, S. O.; Carroll, P. J., New Class of Fischer-Type Carbene Complexes Containing an o-Carboranyl Substituent. Synthesis and Crystal Structure of (CO)5W[C(OMe)(PhC2B10H10)] and (CO)4(PhC2B10H10)Mn[C(OCH3)(CH3)]. *Organometallics* **1998**, 17, 1109-1115.
46. Yoshikai, N.; Nakamura, E., Mechanisms of Nucleophilic Organocopper(I) Reactions. *Chemical Reviews* **2012**, 112, 2339-2372.
47. Robbins, L. K.; Lilly, C. P.; Sommer, R. D.; Ison, E. A., Effect of the Ancillary Ligand on the Mechanism for CO Migratory Insertion in High-Valent Oxorhenium Complexes. *Organometallics* **2016**, 35, 3530-3537.
48. Rao, C. N. R., Transition Metal Oxides. *Annual Review of Physical Chemistry* **1989**, 40, 291-326.
49. Yi, S.; Zhu, Z.; Cai, X.; Jia, Y.; Cho, J.-H., The Nature of Bonding in Bulk Tellurium Composed of One-Dimensional Helical Chains. *Inorganic Chemistry* **2018**, 57, 5083-5088.
50. Szell, P. M. J.; Zablotny, S.; Bryce, D. L., Halogen bonding as a supramolecular dynamics catalyst. *Nature Communications* **2019**, 10, 916.
51. Lawrance, G. A., *Introduction to Coordination Chemistry*. Wiley: **2013**.
52. Bhatt, V., *Essentials of Coordination Chemistry: A Simplified Approach with 3D Visuals*. Elsevier Science: 2015.
53. Guilard, R.; Erker, G.; Raithby, P.; Xu, Q., The diversity of coordination chemistry – A special issue in honor of Prof. Pierre Braunstein. *Coordination Chemistry Reviews* **2017**, 350, 1-2.
54. Mashima, K.; Tsurugi, H., Uniqueness and versatility of iminopyrrolyl ligands for transition metal complexes. *Journal of Organometallic Chemistry* **2005**, 690, 4414-4423.
55. Weiss, D. T.; Altmann, P. J.; Haslinger, S.; Jandl, C.; Pöthig, A.; Cokoja, M.; Kühn, F. E., Structural diversity of late transition metal complexes with flexible tetra-NHC ligands. *Dalton Transactions* **2015**, 44, 18329-18339.

56. Nithya, P.; Simpson, J.; Govindarajan, S., Syntheses, structural diversity and thermal behavior of first row transition metal complexes containing potential multidentate ligands based on 2,6-diacetylpyridine and benzyl carbazate. *Polyhedron* **2018**, 141, 5-16.
57. Bock, C. W.; Markham, G. D.; Katz, A. K.; Glusker, J. P., The Arrangement of First- and Second-shell Water Molecules Around Metal Ions: Effects of Charge and Size. *Theoretical Chemistry Accounts* **2006**, 115, 100-112.
58. Markham, G. D.; Glusker, J. P.; Bock, C. W., The Arrangement of First- and Second-Sphere Water Molecules in Divalent Magnesium Complexes: Results from Molecular Orbital and Density Functional Theory and from Structural Crystallography. *The Journal of Physical Chemistry B* **2002**, 106, 5118-5134.
59. Bogatko, S. A.; Bylaska, E. J.; Weare, J. H., First Principles Simulation of the Bonding, Vibrational, and Electronic Properties of the Hydration Shells of the High-Spin Fe3+ Ion in Aqueous Solutions. *The Journal of Physical Chemistry A* **2010**, 114, 2189-2200.
60. Burgess, J., *Metal Ions in Solution*. Ellis Horwood: **1978**.
61. Hersleth, H.-P.; Ryde, U.; Rydberg, P.; Görbitz, C. H.; Andersson, K. K., Structures of the high-valent metal-ion haem–oxygen intermediates in peroxidases, oxygenases and catalases. *Journal of Inorganic Biochemistry* **2006**, 100, 460-476.
62. Bellissent-Funel, M. C., *Hydration Processes in Biology: Theoretical and Experimental Approaches*. IOS Press: **1999**.
63. Lincoln, S. F.; Richens, D. T.; Sykes, A. G. 1.25 - Metal Aqua Ions. In *Comprehensive Coordination Chemistry II*, McCleverty, J. A.; Meyer, T. J., Eds.; Pergamon: Oxford, **2003**, 515-555.
64. Zong, X.; Li, C. 7 - Photocatalytic water splitting on metal oxide-based semiconductor photocatalysts. In *Metal Oxides in Heterogeneous Catalysis*, Védrine, J. C., Ed.; Elsevier: **2018**, 355-399.
65. Barreca, D.; Carraro, G.; Gasparotto, A.; Maccato, C. 3 - Metal oxide electrodes for photo-activated water splitting. In *Multifunctional Photocatalytic Materials for Energy*, Lin, Z.; Ye, M.; Wang, M., Eds.; Woodhead Publishing: **2018**, 19-48.
66. Petit, A. S.; Pennifold, R. C. R.; Harvey, J. N., Electronic Structure and Formation of Simple Ferryloxo Complexes: Mechanism of the Fenton Reaction. *Inorganic Chemistry* **2014**, 53, 6473-6481.
67. Vlahović, F.; Perić, M.; Gruden-Pavlović, M.; Zlatar, M., Assessment of TD-DFT and LF-DFT for study of d − d transitions in first row transition metal hexaaqua complexes. *The Journal of Chemical Physics* **2015**, 142, 214111.
68. Dobe, C.; Noble, C.; Carver, G.; Tregenna-Piggott, P. L.; McIntyre, G. J.; Barra, A. L.; Neels, A.; Janssen, S.; Juranyi, F., Electronic and molecular structure of high-spin d4 complexes: experimental and theoretical study of the [Cr(D2O)6]2+ cation in Tutton's salts. *Journal of the American Chemical Society* **2004**, 126, 16639-52.
69. Kallies, B.; Meier, R., Electronic Structure of 3d [M(H2O)6]3+ Ions from ScIII to FeIII: A Quantum Mechanical Study Based on DFT Computations and Natural Bond Orbital Analyses. *Inorganic Chemistry* **2001**, 40, 3101-3112.
70. Yaroshevsky, A. A., Abundances of chemical elements in the Earth's crust. *Geochemistry International* **2006**, 44, 48-55.
71. Sangaiya, P.; Jayaprakash, R., A Review on Iron Oxide Nanoparticles and Their Biomedical Applications. *Journal of Superconductivity and Novel Magnetism* **2018**, 31, 3397-3413.
72. Wani, W. A.; Baig, U.; Shreaz, S.; Shiekh, R. A.; Iqbal, P. F.; Jameel, E.; Ahmad, A.; Mohd-Setapar, S. H.; Mushtaque, M.; Ting Hun, L., Recent advances in iron complexes as potential anticancer agents. *New Journal of Chemistry* **2016**, 40, 1063-1090.
73. Link, H. S.; Schmitt, R. J., Iron, Carbon Steel, and Alloy Steel. Materials of Construction Review. *Industrial & Engineering Chemistry* **1961**, 53, 590-595.
74. Wang, N. L.; Hosono, H.; Dai, P., *Iron-based Superconductors: Materials, Properties and Mechanisms*. Jenny Stanford Publishing: **2012**.
75. Angus, H. T., *Cast Iron: Physical and Engineering Properties*. Elsevier Science: **2013**.
76. Litter, M. I.; Quici, N.; Meichtry, M., *Iron Nanomaterials for Water and Soil Treatment*. Jenny Stanford Publishing: **2018**.
77. Aisen, P.; Enns, C.; Wessling-Resnick, M., Chemistry and biology of eukaryotic iron metabolism. *The International Journal of Biochemistry & Cell Biology* **2001**, 33, 940-959.

78. Lieu, P. T.; Heiskala, M.; Peterson, P. A.; Yang, Y., The roles of iron in health and disease. *Molecular Aspects of Medicine* **2001**, 22, 1-87.
79. Visser, S. P. d.; Kumar, D., *Iron-Containing Enzymes: Versatile Catalysts of Hydroxylation Reactions in Nature*. The Royal Society of Chemistry: **2011**, 001-448.
80. Yin, G., Active transition metal oxo and hydroxo moieties in nature's redox, enzymes and their synthetic models: Structure and reactivity relationships. *Coordination Chemistry Reviews* **2010**, 254, 1826-1842.
81. England, J.; Guo, Y.; Farquhar, E. R.; Young Jr, V. G.; Münck, E.; Que Jr, L., The Crystal Structure of a High-Spin Oxoiron(IV) Complex and Characterization of Its Self-Decay Pathway. *Journal of the American Chemical Society* **2010**, 132, 8635-8644.
82. England, J.; Martinho, M.; Farquhar, E. R.; Frisch, J. R.; Bominaar, E. L.; Münck, E.; Que, L., A Synthetic High-Spin Oxoiron(IV) Complex. Generation, Spectroscopic Characterization and Reactivity. *Angewandte Chemie (International ed. in English)* **2009**, 48, 3622-3626.
83. Kaizer, J.; Klinker, E. J.; Oh, N. Y.; Rohde, J.-U.; Song, W. J.; Stubna, A.; Kim, J.; Münck, E.; Nam, W.; Que, L., Nonheme FeIVO Complexes That Can Oxidize the C−H Bonds of Cyclohexane at Room Temperature. *Journal of the American Chemical Society* **2004**, 126, 472-473.
84. Klinker, E. J.; Kaizer, J.; Brennessel, W. W.; Woodrum, N. L.; Cramer, C. J.; Que, L., Structures of Nonheme Oxoiron(IV) Complexes from X-ray Crystallography, NMR Spectroscopy, and DFT Calculations. *Angewandte Chemie International Edition* **2005**, 44, 3690-3694.
85. Grapperhaus, C. A.; Mienert, B.; Bill, E.; Weyhermüller, T.; Wieghardt, K., Mononuclear (Nitrido)iron(V) and (Oxo)iron(IV) Complexes via Photolysis of [(cyclam-acetato)FeIII(N3)]+ and Ozonolysis of [(cyclam-acetato)FeIII(O3SCF3)]+ in Water/Acetone Mixtures. *Inorganic Chemistry* **2000**, 39, 5306-5317.
86. MacBeth, C. E.; Golombek, A. P.; Young, V. G.; Yang, C.; Kuczera, K.; Hendrich, M. P.; Borovik, A. S., O2 Activation by Nonheme Iron Complexes: A Monomeric Fe(III)-Oxo Complex Derived From O2. *Science* **2000**, 289, 938-941.
87. Lacy, D. C.; Gupta, R.; Stone, K. L.; Greaves, J.; Ziller, J. W.; Hendrich, M. P.; Borovik, A. S., Formation, Structure, and EPR Detection of a High Spin FeIV—Oxo Species Derived from Either an FeIII—Oxo or FeIII—OH Complex. *Journal of the American Chemical Society* **2010**, 132, 12188-12190.
88. Rohde, J.; In, J.; Lim, M.; Brennessel, W.; Bukowski, M.; Stubna, A.; Münck, E.; Nam, W.; Que, L., Crystallographic and spectroscopic characterization of a nonheme Fe(IV)-O complex. *Science (New York)* **2003**, 299, 1037-9.
89. Ray, K.; England, J.; Fiedler, A. T.; Martinho, M.; Münck, E.; Que, L., An Inverted and More Oxidizing Isomer of [FeIV(O)(tmc)(NCCH3)]2+. *Angewandte Chemie International Edition* **2008**, 47, 8068-8071.
90. Thibon, A.; England, J.; Martinho, M.; Young, V. G.; Frisch, J. R.; Guillot, R.; Girerd, J.-J.; Münck, E.; Que, L.; Banse, F., Proton- and Reductant-Assisted Dioxygen Activation by a Nonheme Iron(II) Complex to Form an Oxoiron(IV) Intermediate. *Angewandte Chemie (International ed. in English)* **2008**, 47, 7064-7067.
91. Badiei, Y. M.; Siegler, M. A.; Goldberg, D. P., O(2) Activation by Bis(imino)pyridine Iron(II)-Thiolate Complexes. *Journal of the American Chemical Society* **2011**, 133, 1274-1277.
92. Bigi, J. P.; Harman, W. H.; Lassalle-Kaiser, B.; Robles, D. M.; Stich, T. A.; Yano, J.; Britt, R. D.; Chang, C. J., A High-Spin Iron(IV)–Oxo Complex Supported by a Trigonal Nonheme Pyrrolide Platform. *Journal of the American Chemical Society* **2012**, 134, 1536-1542.
93. Jackson, T. A.; Rohde, J.-U.; Seo, M. S.; Sastri, C. V.; DeHont, R.; Stubna, A.; Ohta, T.; Kitagawa, T.; Münck, E.; Nam, W.; Que, L., Axial Ligand Effects on the Geometric and Electronic Structures of Nonheme Oxoiron(IV) Complexes. *Journal of the American Chemical Society* **2008**, 130, 12394-12407.
94. Sastri, C. V.; Park, M. J.; Ohta, T.; Jackson, T. A.; Stubna, A.; Seo, M. S.; Lee, J.; Kim, J.; Kitagawa, T.; Münck, E.; Que, L.; Nam, W., Axial Ligand Substituted Nonheme FeIVO Complexes: Observation of Near-UV LMCT Bands and FeO Raman Vibrations. *Journal of the American Chemical Society* **2005**, 127, 12494-12495.
95. Nam, W., High-Valent Iron(IV)–Oxo Complexes of Heme and Non-Heme Ligands in Oxygenation Reactions. *Accounts of Chemical Research* **2007**, 40, 522-531.
96. Kundu, S.; Thompson, J. V. K.; Ryabov, A. D.; Collins, T. J., On the Reactivity of Mononuclear Iron(V)oxo Complexes. *Journal of the American Chemical Society* **2011**, 133, 18546-18549.
97. Guo, M.; Corona, T.; Ray, K.; Nam, W., Heme and Nonheme High-Valent Iron and Manganese Oxo Cores in Biological and Abiological Oxidation Reactions. *ACS Central Science* **2019**, 5, 13-28.

98. McDonald, A. R.; Que Jr, L., High-valent nonheme iron-oxo complexes: Synthesis, structure, and spectroscopy. *Coordination Chemistry Reviews* **2013**, 257, 414-428.
99. Chan, W. T. K.; Wong, W.-T., A brief introduction to transition metals in unusual oxidation states. *Polyhedron* **2013**, 52, 43-61.
100. Shan, X.; Que, L., High-valent nonheme iron-oxo species in biomimetic oxidations. *Journal of Inorganic Biochemistry* **2006**, 100, 421-433.
101. Hohenberger, J.; Ray, K.; Meyer, K., The biology and chemistry of high-valent iron–oxo and iron–nitrido complexes. *Nature Communications* **2012**, 3, 720.
102. Sharma, V. K., Ferrate(VI) and ferrate(V) oxidation of organic compounds: Kinetics and mechanism. *Coordination Chemistry Reviews* **2013**, 257, 495-510.
103. Balch, A. L.; Chan, Y. W.; Cheng, R. J.; La Mar, G. N.; Latos-Grazynski, L.; Renner, M. W., Oxygenation patterns for iron(II) porphyrins. Peroxo and ferryl (FeIVO) intermediates detected by proton nuclear magnetic resonance spectroscopy during the oxygenation of (tetramesitylporphyrin)iron(II). *Journal of the American Chemical Society* **1984**, 106, 7779-7785.
104. Ortiz de Montellano, P. R.; De Voss, J. J., Oxidizing species in the mechanism of cytochrome P450. *Natural Product Reports* **2002**, 19, 477-493.
105. Boča, R. 1 - Molecular Symmetry. In *A Handbook of Magnetochemical Formulae*, Boča, R., Ed.; Elsevier: Oxford, **2012**, 3-49.
106. Magnasco, V. Chapter 7 - Molecular symmetry. In *Elementary Molecular Quantum Mechanics (Second Edition)*, Magnasco, V., Ed.; Elsevier: Oxford, **2013**, 297-322.
107. di Lauro, C. 3 - Molecular Symmetry and Spectroscopy. In *Rotational Structure in Molecular Infrared Spectra*, di Lauro, C., Ed.; Elsevier: Boston, **2013**, 31-58.
108. Kettle, S. F. A., *Symmetry and Structure: Readable Group Theory for Chemists*. Wiley: **2008**.
109. Altmann, S. L.; Herzig, P., *Point-group theory tables*. Clarendon Press: **1994**.
110. Ladd, M., *Symmetry and Group theory in Chemistry*. Elsevier Science: **1998**.
111. Cotton, F. A., *Chemical Applications of Group Theory*. Wiley India: **2003**.
112. Hartmann, H.; Ilse, F. E., *Zeitschrift für Physikalische Chemie* **1951**, 197, 239.
113. Lever, A. B. P., *Inorganic electronic spectroscopy*. Elsevier: **1984**.
114. Rennie, R.; Law, J., *A Dictionary of Chemistry*. Oxford University Press: **2016**.
115. Ryutaro, T., Absorption Spectra of Co-ordination Compounds. I. *Bulletin of the Chemical Society of Japan* **1938**, 13, 388-400.
116. Griffith, J. S., *The Theory of Transition-Metal Ions*. Cambridge University Press: **1964**.
117. Daul, C.; Zlatar, M.; Gruden-Pavlović, M.; Swart, M. Application of Density Functional and Density Functional Based Ligand Field Theory to Spin States. In *Spin States in Biochemistry and Inorganic Chemistry*, **2015**, 7-34.
118. Swart, M.; Costas, M., *Spin States in Biochemistry and Inorganic Chemistry: Influence on Structure and Reactivity*. Wiley: **2015**.
119. Gayakhe, V.; Bhilare, S.; Yashmeen, A.; Fairlamb, I. J. S.; Kapdi, A. R. Chapter 6 - Transition-Metal Catalyzed Modification of Nucleosides. In *Palladium-Catalyzed Modification of Nucleosides, Nucleotides and Oligonucleotides*, Kapdi, A. R.; Maiti, D.; Sanghvi, Y. S., Eds.; Elsevier: **2018**, 167-195.
120. Lee, C.; Matunas, R. 10.14 - C–O Bond Formation through Transition Metal-mediated Etherification. In *Comprehensive Organometallic Chemistry III*, Mingos, D. M. P.; Crabtree, R. H., Eds.; Elsevier: Oxford, **2007**, 649-693.
121. Ranu, B. C.; Chatterjee, T.; Mukherjee, N.; Maity, P.; Majhi, B. Chapter 2 - Synthesis of Bioactive Five- and Six-Membered Heterocycles Catalyzed by Heterogeneous Supported Metals. In *Green Synthetic Approaches for Biologically Relevant Heterocycles*, Brahmachari, G., Ed.; Elsevier: Boston, **2015**, 7-43.
122. DuBois, M. R., Catalytic applications of transition-metal complexes with sulfide ligands. *Chemical Reviews* **1989**, 89, 1-9.
123. Casado-Sánchez, A.; Uygur, M.; González-Muñoz, D.; Aguilar-Galindo, F.; Nova-Fernández, J. L.; Arranz-Plaza, J.; Díaz-Tendero, S.; Cabrera, S.; Mancheño, O. G.; Alemán, J., 8-Mercaptoquinoline as a Ligand for Enhancing the Photocatalytic Activity of Pt(II) Coordination Complexes: Reactions and Mechanistic Insights. *The Journal of Organic Chemistry* **2019**, 84, 6437-6447.

124. Stepanović, S.; Angelone, D.; Gruden, M.; Swart, M., The role of spin states in the catalytic mechanism of the intra- and extradiol cleavage of catechols by O2. *Organic & Biomolecular Chemistry* **2017**, 15, 7860-7868.
125. Engelmann, X.; Malik, D. D.; Corona, T.; Warm, K.; Farquhar, E. R.; Swart, M.; Nam, W.; Ray, K., Trapping of a Highly Reactive Oxoiron(IV) Complex in the Catalytic Epoxidation of Olefins by Hydrogen Peroxide. *Angewandte Chemie International Edition* **2019**, 58, 4012-4016.
126. Frenking, G.; Deubel, D. V., *Theoretical Aspects of Transition Metal Catalysis*. Springer: **2005**.
127. Saouma, C. T.; Mayer, J. M., Do spin state and spin density affect hydrogen atom transfer reactivity; *Chemical Science* **2014**, 5, 21-31.
128. Costas, M.; Harvey, J. N., Discussion of an open problem. *Nature Chemistry* **2012**, 5, 7.
129. Poli, R.; Harvey, J. N., Spin forbidden chemical reactions of transition metal compounds. New ideas and new computational challenges. *Chemical Society Reviews* **2003**, 32, 1-8.
130. Yang, B.; Gagliardi, L.; Truhlar, D. G., Transition states of spin-forbidden reactions. *Physical Chemistry Chemical Physics* **2018**, 20, 4129-4136.
131. Turro, N. J.; Ramamurthy, V.; Ramamurthy, V.; Scaiano, J. C., *Principles of Molecular Photochemistry: An Introduction*. University Science Books: **2009**.
132. Turro, N. J., *Modern Molecular Photochemistry*. University Science Books: **1991**.
133. Lever, A. B. P., *Excited states and reactive intermediates : photochemistry, photophysics, and electrochemistry / A.B.P. Lever, editor*. American Chemical Society: Washington, DC, **1986**.
134. J., F., *Relaxation Processes in Molecular Excited States*. Relaxation Processes in Molecular Excited States: **1989**.
135. Fromme, B., *d-d Excitations in Transition-Metal Oxides: A Spin-Polarized Electron Energy-Loss Spectroscopy (SPEELS) Study*. Springer Berlin Heidelberg: **2000**.
136. Hüfner, S., *Photoelectron Spectroscopy: Principles and Applications*. Springer Berlin Heidelberg: **2013**.
137. Piela, L., *Ideas of Quantum Chemistry*. Elsevier Science: **2006**.
138. Thomas, L. H., The Motion of the Spinning Electron. *Nature* **1926**, 117, 514-514.
139. Graham, M. J.; Zadrozny, J. M.; Shiddiq, M.; Anderson, J. S.; Fataftah, M. S.; Hill, S.; Freedman, D. E., Influence of Electronic Spin and Spin–Orbit Coupling on Decoherence in Mononuclear Transition Metal Complexes. *Journal of the American Chemical Society* **2014**, 136, 7623-7626.
140. Endicott, J. F. Charge-Transfer Excited States of Transition Metal Complexes. In *Electron Transfer in Chemistry*; **2001**, 238-270.
141. Charge-transfer bands in the electronic spectra of transition-metal complexes. In *Metal-Ligand Bonding*, Janes, R.; Moore, E., Eds.; The Royal Society of Chemistry: **2004**, 75-82.
142. Balzani, V.; Carassiti, V., *Photochemistry of coordination compounds*. Academic Press: **1970**.
143. King, R. B., *Encyclopedia of Inorganic Chemistry*. Wiley: **2005**.
144. Wehry, E. L., Photochemical behaviour of transition-metal complexes. *Quarterly Reviews, Chemical Society* **1967**, 21, 213-230.
145. Endicott, J. F., The Charge Transfer Photochemistry of Coordination Complexes in Aqueous Solution. *Israel Journal of Chemistry* **1970**, 8, 209-226.
146. Chen, J.; Browne, W. R., Photochemistry of iron complexes. *Coordination Chemistry Reviews* **2018**, 374, 15-35.
147. Wolfsberg, M.; Van Hook, W. A.; Paneth, P. The Born–Oppenheimer Approximation: Potential Energy Surfaces. In *Isotope Effects: in the Chemical, Geological, and Bio Sciences*; Springer Netherlands: Dordrecht, **2009**, 37-54.
148. Mustroph, H., Potential-Energy Surfaces, the Born–Oppenheimer Approximations, and the Franck–Condon Principle: Back to the Roots. *ChemPhysChem* **2016**, 17, 2616-2629.
149. Wigner, E., On the Quantum Correction For Thermodynamic Equilibrium. *Physical Review* **1932**, 40, 749-759.
150. Thomas, L. H., The calculation of atomic fields. *Mathematical Proceedings of the Cambridge Philosophical Society* **2008**, 23, 542-548.
151. Fermi, E., A statistical method for the determination of some atomic properties and the application of this methods to the theory of the periodic system of elements. *Z. Phys.* **1928**, 48, 73-79.

152. Szabo, A.; Ostlund, N. S., *Modern Quantum Chemistry: Introduction to Advanced Electronic Structure Theory*. Dover Publications: 1996.
153. Lowe, J. P.; Science, E.; Technology, *Quantum Chemistry*. Academic Press: 1993.
154. Helgaker, T.; Jorgensen, P.; Olsen, J., *Molecular Electronic-Structure Theory*. Wiley: 2014.
155. Veszprémi, T.; Fehér, M., *Quantum Chemistry: Fundamentals to Applications*. Springer US: **1999**.
156. Pilar, F. L., *Elementary Quantum Chemistry*. Dover Publications: **2001**.
157. Cramer, C. J., *Essentials of Computational Chemistry: Theories and Models*. Wiley: **2005**.
158. Harvey, J. DFT Computation of Relative Spin-State Energetics of Transition Metal Compounds. In *Principles and Applications of Density Functional Theory in Inorganic Chemistry I*; Springer Berlin Heidelberg: **2004**; 112, 4, 151-184.
159. Sholl, D.; Steckel, J. A., *Density Functional Theory: A Practical Introduction*. Wiley: **2009**.
160. Geerlings, P.; De Proft, F.; Langenaeker, W., Conceptual Density Functional Theory. *Chemical Reviews* **2003**, 103, 1793-1874.
161. Engel, E.; Dreizler, R. M., *Density Functional Theory: An Advanced Course*. Springer Berlin Heidelberg: **2011**.
162. Parr, R. G.; Weitao, Y., *Density-Functional Theory of Atoms and Molecules*. Oxford University Press: **1994**.
163. Lieb, E. H.; Simon, B., The Thomas-Fermi theory of atoms, molecules and solids. *Advances in Mathematics* **1977**, 23, 22-116.
164. Schrödinger, E., An Undulatory Theory of the Mechanics of Atoms and Molecules. *Physical Review* **1926**, 28, 1049-1070.
165. Hohenberg, P.; Kohn, W., Inhomogeneous Electron Gas. *Physical Review* **1964**, 136, B864-B871.
166. Kohn, W.; Sham, L. J., Self-Consistent Equations Including Exchange and Correlation Effects. *Physical Review* **1965**, 140, A1133-A1138.
167. Harvey, J. N., On the accuracy of density functional theory in transition metal chemistry. *Annual Reports Section "C" (Physical Chemistry)* **2006**, 102, 203-226.
168. Zhao, Y.; Truhlar, D. G., Density Functionals with Broad Applicability in Chemistry. *Accounts of Chemical Research* **2008**, 41, 157-167.
169. Lundberg, M.; Siegbahn, P. E. M., Quantifying the effects of the self-interaction error in DFT: When do the delocalized states appear? *The Journal of Chemical Physics* **2005**, 122, 224103.
170. Grimme, S., Seemingly Simple Stereoelectronic Effects in Alkane Isomers and the Implications for Kohn–Sham Density Functional Theory. *Angewandte Chemie International Edition* **2006**, 45, 4460-4464.
171. Grimme, S., Accurate description of van der Waals complexes by density functional theory including empirical corrections. *Journal of Computational Chemistry* **2004**, 25, 1463-1473.
172. Vosko, S. H.; Wilk, L.; Nusair, M., Accurate spin-dependent electron liquid correlation energies for local spin density calculations: a critical analysis. *Canadian Journal of Physics* **1980**, 58, 1200-1211.
173. Seminario, J. M., *Recent Developments and Applications of Modern Density Functional Theory*. Elsevier Science: **1996**.
174. Bersuker, I., *The Jahn-Teller Effect*. Cambridge University Press: Cambridge, **2006**.
175. Jahn, H. A.; Teller, E.; Donnan, F. G., Stability of polyatomic molecules in degenerate electronic states; **2014**;Orbital degeneracy. *Proceedings of the Royal Society of London. Series A - Mathematical and Physical Sciences* **1937**, 161, 220-235.
176. Giese, T. J.; York, D. M., Density-functional expansion methods: evaluation of LDA, GGA, and meta-GGA functionals and different integral approximations. *The Journal of chemical physics* **2010**, 133, 244107-244107.
177. Becke, A. D., Density-functional exchange-energy approximation with correct asymptotic behavior. *Physical Review A* **1988**, 38, 3098.
178. Cramer, C. J.; Truhlar, D. G., Density functional theory for transition metals and transition metal chemistry. *Physical Chemistry Chemical Physics* **2009**, 11, 10757-10816.
179. Sousa, S. F.; Fernandes, P. A.; Ramos, M. J., General Performance of Density Functionals. *The Journal of Physical Chemistry A* **2007**, 111, 10439-10452.
180. Schultz, N. E.; Zhao, Y.; Truhlar, D. G., Density Functionals for Inorganometallic and Organometallic Chemistry. *The Journal of Physical Chemistry A* **2005**, 109, 11127-11143.

181. Bühl, M.; Kabrede, H., Geometries of Transition-Metal Complexes from Density-Functional Theory. *Journal of Chemical Theory and Computation* **2006**, 2, 1282-1290.
182. de Jong, G. T.; Bickelhaupt, F. M., Oxidative Addition of the Chloromethane C−Cl Bond to Pd, an ab Initio Benchmark and DFT Validation Study. *Journal of Chemical Theory and Computation* **2006**, 2, 322-335.
183. Holthausen, M. C., Benchmarking approximate density functional theory. I. s/d excitation energies in 3d transition metal cations. *Journal of Computational Chemistry* **2005**, 26, 1505-1518.
184. Paier, J.; Marsman, M.; Kresse, G., Why does the B3LYP hybrid functional fail for metals? *The Journal of Chemical Physics* **2007**, 127, 024103.
185. Barden, C. J.; Rienstra-Kiracofe, J. C.; III, H. F. S., Homonuclear 3d transition-metal diatomics: A systematic density functional theory study. *The Journal of Chemical Physics* **2000**, 113, 690-700.
186. Zhao, Y.; Truhlar, D. G., A new local density functional for main-group thermochemistry, transition metal bonding, thermochemical kinetics, and noncovalent interactions. *The Journal of Chemical Physics* **2006**, 125, 194101.
187. Jensen, K. P.; Roos, B. O.; Ryde, U., Performance of density functionals for first row transition metal systems. *The Journal of Chemical Physics* **2007**, 126, 014103.
188. Ghosh, A.; Gonzalez, E.; Tangen, E.; Roos, B. O., Mapping the d−d Excited-State Manifolds of Transition Metal β-Diiminato−Imido Complexes. Comparison of Density Functional Theory and CASPT2 Energetics. *The Journal of Physical Chemistry A* **2008**, 112, 12792-12798.
189. Zhao, Y.; Truhlar, D. G., Comparative DFT Study of van der Waals Complexes: Rare-Gas Dimers, Alkaline-Earth Dimers, Zinc Dimer, and Zinc-Rare-Gas Dimers. *The Journal of Physical Chemistry A* **2006**, 110, 5121-5129.
190. de Jong, G. T.; Geerke, D. P.; Diefenbach, A.; Matthias Bickelhaupt, F., DFT benchmark study for the oxidative addition of CH4 to Pd. Performance of various density functionals. *Chemical Physics* **2005**, 313, 261-270.
191. Adamo, C.; Lelj, F., A hybrid density functional study of the first-row transition-metal monocarbonyls. *The Journal of Chemical Physics* **1995**, 103, 10605-10613.
192. Swart, M.; Gruden, M., Spinning around in Transition-Metal Chemistry. *Accounts of Chemical Research* **2016**, 49, 2690-2697.
193. Labanowski, J. K.; Andzelm, J. W., *Density Functional Methods in Chemistry*. Springer New York: 2012.
194. Farkas, Ö.; Bernhard Schlegel, H., Geometry optimization methods for modeling large molecules. *Journal of Molecular Structure: THEOCHEM* **2003**, 666-667, 31-39.
195. Lenthe, E. v.; Baerends, E. J.; Snijders, J. G., Relativistic total energy using regular approximations. *The Journal of Chemical Physics* **1994**, 101, 9783-9792.
196. Klamt, A.; Schuurmann, G., COSMO: a new approach to dielectric screening in solvents with explicit expressions for the screening energy and its gradient. *Journal of the Chemical Society, Perkin Transactions 2* **1993**, 799-805.
197. Grimme, S.; Antony, J.; Ehrlich, S.; Krieg, H., A consistent and accurate ab initio parametrization of density functional dispersion correction (DFT-D) for the 94 elements H-Pu. *The Journal of Chemical Physics* **2010**, 132, 154104.
198. Grimme, S., Semiempirical GGA-type density functional constructed with a long-range dispersion correction. *Journal of Computational Chemistry* **2006**, 27, 1787-1799.
199. Becke, A. D., Density-functional exchange-energy approximation with correct asymptotic behavior. *Physical Review A* **1988**, 38, 3098-3100.
200. Perdew, J. P., Density-functional approximation for the correlation energy of the inhomogeneous electron gas. *Physical Review B* **1986**, 33, 8822-8824.
201. Perdew, J. P., Erratum: Density-functional approximation for the correlation energy of the inhomogeneous electron gas. *Physical Review B* **1986**, 34, 7406-7406.
202. Brorsen, K. R.; Yang, Y.; Pak, M. V.; Hammes-Schiffer, S., Is the Accuracy of Density Functional Theory for Atomization Energies and Densities in Bonding Regions Correlated? *The Journal of Physical Chemistry Letters* **2017**, 8, 2076-2081.
203. Martin, J. M. L.; Oliveira, G. d., Towards standard methods for benchmark quality ab initio thermochemistry—W1 and W2 theory. *The Journal of Chemical Physics* **1999**, 111, 1843-1856.

204. Hocking, R. K.; Deeth, R. J.; Hambley, T. W., DFT Study of the Systematic Variations in Metal−Ligand Bond Lengths of Coordination Complexes: the Crucial Role of the Condensed Phase. *Inorganic Chemistry* **2007**, 46, 8238-8244.
205. Moltved, K. A.; Kepp, K. P., Chemical Bond Energies of 3d Transition Metals Studied by Density Functional Theory. *Journal of Chemical Theory and Computation* **2018**, 14, 3479-3492.
206. Jean Nono, H.; Bikele Mama, D.; Ghogomu, J. N.; Younang, E., A DFT Study of Structural and Bonding Properties of Complexes Obtained from First-Row Transition Metal Chelation by 3-Alkyl-4-phenylacetylamino-4,5-dihydro-1H-1,2,4-triazol-5-one and Its Derivatives. *Bioinorganic Chemistry and Applications* **2017**, 2017, 15.
207. Frison, G.; Ohanessian, G., A comparative study of semiempirical, ab initio, and DFT methods in evaluating metal–ligand bond strength, proton affinity, and interactions between first and second shell ligands in Zn-biomimetic complexes. *Journal of Computational Chemistry* **2008**, 29, 416-433.
208. De Proft, F.; Martin, J. M. L.; Geerlings, P., Calculation of molecular electrostatic potentials and Fukui functions using density functional methods. *Chemical Physics Letters* **1996**, 256, 400-408.
209. Demircioğlu, Z.; Kaştaş, Ç. A.; Büyükgüngör, O., Theoretical analysis (NBO, NPA, Mulliken Population Method) and molecular orbital studies (hardness, chemical potential, electrophilicity and Fukui function analysis) of (E)-2-((4-hydroxy-2-methylphenylimino)methyl)-3-methoxyphenol. *Journal of Molecular Structure* **2015**, 1091, 183-195.
210. Dostanić, J.; Lončarević, D.; Zlatar, M.; Vlahović, F.; Jovanović, D. M., Quantitative structure-activity relationship analysis of substituted arylazo pyridone dyes in photocatalytic system: Experimental and theoretical study. *Journal of Hazardous Materials* **2016**, 316, 26-33.
211. Kwiatkowski, J. S.; Leszczynski, J., Density functional theory study on molecular structure and vibrational IR spectra of isocytosine. *International Journal of Quantum Chemistry* **1997**, 61, 453-465.
212. Itoh, K.; Kiyohara, T.; Shinohara, H.; Ohe, C.; Kawamura, Y.; Nakai, H., DFT Calculation Analysis of the Infrared Spectra of Ethylene Adsorbed on Cu(110), Pd(110), and Ag(110). *The Journal of Physical Chemistry B* **2002**, 106, 10714-10721.
213. Krishnakumar, V.; Balachandran, V.; Chithambarathanu, T., Density functional theory study of the FT-IR spectra of phthalimide and N-bromophthalimide. *Spectrochimica Acta Part A: Molecular and Biomolecular Spectroscopy* **2005**, 62, 918-925.
214. Daul, C.; Güdel, H. U.; Weber, J., A density functional investigation of the ground- and excited-state properties of ruthenocene. *The Journal of Chemical Physics* **1993**, 98, 4023-4029.
215. Daul, C.; Baerends, E. J.; Vernooijs, P., A Density Functional Study of the MLCT States of [Ru(bpy)3]2+ in D3 Symmetry. *Inorganic Chemistry* **1994**, 33, 3538-3543.
216. Lannoo, M.; Baraff, G. A.; Schlüter, M., Self-consistent second-order perturbation treatment of multiplet structures using local-density theory. *Physical Review B* **1981**, 24, 943-954.
217. Wood, J. H., Atomic multiplet structures obtained from Hartree-Fock, statistical exchange and local spin density approximations. *Journal of Physics B: Atomic and Molecular Physics* **1980**, 13, 1-14.
218. Hellman, A.; Razaznejad, B.; Lundqvist, B. I., Potential-energy surfaces for excited states in extended systems. *The Journal of Chemical Physics* **2004**, 120, 4593-4602.
219. Gross, E. K. U.; Kohn, W. Time-Dependent Density-Functional Theory. In *Advances in Quantum Chemistry*, Löwdin, P.-O., Ed.; Academic Press: **1990**; 21, 255-291.
220. Runge, E.; Gross, E. K. U., Density-Functional Theory for Time-Dependent Systems. *Physical Review Letters* **1984**, 52, 997-1000.
221. Ullrich, C., *Time-Dependent Density-Functional Theory: Concepts and Applications*. OUP Oxford: **2012**.
222. Marques, M. A. L.; Maitra, N. T.; Nogueira, F. M. S.; Gross, E. K. U.; Rubio, A., *Fundamentals of Time-Dependent Density Functional Theory*. Springer Berlin Heidelberg: **2012**.
223. Ullrich, C. A.; Yang, Z.-h., A Brief Compendium of Time-Dependent Density Functional Theory. *Brazilian Journal of Physics* **2014**, 44, 154-188.
224. van Gisbergen, S. J. A.; Groeneveld, J. A.; Rosa, A.; Snijders, J. G.; Baerends, E. J., Excitation Energies for Transition Metal Compounds from Time-Dependent Density Functional Theory. Applications to MnO4-, Ni(CO)4, and Mn2(CO)10. *The Journal of Physical Chemistry A* **1999**, 103, 6835-6844.

225. Autschbach, J. Spectroscopic Properties Obtained from Time-Dependent Density Functional Theory (TD-DFT). In *Encyclopedia of Inorganic Chemistry*; **2009**.
226. Full, J.; González, L.; Daniel, C., A CASSCF/CASPT2 and TD-DFT Study of the Low-Lying Excited States of η5-CpMn(CO)3. *The Journal of Physical Chemistry A* **2001**, 105, 184-189.
227. Rosa, A.; Ricciardi, G.; Baerends, E. J.; van Gisbergen, S. J. A., The Optical Spectra of NiP, NiPz, NiTBP, and NiPc: Electronic Effects of Meso-tetraaza Substitution and Tetrabenzo Annulation. *The Journal of Physical Chemistry A* **2001**, 105, 3311-3327.
228. Ricciardi, G.; Rosa, A.; Baerends, E. J., Ground and Excited States of Zinc Phthalocyanine Studied by Density Functional Methods. *The Journal of Physical Chemistry A* **2001**, 105, 5242-5254.
229. Atanasov, M.; Daul, C. A.; Rauzy, C. A DFT Based Ligand Field Theory. In *Optical Spectra and Chemical Bonding in Inorganic Compounds: Special Volume dedicated to Professor Jørgensen I*, Mingos, D. M. P.; Schönherr, T., Eds.; Springer Berlin Heidelberg: Berlin, Heidelberg, **2004**, 97-125.
230. Atanasov, M.; Daul, C. A.; Rauzy, C., New insights into the effects of covalency on the ligand field parameters: a DFT study. *Chemical Physics Letters* **2003**, 367, 737-746.
231. Roos, B. O. The Multiconfigurational (MC) SCF Method. In *Methods in Computational Molecular Physics*, Diercksen, G. H. F.; Wilson, S., Eds.; Springer Netherlands: Dordrecht, **1983**, 161-187.
232. Shepard, R. The Multiconfiguration Self-Consistent Field Method. In *Ab initio Methods in Quantum Chemistry Part II*, Lawley, K. P., Ed.; John Wiley & Sons Ltd: Chichester, **1987**.
233. Malmqvist, P. A.; Rendell, A.; Roos, B. O., The restricted active space self-consistent-field method, implemented with a split graph unitary group approach. *The Journal of Physical Chemistry* **1990**, 94, 5477-5482.
234. Roos, B. O. Multiconfigurational quantum chemistry for ground and excited states. In *Radiation Induced Molecular Phenomena in Nucleic Acids: A Comprehensive Theoretical and Experimental Analysis*, Shukla, M. K.; Leszczynski, J., Eds.; Springer Netherlands: Dordrecht, **2008**, 125-156.
235. Andersson, K.; Malmqvist, P. Å.; Roos, B. O., Second-order perturbation theory with a complete active space self-consistent field reference function. *The Journal of Chemical Physics* **1992**, 96, 1218-1226.
236. Andersson, K.; Roos, B. O.; Malmqvist, P. Å.; Widmark, P. O., The Cr2 potential energy curve studied with multiconfigurational second-order perturbation theory. *Chemical Physics Letters* **1994**, 230, 391-397.
237. Bartlett, R. J., Many-Body Perturbation Theory and Coupled Cluster Theory for Electron Correlation in Molecules. *Annual Review of Physical Chemistry* **1981**, 32, 359-401.
238. Watts, J. D.; Gauss, J.; Bartlett, R. J., Coupled-cluster methods with noniterative triple excitations for restricted open-shell Hartree–Fock and other general single determinant reference functions. Energies and analytical gradients. *The Journal of Chemical Physics* **1993**, 98, 8718-8733.
239. Dreuw, A.; Wormit, M., The algebraic diagrammatic construction scheme for the polarization propagator for the calculation of excited states. *Wiley Interdisciplinary Reviews: Computational Molecular Science* **2015**, 5, 82-95.
240. Olsen, J., The CASSCF method: A perspective and commentary. *International Journal of Quantum Chemistry* **2011**, 111, 3267-3272.
241. Pulay, P., A perspective on the CASPT2 method. *International Journal of Quantum Chemistry* **2011**, 111, 3273-3279.
242. Du, P.; Davidson, E. R., Ab initio study on the excitation energies of the protonated Schiff base of 11-cis-retinal. *The Journal of Physical Chemistry* **1990**, 94, 7013-7020.
243. Neese, F., A spectroscopy oriented configuration interaction procedure. *The Journal of Chemical Physics* **2003**, 119, 9428-9443.
244. van Leeuwen, R., Mapping from Densities to Potentials in Time-Dependent Density-Functional Theory. *Physical Review Letters* **1999**, 82, 3863-3866.
245. Casida, M. E.; Huix-Rotllant, M., Progress in Time-Dependent Density-Functional Theory. *Annual Review of Physical Chemistry* **2012**, 63, 287-323.
246. Casida, M. E., Time-dependent density-functional theory for molecules and molecular solids. *Journal of Molecular Structure: THEOCHEM* **2009**, 914, 3-18.
247. Hirata, S.; Head-Gordon, M., Time-dependent density functional theory within the Tamm–Dancoff approximation. *Chemical Physics Letters* **1999**, 314, 291-299.

248. Scalmani, G.; Frisch, M. J.; Mennucci, B.; Tomasi, J.; Cammi, R.; Barone, V., Geometries and properties of excited states in the gas phase and in solution: Theory and application of a time-dependent density functional theory polarizable continuum model. *The Journal of Chemical Physics* **2006**, 124, 094107.
249. Furche, F.; Ahlrichs, R., Adiabatic time-dependent density functional methods for excited state properties. *The Journal of Chemical Physics* **2002**, 117, 7433-7447.
250. Chen, D.; Liu, J.; Ma, H.; Zeng, Q.; Liang, W., Analytical derivative techniques for TDDFT excited-state properties: Theory and application. *Science China Chemistry* **2014**, 57, 48-57.
251. Ziegler, T.; Krykunov, M., On the calculation of charge transfer transitions with standard density functionals using constrained variational density functional theory. *The Journal of Chemical Physics* **2010**, 133, 074104.
252. Dreuw, A.; Head-Gordon, M., Failure of Time-Dependent Density Functional Theory for Long-Range Charge-Transfer Excited States: The Zincbacteriochlorin−Bacteriochlorin and Bacteriochlorophyll−Spheroidene Complexes. *Journal of the American Chemical Society* **2004**, 126, 4007-4016.
253. Prlj, A.; Curchod, B. F. E.; Fabrizio, A.; Floryan, L.; Corminboeuf, C., Qualitatively Incorrect Features in the TDDFT Spectrum of Thiophene-Based Compounds. *The Journal of Physical Chemistry Letters* **2015**, 6, 13-21.
254. Seidu, I.; Krykunov, M.; Ziegler, T., Applications of Time-Dependent and Time-Independent Density Functional Theory to Electronic Transitions in Tetrahedral d0 Metal Oxides. *Journal of Chemical Theory and Computation* **2015**, 11, 4041-4053.
255. Stein, T.; Kronik, L.; Baer, R., Reliable Prediction of Charge Transfer Excitations in Molecular Complexes Using Time-Dependent Density Functional Theory. *Journal of the American Chemical Society* **2009**, 131, 2818-2820.
256. Jiang, Y.; Hu, Z.; Zhou, B.; Zhong, C.; Sun, Z.; Sun, H., Accurate Prediction for Dynamic Hybrid Local and Charge Transfer Excited States from Optimally Tuned Range-Separated Density Functionals. *The Journal of Physical Chemistry C* **2019**, 123, 5616-5625.
257. Kronik, L.; Stein, T.; Refaely-Abramson, S.; Baer, R., Excitation Gaps of Finite-Sized Systems from Optimally Tuned Range-Separated Hybrid Functionals. *Journal of Chemical Theory and Computation* **2012**, 8, 1515-1531.
258. Elliott, P.; Goldson, S.; Canahui, C.; Maitra, N. T., Perspectives on double-excitations in TDDFT. *Chemical Physics* **2011**, 391, 110-119.
259. Gritsenko, O. V.; Jan Baerends, E., Double excitation effect in non-adiabatic time-dependent density functional theory with an analytic construction of the exchange–correlation kernel in the common energy denominator approximation. *Physical Chemistry Chemical Physics* **2009**, 11, 4640-4646.
260. Anderson, P. W., New Approach to the Theory of Superexchange Interactions. *Physical Review* **1959**, 115, 2-13.
261. Zlatar, M.; Gruden, M.; Vassilyeva, O. Y.; Buvaylo, E. A.; Ponomarev, A. N.; Zvyagin, S. A.; Wosnitza, J.; Krzystek, J.; Garcia-Fernandez, P.; Duboc, C., Origin of the Zero-Field Splitting in Mononuclear Octahedral MnIV Complexes: A Combined Experimental and Theoretical Investigation. *Inorganic Chemistry* **2016**, 55, 1192-1201.
262. Atanasov, M.; Jan Baerends, E.; Baettig, P.; Bruyndonckx, R.; Daul, C.; Rauzy, C.; Zbiri, M., The calculation of ESR parameters by density functional theory: the g- and A-tensors of Co(acacen). *Chemical Physics Letters* **2004**, 399, 433-439.
263. Senn, F.; Zlatar, M.; Gruden-Pavlovic, M.; Daul, C., Computational analysis of tris(1,2-ethanediamine) cobalt(III) complex ion: calculation of the 59Co shielding tensor using LF-DFT. *Monatsh Chem* **2011**, 142, 593-597.
264. Atanasov, M.; Daul, C. A., A DFT based ligand field model for magnetic exchange coupling in transition metal dimer complexes:: (ii) application to magnetic systems with more than one unpaired electron per site. *Chemical Physics Letters* **2003**, 381, 584-591.
265. Atanasov, M.; Daul, C. A., Modeling properties of molecules with open d-shells using density functional theory. *Comptes Rendus Chimie* **2005**, 8, 1421-1433.
266. Rauzy, C. Modeling the properties of open d-shell molecules with a multideterminantal DFT. These Nr. 1465, Université d Fribourg, Suisse, **2005**.

267. Hecht, K. T. The Wigner—Eckart Theorem. In *Quantum Mechanics*; Springer New York: New York, NY, **2000**, 299-302.
268. Band, Y. B.; Avishai, Y. 3 - Angular Momentum and Spherical Symmetry. In *Quantum Mechanics with Applications to Nanotechnology and Information Science*, Band, Y. B.; Avishai, Y., Eds.; Academic Press: Amsterdam, **2013**, 105-157.
269. Janak, J. F., Proof that ∂Eϑni=ε in density-functional theory. *Physical Review B* **1978**, 18, 7165-7168.
270. Mayer, I., On Löwdin's method of symmetric orthogonalization*. *International Journal of Quantum Chemistry* **2002**, 90, 63-65.
271. Perfetti, M.; Bendix, J., Descriptors of magnetic anisotropy revisited. *Chemical Communications* **2018**, 54, 12163-12166.
272. Zlatar, M.; Gruden-Pavlovic, M.; Guell, M.; Swart, M., Computational study of the spin-state energies and UV-Vis spectra of bis(1,4,7-triazacyclononane) complexes of some first-row transition metal cations. *Physical Chemistry Chemical Physics* **2013**, 15, 6631-6639.
273. Trueba, A.; Garcia-Fernandez, P.; García-Lastra, J. M.; Aramburu, J. A.; Barriuso, M. T.; Moreno, M., Spectrochemical Series and the Dependence of Racah and 10Dq Parameters on the Metal−Ligand Distance: Microscopic Origin. *The Journal of Physical Chemistry A* **2011**, 115, 1423-1432.
274. Boča, R., Zero-field splitting in metal complexes. *Coordination Chemistry Reviews* **2004**, 248, 757-815.
275. Atanasov, M.; Rauzy, C.; Baettig, P.; Daul, C., Calculation of spin-orbit coupling within the LFDFT: Applications to [NiX4]2− (X= F−, Cl−, Br−, I−). *International Journal of Quantum Chemistry* **2005**, 102, 119-131.
276. Petit, L.; Borel, A.; Daul, C.; Maldivi, P.; Adamo, C., A theoretical characterization of covalency in rare earth complexes through their absorption electronic properties: f-f transitions. *Inorg Chem* **2006**, 45, 7382.
277. Ziegler, T.; Rauk, A., On the calculation of bonding energies by the Hartree Fock Slater method. *Theoretica chimica acta* **1977**, 46, 1-10.
278. Uddin, J.; Frenking, G., Energy Analysis of Metal-Ligand Bonding in Transition Metal Complexes with Terminal Group-13 Diyl Ligands (CO)4Fe-ER, Fe(EMe)5 and Ni(EMe)4 (E = B−Tl; R = Cp, N(SiH3)2, Ph, Me) Reveals Significant π Bonding in Homoleptical Molecules. *Journal of the American Chemical Society* **2001**, 123, 1683-1693.
279. Lein, M.; Szabó, A.; Kovács, A.; Frenking, G., Energy decomposition analysis of the chemical bond in main group and transition metal compounds. *Faraday Discussions* **2003**, 124, 365-378.
280. Bayat, M.; von Hopffgarten, M.; Salehzadeh, S.; Frenking, G., Energy decomposition analysis of the metal–oxime bond in [M{RC(NOH)C(NO)R}2] (M = Ni(II), Pd(II), Pt(II), R = CH3, H, F, Cl, Br, Ph, CF3). *Journal of Organometallic Chemistry* **2011**, 696, 2976-2984.
281. Bayat, M.; Salehzadeh, S.; Frenking, G., Energy decomposition analysis of the metal-imine bond in [(CO)4M–SB] (M = Cr, Mo, W; SB: RHCN–CH2CH2–NCHR). *Journal of Organometallic Chemistry* **2012**, 697, 74-79.
282. Bickelhaupt, M.; Baerends, E. Kohn-Sham Density Functional Theory: Predicting and Understanding Chemistry. In *Reviews in Computational Chemistry*, Lipkowitz, K.; Boyd, D., Eds.; **2000**, 1-86.
283. Zhao, L.; von Hopffgarten, M.; Andrada, D. M.; Frenking, G., Energy decomposition analysis. *WIREs Computational Molecular Science* **2018**, 8, e1345.
284. Baerends, E. J.; Rozendaal, A. Analysis of σ-Bonding, π-(Foack)Bonding and the Synergic Effect in Cr(CO)6. Comparison of Hartree-Fock and Xα Results for Metal-CO Bonding. In *Quantum Chemistry: The Challenge of Transition Metals and Coordination Chemistry*, Veillard, A., Ed.; Springer Netherlands: Dordrecht, **1986**, 159-177.
285. Bickelhaupt, F. M.; Ziegler, T.; Schleyer, P. v. R., CH3• Is Planar Due to H−H Steric Repulsion. Theoretical Study of MH3• and MH3Cl (M = C, Si, Ge, Sn). *Organometallics* **1996**, 15, 1477-1487.
286. Filip, V.; Maja, G.; Stepan, S.; Marcel, S., *Density Functional Approximations for Consistent Spin and Oxidation States of Oxoiron Complexes*. **2019**.
287. te Velde, G.; Bickelhaupt, F. M.; Baerends, E. J.; Fonseca Guerra, C.; van Gisbergen, S. J. A.; Snijders, J. G.; Ziegler, T., Chemistry with ADF. *Journal of Computational Chemistry* **2001**, 22, 931-967.
288. Baerends, E. J. A., J.; Berces, A.; Bo, C.; Boerrigter, P. M.; Cavallo, L.; Chong, D. P.; Deng, L.; Dickson, R. M.; Ellis, D. E.; Fan, L.; Fischer, T. H.; Fonseca Guerra, C.; van Gisbergen, S. J. A.; Groeneveld, J. A.; Gritsenko, O. V.; Grüning, M.; Harris, F. E.; van den Hoek, P.; Jacobsen, H.; van Kessel, G.; Kootstra, F.; van Lenthe, E.; Osinga, V. P.; Patchkovskii, S.; Philipsen, P. H. T.; Post, D.; Pye, C. C.; Ravenek, W.; Ros, P.; Schipper, P. R. T.;

Schreckenbach, G.; Snijders, J. G.; Solà, M.; Swart, M.; Swerhone, D.; te Velde, G.; Vernooijs, P.; Versluis, L.; Visser, O.; van Wezenbeek, E.; Wiesenekker, G.; Wolff, S. K.; Woo, T. K.; Ziegler, T.; SCM: Amsterdam.
289. Guerra, C. F.; Snijders, J. G.; teVelde, G.; Baerends, E., Towards an order-N DFT method. *Theoretical Chemistry Accounts* **1998**, 99.
290. Gaussian 09, R. A., M. J. Frisch, G. W. Trucks, H. B. Schlegel, G. E. Scuseria, M. A. Robb, J. R. Cheeseman, G. Scalmani, V. Barone, G. A. Petersson, H. Nakatsuji, X. Li, M. Caricato, A. Marenich, J. Bloino, B. G. Janesko, R. Gomperts, B. Mennucci, H. P. Hratchian, J. V. Ortiz, A. F. Izmaylov, J. L. Sonnenberg, D. Williams-Young, F. Ding, F. Lipparini, F. Egidi, J. Goings, B. Peng, A. Petrone, T. Henderson, D. Ranasinghe, V. G. Zakrzewski, J. Gao, N. Rega, G. Zheng, W. Liang, M. Hada, M. Ehara, K. Toyota, R. Fukuda, J. Hasegawa, M. Ishida, T. Nakajima, Y. Honda, O. Kitao, H. Nakai, T. Vreven, K. Throssell, J. A. Montgomery, Jr., J. E. Peralta, F. Ogliaro, M. Bearpark, J. J. Heyd, E. Brothers, K. N. Kudin, V. N. Staroverov, T. Keith, R. Kobayashi, J. Normand, K. Raghavachari, A. Rendell, J. C. Burant, S. S. Iyengar, J. Tomasi, M. Cossi, J. M. Millam, M. Klene, C. Adamo, R. Cammi, J. W. Ochterski, R. L. Martin, K. Morokuma, O. Farkas, J. B. Foresman, and D. J. Fox, Gaussian, Inc., Wallingford CT, **2016**.
291. Neese, F., The ORCA program system. *Wiley Interdisciplinary Reviews: Computational Molecular Science* **2012**, 2, 73-78.
292. Furche, F.; Ahlrichs, R.; Hättig, C.; Klopper, W.; Sierka, M.; Weigend, F., Turbomole. *Wiley Interdisciplinary Reviews: Computational Molecular Science* **2014**, 4, 91-100.
293. Aquilante, F.; Autschbach, J.; Carlson, R. K.; Chibotaru, L. F.; Delcey, M. G.; De Vico, L.; Fdez. Galván, I.; Ferré, N.; Frutos, L. M.; Gagliardi, L.; Garavelli, M.; Giussani, A.; Hoyer, C. E.; Li Manni, G.; Lischka, H.; Ma, D.; Malmqvist, P. Å.; Müller, T.; Nenov, A.; Olivucci, M.; Pedersen, T. B.; Peng, D.; Plasser, F.; Pritchard, B.; Reiher, M.; Rivalta, I.; Schapiro, I.; Segarra-Martí, J.; Stenrup, M.; Truhlar, D. G.; Ungur, L.; Valentini, A.; Vancoillie, S.; Veryazov, V.; Vysotskiy, V. P.; Weingart, O.; Zapata, F.; Lindh, R., Molcas 8: New capabilities for multiconfigurational quantum chemical calculations across the periodic table. *Journal of Computational Chemistry* **2016**, 37, 506-541.
294. Valiev, M.; Bylaska, E. J.; Govind, N.; Kowalski, K.; Straatsma, T. P.; Van Dam, H. J. J.; Wang, D.; Nieplocha, J.; Apra, E.; Windus, T. L.; de Jong, W. A., NWChem: A comprehensive and scalable open-source solution for large scale molecular simulations. *Computer Physics Communications* **2010**, 181, 1477-1489.
295. Aidas, K.; Angeli, C.; Bak, K. L.; Bakken, V.; Bast, R.; Boman, L.; Christiansen, O.; Cimiraglia, R.; Coriani, S.; Dahle, P.; Dalskov, E. K.; Ekström, U.; Enevoldsen, T.; Eriksen, J. J.; Ettenhuber, P.; Fernández, B.; Ferrighi, L.; Fliegl, H.; Frediani, L.; Hald, K.; Halkier, A.; Hättig, C.; Heiberg, H.; Helgaker, T.; Hennum, A. C.; Hettema, H.; Hjertenæs, E.; Høst, S.; Høyvik, I.-M.; Iozzi, M. F.; Jansík, B.; Jensen, H. J. A.; Jonsson, D.; Jørgensen, P.; Kauczor, J.; Kirpekar, S.; Kjærgaard, T.; Klopper, W.; Knecht, S.; Kobayashi, R.; Koch, H.; Kongsted, J.; Krapp, A.; Kristensen, K.; Ligabue, A.; Lutnæs, O. B.; Melo, J. I.; Mikkelsen, K. V.; Myhre, R. H.; Neiss, C.; Nielsen, C. B.; Norman, P.; Olsen, J.; Olsen, J. M. H.; Osted, A.; Packer, M. J.; Pawlowski, F.; Pedersen, T. B.; Provasi, P. F.; Reine, S.; Rinkevicius, Z.; Ruden, T. A.; Ruud, K.; Rybkin, V. V.; Sałek, P.; Samson, C. C. M.; de Merás, A. S.; Saue, T.; Sauer, S. P. A.; Schimmelpfennig, B.; Sneskov, K.; Steindal, A. H.; Sylvester-Hvid, K. O.; Taylor, P. R.; Teale, A. M.; Tellgren, E. I.; Tew, D. P.; Thorvaldsen, A. J.; Thøgersen, L.; Vahtras, O.; Watson, M. A.; Wilson, D. J. D.; Ziolkowski, M.; Ågren, H., The Dalton quantum chemistry program system. *WIREs Computational Molecular Science* **2014**, 4, 269-284.
296. Shao, Y.; Gan, Z.; Epifanovsky, E.; Gilbert, A. T. B.; Wormit, M.; Kussmann, J.; Lange, A. W.; Behn, A.; Deng, J.; Feng, X.; Ghosh, D.; Goldey, M.; Horn, P. R.; Jacobson, L. D.; Kaliman, I.; Khaliullin, R. Z.; Kuś, T.; Landau, A.; Liu, J.; Proynov, E. I.; Rhee, Y. M.; Richard, R. M.; Rohrdanz, M. A.; Steele, R. P.; Sundstrom, E. J.; Woodcock, H. L.; Zimmerman, P. M.; Zuev, D.; Albrecht, B.; Alguire, E.; Austin, B.; Beran, G. J. O.; Bernard, Y. A.; Berquist, E.; Brandhorst, K.; Bravaya, K. B.; Brown, S. T.; Casanova, D.; Chang, C.-M.; Chen, Y.; Chien, S. H.; Closser, K. D.; Crittenden, D. L.; Diedenhofen, M.; DiStasio, R. A.; Do, H.; Dutoi, A. D.; Edgar, R. G.; Fatehi, S.; Fusti-Molnar, L.; Ghysels, A.; Golubeva-Zadorozhnaya, A.; Gomes, J.; Hanson-Heine, M. W. D.; Harbach, P. H. P.; Hauser, A. W.; Hohenstein, E. G.; Holden, Z. C.; Jagau, T.-C.; Ji, H.; Kaduk, B.; Khistyaev, K.; Kim, J.; Kim, J.; King, R. A.; Klunzinger, P.; Kosenkov, D.; Kowalczyk, T.; Krauter, C. M.; Lao, K. U.; Laurent, A. D.; Lawler, K. V.; Levchenko, S. V.; Lin, C. Y.; Liu, F.; Livshits, E.; Lochan, R. C.; Luenser, A.; Manohar, P.; Manzer, S. F.; Mao, S.-P.; Mardirossian, N.; Marenich, A. V.; Maurer, S. A.; Mayhall, N. J.; Neuscamman, E.; Oana, C. M.; Olivares-Amaya, R.; O'Neill, D. P.; Parkhill, J. A.; Perrine, T. M.; Peverati, R.; Prociuk, A.; Rehn, D. R.; Rosta, E.; Russ, N. J.; Sharada, S. M.; Sharma, S.; Small, D. W.; Sodt, A.; Stein, T.; Stück, D.; Su, Y.-C.; Thom, A. J. W.; Tsuchimochi,

T.; Vanovschi, V.; Vogt, L.; Vydrov, O.; Wang, T.; Watson, M. A.; Wenzel, J.; White, A.; Williams, C. F.; Yang, J.; Yeganeh, S.; Yost, S. R.; You, Z.-Q.; Zhang, I. Y.; Zhang, X.; Zhao, Y.; Brooks, B. R.; Chan, G. K. L.; Chipman, D. M.; Cramer, C. J.; Goddard, W. A.; Gordon, M. S.; Hehre, W. J.; Klamt, A.; Schaefer, H. F.; Schmidt, M. W.; Sherrill, C. D.; Truhlar, D. G.; Warshel, A.; Xu, X.; Aspuru-Guzik, A.; Baer, R.; Bell, A. T.; Besley, N. A.; Chai, J.-D.; Dreuw, A.; Dunietz, B. D.; Furlani, T. R.; Gwaltney, S. R.; Hsu, C.-P.; Jung, Y.; Kong, J.; Lambrecht, D. S.; Liang, W.; Ochsenfeld, C.; Rassolov, V. A.; Slipchenko, L. V.; Subotnik, J. E.; Van Voorhis, T.; Herbert, J. M.; Krylov, A. I.; Gill, P. M. W.; Head-Gordon, M., Advances in molecular quantum chemistry contained in the Q-Chem 4 program package. *Molecular Physics* **2015**, 113, 184-215.

297. Tennyson, J.; Brown, D. B.; Munro, J. J.; Rozum, I.; Varambhia, H. N.; Vinci, N., Quantemol-N: an expert system for performing electron molecule collision calculations using the R-matrix method. *Journal of Physics: Conference Series* **2007**, 86, 012001.

298. Guest , M. F.; Bush, I. J.; Van Dam, H. J. J.; Sherwood, P.; Thomas, J. M. H.; Van Lenthe, J. H.; Havenith, R. W. A.; Kendrick, J., The GAMESS-UK electronic structure package: algorithms, developments and applications. *Molecular Physics* **2005**, 103, 719-747.

299. Car, R.; Parrinello, M., Unified Approach for Molecular Dynamics and Density-Functional Theory. *Physical Review Letters* **1985**, 55, 2471-2474.

300. Delley, B., From molecules to solids with the DMol3 approach. *The Journal of Chemical Physics* **2000**, 113, 7756-7764.

301. Deeth, R. J.; Randell, K., Ligand field stabilization and activation energies revisited: molecular modeling of the thermodynamic and kinetic properties of divalent, first-row aqua complexes. *Inorg Chem* **2008**, 47, 7377-88.

302. Yang, Y.; Ratner, M. A.; Schatz, G. C., Multireference Ab Initio Study of Ligand Field d–d Transitions in Octahedral Transition-Metal Oxide Clusters. *The Journal of Physical Chemistry C* **2014**.

303. Atanasov, M.; Comba, P.; Daul, C.; Neese, F. The Ligand-Field Paradigm. In *Models, Mysteries and Magic of Molecules*, Boeyens, J. A.; Ogilvie, J. F., Eds.; Springer Netherlands: 2008; Chapter 19, pp 411-445.

304. Daniel, C., Electronic spectroscopy and photoreactivity in transition metal complexes. *Coordination Chemistry Reviews* **2003**, 238–239, 143-166.

305. Radoń, M.; Gąssowska, K.; Szklarzewicz, J.; Broclawik, E., Spin-State Energetics of Fe(III) and Ru(III) Aqua Complexes: Accurate ab Initio Calculations and Evidence for Huge Solvation Effects. *Journal of Chemical Theory and Computation* **2016**, 12, 1592-1605.

306. Aguilar, C. M.; De Almeida, W. B.; Rocha, W. R., The electronic spectrum of Fe2+ ion in aqueous solution: A sequential Monte Carlo/quantum mechanical study. *Chemical Physics Letters* **2007**, 449, 144-148.

307. Aguilar, C. M.; De Almeida, W. B.; Rocha, W. R., Solvation and electronic spectrum of Ni2+ ion in aqueous and ammonia solutions: A sequential Monte Carlo/TD-DFT study. *Chemical Physics* **2008**, 353, 66.

308. Bersuker, I. B., *The Jahn-Teller Effect*. Cambridge University Press: **2006**.

309. Jahn, H. A.; Teller, E., *Proceedings of the Royal Society of London. Series A* **1937**, 161, 220.

310. Pápai, M.; Vankó, G.; de Graaf, C.; Rozgonyi, T., Theoretical Investigation of the Electronic Structure of Fe(II) Complexes at Spin-State Transitions. *Journal of chemical theory and computation* **2013**, 9, 509-519.

311. Tregenna-Piggott, P. L.; Spichiger, D.; Carver, G.; Frey, B.; Meier, R.; Weihe, H.; Cowan, J. A.; McIntyre, G. J.; Zahn, G.; Barra, A. L., Structure and bonding of the vanadium(III) hexa-aqua cation. 1. Experimental characterization and ligand-field analysis. *Inorganic Chemistry* **2004**, 43, 8049-60.

312. Marcus, Y., Ionic radii in aqueous solutions. *Chemical Reviews* **1988**, 88, 1475-1498.

313. Beattie, J. K.; Best, S. P., Structures and spectroscopy of hexaaquametal(III) ions. *Coordination Chemistry Reviews* **1997**, 166, 391-415.

314. Cotton, F. A.; Daniels, L. M.; Murillo, C. A.; Quesada, J. F., Hexaaqua dipositive ions of the first transition series: new and accurate structures; expected and unexpected trends. *Inorganic Chemistry* **1993**, 32, 4861-4867.

315. Tregenna-Piggott, P. L. W.; Andres, H.-P.; McIntyre, G. J.; Best, S. P.; Wilson, C. C.; Cowan, J. A., Aqua Ions. 2. Structural Manifestations of the Jahn−Teller Effect in the β-Alums. *Inorganic Chemistry* **2003**, 42, 1350-1365.

316. Becker, E.; Kirchner, K.; Mereiter, K., Hexaaquairon(II) bis[fac-tribromidotricarbonylferrate(II)]. *Acta Crystallographica Section E* **2009**, 65, i71.

317. Stavila, V.; Bulimestru, I.; Gulea, A.; Colson, A. C.; Whitmire, K. H., Hexaaquacobalt(II) and hexaaquanickel(II) bis(mu-pyridine-2,6-dicarboxylato)bis[(pyridine-2,6-dicarboxylato)bismuthate(III)] dihydrate. *Acta crystallographica. Section C, Crystal structure communications* **2011**, 67, 65-8.
318. Johnson, D. A.; Nelson, P. G., Ligand Field Stabilization Energies of the Hexaaqua 3+ Complexes of the First Transition Series. *Inorganic Chemistry* **1999**, 38, 4949-4955.
319. Best, S. P.; Clark, R. J. H., The identification of an electronic Raman transition for the hexa-aquavanadium(III) ion. A direct spectroscopic determination of the trigonal field splitting of the 3T1g ground term. *Chemical Physics Letters* **1985**, 122, 401-405.
320. Neese, F.; Petrenko, T.; Ganyushin, D.; Olbrich, G., Advanced aspects of ab initio theoretical optical spectroscopy of transition metal complexes: Multiplets, spin-orbit coupling and resonance Raman intensities. *Coordination Chemistry Reviews* **2007**, 251, 288-327.
321. Landry-Hum, J.; Bussière, G.; Daniel, C.; Reber, C., Triplet Electronic States in d2 and d8 Complexes Probed by Absorption Spectroscopy: A CASSCF/CASPT2 Analysis of [V(H2O)6]3+ and [Ni(H2O)6]2+. *Inorganic Chemistry* **2001**, 40, 2595-2601.
322. Holmes, O. G.; McClure, D. S., Optical Spectra of Hydrated Ions of the Transition Metals. *The Journal of Chemical Physics* **1957**, 26, 1686-1694.
323. Jørgensen, C. K., *Advan. Chem. Phys* **1963**, 5, 33.
324. Anderson, W. P.; Edwards, W. D.; Zerner, M. C., Calculated spectra of hydrated ions of the first transition-metal series. *Inorganic Chemistry* **1986**, 25, 2728-2732.
325. Zhekova, H. R.; Seth, M.; Ziegler, T., A perspective on the relative merits of time-dependent and time-independent density functional theory in studies of the electron spectra due to transition metal complexes. An illustration through applications to copper tetrachloride and plastocyanin. *International Journal of Quantum Chemistry* **2014**, 114, 1019-1029.
326. Tregenna-Piggott, P. L. W.; Weihe, H.; Barra, A.-L., High-Field, Multifrequency EPR Study of the [Mn(OH2)6]3+ Cation: Influence of π-Bonding on the Ground State Zero-Field-Splitting Parameters. *Inorganic Chemistry* **2003**, 42, 8504-8508.
327. Liakos, D. G.; Ganyushin, D.; Neese, F., A Multiconfigurational ab Initio Study of the Zero-Field Splitting in the Di- and Trivalent Hexaquo−Chromium Complexes. *Inorganic Chemistry* **2009**, 48, 10572-10580.
328. Heidt, L. J.; Koster, G. F.; Johnson, A. M., Experimental and Crystal Field Study of the Absorption Spectrum at 2000 to 8000 Å. of Manganous Perchlorate in Aqueous Perchloric Acid1. *Journal of the American Chemical Society* **1958**, 80, 6471-6477.
329. Jørgensen, C. K., *Absorption Spectra and Chemical Bonding in Complexes*. Pergamon Press: Oxford, England, United Kingdom, **1962**.
330. Cotton, F. A.; Meyers, M. D., Magnetic and Spectral Properties of the Spin-Free 3d6 Systems Iron(II) and Cobalt(III) in Cobalt(III) Hexafluoride Ion: Probable Observation of Dynamic Jahn-Teller Effects. *Journal of the American Chemical Society* **1960**, 82, 5023-5026.
331. Johnson, D. A.; Sharpe, A. G., The preparation of cobalt(III) sulphate and its alums, and the magnetic, spectroscopic, and crystallographic properties of the Co(H2O)63+ ion. *Journal of the Chemical Society A: Inorganic, Physical, Theoretical* **1966**, 798-801.
332. Dobe, C.; González, E.; Tregenna-Piggott, P. L. W.; Reber, C., Spectroscopic effects resulting from interacting singlet and triplet excited states: vibronic structure involving the O–H stretching mode in d–d absorption bands of Ni(H2O)62+. *Dalton Transactions* **2014**, 43, 17864-17870.
333. Neese, F., A critical evaluation of DFT, including time-dependent DFT, applied to bioinorganic chemistry. *JBIC Journal of Biological Inorganic Chemistry* **2006**, 11, 702-711.
334. Pye, C. C.; Ziegler, T., An implementation of the conductor-like screening model of solvation within the Amsterdam density functional package. *Theoretical Chemistry Accounts* **1999**, 101, 396-408.
335. Aakesson, R.; Pettersson, L. G. M.; Sandstroem, M.; Wahlgren, U., Ligand Field Effects in the Hydrated Divalent and Trivalent Metal Ions of the First and Second Transition Periods. *Journal of the American Chemical Society* **1994**, 116, 8691-8704.
336. Perdew, J. P.; Chevary, J. A.; Vosko, S. H.; Jackson, K. A.; Pederson, M. R.; Singh, D. J.; Fiolhais, C., Atoms, molecules, solids, and surfaces: Applications of the generalized gradient approximation for exchange and correlation. *Physical Review B* **1992**, 46, 6671-6687.

337. Swart, M.; Ehlers, A. W.; Lammertsma, K., Performance of the OPBE exchange-correlation functional. *Molecular Physics* **2004**, 102, 2467-2474.
338. Kootstra, F.; Boeij, P. L. d.; Snijders, J. G., Efficient real-space approach to time-dependent density functional theory for the dielectric response of nonmetallic crystals. *The Journal of Chemical Physics* **2000**, 112, 6517-6531.
339. Swart, M.; Solà, M.; Bickelhaupt, F. M., A new all-round density functional based on spin states and SN2 barriers. *The Journal of Chemical Physics* **2009**, 131, 094103.
340. Yanai, T.; Tew, D. P.; Handy, N. C., A new hybrid exchange–correlation functional using the Coulomb-attenuating method (CAM-B3LYP). *Chemical Physics Letters* **2004**, 393, 51-57.
341. Ernzerhof, M.; Scuseria, G. E., Assessment of the Perdew–Burke–Ernzerhof exchange-correlation functional. *The Journal of Chemical Physics* **1999**, 110, 5029-5036.
342. Adamo, C.; Barone, V., Toward reliable density functional methods without adjustable parameters: The PBE0 model. *The Journal of Chemical Physics* **1999**, 110, 6158-6170.
343. Zhao, Y.; Truhlar, D. G., The M06 suite of density functionals for main group thermochemistry, thermochemical kinetics, noncovalent interactions, excited states, and transition elements: two new functionals and systematic testing of four M06-class functionals and 12 other functionals. *Theoretical Chemistry Accounts* **2008**, 120, 215-241.
344. O. Gritsenko, P. Schipper, and E. Baerends, ***1999,*** 302, 199.
345. Wang, F.; Ziegler, T., Time-dependent density functional theory based on a noncollinear formulation of the exchange-correlation potential. *The Journal of Chemical Physics* **2004**, 121, 12191-12196.
346. Wang, F.; Ziegler, T., The performance of time-dependent density functional theory based on a noncollinear exchange-correlation potential in the calculations of excitation energies. *The Journal of Chemical Physics* **2005**, 122, 074109.
347. Daul, C., Density functional theory applied to the excited states of coordination compounds. *International Journal of Quantum Chemistry* **1994**, 52, 867-877.
348. Klamt, A., Conductor-like Screening Model for Real Solvents: A New Approach to the Quantitative Calculation of Solvation Phenomena. *The Journal of Physical Chemistry* **1995**, 99, 2224-2235.
349. Shaik, S.; Shurki, A., Valence Bond Diagrams and Chemical Reactivity. *Angewandte Chemie International Edition* **1999**, 38, 586-625.
350. Shaik, S., Biomimetic chemistry: Iron opens up to high activity. *Nat Chem* **2010**, 2, 347-349.
351. Kazaryan, A.; Baerends, E. J., Ligand Field Effects and the High Spin–High Reactivity Correlation in the H Abstraction by Non-Heme Iron(IV)–Oxo Complexes: A DFT Frontier Orbital Perspective. *ACS Catalysis* **2015**, 5, 1475-1488.
352. Zolnhofer, E. M.; Käß, M.; Khusniyarov, M. M.; Heinemann, F. W.; Maron, L.; van Gastel, M.; Bill, E.; Meyer, K., An Intermediate Cobalt(IV) Nitrido Complex and its N-Migratory Insertion Product. *Journal of the American Chemical Society* **2014**, 136, 15072-15078.
353. Schmidt, A.-C.; Heinemann, F. W.; Maron, L.; Meyer, K., A Series of Uranium (IV, V, VI) Tritylimido Complexes, Their Molecular and Electronic Structures and Reactivity with CO2. *Inorganic Chemistry* **2014**, 53, 13142-13153.
354. Johansson, M. P.; Swart, M., Subtle effects control the polymerisation mechanism in [small alpha]-diimine iron catalysts. *Dalton Transactions* **2011**, 40, 8419-8428.
355. Company, A.; Gomez, L.; Costas, M. Chapter 6 Bioinspired Non-heme Iron Catalysts in C-H and C=C Oxidation Reactions. In *Iron-Containing Enzymes: Versatile Catalysts of Hydroxylation Reactions in Nature*; The Royal Society of Chemistry: **2011**, 148-208.
356. Morimoto, Y.; Kotani, H.; Park, J.; Lee, Y.-M.; Nam, W.; Fukuzumi, S., Metal Ion-Coupled Electron Transfer of a Nonheme Oxoiron(IV) Complex: Remarkable Enhancement of Electron-Transfer Rates by Sc3+. *Journal of the American Chemical Society* **2011**, 133, 403-405.
357. Swart, M., A change in the oxidation state of iron: scandium is not innocent. *Chemical Communications* **2013**, 49, 6650-6652.
358. Vanpoucke, D. E. P.; Bultinck, P.; Cottenier, S.; Van Speybroeck, V.; Van Driessche, I., Aliovalent doping of CeO2: DFT study of oxidation state and vacancy effects. *Journal of Materials Chemistry A* **2014**, 2, 13723-13737.

359. Jacobsen, H.; Kraatz, H. B.; Ziegler, T.; Boorman, P. M., A new look at an old ligand: surprises with thioethers. A density functional study. *Journal of the American Chemical Society* **1992**, 114, 7851-7860.
360. Gruden-Pavlovic, M.; Stepanovic, S.; Peric, M.; Guell, M.; Swart, M., A density functional study of the spin state energetics of polypyrazolylborato complexes of first-row transition metals. *Physical Chemistry Chemical Physics* **2014**, 16, 14514-14522.
361. Hill, E. A.; Weitz, A. C.; Onderko, E.; Romero-Rivera, A.; Guo, Y.; Swart, M.; Bominaar, E. L.; Green, M. T.; Hendrich, M. P.; Lacy, D. C.; Borovik, A. S., Reactivity of an FeIV-Oxo Complex with Protons and Oxidants. *Journal of the American Chemical Society* **2016**, 138, 13143-13146.
362. Padamati, S. K.; Angelone, D.; Draksharapu, A.; Primi, G.; Martin, D. J.; Tromp, M.; Swart, M.; Browne, W. R., Transient Formation and Reactivity of a High-Valent Nickel(IV) Oxido Complex. *Journal of the American Chemical Society* **2017**, 139, 8718-8724.
363. Pirovano, P.; Farquhar, E. R.; Swart, M.; Fitzpatrick, A. J.; Morgan, G. G.; McDonald, A. R., Characterization and Reactivity of a Terminal Nickel(III)-Oxygen Adduct. *Chemistry (Weinheim an der Bergstrasse, Germany)* **2015**, 21, 3785-3790.
364. Fukuzumi, S.; Morimoto, Y.; Kotani, H.; Naumov, P.; Lee, Y.-M.; Nam, W., Crystal structure of a metal ion-bound oxoiron(IV) complex and implications for biological electron transfer. *Nat. Chem.* **2010**, 2, 756-759.
365. Prakash, J.; Rohde, G. T.; Meier, K. K.; Jasniewski, A. J.; Van Heuvelen, K. M.; Münck, E.; Que, L., Spectroscopic Identification of an FeIII Center, not FeIV, in the Crystalline Sc–O–Fe Adduct Derived from [FeIV(O)(TMC)]2+. *Journal of the American Chemical Society* **2015**, 137, 3478-3481.
366. MacBeth, C. E.; Gupta, R.; Mitchell-Koch, K. R.; Young, V. G.; Lushington, G. H.; Thompson, W. H.; Hendrich, M. P.; Borovik, A. S., Utilization of Hydrogen Bonds To Stabilize M−O(H) Units: Synthesis and Properties of Monomeric Iron and Manganese Complexes with Terminal Oxo and Hydroxo Ligands. *Journal of the American Chemical Society* **2004**, 126, 2556-2567.
367. Cho, J.; Jeon, S.; Wilson, S. A.; Liu, L. V.; Kang, E. A.; Braymer, J. J.; Lim, M. H.; Hedman, B.; Hodgson, K. O.; Valentine, J. S.; Solomon, E. I.; Nam, W., Structure and reactivity of a mononuclear non-haem iron(III)–peroxo complex. *Nature* **2011**, 478, 502-505.
368. Kendall, A. J.; Zakharov, L. N.; Gilbertson, J. D., Synthesis and Stabilization of a Monomeric Iron(II) Hydroxo Complex via Intramolecular Hydrogen Bonding in the Secondary Coordination Sphere. *Inorganic Chemistry* **2010**, 49, 8656-8658.
369. Fukuzumi, S.; Morimoto, Y.; Kotani, H.; Naumov, P.; Lee, Y.-M.; Nam, W., Crystal structure of a metal ion-bound oxoiron(IV) complex and implications for biological electron transfer. *Nat Chem* **2010**, 2, 756-759.
370. Mukherjee, J.; Lucas, R. L.; Zart, M. K.; Powell, D. R.; Day, V. W.; Borovik, A. S., Synthesis, Structure, and Physical Properties for a Series of Monomeric Iron(III) Hydroxo Complexes with Varying Hydrogen-Bond Networks. *Inorganic Chemistry* **2008**, 47, 5780-5786.
371. Ogo, S.; Yamahara, R.; Roach, M.; Suenobu, T.; Aki, M.; Ogura, T.; Kitagawa, T.; Masuda, H.; Fukuzumi, S.; Watanabe, Y., Structural and Spectroscopic Features of a cis (Hydroxo)-FeIII-(Carboxylato) Configuration as an Active Site Model for Lipoxygenases. *Inorganic Chemistry* **2002**, 41, 5513-5520.
372. Ogo, S.; Wada, S.; Y., W.; Iwase, M.; Wada, A.; Harata, M.; Jitsukawa, K.; Masuda, H.; Einaga, H., Synthesis, Structure, and Spectroscopic Properties of [Feiii(tnpa)(OH)(PhCOO)]ClO4: A Model Complex for an Active Form of Soybean Lipoxygenase-1. *Angewandte Chemie International Edition* **1998**, 37, 2102–2104.
373. Cook, S. A.; Ziller, J. W.; Borovik, A. S., Iron(II) Complexes Supported by Sulfonamido Tripodal Ligands: Endogenous versus Exogenous Substrate Oxidation. *Inorganic Chemistry* **2014**, 53, 11029-11035.
374. Bukowski, M. R.; Koehntop, K. D.; Stubna, A.; Bominaar, E. L.; Halfen, J. A.; Münck, E.; Nam, W.; Que, L., A Thiolate-Ligated Nonheme Oxoiron(IV) Complex Relevant to Cytochrome P450. *Science* **2005**, 310, 1000-1002.
375. Sun, J.; Perdew, J. P.; Ruzsinszky, A., Semilocal density functional obeying a strongly tightened bound for exchange. *Proceedings of the National Academy of Sciences* **2015**, 112, 685-689.
376. Andris, E.; Navrátil, R.; Jasik, J.; Thibault, T.; Srnec, M.; Costas, M.; Roithova, J., Chasing the Evasive Fe=O Stretch and the Spin State of the Iron(IV)-Oxo Complexes by Photodissociation Spectroscopy. *Journal of the American Chemical Society* **2017**, 10.1021/jacs.6b12291.
377. Swart, M.; Groenhof, A. R.; Ehlers, A. W.; Lammertsma, K., Validation of Exchange−Correlation Functionals for Spin States of Iron Complexes. *The Journal of Physical Chemistry A* **2004**, 108, 5479-5483.

378. Stepanovic, S.; Andjelkovic, L.; Zlatar, M.; Andjelkovic, K.; Gruden-Pavlovic, M.; Swart, M., Role of Spin State and Ligand Charge in Coordination Patterns in Complexes of 2,6-Diacetylpyridinebis(semioxamazide) with 3d-Block Metal Ions: A Density Functional Theory Study. *Inorganic Chemistry* **2013**, 52, 13415-13423.
379. Swart, M., Metal-ligand bonding in metallocenes: differentiation between spin state, electrostatic and covalent bonding. *Inorganica Chimica Acta* **2007**, 360, 179-189.
380. Swart, M., Accurate Spin-State Energies for Iron Complexes. *Journal of Chemical Theory and Computation* **2008**, 4, 2057-2066.
381. Swart, M.; Ehlers, A. W.; Lammertsma, K., The performance of OPBE. *Molecular Physics* **2004**, 102, 2467-2474.
382. Zhou, A.; Kleespies, S. T.; Van Heuvelen, K. M.; Que, L., Characterization of a heterobimetallic nonheme Fe(iii)–O–Cr(iii) species formed by O2 activation. *Chemical Communications* **2015**, 51, 14326-14329.
383. Swart, M.; Bickelhaupt, F. M., QUILD: QUantum-regions Interconnected by Local Descriptions. *Journal of Computational Chemistry* **2008**, 29, 724-734.
384. Van Lenthe, E.; Baerends, E. J., Optimized Slater-type basis sets for the elements 1–118. *Journal of Computational Chemistry* **2003**, 24, 1142-1156.
385. Chong, D. P.; Van Lenthe, E.; Van Gisbergen, S.; Baerends, E. J., Even-tempered slater-type orbitals revisited: From hydrogen to krypton. *Journal of Computational Chemistry* **2004**, 25, 1030-1036.
386. Swart, M., A new family of hybrid density functionals. *Chemical Physics Letters* **2013**, 580, 166-171.
387. van Lenthe, E.; Ehlers, A.; Baerends, E.-J., Geometry optimizations in the zero order regular approximation for relativistic effects. *The Journal of Chemical Physics* **1999**, 110, 8943-8953.
388. van Lenthe, E.; Baerends, E. J.; Snijders, J. G., Relativistic total energy using regular approximations. *The Journal of Chemical Physics* **1994**, 101, 9783-9792.
389. Dirac, P. A. M., Note on Exchange Phenomena in the Thomas Atom. *Mathematical Proceedings of the Cambridge Philosophical Society* **2008**, 26, 376-385.
390. Slater, J. C., A Simplification of the Hartree-Fock Method. *Physical Review* **1951**, 81, 385-390.
391. Franchini, M.; Philipsen, P. H. T.; Visscher, L., The Becke Fuzzy Cells Integration Scheme in the Amsterdam Density Functional Program Suite. *Journal of Computational Chemistry* **2013**, 34, 1819-1827.
392. Becke, A. D., A multicenter numerical integration scheme for polyatomic molecules. *The Journal of Chemical Physics* **1988**, 88, 2547-2553.
393. Chen, H.; Lai, W.; Shaik, S., Exchange-Enhanced H-Abstraction Reactivity of High-Valent Nonheme Iron(IV)-Oxo from Coupled Cluster and Density Functional Theories. *The Journal of Physical Chemistry Letters* **2010**, 1, 1533-1540.
394. Swart, M., A change in oxidation state of iron: scandium is not innocent. *Chemical Communications* **2013**, 49, 6650-6652.

8. Biography

8.1 Biography of the author

Filip Ž. Vlahović was born on June 20th, 1989. in Lazarevac, Serbia. He finished elementary and high school in Ljig. He started his Bachelor studies at the Department of Chemistry, University of Belgrade in 2008. He graduated on September 20th, 2012 with GPA of 8.42/10.00. He started graduate academic studies (MSc) at the Chair of Organic Chemistry, Department of Chemistry, University of Belgrade in October 2012. He finished studies on September 9th 2013 with GPA 8.75/10. He started his PhD studies at the Chair of General and Inorganic Chemistry, Department of Chemistry, University Belgrade in October 2013. From September 2014 he is employed at the Innovation center of the Faculty of Chemistry, as member of the project „Rational Design and Synthesis of Bioactive and Coordination Compounds and Functional Materials Relevant for (bio)Nanotechnology".

Filip Ž. Vlahović has attended the summer school of COST Action "Explicit Control Over Spin-states in Technology and Biochemistry (ECOSTBio)" "*Theory and practice in Spectroscopy and Electrochemistry*" Groningen, July, 9-16, 2016 where he has assisted in performing practical classes. As a part of COST action, has spent three months in Girona (Spain) during a Short-Term Scientific Mission (STSM), where he has attended the "*Predictive Catalysis: Transition-Metal Reactivity by Design*" conference, and presented his scientific achievements. Filip Ž. Vlahović has attended the "*25th Young Investigators Seminar on Analytical Chemistry*" in Graz (Austria), where he has won the third prize in the evaluation of The Best Oral Presentation. Filip Ž. Vlahović has attended the "*26th Young Investigators Seminar on Analytical Chemistry*" in Pardubice (Czech Republic), where he has won the third prize in the evaluation of The Best Oral Presentation. As a part of CEEPUS action, has spent one month in Graz (Austria). One of the published scientific paper was chosen as the cover of the March 2020 issue of the *International Journal of Quantum Chemistry.*

Since the beginning of his Ph.D. dissertation, Filipa Ž. Vlahović is co-author of eight scientific papers published in international journals, of which the author is the first author of four papers.

8.2 Биографија аутора

Филип Ж. Влаховић рођен је 20.06.1989. године у Лазаревцу, Република Србија. Основну и средњу школу завршио је у Љигу. Основне академске студије на студијском програму „Дипломирани хемичар" на Хемијском факултету Универзитета у Београду уписао је школске 2008/09. године, а дипломирао 2012. године са просечном оценом 8,42 (осам и 42/100). Мастер академске студије на студијском програму „Мастер хемичар" уписао је школске 2012/13. године, а мастер тезу одбранио октобра 2013. године са просечном оценом 8.75 (осам и 75/100). Докторске академске студије на студијском програму „Доктор хемијских наука" при Катедри за неорганску хемију на Хемијском факултету Универзитета у Београду уписао је школске 2013/14. године. Све програмом предвиђене испите положио је са просечном оценом 10,00 (десет и 0/100). Од септембра 2014. је запослен у Иновационом центру Хемијског факултета Универзитета у Београду као члан на пројекту „Рационални дизајн и синтеза биоактивних и координационих једињења и функционалних материјала релевантних за (био)нанотехнологију''.

Филип Влаховић је члан *COST* акције *CM1305 (ECOSTBio: Explicit Control Over Spin-states in Technology and Biochemistry)* и учествовао у извођењу практичне наставе на летњој школи "*Theory and practice in Spectroscopy and Electrochemistry*" Гронинген, Холандија, јула 2016. године. У склопу исте *COST* акције Филип Влаховић је боравио у Шпанији, на Универзитету у Ђирони 3 месеца (фебруара - априла 2018.), на *Short-Term Scientific Mission,* током које је

радио на детаљном проучавању серије гвожђе-оксо комплекса. Током ове размене Филип Влаховић је учествовао и презентовао своје научне резултате на конференцији "*Predictive Catalysis: Transition-Metal Reactivity by Design*". Филип Влаховић је учествовао на конференцији "*25th Young Investigators Seminar on Analytical Chemistry*" у Грацу (Аустрија), где је освојио трећу награду при валидацији за најбољу оралну презентацију. Филип Влаховић је учествовао на конференцији "*26th Young Investigators Seminar on Analytical Chemistry*" у Пардубице (Чешка Република), где је освојио трећу награду при валидацији за најбољу оралну презентацију. У склопу *CEPPUS* акције боравио је месец дана на универзитету у Грацу (децембара 2019.). Један од објављених научних радова изабран је за насловницу *International Journal of Quantum Chemistry*, марта 2020.

Од почетка рада на својој докторској дисертацији до сада Филипа Ж. Влаховић је коаутор осам научних радова објављених у међународним часописима, од чега је првопотписани аутор на четири рада.

Изјава о ауторству

Име и презиме аутора **Филип Ж. Влаховић**

Број индекса **ДХ01/2013**

Изјављујем

да је докторска дисертација под насловом

"Теорија функционала густине у проучавању електронских стања аква- и оксо-комплекса прве серије прелазних метала".

"Density functional theory for studying electronic states of aqua- and oxo- first row transition metal complexes".

- резултат сопственог истраживачког рада;
- да дисертација у целини ни у деловима није била предложена за стицање друге дипломе према студијским програмима других високошколских установа;
- да су резултати коректно наведени и
- да нисам кршио ауторска права и користио интелектуалну својину других лица.

Потпис аутора

У Београду,

xx.xx.xxxx.

Изјава о истоветности штампане и електронске верзије докторског рада

Име и презиме аутора **Филип Ж. Влаховић**

Број индекса **ДХ01/2013**

Студијски програм **доктор хемијских наука**

Наслов рада

"Теорија функционала густине у проучавању електронских стања аква- и оксо-комплекса прве серије прелазних метала".

"Density functional theory for studying electronic states of aqua- and oxo- first row transition metal complexes".

Ментори:

Др Маја Груден-Павловић,
редовни професор, Универзитета у Београду Хемијског факултета, Србија

Dr. Marcel Swart,
ICREA Research professor, Institut de Química Computacional i Catàlisi (IQCC), University of Girona, Spain

Изјављујем да је штампана верзија мог докторског рада истоветна електронској верзији коју сам предао ради похрањена у **Дигиталном репозиторијуму Универзитета у Београду.** Дозвољавам да се објаве моји лични подаци везани за добијање академског назива доктора наука, као што су име и презиме, година и место рођења и датум одбране рада. Ови лични подаци могу се објавити на мрежним страницама дигиталне библиотеке, у електронском каталогу и у публикацијама Универзитета у Београду.

Потпис аутора

У Београду,

xx.xx.xxxx.

Изјава о коришћењу

Овлашћујем Универзитетску библиотеку „Светозар Марковић“ да у **Дигитални репозиторијум Универзитета у Београду** унесе моју докторску дисертацију под насловом:

"Теорија функционала густине у проучавању електронских стања аква- и оксо-комплекса прве серије прелазних метала".

"Density functional theory for studying electronic states of aqua- and oxo- first row transition metal complexes".

која је моје ауторско дело.

Дисертацију са свим прилозима предао сам у електронском формату погодном за трајно архивирање. Моју докторску дисертацију похрањену у **Дигиталном репозиторијуму Универзитета у Београду** и доступну у отвореном приступу могу да користе сви који поштују одредбе садржане у одабраном типу лиценце Креативне заједнице (Creative Commons) за коју сам се одлучио/ла.

1. Ауторство (CC BY)

2. Ауторство – некомерцијално (CC BY-NC)

3. Ауторство – некомерцијално – без прерада (CC BY-NC-ND)

4. Ауторство – некомерцијално – делити под истим условима (CC BY-NC-SA)

5. Ауторство – без прерада (CC BY-ND)

6. Ауторство – делити под истим условима (CC BY-SA)

(Молимо да заокружите само једну од шест понуђених лиценци.

Кратак опис лиценци је саставни део ове изјаве).

Потпис аутора

У Београду,

xx.xx.xxxx.

1. **Ауторство.** Дозвољавате умножавање, дистрибуцију и јавно саопштавање дела, и прераде, ако се наведе име аутора на начин одређен од стране аутора или даваоца лиценце, чак и у комерцијалне сврхе. Ово је најслободнија од свих лиценци.

2. **Ауторство – некомерцијално**. Дозвољавате умножавање, дистрибуцију и јавно саопштавање дела, и прераде, ако се наведе име аутора на начин одређен од стране аутора или даваоца лиценце. Ова лиценца не дозвољава комерцијалну употребу дела.

3. **Ауторство – некомерцијално – без прерада**. Дозвољавате умножавање, дистрибуцију и јавно саопштавање дела, без промена, преобликовања или употребе дела у свом делу, ако се наведе име аутора на начин одређен од стране аутора или даваоца лиценце. Ова лиценца не дозвољава комерцијалну употребу дела. У односу на све остале лиценце, овом лиценцом се ограничава највећи обим права коришћења дела.

4. **Ауторство – некомерцијално – делити под истим условима**. Дозвољавате умножавање, дистрибуцију и јавно саопштавање дела, и прераде, ако се наведе име аутора на начин одређен од стране аутора или даваоца лиценце и ако се прерада дистрибуира под истом или сличном лиценцом. Ова лиценца не дозвољава комерцијалну употребу дела и прерада.

5. **Ауторство – без прерада**. Дозвољавате умножавање, дистрибуцију и јавно саопштавање дела, без промена, преобликовања или употребе дела у свом делу, ако се наведе име аутора на начин одређен од стране аутора или даваоца лиценце. Ова лиценца дозвољава комерцијалну употребу дела.

6. **Ауторство – делити под истим условима**. Дозвољавате умножавање, дистрибуцију и јавно саопштавање дела, и прераде, ако се наведе име аутора на начин одређен од стране аутора или даваоца лиценце и ако се прерада дистрибуира под истом или сличном лиценцом. Ова лиценца дозвољава комерцијалну употребу дела и прерада. Слична је софтверским лиценцама, односно лиценцама отвореног кода.